FACULTY OF ENGINEERING AND ARCHITECTURE

# Advancing Industrial High-Temperature Heat Pumps through Financial, Thermodynamic and Technological Evaluation

**Elias Vieren**

Doctoral dissertation submitted to obtain the academic degree of
Doctor of Electromechanical Engineering

**Supervisors**

Prof. Steven Lecompte, PhD - Prof. Michel De Paepe, PhD

Department of Electromechanical, Systems and Metal Engineering
Faculty of Engineering and Architecture, Ghent University

March 2025

GHENT UNIVERSITY

ISBN 978-94-6355-965-2
NUR 961
Wettelijk depot: D/2025/10.500/25

## Members of the Examination Board

### Chair

Prof. Patrick De Baets, PhD, Ghent University

### Other members entitled to vote

Prof. Alessia Arteconi, PhD, KU Leuven
Prof. Jelle Laverge, PhD, Ghent University
Prof. Jan Mertens, PhD, Ghent University
Prof. Emilio Navarro-Peris, PhD, Universitat Politècnica de València, Spain
Manuel Vandevoorde, PhD, Atlas Copco

### Supervisors

Prof. Steven Lecompte, PhD, Ghent University
Prof. Michel De Paepe, PhD, Ghent University

# Preface

Four years ago I started a PhD. I am grateful that I took this opportunity. Over these four years, many people have supported me in achieving my PhD, and I would like to take this opportunity to acknowledge them.

First of all, I would like to express my sincere gratitude to my supervisors, Prof. Steven Lecompte and Prof. Michel De Paepe, for their invaluable guidance and unwavering support throughout my PhD journey. Steven, I am particularly grateful to you for your valuable input and guidance during all the meetings we had. I would also like to thank you for always taking the time to answer my questions, even when I showed up at your office unexpectedly. I can only wonder how many times I might have distracted you from your work.

I would also like to acknowledge all my colleagues who contributed to the scientific aspects of my PhD. In particular, I am deeply grateful to Toon Demeester, Wim Beyne, and Kenny Couvreur for their invaluable guidance and support throughout this journey. I extend special thanks to Kenny for his detailed feedback on my thesis book. Furthermore, I would like to express my gratitude to Prof. Alessia Arteconi and her colleagues at KU Leuven for their valuable input and feedback during the Upheat-INES project, which formed the foundation of my PhD.

During my PhD I also found a close group of welcoming colleagues within the Sustainable Thermo-Fluid Energy Systems research group. To all my colleagues, old and new, thank you for the pleasant times we have had. Particularly, I would like to thank my 'office neighbour' Robin Tassenoy. When I find a new job, I will miss your jokes, our chats and the trips we took after the conferences we attended.

During my PhD, I spent three months at the Technical University of Denmark (DTU) for a research stay, which turned out to be a truly wonderful experience. I would like to express my gratitude to Prof. Brian Elgemaard for the warm welcome I received and the interesting research I was able to help with. It was miserable to hear that you are no longer with us. You will be missed by so many. I would also like to thank everyone else at DTU for the warm welcome. I really enjoyed the 'Coffee Club Breakfast' we had on

Fridays. My special thanks go to Wiebke Meesenburg and Barış Burak Kanbur for the warm welcome you both gave me (and for lending me your DTU cards when I ordered food during the lunch breaks we had). My special thanks also go to Jierong Liang for your guidance on the topic I was working on during my research stay.

I am also grateful to my friends and family. To my friends, thank you for the good times we have had over the years and for distracting me and allowing me to refresh my mind. To my mum, dad, brother and sister, thank you for your support over the years and for always being there for me. I would particularly like to thank my mother for her unwavering support and for taking such good care of me, not only over the last four years but throughout the past twenty-eight years.

Elias Vieren
Gent, December 2024

# Summary

Climate change and the vast amount of pollutants emitted are direct consequences of the ever-increasing global demand for energy. A significant proportion of this energy demand comes from industry, where most of the energy is required in the form of heat. As this heat is mainly produced by burning fossil fuels, replacing fossil fuel boilers represents a significant opportunity to mitigate climate change and reduce pollutants. A promising technology for this are heat pumps. Heat pumps in the industry recover residual heat and use it to provide useful process heat, allowing to significantly reduce primary energy use. Moreover, heat pumps can be powered by electricity, enabling a complete shift away from fossil fuels for heat production.

There are several types of electrically-driven heat pumps, but the focus in this work is on the vapour compression heat pump, which uses an intermediate working fluid. The vapour compression heat pump is the most common type of heat pump. While it is becoming increasingly integrated in the building sector, its use in the industrial sector remains significantly lower. This thesis addresses three main reasons for the poor integration of vapour compression heat pumps in industry.

First, a financial comparison is made with competing heating technologies. This is done to offer clarity on its financial potential and to identify use cases for vapour compression heat pumps. The vapour compression heat pump is compared with the heat transformer, the electric boiler and the natural gas boiler. A heat transformer upgrades residual heat to a higher temperature level by utilizing a thermodynamic cycle. This process involves rejecting a significant amount of heat at a lower temperature to enable the temperature lift. The heat-driven heat pump was excluded from this analysis. This is due to the scarcity of research, and the lack of technological advancements, that would enable the use of this type of heat pump at high temperatures. A key reason for this limitation is that their functionality relies on the presence of a residual heat source at even higher temperatures. First, a generic comparison was made over a range of temperature lifts and availabilities of residual heat. This allows for indicating which technology offers the lowest levelized cost of heat over the investigated range of temperature lifts and availabilities

of residual heat. Furthermore, the analysis was carried out under different energy prices. Overall, it was concluded that the heat transformer is only viable in regions where there is more residual heat available than heat demand. Otherwise, the choice lies between the vapor compression heat pump and the natural gas boiler, depending on the combination of energy prices and temperature lift. The vapour compression heat pump generally performed best in scenarios with high energy prices, low electricity-to-gas price ratios and lower temperature lifts. For other scenarios the technology was typically only viable up to a maximum temperature lift. To gain a deeper insight, a financial comparison of all four technologies was made for two specific case studies with a predefined temperature lift and residual heat availability. Here, variations in technology costs were also taken into account. Depending on the country, different solutions were found to be optimal. In addition, a sensitivity analysis was carried out by varying the annual operating hours, emission trading schemes and residual heat availability. The vapour compression heat pump is favoured in scenarios with high operating hours, high costs associated with emission trading schemes and high residual heat availability. However, in cases where the residual heat greatly exceeds heat demand, the heat transformer may offer the lowest levelized cost of heat.

Second, the study focuses on further improving the performance of vapour compression heat pumps to further increase their adoption. The focus here is on the working fluid selection, particularly focusing on applications where there are temperature glides at the heat sink and/or heat source. In this context, a robust thermodynamic simulation and optimization framework has been developed, aimed at maximizing the Coefficient of Performance. First, applications with large temperature glides at the heat sink and smaller glides at the heat source were examined, with the emphasis on transcritical cycles. The analysis revealed that transcritical cycles outperform conventional subcritical cycles when the temperature glide at the heat sink exceeds 60 K. Nevertheless, for lower temperature glides, transcritical cycles exhibit more favourable operating conditions, including a lower compressor discharge temperature, a reduced pressure ratio, and a higher volumetric heating capacity. However, their main challenge is the associated high compressor discharge pressure. Next, applications with smaller, or no, temperature glides at both the heat source and heat sink were investigated. Here, the focus was on binary (zeotropic) mixtures. It was found that binary zeotropic mixtures can lead to improved performance compared to pure working fluids due to their characteristic temperature glide during phase change. Interestingly, the temperature glide during condensation or evaporation is not necessarily the same, so the use of zeotropic mixtures is not limited to applications with similar temperature glides at the heat source and heat sink. In cases where there

are no glides at the heat source or sink, (near-) azeotropic binary mixtures may still offer advantages over pure working fluids due to a trade-off in their thermophysical properties. After both analyses, cost functions were incorporated in the thermodynamic model, allowing for optimizing the levelized cost of heat rather than just the thermodynamic performance. The corresponding analysis was carried out over a wide range of generic heat source and heat sink temperature profiles, and it was found that the optimum performance does not necessarily correspond to the lowest investment cost. Therefore, a discrepancy was found between the optimal Coefficient of Performance and the optimal levelized cost of heat. Nevertheless, the potential benefits of binary mixtures and transcritical cycles were even more pronounced in these cost-optimized scenarios.

Third, the current state-of-the-art vapour compression heat pumps are limited in supply temperature, which restricts their applications. At present, commercial machines can achieve supply temperatures between 120 °C to 160 °C. To overcome this limitation, a design for a vapour compression heat pump capable of delivering heat up to 200 °C has been made. Either water or a water-ammonia mixture was selected as the working fluid, based on the working fluid screening procedure performed. These working fluids were chosen for their favourable performance and because both are natural working fluids with zero global warming potential, ozone depletion potential, PFAS formation potential, and are either non-flammable or mildly flammable. An oil-free twin-screw compressor with hydrodynamic bearings and working fluid injection was selected for this purpose, featuring a 30 kW drive. The influence of working fluid injection was first analyzed to determine the optimal injection rate. This was followed by a detailed design of the heat pump, including the selection, sizing, and ordering of all components. A 3D model of the machine was then created, and a hazard and operability study along with a control strategy was developed. Future work will involve the commissioning of the machine and conducting an experimental campaign.

# Samenvatting

Klimaatverandering en de uitstoot van grote hoeveelheden vervuilende stoffen zijn directe gevolgen van de steeds toenemende wereldwijde vraag naar energie. Een aanzienlijk deel van deze energievraag is afkomstig van de industrie, waar de meeste energie nodig is in de vorm van warmte. Deze warmte wordt voornamelijk geproduceerd door de verbranding van fossiele brandstoffen. Daarom is het vervangen van industriële boilers die gebruik maken van fossiele brandstoffen een belangrijke aspect om de klimaatverandering te beperken en de uitstoot van vervuilende stoffen te verminderen. Een veelbelovende technologie hiervoor zijn warmtepompen. Warmtepompen in de industrie maken gebruik van restwarmte om zo nuttige proceswarmte te leveren, waardoor het gebruik van primaire energie aanzienlijk kan worden teruggedrongen. Bovendien kunnen warmtepompen worden aangedreven door elektriciteit, waardoor een volledige verschuiving weg van fossiele brandstoffen voor warmteproductie mogelijk wordt.

Er zijn verschillende soorten elektrisch aangedreven warmtepompen, maar in dit werk ligt de nadruk op de dampcompressie warmtepomp, die een tussenliggende koudemiddel gebruikt. De dampcompressie warmtepomp is het meest voorkomende type warmtepomp. Hoewel ze steeds meer geïntegreerd wordt in de bouwsector, blijft het gebruik in de industriële sector aanzienlijk lager. In dit proefschrift worden drie hoofdredenen behandeld voor de beperkte integratie van dampcompressie warmtepompen in de industrie.

Eerst wordt een financiële vergelijking gemaakt met concurrerende verwarmingstechnologieën. Dit wordt gedaan om duidelijkheid te bieden over het financiële potentieel en om applicaties voor dampcompressie warmtepompen te identificeren. De dampcompressie warmtepomp wordt vergeleken met de warmtetransformator, de elektrische ketel en de aardgasketel. Een warmtetransformator verhoogt restwarmte naar een hoger temperatuurniveau door gebruik te maken van een thermodynamische cyclus. Dit proces vereist de afvoer van een aanzienlijke hoeveelheid warmte op een lagere temperatuur om de temperatuursverhoging mogelijk te maken. De warmte-aangedreven warmtepomp is buiten beschouwing gelaten in deze analyse. Dit door het gebrek aan onderzoek, en de afwezigheid van technologische vooruitgang,

die het gebruik van dit type warmtepomp voor hoge temperaturen mogelijk maakt. Dit is voornamelijk toe te wijten omdat hun werking afhankelijk is van de aanwezigheid van een restwarmtebron bij nog hogere temperaturen. Eerst wordt een generieke vergelijking gemaakt voor een reeks temperatuursverhogingen en beschikbaarheden van restwarmte. Hieruit volgt welke technologie de laagste gekapitaliseerde kost van warmte biedt over het onderzochte bereik van temperatuurverhogingen en beschikbaarheden van restwarmte. Bovendien werd deze analyse uitgevoerd onder verschillende energieprijzen. In het algemeen werd geconcludeerd dat de warmtetransformator alleen rendabel is wanneer meer restwarmte beschikbaar is dan warmtevraag. Anders is de keuze tussen de dampcompressie warmtepomp en de aardgasketel. Deze keuze hangt af van de combinatie van energieprijzen en temperatuurverhoging. De dampcompressie warmtepomp presteerde over het algemeen het beste in scenario's met hoge energieprijzen, lage elektriciteit-gasprijsverhoudingen en lagere temperatuurverhogingen. Voor andere scenario's was de technologie meestal alleen financieel interessant tot een maximale temperatuurverhoging. Om meer inzicht te krijgen, werd ook een financiële vergelijking van alle vier de technologieën gemaakt voor twee specifieke case studies met een vooraf gedefinieerde temperatuurverhoging en beschikbaarheid van restwarmte. Hierbij werd bovendien ook rekening gehouden met variaties in technologiekosten. Afhankelijk van het land bleken verschillende oplossingen optimaal te zijn. Daarnaast werd er een sensitiviteitsanalyse uitgevoerd door het varieren van de jaarlijkse bedrijfsuren, $CO_2$ emissie kosten en restwarmtebeschikbaarheid. De dampcompressie warmtepomp is het meest interessant in scenario's met hoge bedrijfsuren, hoge $CO_2$ emissie kosten en een hoge beschikbaarheid van restwarmte. In gevallen waarin de restwarmte echter veel hoger is dan de warmtevraag, kan de warmtetransformator de technologie zijn met de laagste gekapitaliseerde kost van warmte.

Ten tweede richt het onderzoek zich verder op het verbeteren van de prestaties van dampcompressie warmtepompen om het toepassingsgebied ervan verder te vergroten. De focus ligt hierbij op de selectie van het koudemiddel, met een specifieke focus op toepassingen waar sprake is van temperatuur variaties bij het proces en/of de warmtebron. In deze context is een robuust thermodynamisch simulatie- en optimalisatiekader ontwikkeld, met het doel om de prestatiecoëfficiënt te optimaliseren. Eerst werden toepassingen met grote temperatuur variaties bij het proces en kleinere temperatuur variaties bij de warmtebron onderzocht, met de nadruk op transkritische cycli. Uit de analyse bleek dat transkritische cycli beter presteren dan conventionele subkritische cycli wanneer de temperatuur variatie bij het proces groter is dan 60 K. Voor lagere temperatuur variaties vertonen transkritische cycli echter al gunstigere operationele condities, waaronder een lagere temperatuur aan de

compressoruitlaat, een lagere drukverhouding en een hogere volumetrische verwarmingscapaciteit. Hun grootste uitdaging is echter de bijbehorende hoge druk aan de compressoruitlaat. Vervolgens werden toepassingen met kleinere, of geen, temperatuurvariaties bij zowel de warmtebron als het proces onderzocht. Hier lag de focus op binaire (zeotrope) mengsels. Het bleek dat binaire zeotrope mengsels tot betere prestaties kunnen leiden vanwege hun karakteristieke temperatuurvariatie tijdens de faseovergang. Interessant is dat de temperatuurvariatie tijdens condensatie en verdamping niet noodzakelijkerwijs hetzelfde is, zodat het gebruik van zeotrope mengsels niet beperkt is tot toepassingen met vergelijkbare temperatuurvariatie bij de warmtebron en het proces. In gevallen waar er geen temperatuur variaties zijn bij de warmtebron of het koellichaam, kunnen (bijna-) azeotrope binaire mengsels nog steeds voordelen bieden ten opzichte van zuivere koudemiddelen vanwege een afweging in hun thermofysische eigenschappen. Na beide analyses werden kostfuncties opgenomen in het thermodynamisch model, wat het mogelijk maakt om de gekapitaliseerde kost van warmte te optimaliseren in plaats van alleen de thermodynamische performantie. De overeenkomstige analyse werd uitgevoerd over een breed bereik van generieke warmtebron- en procestemperatuurprofielen. Het bleek dat de optimale prestatie niet noodzakelijkerwijs overeenkomt met de laagste investering kosten. Daarom werd er een verschil gevonden tussen de optimale prestatiecoëfficiënt en de optimale gekapitaliseerde kosten van warmte. Desondanks waren de potentiële voordelen van binaire mengsels en transkritische cycli nog duidelijker in deze scenario's met geoptimaliseerde kosten.

Ten derde zijn de huidige dampcompressie warmtepompen beperkt in de toevoertemperatuur, wat hun toepassingen beperkt. Op dit moment kunnen commerciële machines temperaturen tussen 120 °C en 160 °C bereiken. Om deze beperking te overwinnen is er een ontwerp gemaakt voor een dampcompressie warmtepomp die warmte tot 200 °C kan leveren. Als koudemiddel werd water of een water-ammoniakmengsel gekozen op basis van de uitgevoerde screeningprocedure voor koudemiddelen. Deze vloeistoffen zijn gekozen vanwege hun gunstige prestaties en het feit dat het beide natuurlijke koudemiddelen zijn, die geen aardopwarmingspotentieel, geen ozonafbrekingspotentieel, geen PFAS-vormingspotentieel hebben en niet of slechts licht ontvlambaar zijn. Hiervoor werd een olievrije dubbelschroefcompressor met hydrodynamische lagers en koudemiddelinjectie geselecteerd, met een aandrijving van 30 kW. De invloed van de koudemiddelinjectie werd eerst geanalyseerd om het optimale injectiedebiet te bepalen. Daarna volgde een gedetailleerd ontwerp van de warmtepomp, inclusief de selectie, dimensionering en bestelling van alle componenten. Vervolgens werd er een 3D-model van de warmtepomp gemaakt en werd er een gevaren- en werkbaarheids-

studie uitgevoerd, samen met het ontwikkelen van een controle strategie. Toekomstig werk omvat de inbedrijfstelling van de machine en het uitvoeren van een experimentele campagne.

# Nomenclature

These lists give a non-exhaustive overview of the acronyms and symbols used throughout the thesis.

## Acronyms

| | |
|---|---|
| BIP | Binary interaction parameter |
| CFC | Chlorofluorocarbon |
| CHP | Compression heat pump |
| DWC | Dividing-wall column |
| EB | Electric boiler |
| ETS | Emission trading scheme |
| GCHP | Gas compression heat pump |
| GWP | Global warming potential |
| HCFC | Hydrochlorofluorocarbon |
| HCFO | Hydrochlorofluroolefin |
| HFC | Hydrofluorocarbon |
| HFO | Hydrofluoroolefin |
| HHP | Heat-driven heat pump |
| HPT | Heat Pumping Technologies |
| HTC | Heat transfer coefficient |
| HTF | Heat-driven heat transformer |
| HTHP | High-temperature heat pump |
| IEA | International Energy Agency |
| IHX | Internal heat exchanger |
| MVR | Mechanical vapour recompression |
| NGB | Natural gas boiler |
| ODP | Ozone depletion potential |
| ORC | Organic Rankine cycle |
| PFAS | Polyfluoroalkyl substance |
| SC | Subcritical |
| SGHP | Steam generating heat pump |
| SSD | Superheated steam drying |
| TC | Transcritical |

| | |
|---|---|
| TFA | Trifluoroacetic acid |
| TRL | Technology readiness level |
| TVR | Thermal vapour recompression |
| VCHP | Vapour compression heat pump |
| VLE | Vapour-liquid equilibrium |

## Greek symbols

| | | |
|---|---|---|
| $\alpha$ | heat transfer coefficient | $W/(m^2 \cdot K)$ |
| $\Delta$ | difference | - |
| $\epsilon$ | effectiveness | - |
| $\eta$ | efficiency | - |
| $\rho$ | density | $kg/m^3$ |
| $\chi$ | vapour quality | - |

## Latin symbols

| | | |
|---|---|---|
| $A$ | Heat transfer area | $m^2$ |
| $C$ | Cost | € |
| $CEPCI$ | Chemical Engineering Plant Cost Index | - |
| $COP$ | Coefficient of Performance | - |
| $EGPR$ | Electricity to gas price ratio | - |
| $F$ | Factor | - |
| $GTL$ | Gross temperature lift | K |
| $LCOH$ | Levelized cost of heat | €/kWh |
| $LMTD$ | Log mean temperature difference | K |
| $NBP$ | Normal boiling point | K |
| $PPTD$ | Pinch point temperature difference | K |
| $PR$ | Pressure ratio | - |
| $RHR$ | Residual heat ratio | - |
| $TCI$ | Total cost of investment | € |
| $T$ | Temperature | K |
| $U$ | Overall heat transfer coefficient | $W/(m^2 \cdot K)$ |
| $VHC$ | Volumetric heating capacity | $kJ/m^3$ |
| $h$ | Hours | h |
| $h$ | Specific enthalpy | J/(kg) |
| $i$ | Interest rate | % |
| $n$ | Number | - |
| $p$ | Pressure | Pa |
| $s$ | Specific entropy | J/(kg · K) |
| $t$ | Time | Year |

| | | |
|---|---|---|
| $x_{mole}$ | Molar fraction first constituent | - |
| $\dot{E}$ | Energy input rate | W |
| $\dot{m}$ | Mass flow rate | kg/s |
| $\dot{Q}$ | Heat transfer rate | W |
| $\dot{V}$ | Volume flow rate | $m^3/s$ |
| $\dot{W}$ | Power | W |

## Subscripts

| | |
|---|---|
| $a$ | annual |
| $BM$ | bare module |
| $CAPEX$ | capital expenditures |
| $c$ | cold |
| $comp$ | compressor |
| $cd$ | condenser |
| $d$ | discharge |
| $el$ | electrical |
| $exp$ | expander |
| $ev$ | evaporator |
| $h$ | hot |
| $hex$ | heat exchanger |
| $i$ | in |
| $in$ | inlet |
| $inv$ | investment |
| $is$ | isentropic |
| $l$ | low |
| $maint$ | maintenance |
| $m$ | medium |
| $max$ | maximum |
| $o$ | out |
| $OPEX$ | operational expenditures |
| $out$ | outlet |
| $rej$ | rejected |
| $sc$ | subcooling |
| $sf$ | secondary fluid |
| $sh$ | superheat |
| $sm$ | secondary medium |
| $spec$ | specific |
| $temp$ | temperature |
| $th$ | thermal |
| $TM$ | total module |
| $tot$ | total |

| | |
|---|---|
| $vol$ | volumetric |
| $wf$ | working fluid |

# Contents

# 1 Introduction

## 1.1 The need for fossil-fuel-free industrial heat

The global atmospheric concentration of greenhouse gases, such as carbon dioxide ($CO_2$), has increased significantly since the industrial revolution due to human activity. These anthropogenic greenhouse gases are causing global warming and climate change, which means a rise in global temperatures and sea levels, and a greater occurrence and magnitude of floods, droughts, heat waves and hurricanes [1]. Therefore, in December 2015, the world leaders gathered at the 21st Conference of the Parties (COP21) in Paris and agreed to a two headed temperature goal: "Limit the increase in the global average temperature to well below 2 °C above pre-industrial levels and pursuing efforts to limit the temperature increase to 1.5 °C" [2]. However, 2023, eight years later, was by far the warmest year on record since global records began in 1850. The Earth's temperature was 1.35 °C above the pre-industrial average (1850-1900) [3]. Therefore, it is often stated that "the current level of global effort is not sufficient to achieve what is required to limit warming to 1.5 °C" [4]. In order to step up the global efforts, and achieve the goals of the Paris Agreement, it is vital to understand what the main greenhouse gases are and where they come from.

It is well known that the main greenhouse gas is $CO_2$ and mainly originates from fossil fuel combustion and deforestation. $CO_2$ alone was responsible for about 76 % of the global greenhouse emissions in 2019 [5]. Other greenhouse

gas emissions include 13 % methane ($CH_4$), 7 % sulfur dioxide, 3 % nitrous oxide ($N_2O$), and 1 % fluorinated gases. Because $CO_2$ is the main greenhouse gas, greenhouse gas emissions are often expressed in terms of $CO_2$ equivalent ($CO_{2,eq}$). An overview of the relative greenhouse gas emissions among different sectors can be found in Figure 1.1.

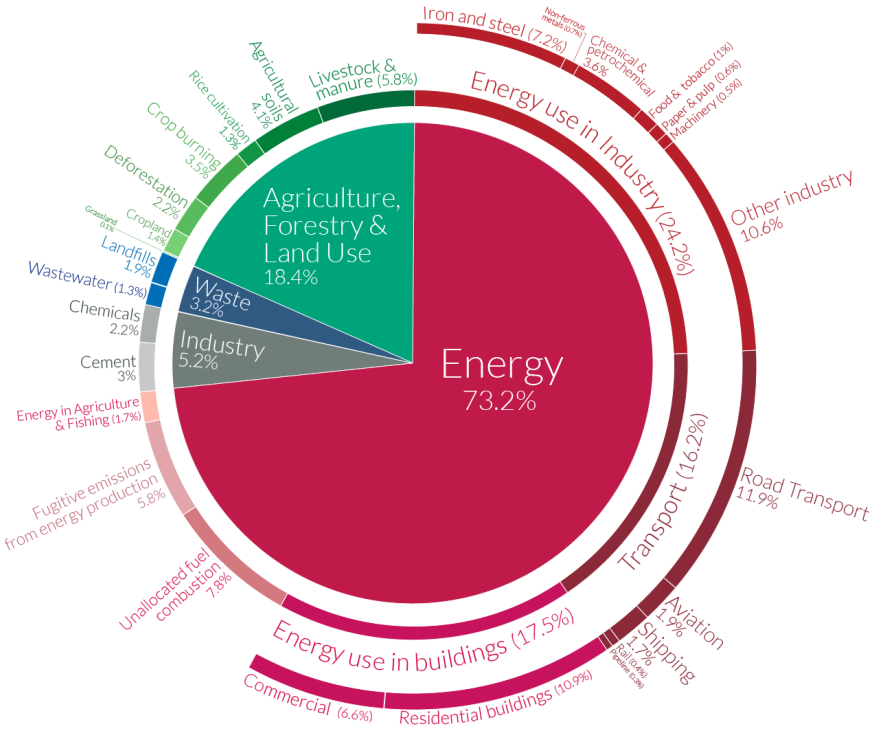


Figure 1.1: Percentage of global greenhouse gas emissions by sector. Figure reproduced from Ritchie [6].

From this figure it can be observed that greenhouse gas emissions allocated to direct energy use has the largest contribution (73.2 %). Within this classification, the energy use in industry has the largest contribution to greenhouse gasses, responsible for 24.2 % of all greenhouse gas emissions. Other studies indicate that a large share of the industrial sector greenhouse gas emissions results from one single process: the generation of heat (i.e. thermal energy). According to de Boer et al. [7], the demand in heat was responsible for 77 % of the energy demand in the European industry in 2019. In their study it was found that 11 % of the energy demand in industry was due to space heating, while 66 % was due to the demand in process heat. According to the Global Carbon Project report [8], the heat demand in industry was even responsible

for 21 % of the global $CO_2$ emissions in 2016. Furthermore, when fossil fuels like coal, oil and natural gas are burned they release a variety of pollutants, including particulate matter, which can cause respiratory and cardiovascular diseases as well as premature deaths [9, 10]. Because of the above-mentioned reasons, there is a clear need for fossil-fuel-free heat.

The technologies to defossilize industrial heat may vary depending on the temperature level of the heat demand [11]. Therefore, the heat demand is often classified according to its temperature level. This classification, for the European industry, was also made in the work of de Boer et al. [7], as visualized in Figure 1.2. The data shown here only focuses on process heat and does not include the demand for space heating in industry. Particularly interesting is that the study shows that 37 % of the process heat demand is at temperatures below 200 °C. Heat demand at these temperatures can be more conveniently decarbonized. Particularly interesting and increasingly put forward is the use of heat pumps to provide industrial heat up to 200 °C, avoiding the use of fossil fuels. Heat pumps generally become less attractive for heat demands above 200 °C. This is because their performance decreases as a result of the higher temperature lift associated with higher supply temperatures. In addition, their complexity and cost increase with increasing temperature lift and supply temperature. Therefore, boiler solutions based on renewable electricity, renewable hydrogen, sustainable biomass, or natural gas with carbon capture and utilization are required for heat demands above 200 °C. Alternatively, direct renewable sources such as solar or geothermal energy could be used.

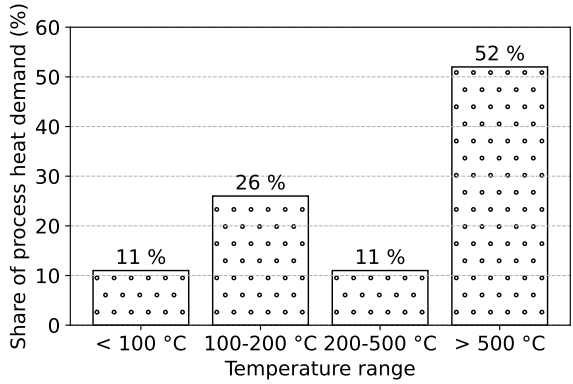


Figure 1.2: Breakdown of the European process heat demand according to its temperature level. Figure based on data from de Boer et al. [7].

## 1.2 High-temperature heat pumps as a solution for fossil-fuel-free industrial heat

The interest in heat pump technologies within the industry is gradually increasing. Heat pumps can extract heat from a residual heat stream and transfer it to a process requiring heat at higher temperatures. They can be driven by mechanical work, mostly done by using an electrical motor or by a change in chemical equilibrium, done by using a heat source. The valorization of residual heat typically results in substantial reductions in primary energy input and thus $CO_2$ emissions and pollutants. Next to the significant improvement in energy efficiency, heat pumps result in the uptake of a sustainable energy source and are therefore able to completely omit $CO_2$ emissions and pollutant emissions.

The term 'industrial heat pump' is frequently used to describe heat pumps used in an industrial setting. The term 'high-temperature heat pump' (HTHPs) on the other hand is frequently used to classify industrial heat pumps providing heat at high temperatures. Different boundaries are used in the literature as a threshold value to classify the definition of 'high temperature', but 100 °C is often used as minimum supply temperature for a HTHP [12]. Multiple HTHP technologies exist, but the closed-cycle vapour compression heat pump is the most widely used and studied [12]. This heat pump extracts heat from a heat source and transfers it to a heat sink at a higher temperature. The heat source and sink are often referred to as the 'secondary media'. This process is facilitated by a thermodynamic cycle, which relies on an intermediate working fluid. The cycle is powered by a primary energy source, typically electricity, which drives the compressor.

The technology readiness level (TRL) of the closed-cycle vapour compression HTHP depends on the maximum supply temperature level of the heat it can supply. HTHPs with a maximum supply temperature of 120 °C are currently in commercial roll-out. For supply temperatures between 120 °C and 160 °C, the technology is currently in the demonstration phase, while HTHPs supplying heat above 160 °C are still in the prototype phase [13]. For even higher temperatures, up to 200 °C, the technology is only at the concept or lab phase [13]. For all the industrial heat pumps there are still several challenges to overcome before widespread adoption is reached. This is especially true for these that extend the boundaries of achievable supply temperatures.

## 1.3 Challenges in de-fossilizing industrial heat with high-temperature heat pumps

Some of the main challenges in de-fossilizing industrial heat up to 200 °C through vapour compression HTHPs are:

1. There is a limited understanding of the technical capabilities and economically viable applications of HTHPs among stakeholders such as users, consultants, investors, plant designers, manufacturers, and installers [7, 12].
2. There is a lack of understanding regarding the integration of HTHPs into industrial processes. Custom designs often result in costly integration within existing systems [7, 12].
3. HTHPs have higher initial investment costs compared to natural gas or oil-fired boilers [12].
4. Competing heating technologies which use fossil fuels can have lower operational cost due to low energy prices [12]. In addition, for the different types of heat pump technologies, it is generally not clear for which type of heat pump to match with a specific application from a financial point of view.
5. There is a lack of working fluids with a low global warming potential that can be used in the high temperature range [12]. Particularly found lacking in the current state-of-the-art HTHPs are working fluids which, during heat transfer, matches their temperature profile with the temperature profile of the secondary media. This can strongly increase the performance, and thus adoption rate, of the heat pump. Furthermore, overall there is a particular lack in research on suitable working fluids for heat supply temperatures between 100 °C and 200 °C.
6. Depending on the application, the heat pump technology may not be available, particularly at higher temperatures [7, 14]. Furthermore, for some industries, there may be concerns regarding potential flammability of the working fluid of the heat pump available.

## 1.4 Objective of the dissertation

The objective of the study is to advance industrial HTHPs through financial, thermodynamic and technological evaluation. This objective aligns well with tackling the challenges listed in Section 1.3. A particular focus will be placed on challenges 4, 5 and 6. In what follows it will be briefly explained how these challenges will be tackled.

## 1.5 Approach of the dissertation

The dissertation is divided in three main parts, which are respectively related to challenges 4, 5 and 6.

The first part (Chapter 2 and 3) concerns the assessment of the financial competitiveness of closed-loop vapour compression HTHPs and is therefore related to Challenge 4. It involves a comparison with fossil fuel and electric boilers. In addition, a comparison is also made with the heat transformer, another type of HTHP. For each technology the application areas are shown in a generic and intuitive way in the form of contour plots. This is achieved through the development of a generic financial model. The analysis shows that the vapour compression heat pump is the most cost-efficient heating technology for a wide range of applications. This confirms the relevance of the technology and the scope of the dissertation. After this part, the focus is solely on the vapour compression heat pump.

The second part (Chapter 4 and 5) addresses Challenge 5 in two steps. Firstly, a thermodynamic simulation and optimization model is developed. The model aims at selecting suitable working fluids for vapour compression HTHPs from a thermodynamic point of view. The focus is on applications with supply temperatures between 160 °C and 200 °C. Secondly, this work is extended with a techno-economic analysis by introducing financial considerations.

The third part (Chapter 6) is focused on the design of a heat pump which can (a) supply heat at temperatures up to 200 °C and (b) proves and characterize the concept of the water and ammonia mixtures. Based on the results of the second part, pure water and the zeotropic mixture of water and ammonia were selected as working fluids due to their promising performance, low or no flammability risks, and their status as natural working fluids. While pure water is more suitable for applications without temperature glide (e.g. steam production), the mixture of water and ammonia is more suitable for applications with temperature glides (e.g. thermal oil heating).

A brief overview of the chapters of this book is given below:

- **Chapter 2:** Provides a general overview of HTHP technology with a focus on its classifications and general working principle, technology readiness level, cost and applications. The aim of this chapter is also to provide a concise and generic overview of heat pump technologies as a basis for the next chapter.
- **Chapter 3:** In this chapter the financial comparison of a natural gas boiler, electric boiler, vapour compression heat pump and heat transformer is performed and presented based on a high-level financial

model. The potential of vapour compression heat pumps is highlighted here.

- **Chapter 4:** In this chapter a thermodynamic screening for a large set of working fluids is performed and presented. A particular focus is placed upon the match in temperature profiles between the working fluid and the secondary medium.
- **Chapter 5:** Extends Chapter 4 by also considering costs associated to the heat pump components. Hence, the comparison is performed from a techno-economic point of view rather than a thermodynamic point of view.
- **Chapter 6:** Introduces and explains the specific design of the water and water and ammonia mixture HTHP concept. In Chapter 4 and Chapter 5 it was shown that these working fluids are promising from a technical, thermodynamic and cost perspective.
- **Chapter 7:** Provides a general conclusion about the dissertation and introduces future work.

A list of Journal and Conference publications published during the dissertation can de found in Appendix A.

# 2

# General overview of high-temperature heat pump technologies for industry

*This Chapter is mainly based on unpublished work, but contains parts of the Journal paper:*

*E. Vieren, T. Demeester, W. Beyne, C. Magni, H. Abedini, C. Arpagaus, S. Bertsch, A. Alessia, M. De Paepe and S. Lecompte, "The potential of vapor compression heat pumps supplying process heat between 100 and 200 °c in the chemical industry",* Energies*, vol. 16, no. 18, 2023, ISSN: 1996-1073. DOI:* 10.3390/en16186473*. [Online]. Available:* https://www.mdpi.com/1996-1073/16/18/6473

## 2.1 Introduction

This chapter provides a brief and general introduction to HTHP technologies, among others aimed at providing a basis for the next chapter (Chapter 3). It starts with classifying the different heat pump technologies and explains their general working principle in terms of energy flows (Section 2.2). Next, an indication of the cost and TRL is given for each technology (Section 2.3).

At last, an indication of relevant industrial applications is given in Section 2.4.

## 2.2 Classifications of heat pump technologies and their general working principle

Multiple classifications of heat pump technologies exists. The classification made here can be found in Figure 2.1. The first breakdown is made depending whether the system is a closed loop or open loop. The closed-loop systems use an intermediate working fluid (sometimes referred to as the refrigerant), while in the open-loop systems the process medium is directly used in the heat pump system. The second breakdown is made depending whether the driving energy input of the heat pump is mechanical energy or heat. The mechanically-driven systems are driven by a compressor. As the compressor is usually electrically driven, these heat pumps are sometimes referred to as 'electrically-driven heat pumps'. Depending on these two classifications five main types of heat pumps can be classified, named and abbreviated 'Thermal vapour recompression (TVR)', 'Mechanical vapour recompression (MVR)', 'Heat-driven heat transformer (HTF)', 'Heat-driven heat pump (HHP)' and 'Compression heat pump (CHP)'. Furthermore, the HTF and HHP can be based on absorption, adsorption or chemical processes. The CHP on the other hand is either based on the vapour compression or gas compression cycle. The vapour compression heat pump operates based on the reversed Rankine cycle, while the gas compression heat pump can operate either based on the reversed Brayton cycle or the reversed Stirling cycle.

In what follows a high-level thermodynamic description of the five main technologies (i.e. TVR, MVR, HTF, HHP and CHP) will be given. For further information such as the technical operating principles, references to the literature are made.

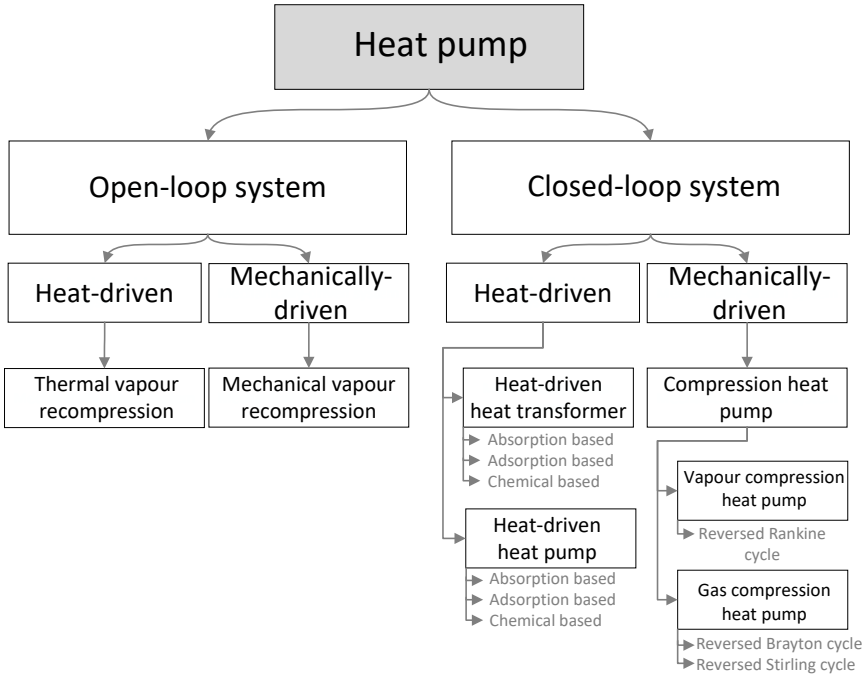


Figure 2.1: Overview of the heat pump classification.

### 2.2.1 Closed-loop systems

In this subsection the three closed-loop systems (i.e. CHP, HHP and HTF) are discussed. An indication of typical energy flows of each heat pump type is given in Figure 2.2. These energy flows are based on a supply of 1 $MW_{th}$ process heat. Moreover, in this figure, each arrow colour is associated with a different type of energy flow, clarified by the legend at the bottom of the figure. Furthermore, the relative temperature levels are shown for the associated heat flows. For the estimation of the capacities of the energy flows, typical values for the Coefficient of Performances (COPs) reported within the literature are used [16–18]. For all these technologies, the COP is defined by the ratio of the rate of useful process heat ($\dot{Q}_{usefull}$) supply to the rate of driving energy input ($\dot{E}_{driving}$) as shown in Equation 2.1. Moreover, a distinction is made between a medium temperature lift ($\sim$ 45 K) and a large temperature lift ($\sim$ 90 K) in order to indicate the dependency of the COP and energy flows on the temperature lift.

$$COP = \frac{\dot{Q}_{usefull}}{\dot{E}_{driving}} \tag{2.1}$$

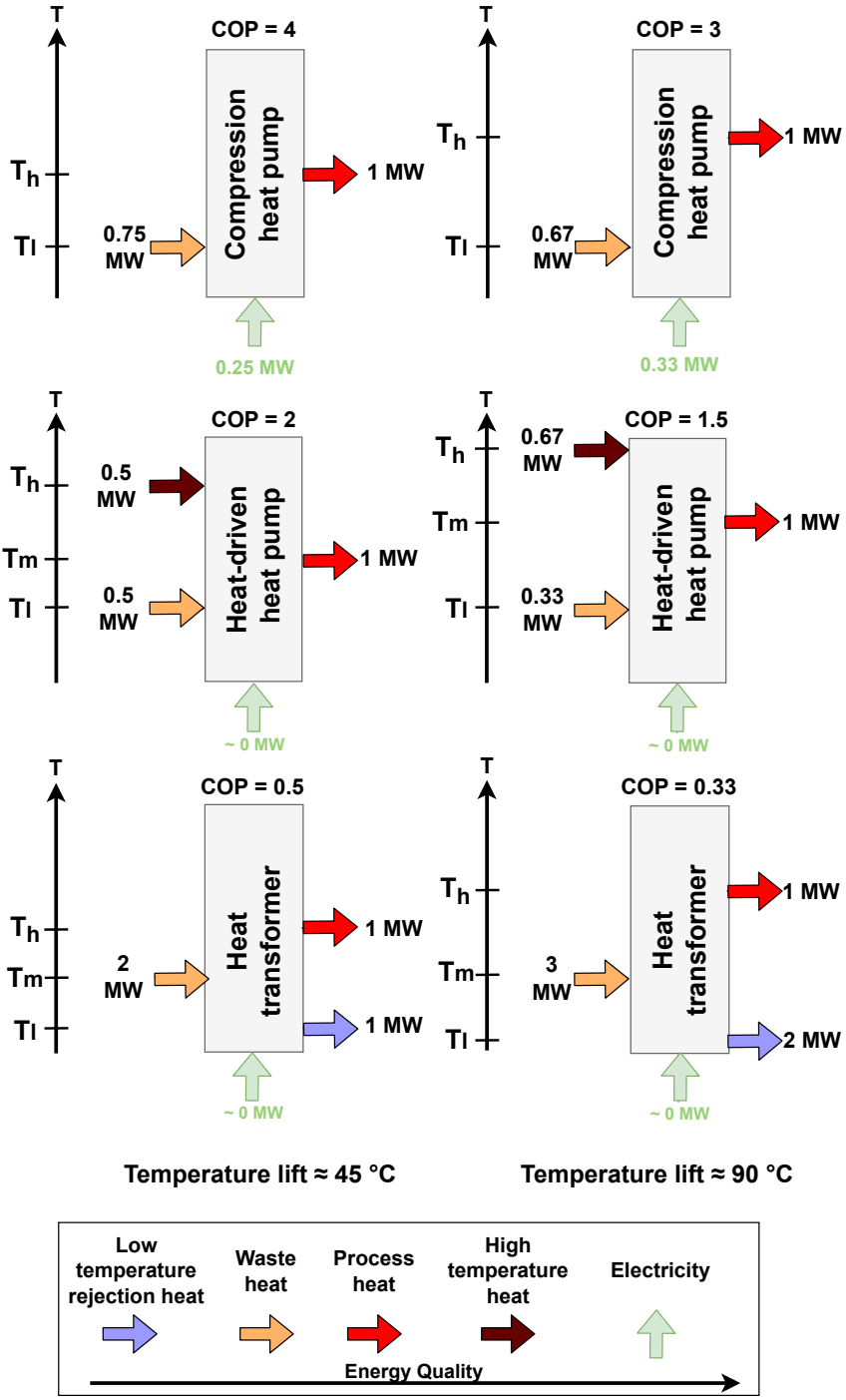


Figure 2.2: Typical energy flows of a CHP, HHP and HTF.

#### 2.2.1.1 Mechanically-driven system

**Compression heat pump**
A CHP transfers heat from a (residual) heat source ($\dot{Q}_{residual}$) at temperature level $T_l$ to a higher temperature stream ($\dot{Q}_{process}$) at temperature level $T_h$. This process is possible because of a compressor which requires an amount of work ($\dot{W}_{comp}$). The maximum theoretical ratio of heat delivery to compressor power, at constant heat source and heat sink temperatures, is defined by the Carnot COP:

$$COP_{max} = \frac{\dot{Q}_{process}}{\dot{W}_{comp}} = \frac{T_h}{T_h - T_l} \tag{2.2}$$

In practical applications, with temperature lifts between 30 K to 100 K, the actual COP typically varies between 2 to 5 [12, 13]. As the compressor is commonly electrically driven, the CHP technology is theoretically able to operate entirely emission free when the electricity originates from renewable energy. Moreover, due to the addition of compression work in the energy balance, shown in Equation 2.3, an increased amount of heat is delivered at the heat sink compared to the amount of heat extracted from the heat source ($\dot{Q}_{residual}$) (i.e. $\dot{Q}_{process} > \dot{Q}_{residual}$).

$$\dot{Q}_{residual} + \dot{W}_{comp} = \dot{Q}_{process} \tag{2.3}$$

As indicated earlier, the CHP can either be classified as a vapour compression heat pump (VCHP) or a gas compression heat pump (GCHP). With the VCHP operating according to the reversed Rankine cycle and the GCHP operating according to the reversed Brayton cycle or the reversed Stirling cycle. More information on CHPs can be found in the literature [12, 19–23].

#### 2.2.1.2 Heat-driven system

**Heat-driven heat pump**
HHPs transfer heat from two inlet streams to one process heat stream. Next to the low-temperature (residual) heat stream ($\dot{Q}_{residual}$) at temperature level $T_l$, there is a need for a high-temperature heat input ($\dot{Q}_{high}$) at temperature level $T_h$. The output of a HHP system is process heat ($\dot{Q}_{process}$) at an intermediate temperature level $T_m$. The maximum theoretical COP, when the heat source and heat sink temperatures are held constant, is defined by [24]:

$$COP_{max} = \frac{\dot{Q}_{process}}{\dot{Q}_{high}} = \left(1 - \frac{T_l}{T_h}\right) \cdot \left(\frac{T_m}{T_m - T_l}\right) \tag{2.4}$$

This COP is essentially a multiplication of the Carnot heat engine efficiency and the Carnot COP of a CHP. Consequently, lower COPs are obtained compared to CHPs. However, the driving energy input (high-temperature heat) usually comes at a lower cost than electricity. In practical implementations the COP typically varies between 1.3 to 2.2 [18]. Due to the addition of the

high-temperature heat input ($\dot{Q}_{high,temp}$) in the energy balance (Equation 2.5), a reduced amount of low-grade residual heat is required to provide a specific amount of process heat ($\dot{Q}_{process} >> \dot{Q}_{residual}$).

$$\dot{Q}_{residual} + \dot{Q}_{high,temp} = \dot{Q}_{process} \tag{2.5}$$

The driving energy input mainly comes from gas-driven heat sources and to a lesser extent from high-temperature residual heat, bioenergy, geothermal or solar heat sources. The technology is thus often referred to as 'gas-driven heat pumps' [25]. The operating principle can either be based on adsorption, absorption or chemical processes. More information on the operating principles of HHPs can be found in the literature [17, 26–29].

**Heat-driven heat transformer**
A HTF transfers (residual) heat ($\dot{Q}_{residual}$) at an intermediate temperature $T_m$ to two output flows: a high-temperature flow ($\dot{Q}_{process}$: i.e., upgraded heat) at temperature level $T_h$ and a low-temperature flow ($\dot{Q}_{rej}$: i.e., rejected heat) at temperature level $T_l$. Consequently, the process requires negligible amounts of electricity, contrary to the CHP. Neither does it require high-temperature heat sources in contrast to the HHP. The technology therefore has low operational cost, except for some auxiliary power requirements. The maximum theoretical COP is defined as:

$$COP_{max} = \frac{\dot{Q}_{process}}{\dot{Q}_{residual}} = \left(1 - \frac{T_l}{T_m}\right) \cdot \left(\frac{T_h}{T_h - T_l}\right) \tag{2.6}$$

As a substantial amount of low-grade heat is rejected, HTFs always have a COP below 1. For low temperature lifts (~50 K), COPs of about 0.5 are reported [16, 18, 30], whereas for high temperature lifts (~140 K) COPs around 0.23 are reported [16, 18, 30]. Therefore, only a quarter to half of the residual heat can be valorized. The remaining part is rejected as low-temperature heat ($\dot{Q}_{low,temp}$) as shown in the energy balance (Equation 2.7). This gives rise to a poor residual heat utilization ($\dot{Q}_{process} << \dot{Q}_{residual}$).

$$\dot{Q}_{residual} = \dot{Q}_{process} + \dot{Q}_{low,temp} \tag{2.7}$$

As for the HHP, the operating principle can either be based on adsorption, absorption or chemical processes. More information on the operating principles of HTFs can be found in the literature [16, 18, 26, 30–33].

## 2.2.2 Open-loop systems

### 2.2.2.1 Mechanically-driven system

**Mechanical vapour recompression**
In terms of energy flows and thermodynamic performance, the MVR follows the same principles as the CHP. The main difference is that no heat exchangers

are present in the MVR. For the CHP heat is extracted from a heat source and delivered to a heat sink at higher temperatures, both through the use of heat exchangers. This separates the heat source from the heat sink. In an MVR, the heat source is directly used and upgraded to the desired pressure and temperature level through compression. The heat source thus becomes the useful stream. The COP definition of the CHP and the energy flows shown in Figure 2.2 remain valid.

A limitation of the MVR is that the heat source has to be a vapour stream, which can be compressed. MVR can thus not be directly used for example to heat thermal oil using moist air as a heat source. Furthermore, the vapour streams available might pose challenges related to the compressor design. Using an intermediate working fluid might result in a much simpler compressor design. Advantages include simpler cycle layouts and often higher performance. A typical application is the recompression of residual low-pressure steam to a pressure where there is a steam demand.

#### 2.2.2.2 Heat-driven system

**Thermal vapour recompression**
Similar to the MVR, the TVR does not use heat exchangers. This contrasts with the closed-system counterpart, the HHP, where heat is extracted from both the low-temperature and high-temperature heat sources and transferred to a heat source at an intermediate temperature. Instead, the low-temperature heat source and high-temperature heat source are send to an ejector where the medium temperature heat is an output. The COP definition of the CHP and the energy flows shown in Figure 2.2 remain valid.

Again, the TVR is mostly limited to the application of steam upgrading.

## 2.3 Indication of technology readiness level and cost

Within the International Energy Agency (IEA) Heat Pumping Technologies (HPT) Annex 58 [13] an overview is provided about the commercial available HTHPs, or HTHPs currently in the development phase. This overview provides information regarding the capacities, maximum supply temperatures, TRL, cost, heat pump design, etc. The data is however not third party verified. This data is processed and summarized in Task 1 of the Annex 58 [34] and also in the review paper of Klute et al. [35], who also included information on the state of the art from the literature.

The main conclusions of these two works, regarding the maximum supply temperature levels of the different heating technologies are:

- **Heat-driven heat pump**: No data is collected on the HHP within Annex 58. This is because the outlet temperatures of HHP are typically below 90 °C and within the Annex the focus is on heat pump technologies with supply temperatures above 100 °C.
- **Compression heat pump**: Regarding the CHP there is a difference in TRL depending whether the heat pump technology is a VCHP or a GCHP. The VCHPs are currently (2024) in the commercial roll-out for temperatures up to 120 °C. For temperatures between 120 °C to 160 °C demonstrators are available, while for temperatures above 160 °C the technology is mainly in the prototype phase. Regarding the GCHPs higher TRLs are reported. Claims of TRLs of 9 up to 200 °C, or TRLs of 7 up to 250 °C, are reported.
- **Mechanical vapour recompression**: Some MVR technologies are identified with TRLs of 9 for supply temperatures above 200 °C.
- **Thermal vapour compression**: Some TVR technologies are identified with TRLs of 9 for supply temperatures above 200 °C.
- **Heat-driven heat transformer**: One manufacturer with TRL of 9 above 200 °C, otherwise typically limited to 150 °C.

Overall it can be concluded that the HHP has the lowest maximum supply temperature, followed by the VCHP. The GCHP, MVR, TVR and HTF all have TRLs of 9 at maximum supply temperatures above 200 °C. Although for the HTF and GCHP this is only for one manufacturer.

Another important factor is the investment cost. Here, a relative ranking is made. According to Klute et al. [35], TVRs have the lowest cost, followed by MVRs, VCHP and then HHPs. Second most expensive are the GCHPs and by far the most expensive are the HTFs. The cost functions fitted can be found in the review paper [35]. Although this gives an indication about the investment cost of the technology, no direct comparison between the investment cost is possible as the operational costs may highly differ due to differences in driving energy input and performance.

## 2.4 Industrial applications of high-temperature heat pumps

In this section a general overview of applications is first provided (Section 2.4.1). Afterwards, a more detailed description is given on highly relevant

applications (Section 2.4.2). Lastly, case studies of relevant applications are introduced (Section 2.4.3). These case studies will be used as boundary conditions throughout this manuscript.

### 2.4.1 General overview of applications

The main application of HTHPs is the supply of process heat in industry. Typical sectors with a large application potential include, but are not limited to, the paper industry, food and beverages industry, chemical industry and metal industry [12, 14, 36]. An overview of the most relevant applications among different sectors, with typical process temperature ranges can be found in Figure 2.3.

The figure shows a wide variety of applications among different sectors. It also shows that distillation, drying and injection molding are applications which demand heat at higher temperatures, up to 200 °C and even above. Yet no VCHP technology is commercially available. Furthermore, because of the widespread use of distillation and drying in the industry the next subsection will discuss these two relevant applications in more detail.

Noteworthy is that in practice the heat generation technology often is not directly integrated in the process. Instead, the industry often employs heat exchanger networks using intermediate fluids such as steam or thermal oil which transfer the heat. Direct integration could involve topological disadvantages, limited operational flexibility and controllability of the overall plant and chemical and safety hazards [37]. Heat exchanger networks covers these disadvantages, but at reduced energy conservation opportunities because of the exergy destruction impaired in employing an intermediate heat carrier. The most used intermediate heat carrier is steam, which is common for industrial applications [38–42]. Consequently, due to its deep integration and industrial relevance, steam generation is also further discussed as a relevant application.

Next to the supply of industrial process heat, HTHPs are also frequently put forward for district heating, which typically has supply temperatures between 60 °C to 135 °C [43]. Therefore, for the higher temperature district heating networks ($>$ 100 °C), HTHP could be an interesting alternative heating method. Another application with increased attention are Carnot batteries, which is a type of thermo-mechanical electrical energy storage system [44]. For the charging cycle, where electrical energy is converted in thermal energy, HTHPs are increasingly put forward [44]. No further focus is however placed upon these applications in the next sections.

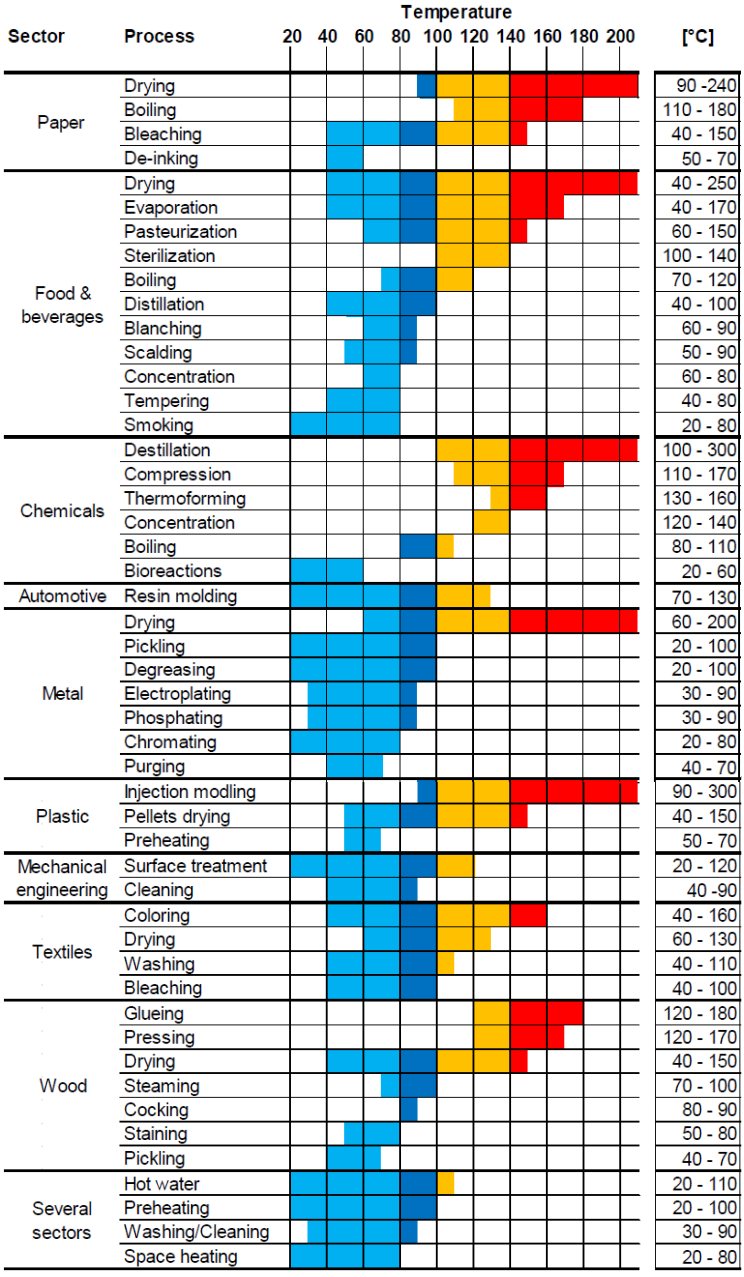


Figure 2.3: Overview of the most relevant applications of HTHPs among different sectors, combined with typical process temperatures indicated. Figure copied from Arpagaus et al. [12].

## 2.4.2 Detailed overview of highly relevant applications

### 2.4.2.1 Distillation

Distillation is a frequently used process in the industry, and is of particular importance in the chemical industry. Distillation is commonly used to separate liquid mixtures, by utilizing selective boiling and condensation. As boiling and condensation are energy-intensive tasks, distillation alone globally accounts for about 40 % of the energy used in the chemical process industry [45].

In its simplest form, as illustrated in Figure 2.4.a, a distillation column consists of a reboiler at the bottom of the column and a condenser at the top of the column. In the reboiler, high-quality heat is supplied to evaporate the mixture, while in the condenser low-quality heat is rejected as the vapour condenses. The heat released at the condenser is often extracted by means of cooling water, whereas the heat supplied in the reboiler is typically delivered by steam.

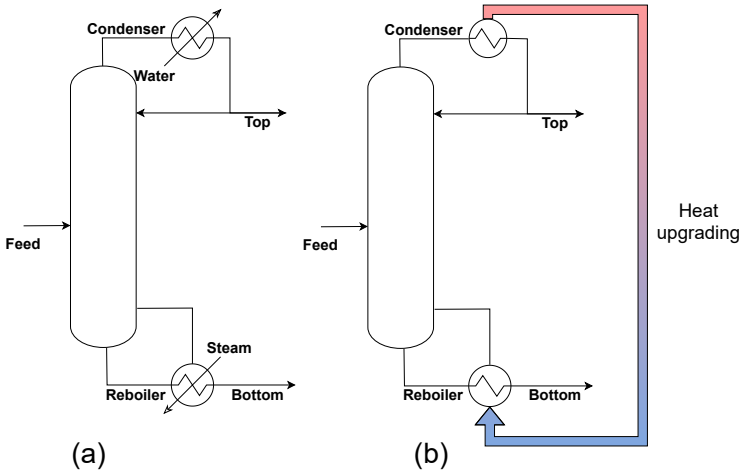


Figure 2.4: Scheme of a simple distillation column, with (a) the conventional heating method and (b) heat pump integration.

In ideal circumstances, no heat is lost in a distillation process, but it is degraded to lower a temperature. Moreover, the operation temperatures are typically in the temperature range of 100 °C to 300 °C and are often below 200 °C. Hence, heat pumps are an effective technology for upgrading the low-temperature heat back to its original temperature, while simultaneously providing cooling as shown in Figure 2.4.b. Integrating heat pumps into distillation processes is generally an attractive option, as the heat availability and demand are similar. Moreover, the heat source and sink are part of the same

integrated process, facilitating easier integration of the heat pump.

Due to the immense potential of heat pumps in distillation processes, heat pump assisted distillation is often studied in the literature [40, 46–51]. Both open-loop and closed-loop systems are studied.

#### 2.4.2.2 Drying

Drying of particulate products is a common process in the industry [38]. It is an energy-intensive process due to the high latent heat of vaporization and therefore globally accounts for up to 15 % of all energy use in industry [52] and 5 % in the chemical industry [53]. A large number of drying methods exists [53]. Here the focus is placed upon two of the most important methods, spray drying and superheated steam drying.

**Spray drying**

Within the literature, or research projects, heat pump assisted heat recovery from the exhaust air of spray dryers is often studied [38, 54–56]. In these studies, ambient air typically needs to be heated to between 158 °C and 210 °C, with most processes operating in the higher temperature range. The outlet temperature of the humid exhaust air for these cases varies between 52 °C to 76 °C. Air recirculation is often avoided to prevent bacterial growth and reduced drying rates [57]. Therefore, the exhaust air is typically first used for preheating the ambient inlet air. After the air preheating, the remaining heat from the exhaust air can be transferred to the drying air by means of a heat pump. However, some energy is lost to the environment and is transferred to the dried product. As a consequence of the air preheating and the energy transferred to the drying product and environment, no complete energy recovery can be made between the residual heat available and the heat demanded. Extracting too much heat from the air would result in too high temperature lifts and/or sub-ambient temperatures, as indicated in Figure 2.5. Therefore, an auxiliary heating system (e.g. electric heater) is necessary to heat the air to its final temperature. An alternative option is utilizing an external waste heat source with a suitable temperature level and energy content so that the air can be heated to the desired temperature without the use of an auxiliary heating system. For heat pump integration in hot air based drying processes, closed-loop heat pumps are typically used.

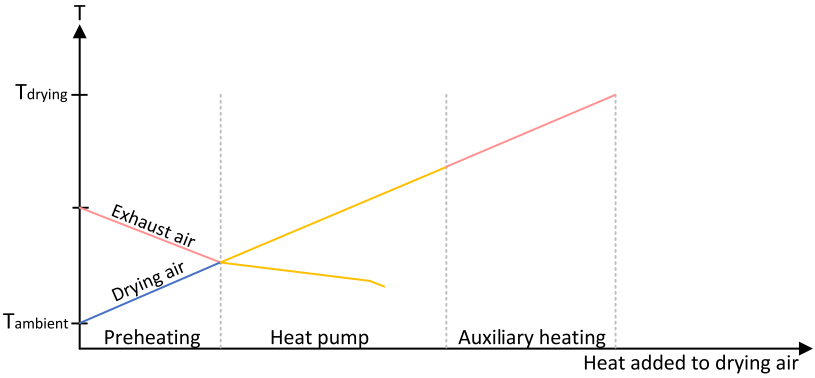


Figure 2.5: Illustration of theoretic temperature profiles within air drying applications.

**Superheated steam drying**

Superheated steam drying (SSD) is an emerging closed-loop technology with several advantages over other drying technologies [53, 58, 59]. The technology recently has gained importance and became commercially viable [60]. The process is often a closed-loop process where the majority of the steam is recirculated to be superheated. A particular advantage for the integration of heat pumps is that the exhaust of the SSD process is also steam, which can be recirculated. In SSD an exhaust amount of steam, equal to the amount of water evaporated from the dried product, is produced. This slightly superheated excess steam can be used as residual heat source at constant temperature when condensed, contrary to drying methods based on hot air. By doing so, an acceptable temperature lift and hence performance of the heat pump can be achieved when heat is transferred from the residual steam to superheat the drying steam, as illustrated in Figure 2.6. Therefore, no auxiliary heating system is needed. Both open-loop as closed-loop heat pumps can be used for SSD.

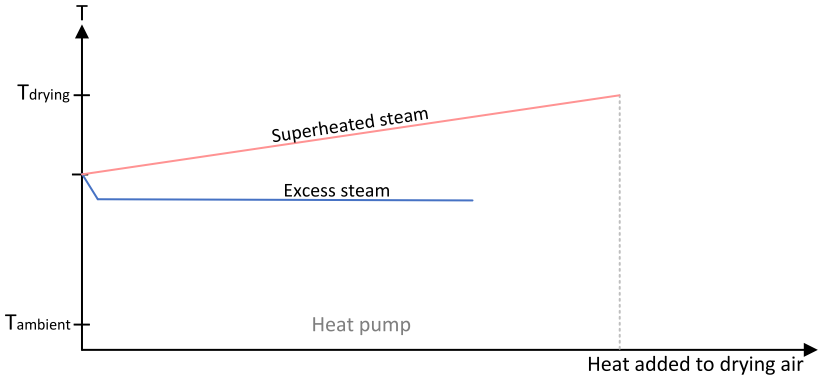


Figure 2.6: Illustration of temperature profiles within superheated steam drying.

#### 2.4.2.3 Steam production

Steam is the main heat transfer medium in the industry. Because of the relevance and the deep integration of steam networks, researchers and heat pump manufacturers often focus on steam generating heat pumps (SGHPs) [12, 61].

SGHPs can be both closed-loop as open-loop heat pumps. For open-loop heat pumps, the process is quite simple. Low-pressure steam is compressed to high-pressure steam. For closed-loop heat pumps different configurations exists. The steam can either be produced by directly heating (pressurized) hot water until it evaporates, or indirectly by heating hot water and subsequently flash it. Moreover, a hybrid combination between open loop and closed loop is possible. In what follows, the two closed-loop methods and the hybrid method are discussed.

**Closed loop: Direct steam production**
In direct steam production, pressurized water is heated until it evaporates. However, as the difference in density between the liquid and vapour phase is significant for water, extremely large heat exchangers would be needed. A potential solution to avoid large heat exchangers can be found by directly integrating the heat pump in a boiler as illustrated in Figure 2.7. In this configuration the generated saturated steam is extracted at the top of the boiler, while at the bottom an equal amount of feed water is supplied. The temperature of the boiler can be set by controlling the pressure in the steam boiler.

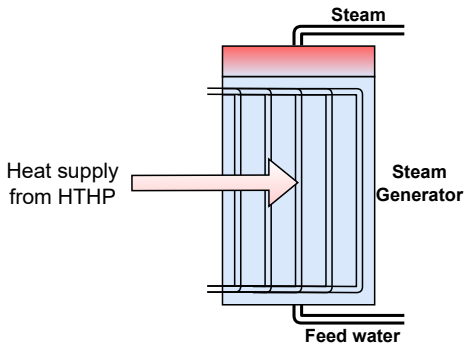


Figure 2.7: Illustration of a heat pump directly generating steam with use of a steam generator.

**Closed loop: Steam flashing**

Next to direct steam generation, SGHPs often produce steam through a flashing process [62–64], as shown in Figure 2.8. In this process the HTHP transfers heat to pressurized water, which is flashed afterwards to a liquid-vapour mixture in a flash tank (i.e. phase separator). Consequently, a small fraction of the water becomes steam. The saturated steam can be extracted at the top of the flash tank, while water is collected at the bottom of the tank. The water at the bottom of the tank is then pressurized and recirculated to the heat pump by a pump. Because here the heat pump solely heats up (pressurized) water, the disadvantage of large heat exchangers is avoided as well.

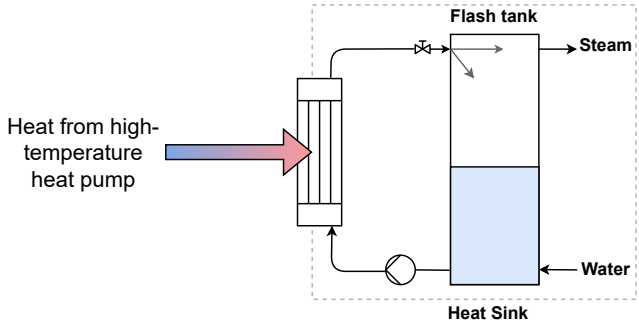


Figure 2.8: Illustration of a SGHP with flash evaporation.

A trade-off in flash tank inlet temperature is involved in the design of this system [65], as illustrated by Figure 2.9. In case of relatively low temperatures (blue cycle) the quality and consequently the steam yield will be low. As a result, a high mass flow rate will be needed to meet a specific steam demand,

resulting in over-sizing of the equipment and/or additional pumping power. However, due to the overall lower heat sink temperatures, the heat pump will operate at a relatively high COP. For a high flash tank inlet temperature (orange cycle) the opposite will occur, namely that the yield will be high while the COP will be reduced.

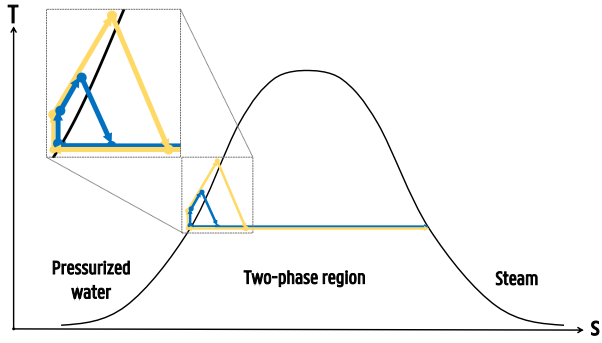


Figure 2.9: Illustration of the flash tank inlet temperature trade-off, based on the T-s diagram of water.

**Hybrid configuration: open loop combined with closed loop**

In practice, closed-loop systems often produce low-pressure steam through direct steam production or flashing. The pressure and temperature are then increased by an open-loop system, either by use of MVR or TVR. Some trade-offs are typically involved here.

MVR is often employed because it allows for lower energy use. Bless et al. [61] found an energy use reduction of about 40 % when comparing a CHP with MVR to a CHP without MVR. However, high compression ratios are required for steam compression and the steam strongly superheats during compression. Therefore, three water-injected compression stages were required next to the CHP. Furthermore, the density of water vapour at suction conditions is low, so that large and therefore more expensive compressors are required. On top of that the need for multiple compression stages and cooling techniques decreases the reliability and increases the maintenance cost. Hence, use of MVR involves multiple trade-offs.

Next to MVRs, the heat may also be upgraded using TVRs.

### 2.4.3 Selected case studies

In this section several case studies, representative for actual industrial applications are introduced, which will be used throughout the manuscript. The case studies are either obtained from bilateral meetings with industrial companies, or from data reported in the literature. Regarding the case studies of industrial companies, the focus was on heat carrier networks. For the case studies from the literature, the focus was on actual industrial processes. All case studies are presented in Appendix B. The case studies on heat carrier networks covers steam production (Appendix B.1), thermal oil heating (Appendix B.2) and pressurized hot water production (Appendix B.3). The case studies on actual industrial processes covers superheated steam drying (Appendix B.4), spray drying with external heat source (Appendix B.5) and distillation (Appendix B.6).

An overview of the most relevant process parameters of the selected case studies can be found in Table 2.1.

Table 2.1: Overview of the selected case studies with $p$ the pressure, $\dot{m}$ the mass flow rate, $T$ the temperature, $x$ the quality and $\dot{Q}$ the heat flow rate.

| Stream | Media | $p$ [bar] | $\dot{m}$ [kg/s] | $T_{in}$ [°C] | $T_{out}$ [°C] | $x_{in}$ [-] | $x_{out}$ [-] | $\dot{Q}$ [kW] |
|---|---|---|---|---|---|---|---|---|
| *Steam production (Appendix B.1)* | | | | | | | | |
| Heat source | Water | 1 | 9.32 | 78 | 60 | - | - | 702.3 |
| Heat sink | Water | 1.58 | 0.213 | - | - | 0 | 1 | 474 |
| *Thermal oil heating (Appendix B.2)* | | | | | | | | |
| Heat source | Water | 20 | 20 | 100 | - | - | - | - |
| Heat sink | Therminol 66 | 1 | 10 | 140 | 200 | - | - | 1254 |
| *Pressurized hot water production (Appendix B.3)* | | | | | | | | |
| Heat source | Water | 3 | 70 | 110 | - | - | - | - |
| Heat sink | Water | 55 | 30 | 140 | 200 | - | - | 7860 |
| *Superheated steam drying (Appendix B.4)* | | | | | | | | |
| Heat source | Superheated steam | 1 | 0.13 | 115 | - | - | - | - |
| Heat sink | Superheated steam | 1 | 2.27 | 116 | 197 | - | - | 970 |
| *Spray drying with external heat source (Appendix B.5)* | | | | | | | | |
| Heat source | Water | 1.5 | 1.69 | 100 | - | - | - | - |
| Heat sink | Dry air | 1 | 1 | 95 | 200 | - | - | 106.2 |
| *Distillation (Appendix B.6)* | | | | | | | | |
| Heat source | 99.5 % Benzene 0.5 % Toluene | 1.65 | 17.5 | 97.3 | 97.2 | - | - | 6654 |
| Heat sink | 93.7 % Ethylbenzene 0.5 % Toluene | 2 | 26.56 | 161.2 | 162 | - | - | 6974 |

# 3

# Financial appraisal of high-temperature heat pump technologies

*This Chapter contains parts of the Journal paper:*

*E. Vieren, T. Demeester, W. Beyne, C. Magni, H. Abedini, C. Arpagaus, S. Bertsch, A. Alessia, M. De Paepe and S. Lecompte, "The potential of vapor compression heat pumps supplying process heat between 100 and 200 °c in the chemical industry",* Energies*, vol. 16, no. 18, 2023, ISSN: 1996-1073. DOI:* 10.3390/en16186473. *[Online]. Available:* https://www.mdpi.com/1996-1073/16/18/6473

*Furthermore, it is also based on the Conference paper:*

*E. Vieren, W. Beyne, T. Demeester, M. De Paepe and S. Lecompte, "Theoretical assessment of industrial heating technologies up to 250°c", in* Proceedings of 26th IIR International Congress of Refrigeration (ICR2023)*, Paris, France: International Institute of Refrigeration (IIR), 2023. [Online]. Available:* http://doi.org/10.18462/iir.icr.2023.0324

*The boundary conditions used in the Conference paper, however, are adapted here to align with those in the Journal paper.*

## 3.1 Introduction

Within the literature high-level financial comparisons of HTHP technologies are often performed. Typically this is performed for VCHPs [57, 67–71] and HTFs [72, 73] individually. Within these studies, the financial comparison is often made with fossil-fuel boiler or electric boilers acting as the baseline. Generally, there is no comparison with other heat pump technologies, although some literature compares the financial aspects of VCHP and solar thermal systems [74, 75]. There is thus a general lack of a financial comparison between the different heat pump technologies and the baseline heating technologies.

Furthermore, the financial performance of the technology is often based on one single case study. Although interesting, these results are not generally applicable, because the financial performance of the different technologies is often highly sensitive to the financial boundary conditions applied and the case study investigated. A generic study is therefore needed to provide a general applicable overview of the financial performance of the different technologies. This would also allow to indicate the preferred application area per technology.

This chapter shows a financial comparison between the natural gas boiler (NGB), electric boiler (EB), vapour compression heat pump (VCHP) and heat transformer (HTF) in a generic way, aimed at indicating the application area of these technologies at different conditions. The use of TVRs or HHPs are excluded from this analysis. The financial performance of these technologies strongly depends on the temperature level of the high-temperature heat source and whether or not this heat source is freely available or needs to be generated at a certain cost. Even if the high-temperature heat source would be freely available an opportunity cost should be considered as this heat could be directly used for process heat demand. Furthermore, the HHP is only mature for temperatures up to 90 °C, with no to few research looking in enhancing this temperature, and the TVR can only be used for steam systems. The MVR system is not directly included but can be covered by the VCHP as they have the same type of energy flows.

## 3.2 Methods

The method section starts with explaining the thermodynamic performance evaluation of the different technologies (Section 3.2.1). This thermodynamic performance is then used as input for the financial evaluation of the technologies (Section 3.2.2). Thereupon, the application cases for the financial model are explained (Section 3.2.3). Two types of application cases are considered,

namely the 'generic thermodynamic boundary conditions' and the 'specific thermodynamic boundary conditions'. In the former, a sweep is made over different parameters which are key for the financial performance, allowing to indicate the most suitable technology over these parameters. In the latter, specific case studies within the industry are considered, giving deeper insights.

### 3.2.1 Thermodynamic performance evaluation

For the heat pump technologies the performance is characterized using the COP, whereas for the boiler systems, the performance is described by a thermal boiler efficiency. The COP of the heat pump technologies is estimated based on data available in the literature rather than using thermodynamic cycle calculations. This allows for the use of actual performance data of (near-) commercial heat pumps. The boiler efficiencies are also determined based on performance data reported in the literature.

#### 3.2.1.1 Vapour compression heat pump

The maximum COP (i.e. Carnot COP) of a VCHP is a function of the heat sink temperature ($T_{sink}$) and the temperature lift ($T_{sink}$-$T_{source}$), as has been shown in Equation 2.2. Further simplification allows expressing the COP as a function of the temperature lift as often done in the literature [76, 77].

When the secondary media are no longer constant and have temperature glides, multiple definitions exists to characterize the temperature lift. In this work, the gross temperature lift (GTL) is used to characterize the temperature lift. The GTL is defined as the temperature difference between the heat sink outlet ($T_{sink,out}$) and the heat source outlet ($T_{source,out}$) as shown in Equation 3.1. The outlet temperatures are selected because these typically determine the evaporation or condensation pressure. Other definitions to quantify the temperature lift may also have its merits, but are not considered here.

$$GTL = T_{sink,out} - T_{source,out} \tag{3.1}$$

The COP for VCHPs is correlated as a function of the GTL based on manufacturer data reported in the framework of the IEA HPT Annex 58 on HTHPs [13]. Within this Annex, performance data of well-known VCHP manufacturers such as Heaten, Mayekawa, MAN, Kobelco, Turboden and Siemens is collected, given the operating conditions. All reported COPs are for heat sink temperatures above 100 °C, which is an important aspect as the COP also depends on this temperature. The data points with a corresponding curve fit can be found in Figure 3.1.

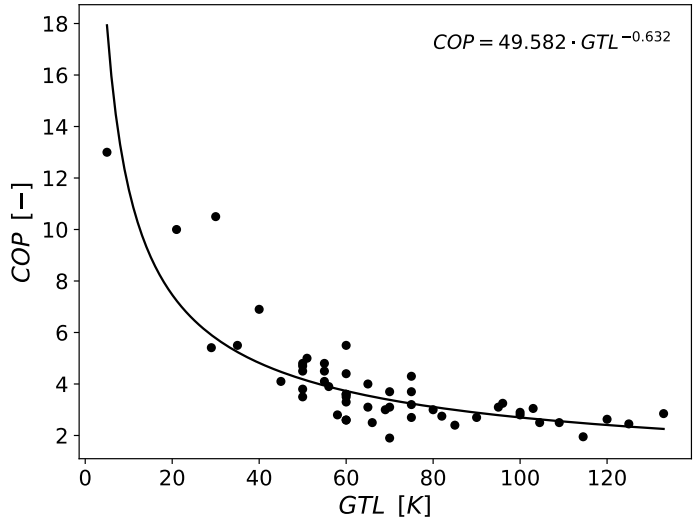


Figure 3.1: Data points and correlation of the COP of VCHPs as a function of GTL, based on manufacturer data reported in the IEA HPT Annex 58 [13].

The corresponding COP correlation can be found in Equation 3.2:

$$COP = 49.582 \cdot GTL^{-0.632} \tag{3.2}$$

The regression has a coefficient of determination ($R^2$) of 0.7, a mean absolute deviation of 0.732, a bias of -0.072 and a maximum deviation of 4.930. These are rather large variabilities. However, for GTLs above 40 K, the mean absolute deviation, bias and the maximum deviation reduces to 0.496, 0.0147 and 1.482 respectively.

#### 3.2.1.2 Heat transformer

The COP of the HTF is also correlated as a function of the GTL. Because HTF technology is less commonly used and has fewer manufacturers, limited manufacturer data is available, including within the IEA HPT Annex 58. Consequently, the COP is correlated based on typical COP values at a GTL of 50 K, 80 K and 140 K reported by Donnellan et al. [31], as shown in Figure. 3.2.

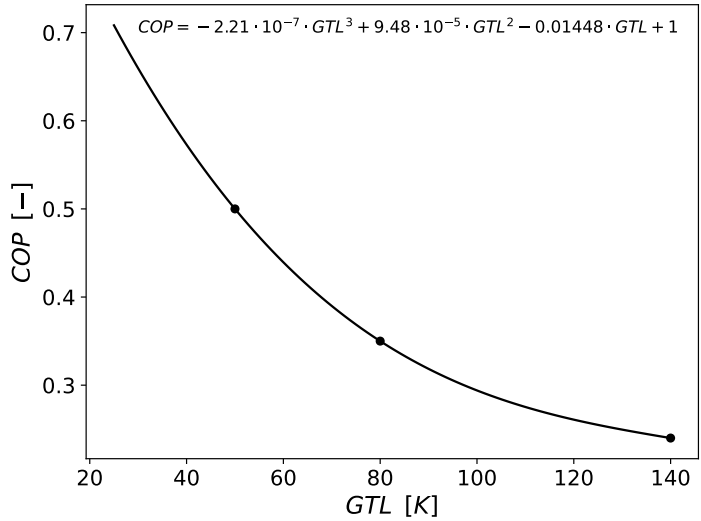


Figure 3.2: Data points and correlation of the COP of HTFs as a function of GTL, based on Donnelan et al. [31].

Based on these three data points, the COP can be correlated as shown in Equation 3.3.

$$COP = -2.21 \cdot 10^{-7} \cdot GTL^3 + 9.48 \cdot 10^{-5} \cdot GTL^2 - 0.01448 \cdot GTL + 1 \quad (3.3)$$

Because this regression is of the third order, and only three data points are used, the regression perfectly fits these data points.

It should also be noted that the HTF also uses a small amount of electricity. However, due to its small contribution, the electricity use is not considered in this analysis.

#### 3.2.1.3 Electric boiler

Regarding the EB a thermal efficiency of 100 % is considered [78]. The thermal efficiency of the electrical boiler ($\eta_{el,boiler}$) is defined as the ratio of the heat supply to the heat sink ($\dot{Q}_{sink}$) to the electrical energy use ($\dot{W}_{el}$), as shown in Equation 3.4.

$$\eta_{el,boiler} = \frac{\dot{Q}_{sink}}{\dot{W}_{el}} \quad (3.4)$$

#### 3.2.1.4 Natural gas boiler

Regarding the NGB a thermal efficiency of 90 % is considered [79, 80]. The thermal efficiency of the natural gas boiler ($\eta_{ng,boiler}$) is defined as the ratio of

the heat supply to the heat sink ($\dot{Q}_{sink}$) to the energy use rate ($\dot{E}_{in}$), as shown in Equation 3.5.

$$\eta_{ng,boiler} = \frac{\dot{Q}_{sink}}{\dot{E}_{in}} \tag{3.5}$$

### 3.2.2 Financial evaluation

Within the financial evaluation, the levelized cost of heat (LCOH) of the different technologies will be compared. In what follows the computation of the LCOH and the corresponding financial boundary conditions are explained.

#### 3.2.2.1 Levelized cost of heat

The LCOH is the total cost per unit of heat generated (€/$kWh_{th}$) over the lifetime of the machine. It is defined by the ratio of the discounted expenses and discounted heat production [81] as shown in Equation 3.6:

$$LCOH = \frac{C_{CAPEX} + \sum_{t=1}^{n} \frac{C_{OPEX,t}}{(1+i)^t}}{\sum_{t=1}^{n} \frac{Q_t}{(1+i)^t}} \tag{3.6}$$

In this equation $C_{CAPEX}$ represents the capital expenditure (€), $n$ the number of years over which the LCOH is defined, $C_{OPEX,t}$ the yearly operational expenditure (€/year), $Q_t$ the yearly amount of heat produced ($kWh_{th}/year$) and $i$ the interest rate.

**Operational expenditures**
The operational expenditure is calculated based on the specific energy costs $c_{energy}$ (€/kWh), the energy use rate $\dot{E}_{use}$ (kW) and the operational hours $h_a$ (h). Moreover, a maintenance cost, assumed to be a fraction ($f_{maint}$) of the capital expenditure, is included. Consequently, the operational expenditure is calculated as shown in Equation 3.7.

$$C_{OPEX,t} = c_{energy} \cdot \dot{E}_{use} \cdot h_a + f_{maint} \cdot C_{CAPEX} \tag{3.7}$$

**Capital expenditures**
The capital expenditure is computed by multiplying the heating capacity $\dot{Q}_{heating}$ ($kW_{th}$) with the specific investment cost of the heating technology $c_{spec,inv}$ (€/$kW_{th}$) as shown in Equation 3.8.

$$C_{CAPEX} = c_{spec,inv} \cdot \dot{Q}_{heating} \tag{3.8}$$

#### 3.2.2.2 Financial boundary conditions

The selected financial boundary conditions are given in Table 3.1. These boundary conditions are selected to represent a heat recovery project in a large-scale industrial site.

Table 3.1: Boundary conditions for the financial model.

| Financial parameter | Value | Reference |
|---|---|---|
| Annual operating time, $h_a$ (hour) | 8000 | [40, 41] |
| Vapour compression heat pump lifetime, $n_{VCHP}$ (year) | 15 | [82, 83] |
| Heat transformer lifetime, $n_{HTF}$ (year) | 15 | [84] |
| Natural gas boiler lifetime, $n_{NGB}$ (year) | 15 | [85] |
| Electric boiler lifetime, $n_{EB}$ (year) | 15 | [86] |
| Discount rate, $i$ (%) | 5 | [83] |
| Yearly maintenance cost fraction, $f_{maint}$ (% of investment cost) | 6 | [87] |

Another important factor is the specific investment cost of the different technologies.

According to Arpagaus et al. [12], specific investment cost for industrial VCHPs varies between 250 €/$kW_{th}$ and 800 €/$kW_{th}$. Meyers et al. [75] reported specific investment costs between 300 €/$kW_{th}$ and 900 €/$kW_{th}$ for industrial VCHPs larger than 100 $kW_{th}$ and showed that the specific investment cost decreases with the heat pump size. Moreover, they reported that the industrial average is about 400 €/$kW_{th}$. Schlosser et al. [69] used a specific investment cost of 420 €/$kW_{th}$ in their analysis for large-scale industrial VCHPs. It is thus expected that the specific investment cost for VCHPs varies between 250 €/$kW_{th}$ and 900 €/$kW_{th}$. In this analysis a cost of 550 €/$kW_{th}$ is therefore assumed, which is close to the average of the upper and lower cost values. This cost is also in line with the data reported by VCHP manufacturers in the framework of IEA HPT Annex 58 [13] and by Klute et al. [35].

For the HTF much larger investment costs are expected. Within the IEA HPT Annex 58 [13], investment costs ranging between 1000 €/$kW_{th}$ and 2000 €/$kW_{th}$ are reported. Lee [88] reports HTF investment costs that are 75 % to 85 % higher than for VCHPs. Enslin [89] reported investment cost of about 1300 €/$kW_{th}$, based on a breakdown of the costs to the component levels. It is thus likely that the specific investment cost for HTFs ranges between 1000 €/$kW_{th}$ to 2000 €/$kW_{th}$, with the more likely values in the lower range of the costs. Furthermore, HTFs are a less mature technology so their specific investment cost might still decrease over time. Therefore, a specific investment cost of 1200 €/$kW_{th}$ is chosen.

The investment cost of these heat pump technologies is much higher compared to industrial boilers. NGBs have a specific investment cost of about 100

€/$kW_{th}$ [90], while the EBs have an even lower investment cost of about 50 €/$kW_{th}$ [91].

The specific investment cost for each technology is summarized in Table 3.2. Ideally, these costs would be a function of the heating capacity and the supply temperature, as economies of scale applies with larger heating capacities and the component cost may increase with increasing temperature. However, due to the lower commercial availability of these heat pump technologies at higher temperatures there is a lack of data to develop such cost functions. Nevertheless, to illustrate the influence of sensitivity on the investment costs, a minimum and maximum investment cost for the VCHP and the HTF is considered based on the cost ranges discussed above.

Table 3.2: Selected specific investment cost and minimum and maximum cost of each heating technology.

| **Technology** | **Considered cost** [€/$kW_{th}$] | **Minimum cost** [€/$kW_{th}$] | **Maximum cost** [€/$kW_{th}$] |
|---|---|---|---|
| Vapour compression heat pump | 550 | 250 | 900 |
| Natural gas boiler | 100 | - | - |
| Electric boiler | 50 | - | - |
| Heat transformer | 1200 | 1000 | 2000 |

## 3.2.3 Application cases

The LCOH of the different technologies will first be calculated for generic thermodynamic boundary conditions. These boundary conditions differ in terms of temperature lifts and heat flows. This is done to give a more general overview of the technology with the lowest LCOH. Furthermore, contour plots will be made, exploiting the preferred operational areas of each technology. Afterwards, the LCOH of the different technologies will be calculated for actual case studies introduced in Section 2.4.3.

### 3.2.3.1 Generic thermodynamic boundary conditions

First the financial evaluation will be performed on a set of generic thermodynamic boundary conditions. In the generic thermodynamic boundary conditions a sweep is performed over the following parameters:

- **Gross temperature lift (GTL)**: Because of the large influence of the GTL on the performance of the heat pump technologies the GTL will be varied. The GTL will be varied from 20 K to 120 K, which is a typical application range for heat pump technologies [12].

- **Residual heat ratio (RHR)**: The heat pump technologies rely on the use of residual heat. In actual applications there is typically a limitation in the residual heat available. Therefore, the amount of residual heat available will be varied. The amount of residual heat available will be characterized by the residual heat ratio (RHR). The RHR is defined as the ratio of the residual heat available ($\dot{Q}_{residual}$) to the amount of heat demanded by the process ($\dot{Q}_{process}$), as shown in Equation 3.9.

$$RHR = \frac{\dot{Q}_{residual}}{\dot{Q}_{process}} \tag{3.9}$$

  The minimum required RHR to deliver all heat demand depends on the heating technology. For the VCHP the minimum RHR is always lower than 1, should it want to operate as stand-alone technology. For the HTF however the minimum RHR should always be larger than 1, should it want to operate as stand-alone system. For both heat pump technologies, the minimum required RHR to fulfill the complete heat demand depends on the COP. For the NGB and the EB, which does not require residual heat, the minimum required RHR is zero. An overview of the theoretical minimum required RHR ratio for each heating technology is shown in Table 3.3.

Table 3.3: Minimum required RHR with typical values for each heating technology.

| Technology | Minimum required RHR | Typical value |
|---|---|---|
| Vapour compression heat pump | $(1 - \frac{1}{COP})$ | 0.5-0.8 |
| Heat transformer | $\frac{1}{COP}$ | 2-4 |
| Natural gas boiler | 0 | 0 |
| Electric boiler | 0 | 0 |

  As the minimum required RHR is maximum 4, considering common applications, the RHR will range between 0 to 4. If the RHR is too low, and the amount of residual heat available is insufficient for the heat pump technology to meet all the heat demand, an auxiliary EB is used. This boiler then provides all additional heat required.

Based on this sweep the technology with the lowest LCOH will be presented for each GTL and RHR.

Other important factors are the energy prices. The electricity and gas prices however strongly depends on the location, the industry sector and the time. In this generic analysis two electricity prices will be considered, a high price and a low price. The electricity price during 2021 for non-household

consumers with an annual electricity use of 500 $MWh_e$ to 2000 $MWh_e$ in the EU-27 will be selected as the 'high electricity price' reference [92]. According to Eurostat most of the EU consumers falls within these bands. Subsequently, this price dived by two is taken as the 'low electricity price' reference, being more representative for electricity costs before the energy crisis [92]. An overview of the corresponding electricity prices, excluding VAT and other recoverable taxes and levies, can be found in Table 3.4.

Table 3.4: Considered electricity prices scenarios for the generic thermodynamic boundary conditions

| **Scenario** | **Electricity price** [€/$kWh_e$] |
|---|---|
| High electricity price | 0.0945 |
| Low electricity price | 0.04725 |

The natural gas prices are subsequently defined through an electricity to gas price ratio (EGPR), which is defined as the ratio of the electricity price ($c_{el}$) to the natural gas price ($c_{ng}$) as shown in Equation 3.10. Potential increases in the cost of using natural gas through the emission trading scheme (ETS) can be lumped in the natural gas price.

$$EGPR = \frac{c_{el}}{c_{ng}} \tag{3.10}$$

Three different EGPRs will be considered, namely 1.5, 2 and 3, both for the high as the low electricity price scenario. Consequently, six different contour plots will be made, indicating the technology with the lowest LCOH. Before showing these contour plots however, the LCOH of each technology under the varying GTLs, RHR and energy prices is given first.

#### 3.2.3.2 Specific thermodynamic boundary conditions

To get a deeper insight into the results, the financial comparison is also performed on specific, but relevant, case studies reported in Appendix B and Table 2.1. The two following case studies are considered:

1. Superheated steam drying case study, explained in Appendix B.4.
2. Steam production case study, explained in Appendix B.1.

The GTL and RHR of each case study is summarized in Table 3.5

Table 3.5: GTL and RHR of the considered case studies.

| **Case study** | **GTL** [K] | **RHR** [-] |
|---|---|---|
| Superheated steam drying | 81 | 0.805 |
| Steam production | 51.4 | 1.482 |

Regarding the electricity and natural gas prices, a sweep over a range of electricity and natural gas prices can now be performed as the GTL and RHR are fixed by the case study. The electricity cost will be varied from 0.05 €/kWh to 0.15 €/kWh, while the natural gas price will be varied between 0.02 €/kWh to 0.08 €/kWh. Due to the increasing importance of net-zero carbon emissions, the cost of gas and electricity is expected to increase. Hence, both price ranges are predominantly extended towards the higher prices compared to the data reported within Eurostat [92, 93].

Furthermore, next to the sweep over the energy prices, the financial appraisal is also reported and compared at a country scale. For this the average prices reported by Eurostat [92, 93] between 2016 and 2020 for non-household consumer among different European countries are considered. The corresponding electricity prices, gas prices and associated price ratios can be found in Table 3.6.

Table 3.6: Average electricity and gas prices for several EU countries 2016-2020, excluding VAT and other recoverable taxes and levies [92, 93].

| **Country** | **Electricity price** [€/kWh] | **Gas price** [€/kWh] | **Price ratio** [-] |
|---|---|---|---|
| Finland | 0.0649 | 0.0518 | 1.25 |
| Denmark | 0.0612 | 0.0326 | 1.88 |
| France | 0.0732 | 0.0357 | 2.05 |
| Germany | 0.0799 | 0.0312 | 2.56 |
| Belgium | 0.0806 | 0.0235 | 3.43 |
| UK | 0.0987 | 0.0256 | 3.85 |
| EU-27 | 0.0792 | 0.0307 | 2.58 |

The numbers reported in Table 3.6 do not include the impact of the ETS. The cost of ETS in the EU went from 30 €/tonne $CO_2$ at the start of 2021 to 80 €/tonne $CO_2$ at the start of 2022 [94]. Since NGBs have specific $CO_2$ emissions of about 0.22 kg $CO_2$ per kWh [79, 95], the real natural gas price would therefore increase with 0.0176 €/kWh compared to the values reported in Table 3.6, due to the cost related to carbon emissions. This would increase the natural gas price in Belgium with about 70 %. Albeit this scenario introduces a cost to the usage of natural gas, it still results in a low natural gas price.

However, it does not account a potential cost increase of electricity generation, which might take place in a realistic scenario.

## 3.3 Results

In this section, the obtained results of the financial model applied to the generic thermodynamic boundary conditions are first discussed (Section 3.3.1). Afterwards, the results are discussed when the financial model is applied to the specific case studies (Section 3.3.2).

### 3.3.1 Results for the generic thermodynamic boundary conditions

First, the LCOH of each technology is analyzed as a function of the RHR, GTL, and energy prices. Next, an overview is provided of the technology with the lowest LCOH as a function of the RHR, GTL, and EGPR at two different electricity price levels. In this overview first only the renewable technologies are considered (VCHP, HTF and EB). Thereafter, an overview of all technologies is considered by introducing the NGB.

#### 3.3.1.1 Generalized vapour compression heat pump financial performance

The LCOH of the VCHP as function of the GTL and RHR for the low and high electricity price scenario can be found in Figure 3.3. The figure also shows the minimum required RHR for the VCHP, as defined in Table 3.3, in green. Above this line the VCHP can operate as stand-alone system. Below this line an auxiliary EB is required.

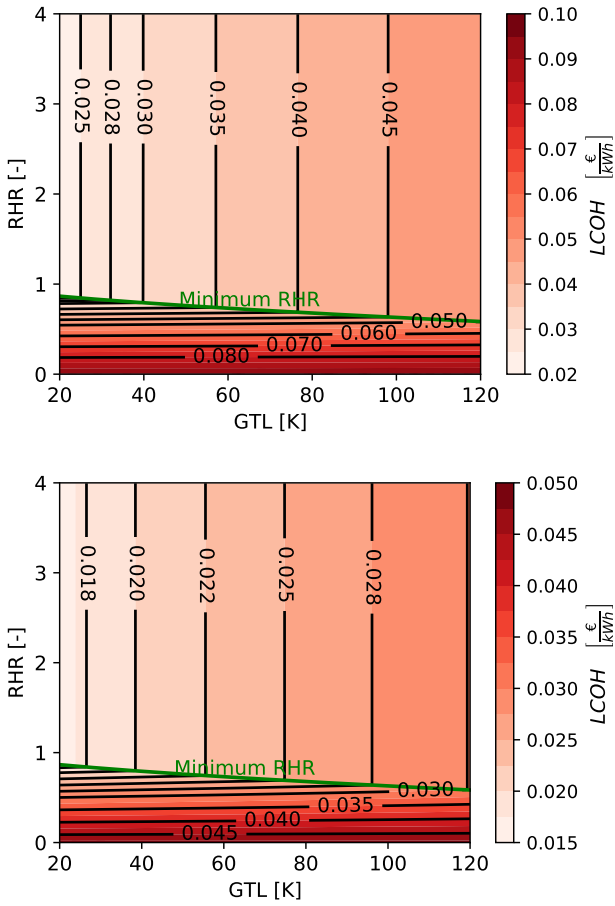


Figure 3.3: LCOH of a VCHP as a function of the GTL and RHR, for an electricity price of 0.0945 €/$kWh_e$ (top) and 0.04725 €/$kWh_e$ (bottom) at the nominal financial boundary conditions.

Based on Figure 3.3 several observations can be made:

- As expected, the LCOH strongly depends on the electricity price. For the high electricity price scenario considerably higher LCOHs are obtained compared to the low electricity price scenario. For lower GTLs, and thus higher COPs and lower electricity use, the relative difference in LCOH however decreases. This is because the VCHP investment cost contributes to a constant LCOH independent on the GTL.
- It can be observed that below the minimum required RHR, described in Table 3.3, the LCOH drastically increases due to the addition of the EB

which seems to be cost-inefficient compared to the VCHP.

- Above the minimum required RHR, the LCOH strongly depends on the GTL, as this determines the COP.
- Below the minimum required RHR, the GTL has little effect on the LCOH. This is because at higher GTLs, and thus lower COPs, more process heat will be delivered by the VCHP considering that the compressor work increases while the residual heat available stays fixed. Consequently, less electricity use from the electrical boiler will be required. The figure suggests that the increase in compressor power gives rise to an equal decrease in EB power. The line of constant LCOH is however not completely horizontal in this region. This is because when more process heat will be delivered by the VCHP at higher GTLs, the total investment cost will increase as the heating capacity shifts from the EB to the VCHP. The reasoning above is however only valid when the available RHR is always below the minimum required RHR, which is a function of the COP and thus GTL.

In Appendix C Section C.1 the same figures as in Figure 3.3 are shown, but for a specific investment cost of 250 €/$kW_{th}$ and 900 €/$kW_{th}$ for the VCHP. Overall, the same trends can be observed. Logically, the higher specific investment cost the higher the LCOH and vice versa. At the higher investment costs, the fact that the lines of constant LCOH are not horizontal below the minimum required RHR is more apparent.

#### 3.3.1.2 Generalized heat transformer financial performance

The LCOH of the HTF as function of the GTL and RHR for the low and high electricity price scenario can be found in Figure 3.4. The figure also shows the minimum required RHR for the HTF, as defined in Table 3.3, in green. Above this line the HTF can operate as stand-alone system. Below this line an auxiliary EB is required.

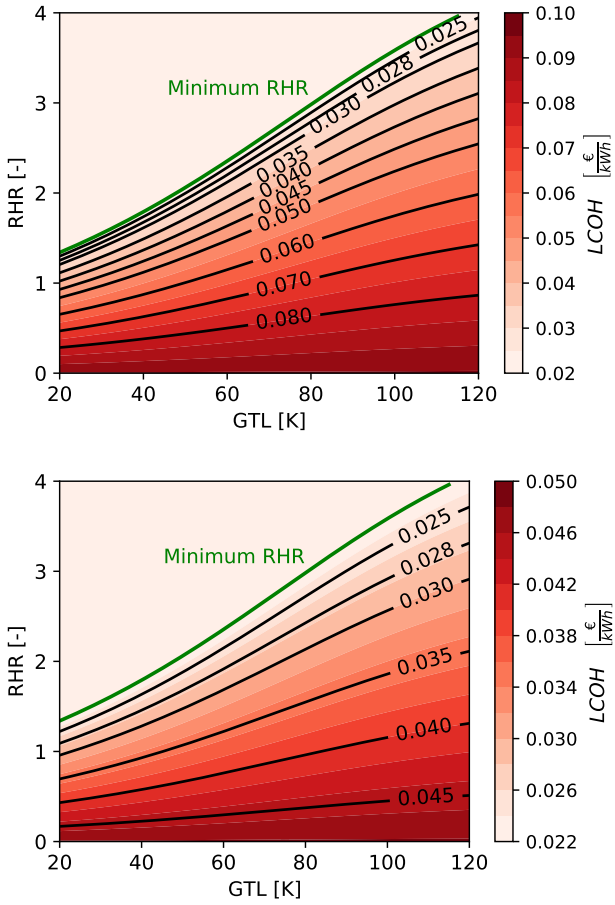


Figure 3.4: LCOH of a HTF as a function of the GTL and RHR, for an electricity price of 0.0945 €/$kWh_e$ (top) and 0.04725 €/$kWh_e$ (bottom) at the nominal financial boundary conditions.

Based on Figure 3.4 several conclusions can be formulated:

- As for the VCHP, the RHR has significant impact on the LCOH when it is below the minimum RHR. Below the minimum required RHR, the EB also starts operating, leading to a significant increase in LCOH. This is because the auxiliary EB is cost-inefficient compared to the HTF.
- Compared to VCHP, much higher RHRs are required for the HTF to operate as a pure stand-alone unit. RHRs between 1.3 and 4 are required for the HTF to operate as a stand-alone system and for the LCOH to become independent of the RHR.

- The minimum required RHR increases with the GTL, while for the VCHP an opposite trend was observed. This is why, when the minimum RHR is not met, the LCOH increases at constant RHR for increasing GTLs.
- When the minimum RHR is met, the LCOH becomes independent of the GTL, which is a highly favourable characteristic.
- Above the minimum required RHR, the LCOH becomes independent of electricity costs, as the HTF theoretically does not use electricity. Below the minimum required RHR there is a strong dependency on the electricity price. It is thus expected that the HTF is an especially favourable technology for applications with both a high RHR and high energy costs and potentially higher GTLs.

In Appendix C Section C.2 the same figures as in Figure 3.4 are shown but for a specific investment cost of 1000 €/$kW_{th}$ and 2000 €/$kW_{th}$. Overall, the same trends can be observed. Logically, the LCOHs are again higher at the higher specific investment cost and vice versa. At the higher investment costs, it can be observed that the contribution of the specific investment cost is particularly high.

#### 3.3.1.3 Generalized electric boiler financial performance

The LCOH of the EB is independent on the GTL and the RHR, but is directly linked to the electricity cost. The LCOH at the considered electricity costs is shown in Table 3.7.

Table 3.7: LCOH of the EB for the two electricity prices at the nominal financial boundary conditions.

| **Electricity price** [€/$kWh_e$] | **LCOH** [€/$kWh_{th}$] |
|---|---|
| 0.0945 | 0.0955 |
| 0.04725 | 0.0482 |

Because of the low investment cost of the EB and the power-to-heat conversion efficiency of 100 % the LCOH is only slightly higher than the electricity price.

#### 3.3.1.4 Generalized natural gas boiler financial performance

The LCOH of the NGB is also independent on the GTL and the RHR, but is directly linked to the natural gas cost. The natural gas price is here defined by the electricity price and EGPR. The LCOH of the NGB as a function of the EGPR for the two considered electricity prices can be found in Table 3.8.

Table 3.8: LCOH of the NGB for the different EGPRs and electricity prices at the nominal boundary conditions.

| **Electricity price** (€/$kWh_e$) | **Natural gas price** (€/$kWh_{th}$) | **LCOH** (€/$kWh_{th}$) |
|---|---|---|
| | *EGPR = 1.5* | |
| 0.0945 | 0.0630 | 0.07190 |
| 0.04725 | 0.0315 | 0.03690 |
| | *EGPR = 2* | |
| 0.0945 | 0.04725 | 0.05440 |
| 0.04725 | 0.023625 | 0.02815 |
| | *EGPR = 3* | |
| 0.0945 | 0.0315 | 0.03690 |
| 0.04725 | 0.01575 | 0.01940 |

As might be expected, the LCOH of a NGB strongly varies with the natural gas price. Because of the thermal efficiency of 90 % and the investment cost of the NGB, the LCOH is somewhat increased compared to the natural gas price.

#### 3.3.1.5 Generalized financial performance comparison of all renewable technologies

The renewable technology (EB, VCHP or HTF) with the lowest LCOH as function of RHR and GTL is shown in Figure 3.5 for both a high electricity price and low electricity price scenario. The relative difference in LCOH (%) of the technology with the lowest LCOH compared to the technology with the second lowest LCOH is also shown by the lines in red.

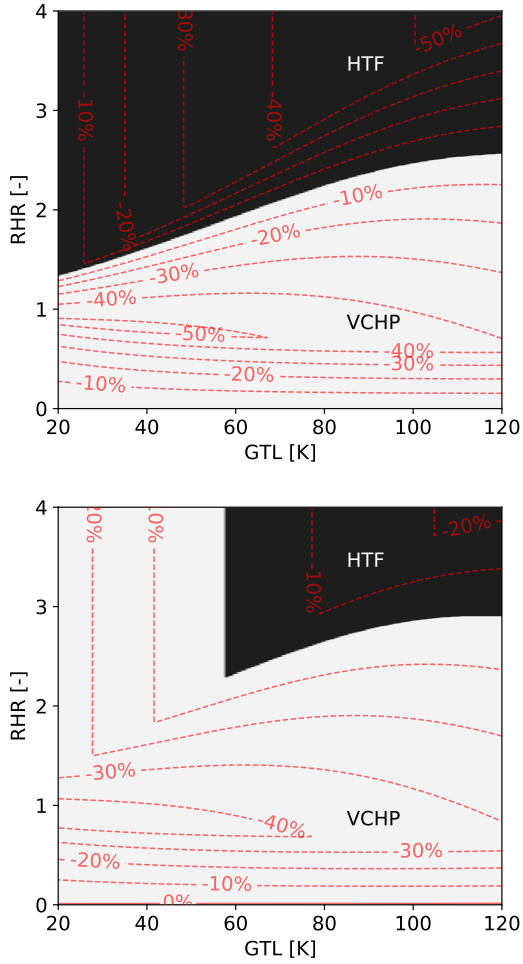


Figure 3.5: Renewable technology with the lowest LCOH as a function of the GTL and RHR, for an electricity price of 0.0945 €/$kWh_e$ (top) and 0.04725 €/$kWh_e$ (bottom) at the nominal financial boundary conditions. Red lines indicate the relative difference in LCOH (%) between the technology with the lowest LCOH and the second-lowest LCOH.

The figure shows that either the HTF or VCHP has the lowest LCOH and that the EB is never the best choice. Although it is used as an auxiliary technology it is not recommended as stand-alone technology. An obvious exception is the scenario where no residual heat is available, but this is not visible on the figure. The HTF is only optimal at higher RHRs, typically above 1. The RHR where the HTF becomes the technology with the lowest LCOH depends on the GTL.

This is because the minimum required RHR of the HTF is a function of the GTL as has been shown in Figure 3.4. For high energy prices, the HTF can result in an LCOH that is more than 50 % lower than that of the VCHP, particularly in regions with higher GTLs and RHRs. For the lower energy prices this decreases to slightly above 20 %. For lower energy prices the potential benefits of the HTF over the VCHP becomes less outspoken, because the LCOH of the VCHP is strongly linked to the OPEX (in contrast to LCOH of HTF). Outside the region where the HTF is optimal, the VCHP is the option with the lowest LCOH. For high energy prices the VCHP can lead to LCOH decreases higher than 50 % compared to the HTF. For low energy prices the LCOH decrease is still above 40 %. It is thus worth noting that the region where the HTF is optimal strongly changes with the electricity price. With higher electricity prices the range where the HTF is the cheapest technology increases, while for lower electricity prices the opposite happens. This behaviour is expected as this technology theoretically does not use electricity when no back-up EB is needed. The HTF is thus a particularly favourable technology at high electricity prices. However, to unlock this potential, RHRs above 1 are typically required. This is however in many industrial applications not the case.

The same figure as Figure 3.5 is also made for a high technology investment cost and a low technology investment cost, as given in Table 3.2. The figures can be found in Appendix C.3. Overall, the same conclusions are true. At the high technology investment cost however, the region where the HTF is optimal strongly decreases. Moreover, in the event of low electricity costs the VCHP is always optimal. Remarkable is that also at the lower technology investment cost the region where the HTF is optimal decreases. This can be related to the fact that the nominal HTF cost was close to the minimal HTF cost, which was not the case for the VCHP.

#### 3.3.1.6 Generalized financial performance comparison of all heating technologies

Now the NGB is also considered. To characterize the natural gas price the proposed EGPRs of 1.5, 2 and 3 are used, considering the two electricity prices. An overview of the technology with the lowest LCOH for the different electricity prices and EGPRs can be found in Figure 3.6. Again, the relative difference (%) in LCOH of the technology with the lowest LCOH compared to the technology with the second lowest LCOH is shown in red. This second best technology is either the NGB, HTF or VCHP.

Figure 3.6 shows that at the high electricity price, and the EGPRs of 1.5 and 2, the NGB replaces part of the region where the VCHP had the lowest LCOH. The region that is replaced by the NGB is part of the region where the minimum RHR of the VCHP is not met, and an auxiliary EB with high

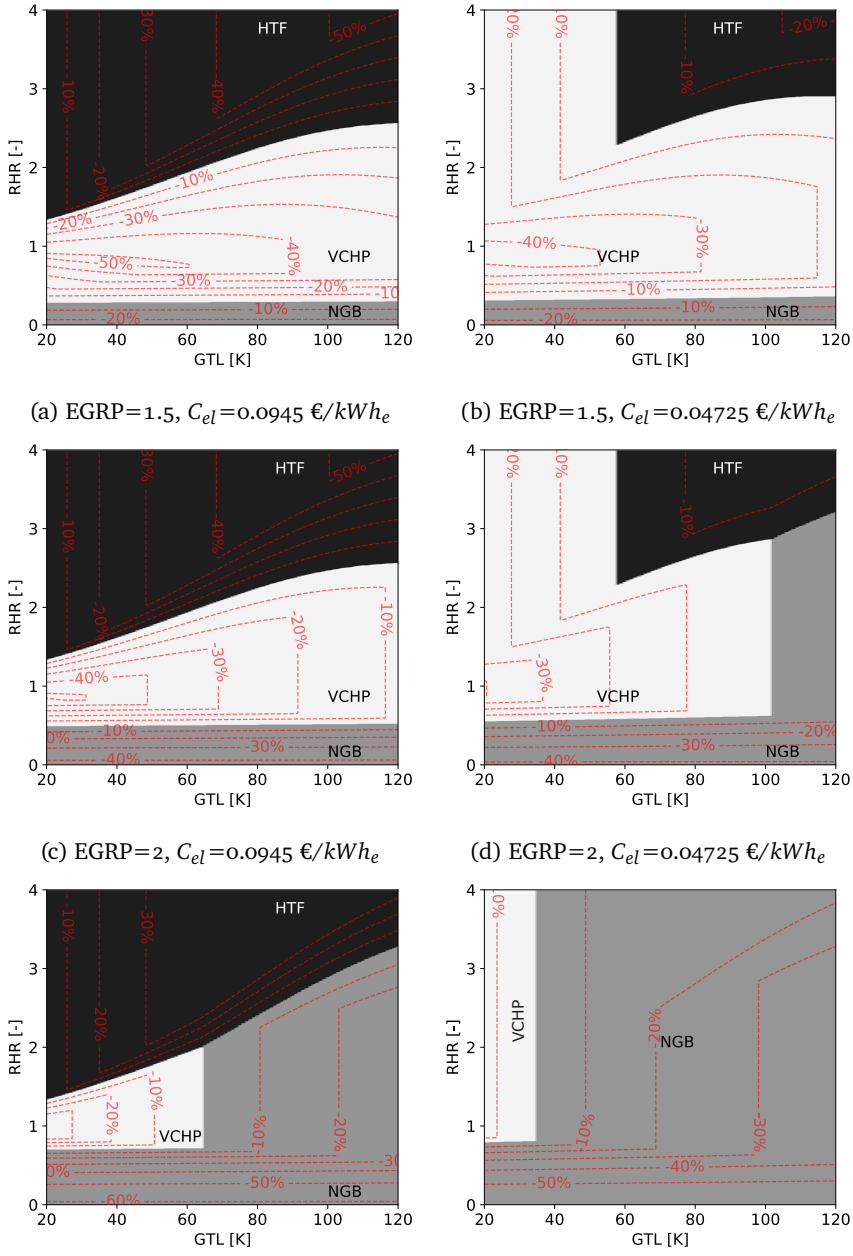


(a) EGRP=1.5, $C_{el}$=0.0945 €/$kWh_e$

(b) EGRP=1.5, $C_{el}$=0.04725 €/$kWh_e$

(c) EGRP=2, $C_{el}$=0.0945 €/$kWh_e$

(d) EGRP=2, $C_{el}$=0.04725 €/$kWh_e$

(e) EGRP=3, $C_{el}$=0.0945 €/$kWh_e$

(f) EGRP=3, $C_{el}$=0.04725 €/$kWh_e$

Figure 3.6: Technology with the lowest LCOH as a function of the RHR and GTL, for the different electricity prices and EGPRs. Red lines indicate the relative difference in LCOH (%) between the technology with the lowest LCOH and the second-lowest LCOH.

operational costs is necessary. When there is sufficient residual heat available the VCHP has a lower LCOH than the NGB. At these conditions, the NGB does not reduce the region where the HTF is optimal. When the EGPR however reaches 3, the NGB may have a lower LCOH than the VCHP, even for scenarios where there is sufficient residual heat available. This is particularly the case at higher GTLs, where the COP of the heat pump decreases. Consequently, the VCHP only becomes viable for GTLs up to 65 K. Furthermore, the NGB even replaces part of the region where the HTF was optimal, although in a more limited extend.

At the lower electricity price and the EGPR of 1.5 the NGB again replaces part of the region where the VCHP was optimal, but only at lower RHRs, below the minimum required RHR for the VCHP. At an EGPR of 2, the minimum RHR for the VCHP to be optimal further increases. Furthermore, the VCHP is never the best technology for GTLs above 100 K. Above these temperature lifts, the NGB also reduces part of the region where the HTF was optimal. When the EGPR increases to 3, the NGB replaces the complete region where the HTF was optimal. The VCHP is only viable at a RHRs higher than 0.8 and a maximum GTL of 35 K.

Overall, it can be concluded that both VCHP and HTF are advantageous compared to the NGB in scenarios of high energy prices, particularly the HTF. This is because the technologies have a high investment costs compared to the NGB. At higher energy prices, the potential revenue through the use of these technologies can increase, resulting in faster pay back of the technology. Moreover, as expected, the heat pump technologies become more advantageous at lower EGPRs. With both the trend of increasing electricity prices and decreasing EGPRs in the industry there exist promising potential for heat pump integration.

The same figure as Figure 3.6 is also made for a high technology investment cost and a low technology investment cost, both costs given in Table 3.2. These figures can be found in Appendix C.4. As indicated before, at higher technology costs, the region where the NGB has the lowest LCOH increases.

### 3.3.2 Results for the specific thermodynamic boundary conditions

In this section the financial framework is applied to the superheated steam drying case study and the steam production case study, both presented in Section 3.2.3.2. For both case studies, the LCOH of the VCHP and the EB will be plotted against the electricity price. The LCOH of the NGB will be plotted against the natural gas price. This also allows for conveniently considering two auxiliary technologies for the HTF, namely the NGB or EB. Consequently,

the technology can be defined as 'HTF+NGB' or 'HTF+EB'. Depending on the auxiliary technology, the LCOH of the HTF will be plotted against the natural gas price or the electricity price.

#### 3.3.2.1 Financial performance comparison for the superheated steam drying case study

Employing the COP correlation for VCHPs (Equation 3.2) and HTFs (Equation 3.3), a COP of respectively 3.084 and 0.332 is obtained as the case study has a GTL of 81 K. As a result of the HTF COP of 0.332, about 1115 $kW_{th}$ of residual heat is required to deliver the heat duty of 370 $kW_{th}$. However, since only 298 $kW_{th}$ of residual heat is available, the HTF can just supply about 99 $kW_{th}$ of the heat demand. Consequently, 271 $kW_{th}$ of heat needs to be delivered by an auxiliary heating system.

The LCOH for the VCHP, EB and HTF+EB as a function of the electricity price can found in Figure 3.7. The LCOH for the NGB and HTF+NGB as a function of the natural gas price can be found in Figure 3.8. In these figures, the solid lines present the LCOH of the technology at the nominal investment cost, while the dashed lines show the LCOH at the minimum and maximum considered investment costs for the heat pump technologies. Since the investment costs chosen are independent on the electricity cost, the dashed lines have a fixed offset from the solid lines.

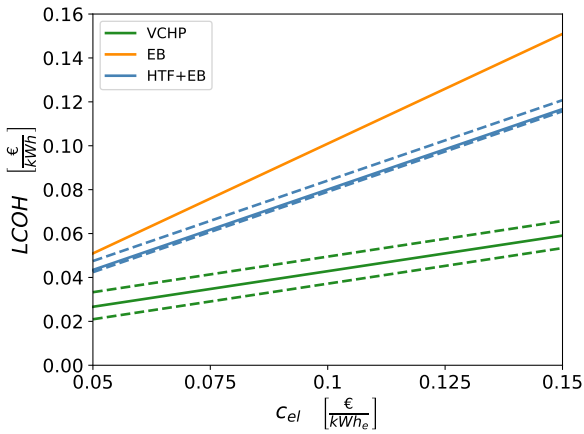


Figure 3.7: LCOH of EB, VCHPs and HTF+EB as a function of the electricity price for the SSD case study, with the dashed lines the sensitivity on the investment cost.

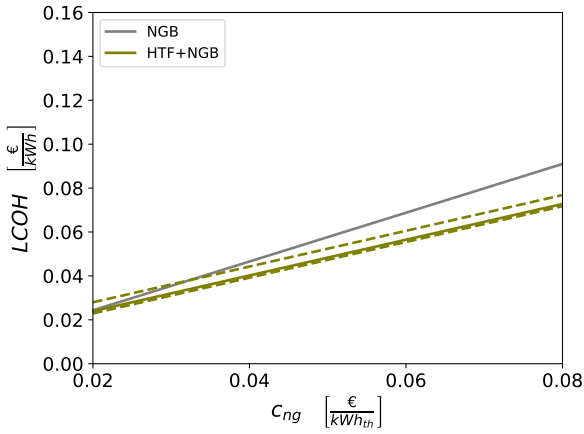


Figure 3.8: LCOH of NGB and HTF+NGB as a function of the natural gas price for the SSD case study, with the dashed lines the sensitivity on the investment cost.

The figure shows that for the electrical options, VCHPs are by far the most financially interesting over the studied electricity price range. EBs are always the most expensive solution. Using a HTF+EB allows to reduce the LCOH compared to EBs. However, for this case study, the decrease is not significant, because the HTF is only able to deliver a small fraction of the total heat demand. For low electricity prices the LCOH of the HTF+EB and EB would even coincide and the optimal technology may shift to the EB. When electricity prices are low, the potential profit from electricity savings is reduced, making it more difficult to pay back the high investment costs of the HTF. The dashed lines in the figure shows that the uncertainty in the LCOH due to the investment costs of the VCHP is relatively high. If the maximum investment cost is considered the LCOH increases with +0.0066 €/$kWh_{th}$, while for a minimum investment cost the LCOH decreases with -0.0057 €/$kWh_{th}$ compared to the base investment cost. Although the investment cost of the HTF can vary over a wider range, the variation on the LCOH of the HTF+EB due to the uncertainty in investment cost is rather small. This is because the HTF only supplies a small fraction of the heat demand. For this specific use case, the LCOH of the HTF+EB can vary with -0.0010 €/$kWh_{th}$ to +0.0041 €/$kWh_{th}$ due to the sensitivity on investment cost. Overall, for the considered price range, the uncertainty on the investment cost does not influence which technology has the lowest LCOH.

For the natural gas options, the HTF+NGB is on the boundary of being consistently more cost effective then the NGB. When the natural gas price

is high, a HTF could reduce the LCOH of a NGB by about 25 %. For lower natural gas prices, NGBs become the best option, again because of the high investment cost of the HTF. At the high HTF investment cost however, the NGB can already become the best option at a natural gas price of 0.0320 €/$kWh_{th}$.

Based on the specific electricity and natural gas costs reported in Table 3.6 and the financial results reported in Figure 3.7 and Figure 3.8, the LCOH for each technology in a specific country can be derived. The corresponding results are reported in Figure 3.9. The uncertainty on the investment cost is not considered in this figure.

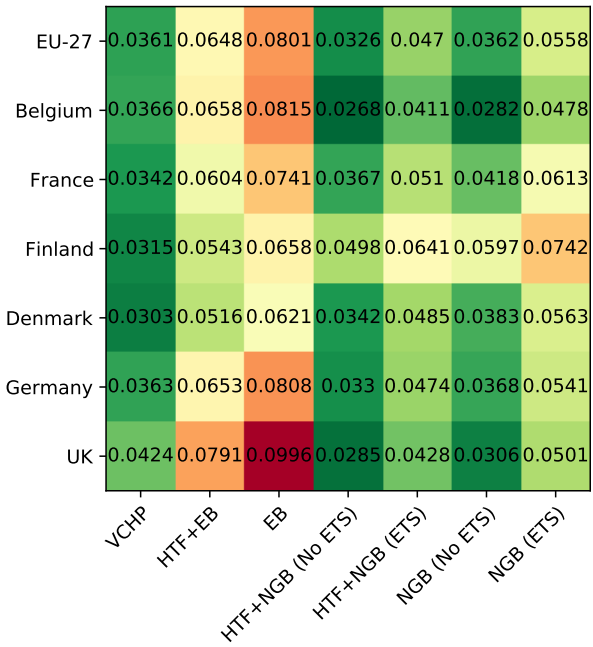


Figure 3.9: LCOH (€/$kWh_{th}$) for the SSD case for each considered technology and country, with and without ETS for natural gas boilers.

Figure 3.9 shows that for the three electrical options, the VCHP is the most cost-effective option in all countries. The LCOH of a VCHP is about 1.7 to 1.8 times lower compared to a HTF+EB and 2.1 to 2.35 times lower compared to the EB. Although the HTF is able to reduce the LCOH with about 20 % compared to the EB, it is not competitive against the VCHP for this case study. For the natural gas options it can be observed that the HTF+NGB is financially the most competitive for all countries. However, since the averaged gas prices between 2016-2020 were quite low, the difference with the NGB is often low, usually in the order of 10 %.

When considering both electricity and natural gas as an energy carrier, different technologies have the lowest LCOH. When no ETS cost is considered, a VCHP is only more cost-effective than a NGB in countries with a low or average EGPR (i.e. France, Finland, Denmark, Germany and the EU-27 average). In countries with a high EGPR (i.e. Belgium and the UK) a NGB is financially more interesting than a VCHP. When comparing a VCHP with a HTF+NGB, VCHPs are only financially cost effective in countries with low EGPRs (i.e. France, Finland and Denmark). When an ETS cost is being applied, the VCHP is for all countries the most interesting option. For some countries such as Finland, an EB becomes even more interesting than a NGB.

#### 3.3.2.2 Financial performance comparison for the steam production case study

For the steam production case study, with a GTL of 51.4 K, the developed COP correlations results in a VCHP COP of 4.11 and HTF COP of 0.474. Now, with a HTF COP of 0.474 and residual heat availability of 702.3 $kW_{th}$, the HTF is able to deliver a heat duty of 332.9 $kW_{th}$. As 474 $kW_{th}$ of heat is demanded by the steam production process, the auxiliary boiler should deliver a heat duty of 141.1 $kW_{th}$. Because two different processes are coupled (i.e. cooling loop and steam network), the HTF is able to deliver about 70 % of the total heat demand, whereas in the SSD stand-alone process the HTF was only able to deliver about 27 % of the total heat demand. Henceforth, more favourable financial aspects may now be expected for the HTF.

The LCOH for the VCHP, EB and HTF+EB as a function of the electricity price is given in Figure 3.10. The LCOH for the NGB and HTF+NGB as a function of the natural gas price is shown in Figure 3.11. Again, the influence of a high and low investment cost of the heat pump technologies is illustrated by the dashed lines. It can now be seen that the variation in LCOH due to the variation in investment cost is higher for the HTF, as the HTF now provides 70 % of the heat demand. The difference in LCOH when considering the minimum and maximum investment cost of the HTF is now -0.0027 €/$kWh_{th}$ and +0.0106 €/$kWh_{th}$ respectively. Whereas, for the VCHP this stays between -0.0057 €/$kWh_{th}$ and +0.0066 €/$kWh_{th}$. In these figures it can also be observed that, when employing an EB or NGB, the same LCOHs are observed as for the SSD case study as their LCOH only depends on the electricity or gas price. Compared to the previous case study, the solutions using VCHPs or HTFs, now have lower LCOHs because of the higher COPs and the higher availability of residual heat for the HTF.

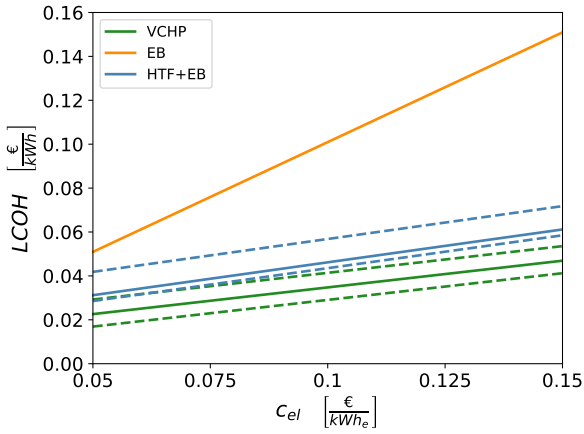


Figure 3.10: LCOH of VCHP, EB and HTF+EB as a function of the electricity price for the steam production case study, with the dashed lines the sensitivity on the investment cost.

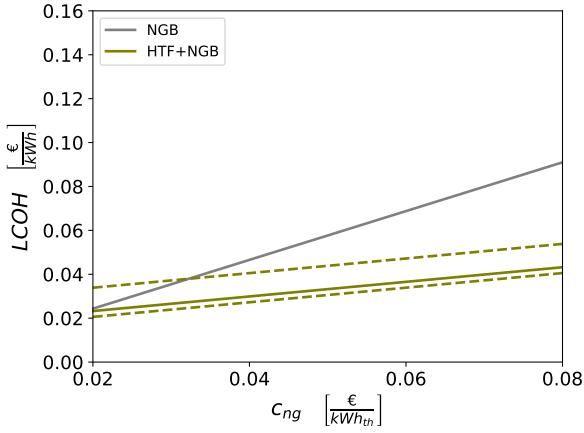


Figure 3.11: LCOH of NGB and HTF+NGB as a function of the natural gas price for the steam production case study, with the dashed lines the sensitivity on the investment cost.

When using electricity as energy carrier, VCHPs are the most interesting option while EBs are the least profitable option. Whereas for the SSD case study the LCOH of the HTF+EB was close to the LCOH of the EB, now its LCOH is relatively close to these of the VCHP. However, even when considering a high VCHP investment cost and a low HTF investment cost the VCHP is still the

best option, although by a marginal difference.

If natural gas is considered as energy carrier, it can be observed that the HTF+NGB is now far more interesting compared to the NGB, especially for high natural gas prices. For low natural gas prices however, the difference reduces and both technologies become financially equal. If the HTF however has a high investment cost, the NGB already becomes the most profitable at a natural gas price of 0.0325 €/$kWh_{th}$.

The LCOH of each technology for the studied countries, considering their nominal investment cost, can be found in Figure 3.12.

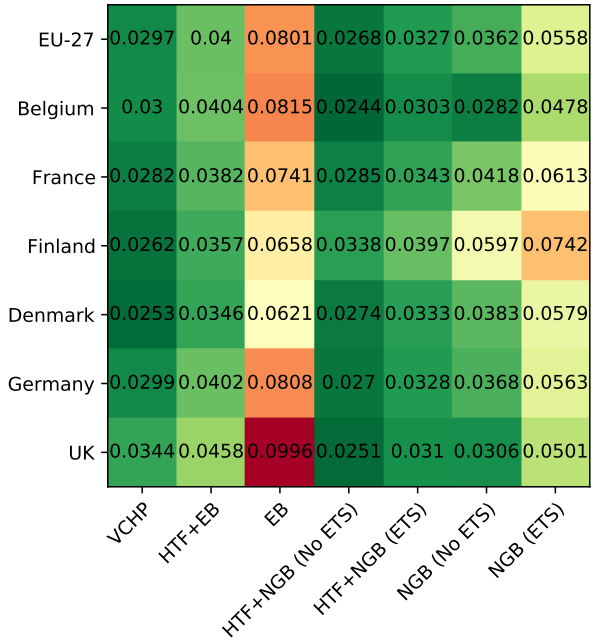


Figure 3.12: LCOH (€/$kWh_{th}$) for the steam production case for each considered technology and country, with and without ETS for natural gas boilers.

Figure 3.12 shows that for the electrical technologies, VCHPs have an LCOH which is about 26 % lower compared to the HTF+EB and about 63 % lower compared to the EB. For the technologies using natural gas, it can be observed that the LCOH of a HTF+NGB is about 26 % lower compared to the LCOH of the NGB. When taking an ETS cost into account this increases to about 40 %. When considering all technologies, it can be observed that even when no ETS costs are applied, VCHPs are more cost effective than NGBs with the exception of the UK and Belgium because of the high EGPR in these countries. When an

ETS is applied, VCHPs are financially more cost effective compared to NGBs in all countries. However, for this case study, VCHPs are only competitive against HTFs+NGBs in countries where the EGPR is low (i.e. France, Finland and Denmark) when no ETS is applied. If an ETS is applied they are always more interesting.

## 3.4 Sensitivity analysis

This work uses financial boundary conditions that are common in the energy intensive industry. However, to illustrate the impact of these boundary conditions, a sensitivity analysis is presented, which is performed on the case studies. Specifically, the sensitivity of the LCOH to changes in annual operating hours, ETS carbon pricing and residual heat availability is examined.

### 3.4.1 Influence of the annual operating hours

In the analysis 8000 annual operating hours were considered. A sensitivity analysis on the annual operation hours is performed by varying this value between 4000 and 8500 hours and computing the respective LCOH for the different heating technologies. It is important to note that the lifetime of the heating system is here assumed to be independent of these operating hours. The LCOH values for the different heating technologies and annual operating hours for both the SSD and the steam production case studies are shown in Figure 3.13 and Figure 3.14 respectively.

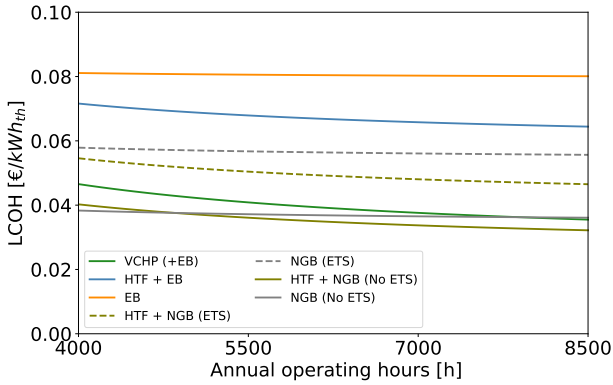


Figure 3.13: LCOH for the SSD case study for the different technologies as a function of the annual operating hours.

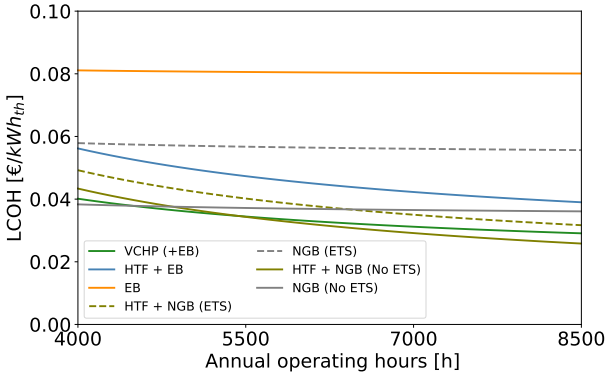


Figure 3.14: LCOH for the steam production case study for the different technologies as a function of the annual operating hours.

From figures 3.13 and 3.14, it is evident that the LCOH of the EB and NGB shows minimal sensitivity to the annual operating hours. On the other hand, the LCOH of VCHP and HTF shows a higher dependency on the operating hours, due to their higher investment costs. It should be taken into account that in both case studies, the HTF can only meet a portion of the total heat demand. As this fraction increases, the dependence on annual operating hours becomes more pronounced, as evident when comparing Figure 3.14 with Figure 3.13. Furthermore, the relationship between LCOH and annual operating hours is non-linear for the heat pump technologies, with a pronounced increase below 5500 operating hours. It is thus crucial for these heat pump technologies to operate in applications with a high number of annual operating hours. Although even at lower annual operating hours, these technologies may still offer favourable financial benefits, particularly when ETS costs are considered for the NGB.

### 3.4.2 Influence of the ETS carbon pricing

In the financial evaluation of the case studies, a carbon price of 80 €/tonne $CO_2$ was considered for the technologies that directly rely on fossil fuel use [96]. To illustrate the sensitivity of this carbon price, it is varied between 0 and 140 €/tonne $CO_2$. The LCOH for the different technologies and carbon prices, for the SSD and the steam production case studies, are shown in Figure 3.15 and Figure 3.16 respectively.

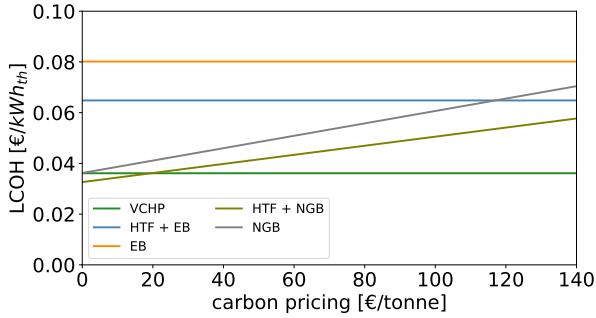


Figure 3.15: LCOH for the SSD case study for the different technologies as a function of the carbon price for fossil fuel usage.

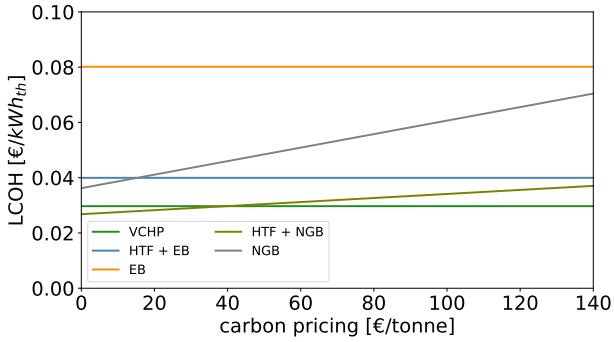


Figure 3.16: LCOH for the steam production case study for the different technologies as a function of the carbon price for fossil fuel usage.

As anticipated, both figures indicate that the LCOH of all electric technologies, or technologies using residual heat only, remains unaffected by the carbon price, whereas the LCOH of natural gas-based technologies is influenced. Notably, the stand-alone NGB shows a strong dependency on the carbon price. In both case studies, the LCOH of the NGB nearly doubles when considering a carbon price of 140 EUR/tonne of $CO_2$ compared to zero carbon pricing. The LCOH of the HTF, on the other hand, is independent of the carbon price. However, when an auxiliary NGB is used, the overall system is affected. In the SSD case study, where the HTF can supply only 27 % of the heating load, the LCOH of the entire system becomes highly dependent on the carbon price when an auxiliary NGB is used. In contrast, in the steam production case study, where the HTF can supply 70 % of the heating load, the overall system is less dependent on the carbon price.

### 3.4.3 Influence of the residual heat availability

When coupling different processes, the ratio of residual heat to process heat can vary. Here, variations in residual heat for the steam production case study, with a heat demand of 474 $kW_{th}$, is studied. To study its effect, the residual heat availability is varied between 0 and 1000 $kW_{th}$. The LCOH of the different heating technologies as a function of the residual heat availability for the steam production case study can be found in Figure 3.17. This figure also shows the RHR next to the residual heat availability.

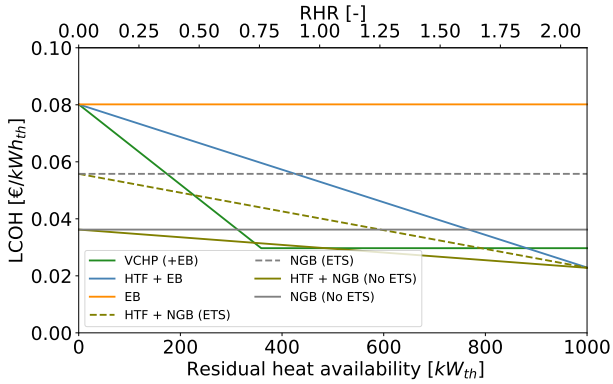


Figure 3.17: LCOH for the steam production case study for the different technologies as a function of the residal heat availability.

As the EB and the NGB do not require residual heat, their LCOH is independent of residual heat available. For the VCHP, 357 $kW_{th}$ of residual heat is required for the LCOH to become independent of the residual heat available. For the HTF 1000 $kW_{th}$ of residual heat is required. If these quantities of residual heat are not available, auxiliary heating will be needed. In such scenarios the LCOH increases for lower residual heat availabilities for both instances, until the residual heat availability becomes zero. At this point the LCOH is the same as for the auxiliary heating technology, as the HTF and VCHP are not able to supply any heat. For high residual heat availabilities the HTF can become more cost effective than a VCHP. Depending on the auxiliary heating system used and whether ETS are being applied this happens between residual heat availabilities between 500 $kW_{th}$ and 900 $kW_{th}$.

## 3.5 Discussion

In this chapter, the financial performance of the NGB, EB, VCHP and HTF are compared in terms of LCOH. The comparison is first done in a generic way

where the technology with the lowest LCOH is plotted as a function of the GTL and RHR. By doing so, all typical industrial processes are covered. Furthermore, it allows to give a generic overview of the most suitable integration area of each technology. This plot is made for two different electricity costs and three different EGPRs, so that the plot is presented six times under one figure (Figure 3.6). Furthermore, to analyze the sensitivity of the investment cost, this figure is also shown for a low investment cost scenario and a high investment cost scenario in Appendix C. One should however not be deceived by the span of the area indicating an optimal technology (i.e. lowest LCOH) on these plots. One could for example think that the HTF has the largest application area. However, the HTF is never optimal in scenarios of RHR lower than 1. In practical applications however the RHR is frequently below 1. Consequently, for typical applications, it is the VCHP or the NGB that will be most relevant. The choice between the VCHP and NGB then strongly depends on the energy price and the EGPR. The VCHP is most suited in scenarios with a high energy price and a low EGPR. The NGB on the other hand is most suited in scenarios with low energy prices and high EGPRs. With the overall trend of rising energy prices and decreasing EGPRs, among others through the ETS, VCHPs are a promising technology for the future.

After the generic comparison, the financial method is applied to two relevant case studies, confirming the statements given above. However, here an additional combination of technologies was considered, namely the combination of a HTF and a NGB. This option typically has a lower LCOH than a stand-alone NGB, increasing the competitiveness of the HTF with the VCHP. However, it only allows for partial decarbonization of the heat demand and therefore was not considered in the section of the generic boundary conditions.

The study however has some limitations, listed below:

- There is a lack of detailed cost data of the heat pump technologies. Particularly lacking is the technology cost as a function of the temperature lift and supply temperature. Furthermore, the cost ideally should depend on the heating capacity. Whereas, scaling information might be available for the latter, it would require plotting the overview of the best technology under different heating capacities. This would make the result section unclear and no generic conclusions or comparisons can be made. Therefore, to show the sensitivity of LCOH to investment costs, a minimum and maximum cost is considered for each heat pump technology.
- It could be argued that the financial model considers the available residual heat as 'free heat', as is commonly done in the literature [76, 97–99]. However, residual heat at a purposeful temperature level is required to enable competitive COPs. Residual heat at these temperatures

could already be valuable for pre-heating industrial processes, or for space heating and domestic hot water purposes of offices or nearby residential areas, e.g. by feeding the heat into a district heating network [100–102]. This aspect is not considered in the current study, but it is highlighted here. If a cost would be applied to the residual heat, it would be disadvantageous for the heat pump technologies. Particularly for the HTF it would be disadvantageous as it requires a large amount of residual heat. Therefore, a substantial part of the region, or even the complete region, where the HTF was optimal may be replaced by the VCHP or the NGB. On the other hand, when the residual heat cannot be directly used, the heat pump technologies might provide cooling, which becomes an additional revenue.

- The study does not take into account the integration costs of the technology. As the heat pump technologies may require a heat recovery installation and a connection to the residual heat source, higher integration costs could be expected compared to the boiler technologies. Although the study somehow considers the influence of integration costs by considering different investment cost scenarios. On the other hand, it could be argued that the need for cooling infrastructure is reduced, or eliminated, by the heat pump technology.
- The study considers a relatively high amount of annual operating hours (8000 h). For a lower amount of operating hours, technologies with a lower investment cost, such as the boiler technologies, will become more interesting as shown in the sensitivity analysis. VCHPs and particularly HTFs, will become less interesting for lower operating hours. This is because there is annually less time for the investment to have a return on investment.

## 3.6 Conclusion

In this chapter the financial performance of the HTF, VCHP and EB were compared with each other first in a generic way and subsequently also with the NGB. The generic comparison was done by varying the residual heat availability and the temperature lift. Subsequently, two actual industrial case studies were studied.

The main conclusion is the no technology is always optimal. This is because the LCOH depends on a multitude of factors that can vary significantly, such as the temperature lift, residual heat availability, energy prices, operating hours, and technology costs. Depending on these parameters any technology can be optimal. An overview of the influence of these parameters on the LCOH of

each technology is given in Table 3.9.

Table 3.9: Overview of the sensitivity of the LCOH under different parameters of each technology. 0: not directly sensitive, 1: slightly sensitive, 2: moderately sensitive, 3: highly sensitive.

| Parameter | Electric boiler | Natural gas boiler | Vapour compression heat pump | Heat transformer |
|---|---|---|---|---|
| **Electricity cost** | 3 | 0 | 2/3 | 0 unless auxiliary electric boiler |
| **Natural gas cost** | 0 | 3 | 0 | 0 |
| **Technology cost** | 1 | 1 | 2 | 3 |
| **Temperature lift** | 0 | 0 | 3 | 3 if few residual heat available otherwise 0 |
| **Residual heat availability** | 0 | 0 | 3, but independent at rather low residual heat availability | 3, but independent at high residual heat availability |
| **Operational hours** | 1 | 1 | 2 | 3 |

It was however found that the HTF is never the preferred technology when the heat demand exceeds the residual heat available in terms of heat flows. In these cases, the VCHP or the NGB is thus often the best choice, with the VCHP being typically the best choice at higher energy prices and a lower EGPR. These pricing scenarios are expected in the coming times. If this should not be the case, the VCHP can still be the preferred application, but only up to a maximum temperature lift.

This confirms the application potential of VCHPs, thereby validating the scope of this dissertation. An overview of the working principles of VCHPs and the and working fluids used is provided in Appendix D. The remainder of this dissertation focuses on this heat pump technology, which will henceforth be referred to as HTHPs, as is common in the literature.

# 4

# Thermodynamic screening of vapour compression high-temperature heat pump working fluids

*This Chapter is based on the Journal paper:*

*E. Vieren, T. Demeester, W. Beyne, A. Arteconi, M. De Paepe and S. Lecompte, "The thermodynamic potential of high-temperature transcritical heat pump cycles for industrial processes with large temperature glides",* Applied Thermal Engineering*, vol. 234, p. 121 197, 2023, ISSN: 1359-4311. DOI:* https://doi.org/10.1016/j.applthermaleng.2023.121197*. [Online]. Available:* https://www.sciencedirect.com/science/article/pii/S1359431123012267

*In this Journal paper the focus is on transcritical cycles. The Chapter however also includes the use of zeotropic mixtures. The literature study and the results related to zeotropic mixtures is unpublished work.*

## 4.1 Introduction

In Chapter 3 it has been shown that VCHPs[1] often are the most cost-effective technology when compared to the NGB and the HTF. Moreover, due to their high power-to-heat efficiency, they allow for a significant reduction in GHG emissions compared to NGB, even under the current European power generation mix [7]. Further enhancing their performance would allow for even further improved cost-efficiencies and lower GHG emissions, increasing the adoption rate of the technology.

One way to increase the performance of vapour compression HTHPs is by reducing exergy losses in the heat exchangers. Knowing that heat transfer is a main source of exergy destruction in HTHPs [104], it can be minimized by closely matching the temperature profile of the working fluid and secondary medium. Two strategies are here considered to match the temperature profile of the working fluid and the secondary medium, namely by the selection of a working fluid that operates in the transcritical regime, or by mixing two pure working fluids which may result in a zeotropic mixture. These two methods are discussed and analyzed separately.

This introduction first provides background information on transcritical operation (Section 4.1.1) and zeotropic mixtures (Section 4.1.2). The research scope is then outlined in Section 4.1.3. Following this, the literature review on transcritical operation (Section 4.1.4) and zeotropic mixtures (Section 4.1.5), in the context of the research scope, is presented. This helps to identify the research gaps.

### 4.1.1 Transcritical operation

An important aspect for transcritical cycles is the critical point. The critical point is the end of a phase equilibrium curve where distinct liquid and vapor phases cease to exist. It is defined by the critical temperature and pressure, beyond which the substance becomes a supercritical fluid. Depending whether the heat rejection and absorption happens below or above this critical point of the working fluid, three operational modes for heat pump cycles can be identified as shown in Table 4.1.

Table 4.1: Overview of the three operational modes of heat pump cycles.

| Operational mode | Heat absorption | Heat rejection |
|---|---|---|
| Subcritical | Below critical point | Below critical point |
| Transcritical | Below critical point | Above critical point |
| Supercritical | Above critical point | Above critical point |

[1] An overview of the working principle and working fluids of VCHP is provided in Appendix D

In practice, the majority of the heat pump cycles operate in subcritical mode [105]. For this mode, the main part of the heat absorption and rejection happens during the latent phase change of the working fluid, which, in case of pure working fluids, takes place at constant temperatures in the evaporator and condenser. In the transcritical cycle, the heat absorption also occurs through a phase change in the evaporator. For the heat rejection, which happens at pressures above the critical pressure, the heat is rejected in a gas cooler, through the cooling of the supercritical fluid. In a supercritical cycle, the heat absorption also happens above the critical pressure. Thus, instead of evaporating a two-phase flow, a supercritical fluid is heated in a gas heater. An overview of the T,s-diagram of a subcritical cycle, transcritical cycle and supercritical cycle can be found in Figure 4.1. The figure also shows that the higher the critical temperature of the working fluid, the more it tends towards operation as a subcritical cycle, while the lower it is the more it tends towards operation as a transcritical or supercritical cycle. It should be mentioned that the supercritical cycle can be classified as a gas compression cycle. Although gas compression cycles can also operate below the critical pressure.

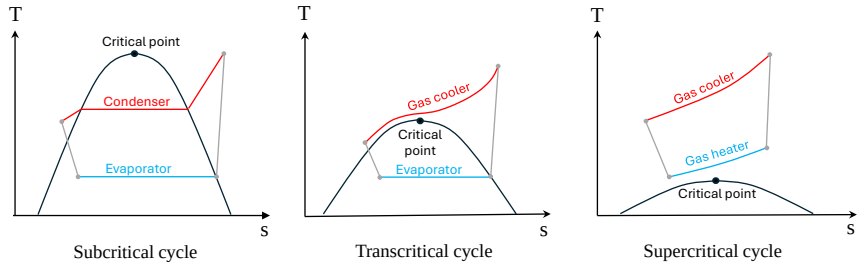


Figure 4.1: T,s-diagram of a subcritical cycle, transcritical cycle and supercritical cycle.

Depending on the application, the temperature change impaired in cooling or heating the supercritical fluid can have advantages and disadvantages. Overall, it is desired that the temperature profile of the working fluid matches the temperature profile of the secondary medium. The match in temperature profile reduces the exergy destruction caused by heat transfer, which can be beneficial for the performance of the heat pump. Figure 4.2 illustrates two examples of the temperature profiles of the working fluid and heat sink in a condenser (subcritical cycle) or gas cooler (transcritical or supercritical cycle), for heat sinks with and without temperature glide.

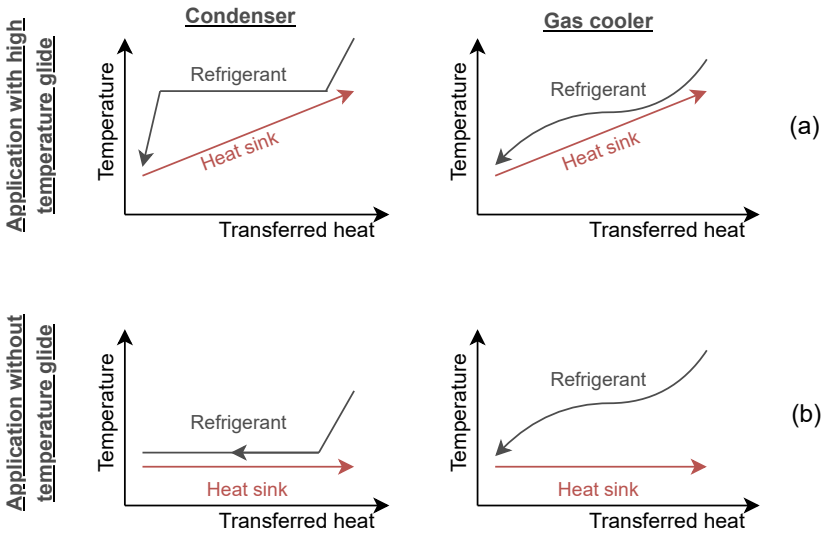


Figure 4.2: Temperature profile during heat rejection for subcritical operation (condenser) and transcritical or supercritical operation (gas cooler), for an application with and without heat sink temperature glide.

This figure shows that transcritical cycles can be more favourable than subcritical cycles in terms of temperature matching for applications with a (large) temperature glide (Figure 4.2 a). For applications with a small or no temperature glide, more favourable temperature matching can be expected with subcritical cycles (Figure 4.2 b), or zeotropic mixtures.

### 4.1.2 Zeotropic mixtures

Combining two or more pure working fluids changes the thermodynamic properties of the resulting mixture. These mixtures may achieve a compromise between beneficial and detrimental properties of the individual mixtures. The mixing of pure working fluids may also result in different thermodynamic behaviour. Mixed pure working fluids may for example have a non-isothermal phase change. This means that they can have a temperature variation during phase change, often referred to as the 'temperature glide', which is defined by the temperature difference between the dew point and the bubble point. Because of this characteristic, mixtures are often classified in three groups; azeotropes, near-azeotropes and zeotropes. With azeotropes referring to mixtures without temperature glide, and thus a constant composition of the liquid and vapour during phase change, near-azeotropes to mixtures with a

negligable temperature glide and zeotropes to mixtures with a temperature glide during phase change. Zeotropic mixtures thus have a different mixture composition of the vapour and liquid phase.

Zeotropic mixtures are increasingly being studied for both HTHPs [106–109] as for organic Rankine cycles (ORCs) [110, 111]. Due to the presence of their temperature glide, the temperature profile of the mixture during heat transfer can be matched with the temperature profile of the heat source and/or sink when these have a temperature glide, as shown in Figure 4.3 a. This temperature match may result in increased performance as a result of the decreased exergy destruction because of the overall lower temperature differences between the working fluid and heat sink/source. However, for a heat source without temperature glide (Figure 4.3 b), the non-isothermal phase change would result in increased exergy destruction because of the overall higher temperature differences between the working fluid and heat sink/source. Notably, the non-isothermal nature of the phase change can lead to reduced heat transfer coefficients, as extensively documented by Zhang et al. [112]. Their experimental study on the condensation heat transfer of the R134a/R245fa mixture in plate heat exchangers confirmed this effect, demonstrating that the heat transfer coefficient at a specific composition is lower than the weighted average of the heat transfer coefficients of the pure components.

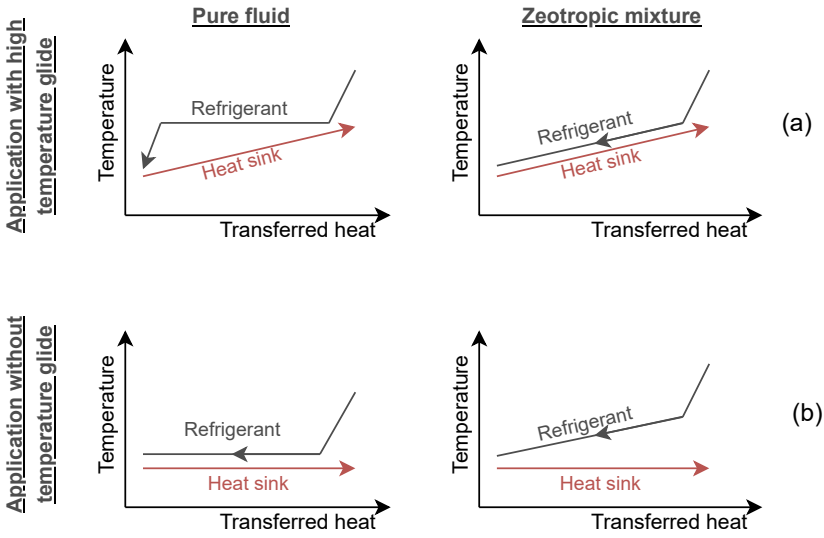


Figure 4.3: Temperature profile during heat rejection for pure working fluids and zeotropic mixture.

Obtaining large temperature glides with zeotropic mixtures however poses a risk for composition shift due to fractionation [113, 114]. Fractionation is the phenomenon where in the two-phase region the liquid phase is richer in the least volatile component, while the vapour phase is richer in the most volatile component. Working fluid leakages, working fluid holdup, or different solubilities in lubricants may then result in different circulating compositions [115]. Therefore, zeotropic mixtures are often proposed for applications with smaller temperature glides. Furthermore, the benefit can be that, in contradiction to transcritical cycles, zeotropic mixtures experience both a temperature glide at the heat source and heat sink.

### 4.1.3 Scope of the research

This analysis first focuses on large temperature glides at the heat sink side ($\geq$ 60 K), which are common in industrial applications such as drying (e.g. spray drying or superheated steam drying), thermal oil heating, pressurized hot water production, air preheating or fluid (pre)heating. For these applications, use of zeotropic mixtures may be less interesting because of the risk of composition shift. Furthermore, the strongly different temperature glides of the heat source and heat sink may severely limit the obtainable efficiency gain of zeotropic mixtures. Transcritical cycles however, are well suited for these types of temperature glides.

The analysis then focuses on applications with more moderate temperature glides ($<<$ 60 K) at both the heat source and the heat sink side. For these applications the use of zeotropic mixtures are investigated. For both aspects there are clear gaps in the literature as indicated in the next two subsections.

### 4.1.4 Literature study and research gaps on transcritical heat pump cycles

The transcritical vapour compression cycle was proposed by Lorentzen in 1990 [116], who identified $CO_2$ as a near-ideal working fluid [117]. Since the publication by Lorentzen much research has been performed on transcritical $CO_2$ cycles; an overview of transcritical $CO_2$ heat pumps and their relevance can be found in several review articles [118–121]. $CO_2$ however has a low critical temperature of 31 °C and a high critical pressure of 73.6 bar. Consequently, pressures in $CO_2$ systems are typically 5-10 times higher compared to other working fluids [122]. This may cause several challenges in component design and safety concerns, especially when high operational temperatures are targeted [122]. Moreover, to keep heat transfer at the heat source in the two-phase region, low temperatures are required at the evaporator side (25-30

°C) [123]. These transcritical cycles will only be suitable for very large heat sink temperature glides. Because of these reasons its use in high-temperature applications is commonly limited to heat sinks with outlet temperatures of 120 °C and considerably lower heat sink inlet temperatures (resulting in large temperature glides) [12, 124].

Whereas transcritical operation is common practice for $CO_2$ heat pump cycles, few transcritical HTHPs are found operating with other working fluids. Besbes et al. [125] constructed a 30 $kW_{th}$ transcritical heat pump prototype with R32 as working fluid, to be implemented in drying plants. In the set-up, air was heated from 60 °C to 120 °C, with effluents available at 50 °C. A COP of 3.69 was observed, which corresponds to an exergy efficiency of 63 %. Chehla et al. [126] adapted the set-up constructed by Besbes et al. [125] for use of HFOs as working fluid. In their work, air heating at 90 °C or 100 °C to 150 °C is experimentally investigated, using effluents at 82 °C. The adapted heat pump reached COPs up to 3.72. Kimura et al. [127] developed a transcritical butane (R600) HTHP with as goal to raise the temperature of thermal oil from 80 °C to 180 °C, employing a hot water heat source at 80 °C. The targeted COP is 3.5. Newly designed oil-free centrifugal compressors with active magnetic bearings were used. The heat pump system has a capacity of 300 $kW_{th}$. Verdnik and Rieberer [128], designed a single-stage HTHP prototype with a suction-gas-cooled reciprocating compressor, low pressure suction accumulator and internal heat exchanger (IHX), also using R600 as working fluid. Transcritical operation enabled to raise the temperature of the heat sink from 80 °C to 160 °C. A COP of 3.1 and a heating capacity of 24.2 $kW_{th}$ was achieved with a heat source cooled from 60 °C to 55 °C. Moreover, the influence of the discharge pressure and suction gas superheat in the IHX on the COP and heating capacity was studied.

Whereas some experimental research is performed on transcritical industrial heat pumps with working fluids other than $CO_2$, few working fluid screenings are performed for temperatures up to 200 °C. This may raise the question whether the working fluids used in the experimental research and transcritical HTHP development are truly optimal. Furthermore, few relevant applications for transcritical HTHPs up to 200 °C are presented.

Sarkar et al. [124] considered subcritical and transcritical cycles for, among others, a generic case study with heat sink outlet temperatures up to 200 °C, but only considered four working fluids (i.e. carbon dioxide, ammonia, propane and isobutane). Wang et al. [55] compared subcritical and transcritical heat pump cycles for spray dryers operating at 200 °C, where most working fluids in Engineering Equation Solver (EES) were assessed. However, due to the lack of a heat source with a suitable energy content, the heat sink outlet temperatures were limited to 110 °C. For these conditions the high GWP

working fluid R134a was proposed as most promising, with R32 and R290 also showing good energy efficiency. Arpagaus et al. [129], modelled a transcritical heat pump cycle with and without IHX and a transcritical heat pump cycle with parallel compression. Two case studies are considered, namely, air heating from 30 °C to 200 °C with a hot water heat source at 80 °C, and water heating from 100 °C to 200 °C with use of moist air at 30 °C as heat source. The investigated working fluids were R245fa, four low-GWP HFOs and the hydrocarbons R601 and R600. The results show that the cycle with IHX has the highest performance and lowest discharge pressure. Moreover, this cycle is convenient to control. The results also showed that the gas cooler pressure has a large impact on the COP.

In conclusion, it is unclear for transcritical HTHPs what the technology potential is for high temperature needs (up to 200 °C), how these HTHPs should be optimally designed and what further challenges remain. In this work, three relevant industrial case studies, with different temperature glides, are proposed as a starting ground. The need to analyze different temperature profiles is also emphasized by Arpagaus et al. [129], who suggest that future research into transcritical cycles should include more temperature conditions. By doing so it can be determined for which boundary conditions (i.e. applications) transcritical operation becomes more beneficial than classical subcritical operation. Moreover, suitable working fluids for transcritical or subcritical operation can be identified for the targeted applications, since all working fluids within REFPROP 10.0 [130] are considered in this work. This is also stressed in the recent review paper of Adamson et al. [105] on transcritical heat pump cycles, which state that one of the challenges is: "The identification of efficient working fluids (or working fluid blends), beyond $CO_2$, to maximise COP for specific applications while keeping within pressure limits". In addition, suitable working fluids will be presented for heat pump supply temperatures up to 200 °C in general, which is scarcely studied in the literature. Furthermore, this study considers and compares the influence of flammability and the use of an IHX for the different case studies.

### 4.1.5 Literature study and research gaps on heat pump cycles using zeotropic mixtures

Zeotropic mixtures are increasingly being studied for use in HTHPs. Some experimental research exists for heat pumps using zeotropic mixtures [107, 131–133]. However, the maximum heat sink temperatures are typically limited to 100 °C. Furthermore, several research papers exist in the literature which shows the potential of using zeotropic mixtures compared to pure working fluids from a simulation point of view.

Liu et al. [134], studied low-GWP ternary zeotropic mixtures with large temperature glides for HTHPs to be used for waste heat recovery. The zeotropic mixtures were composed of CO2 and R1233zd(E) and one of the following flammable working fluids: R600a, R290, R1270 or RE170. For the method and screening they applied, the ternary zeotropic mixture CO2/R600a/R1233zd(E) with the respective mass fractions of 0.2/0.7/0.1 was found to be the working fluid with the highest COP (3.22) for the considered case study. In this case study hot water was heated from 35 °C to 90 °C, using chilled water with an inlet temperature of 20 °C and outlet temperature of 5 °C.

Gómez-Hernández et al. [135] proposed the use of a zeotropic mixture of $CO_2$ and acetone for use in HTHPs and studied its use in the supply temperature range of 150 °C to 220 °C. Considering a heat sink outlet temperature of 200 °C and a temperature difference between heat sink outlet and heat source inlet of 70 °C, a mixture of 5 % CO2 and 95 % acetone (mass fractions) showed the best performance. The mixture showed a COP improvement of 46 % compared to pure acetone.

Ganesan and Eikevik [136] considered a two-stage cascade refrigeration system for HTHP applications. A CO2/butane mixture was used in the low stage while a CO2/pentane mixture was used in the high stage. A heat source temperature between 10 °C to 50 °C was considered, while hot water production up to 115 °C is targeted. The mixture showed an improvement of 20 % compared to pure working fluids.

Zühlsdorf et al. [106] considered 14 natural working fluids for heat pump applications with large temperature glides at the sink side and smaller temperature glide at the source side. In the study four different boundary conditions were considered. For all these boundary conditions, the heat sink was heated from 40 °C to 80 °C. The variations in boundary conditions could be found in the outlet temperature of the heat source. The results showed that, depending on the boundary conditions, a performance increase up to 20 % can be achieved for simple cycles and 27 % if superheating can be avoided.

Dai et al. [137] considered mixtures of CO2 and 10 other working fluids for use in drying processes. They found that these mixtures could enhance the COP and reduce the compressor discharge pressure compared to pure CO2. The highest COP was achieved using CO2/R32 under the mass fraction of 0.1/0.9, which was found to be 7.42 % higher compared to pure CO2. The temperature of the hot air supplied is rather low (<70 °C).

Although some literature exists on the use of zeotropic mixtures, it is often limited by one of the following constraints:

- The heat sink outlet temperatures is far below 200 °C or even below 100 °C.
- The boundary conditions selected is limited to one case study, for which

zeotropic mixtures may show particularly favourable results. No case studies are introduced where zeotropic mixtures may not be favourable.

- The selecting working fluids are limited to (a) one zeotropic mixture, (b) multiple zeotropic mixtures but always with one or two constituents which are always present, e.g. $CO_2$, (c) a pool of mixtures, but only considering limited working fluids.

The research presented here is not limited by these constraints. A large pool of binary mixtures will be considered for use in HTHPs with supply temperatures in the range of 200 °C. This will be done for four generic case studies. The first case study has a temperature glide at both the heat source and heat sink, the second case study has a temperature glide only at the heat source, the third case study has a temperature glide only at the heat sink and the fourth case study has no temperature glides at all.

## 4.2 Methods

To demonstrate when transcritical cycles, or cycles employing zeotropic mixtures, are relevant, an optimization model is developed. The model differentiates from most models reported in the literature [138–141] in the sense that it includes a robust optimization algorithm. This algorithm optimizes, among others, the pressure during heat delivery and the amount of subcooling. Both parameters have a large influence on the COP for transcritical, or near-transcritical, cycles [124, 128]. Moreover, an optimized subcooling also has a strong impact on the COP for subcritical cycles when used for applications with large temperature glides [142]. The model also optimizes the pressure during heat extraction and the amount of superheat, and covers a wet compression detection. In the event of binary mixtures, it also optimizes the mixture composition. Furthermore, it includes a proper post-processing so that only working fluids are reported that are practically relevant.

The basis of the optimization model is a thermodynamic model, which takes the industrial application (i.e. boundary conditions) and the heat pump operating conditions as input as shown in Figure 4.4. On top of this thermodynamic model a global optimizer maximizes the COP by varying the heat pump operating conditions. In order to find a technically feasible solution, several optimization constraints are applied to the global optimizer. The optimization is performed on a large set of working fluids. This set is obtained starting from the REFPROP 10.0 database of pure working fluids [130] subjected to a first fluid screening step. Once all optimal operating conditions and cycle variables are determined for each working fluid, post-processing is performed on these intermediate results by applying technical constraints, which eventually leads

to the reported results in this work. In what follows each of the steps in the methodology are explained in detail.

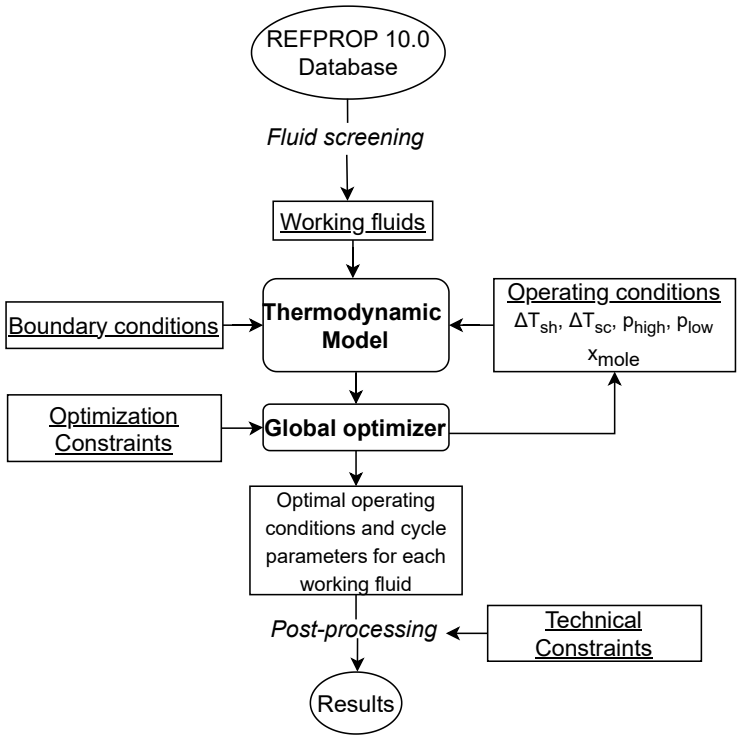


Figure 4.4: Flowchart of the thermodynamic optimization model.

### 4.2.1 Thermodynamic model

In order to estimate the performance of the heat pump cycle, a thermodynamic model in Python is developed. The model simulates a heat pump cycle which consists of a compressor, evaporator, condenser/gas cooler, expansion valve and optionally an IHX as shown in Figure 4.5. In this figure a number, or letter, for each state is given. These numbers, or letters, will be used throughout the result section to indicate the respective states. Depending on the case study, more complex cycles could be beneficial to increase the performance of the heat pump. However, it was not included in the scope of this work. In the literature, transcritical operation or binary zeotropic mixtures are frequently seen as a solution to increase performance without adding additional components to the cycle.

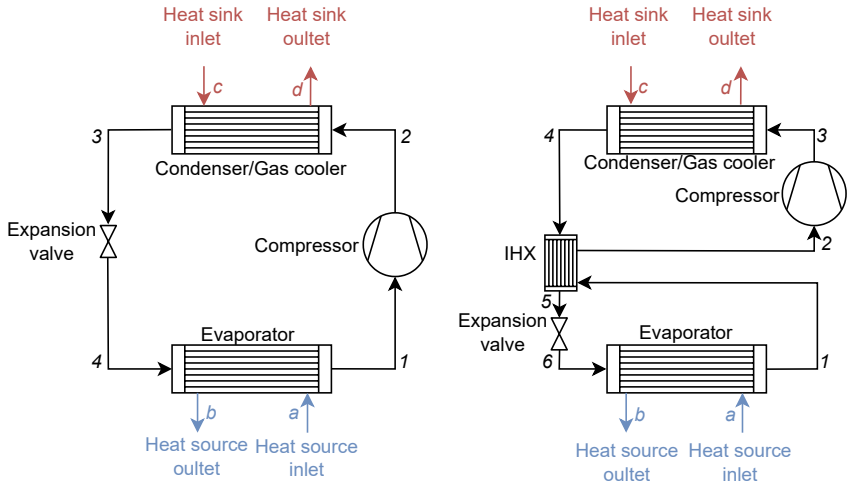


Figure 4.5: Single-stage heat pump cycle, without and with IHX.

The input parameters of the thermodynamic model are: heat sink inlet and outlet state, heat sink mass flow rate, heat pump operating conditions, the inlet state of the heat source and the mass flow rate of the heat source. Note that the heat sink is completely defined a priori, in contrast to the heat source outlet state, which depends on the amount of heat extracted and thus is a function of both the COP and the amount of heat supplied.

The variables defining the heat pump operating conditions are: pressure during heat extraction ($p_{low}$) and delivery ($p_{high}$), amount of superheat at the evaporator outlet ($\Delta T_{sh}$) and amount of subcooling at the condenser or gas cooler outlet ($\Delta T_{sc}$). For operation above the critical point (i.e. transcritical operation), subcooling is defined with respect to the critical temperature. Consequently, according to this definition, the subcooling can have a negative or positive sign. The definition of the superheat and subcooling remains valid when an IHX is used. Moreover, for the binary mixtures the molar fraction of the first constituent ($x_{mole}$) is also a variable. The different components of the heat pump cycle are modelled as described in the upcoming sections.

#### 4.2.1.1 Compressor model

The compressor is modelled by considering a fixed isentropic efficiency ($\eta_{is}$) of 75 % [12, 57] and a volumetric efficiency ($\eta_{vol}$) of 90 % [143]. Similar values were also found in experimental research, such as in the work of Mateu-Royo et al. [144], who constructed a prototype HTHP using R245fa as the working fluid. They performed an energy and exergy analysis for heat source

temperatures between 60 °C and 80 °C, and heat sink temperatures between 90 °C and 140 °C. The results showed an isentropic efficiency varying between from just under 70 % to somewhat over 80 %. Furthermore, volumetric efficiencies ranging from around 87 % to almost 100 % were observed.

Whereas advanced models exist that estimate these efficiencies based upon the operating conditions and/or fluid properties and/or compressor geometry, these are always developed for a specific compressor type and are only valid within a certain range of volume flow rates [83, 145, 146]. These compressor models can also accommodate zeotropic mixtures, with a dependency on the mixture composition [147]. When such models are employed, the optimal mixture composition will shift towards the component with the best individual compressor performance compared to scenarios assuming fixed efficiencies. However, in order to have a generally valid compressor model, fixed efficiencies are used in this work.

The compressor power ($\dot{W}_{comp}$) is calculated as the product of the working fluid mass flow rate ($\dot{m}_{wf}$) and the enthalpy difference over the compressor as shown in Equation 4.1:

$$\dot{W}_{comp} = \dot{m}_{wf} \cdot (h_{comp,out} - h_{comp,in}) \tag{4.1}$$

The enthalpy at the compressor outlet ($h_{comp,out}$) is calculated based on the enthalpy at the inlet of the compressor ($h_{comp,in}$) and the considered isentropic efficiency. An ideal mechanical and drive efficiency is considered, as such the calculated compressor work is equal to the electrical power. Furthermore, within the developed model, the occurrence of two-phase wet compression is monitored and the superheat can be increased if necessary to avoid wet compression.

#### 4.2.1.2 Heat exchanger model

Underwood [148] suggests that in close-coupled packaged plants, the pressure losses of the working fluid during heat transfer can be disregarded since they are typically insignificant. Therefore, pressure drops are not considered here. Furthermore, the heat losses to the environment are set to zero. Therefore, the heat transferred between the working fluid and secondary fluid can be considered equal. In the literature [20, 146, 149–151] both losses are commonly set to zero due to their minimal effects.

The heat transfer rate is calculated by multiplying the mass flow rate of the medium ($\dot{m}$) with the absolute value of enthalpy difference at the heat exchanger inlet ($h_{in}$) and outlet ($h_{out}$) as shown in Eq 4.2:

$$\dot{m}_{wf} \cdot |h_{wf,in} - h_{wf,out}| = \dot{m}_{sf} \cdot |h_{sf,in} - h_{sf,out}| \tag{4.2}$$

where the subscript 'wf' refers to 'working fluid' and the subscript 'sf' refers to 'secondary fluid'. The evaporator and condenser/gas cooler are sized assuming a theoretical limiting case by setting a predetermined pinch point temperature difference (PPTD), and the outlet states are defined by the imposed superheat or subcooling.

It should be noted, however, that with a suitable temperature match between working fluid and heat sink, transcritical cycles or zeotropic mixtures can introduce an overall small temperature difference during heat transfer, as shown in Figure 4.2 and Figure 4.3. This generally requires larger heat transfer surfaces when considering a fixed PPTD. Examining a fixed heat transfer surface for the heat exchanger is impractical due to the dependency of accurate heat transfer correlations in the literature that adequately model subcritical and supercritical heat exchangers for various working fluids under consideration [152]. Furthermore, the aim of this research is to examine the thermodynamic potential, rather than the financial potential. For the latter it should also be taken into account that transcritical cycles generally require smaller compressors [124]. However, it should be emphasized that in practical applications, a compromise may have to be made between the PPTD and the size of the heat exchanger. More information on the PPTD can be found in Section 4.2.2.

For the IHX, where no phase change occurs, a fixed effectiveness of 0.75 is used. To facilitate a valid comparison between the cycle with and without the IHX, the IHX has been engineered to exhibit a relatively high heat exchange effectiveness. Nevertheless, the effectiveness used is still within the range of the values reported within the literature [153–157]. Based on this effectiveness the working fluid outlet states can be determined.

#### 4.2.1.3 Expansion valve model

The expansion valve is assumed to be isenthalpic. The expansion losses in heat pumps employing conventional working fluids are generally small [118]. For transcritical cycles however, the larger pressure difference results in a higher potential of recovering the expansion work. Often studied expansion work recovery devices are expanders [158, 159] and ejectors [160, 161]. While the use of an expansion recovery device could be beneficial, its investigation is beyond the scope of this study. Therefore, these components are omitted. The potential of integrating an expander or ejector in transcritical cycles is however stressed.

#### 4.2.1.4 Heat pump performance parameters

Once all heat pump cycle states are determined, the COP can be calculated. The COP is calculated based on the amount of process heat supplied ($\dot{Q}_{process}$) and the compressor power ($\dot{W}_{comp}$) as shown in Equation 4.3:

$$COP = \frac{\dot{Q}_{process}}{\dot{W}_{comp}} \tag{4.3}$$

Next to the COP, the volumetric heating capacity (VHC) is a particularly important parameter as it gives an indication of the compressor size. For low VHCs, large compressors or high-speed compressors will be needed, driving up the heat pump investment cost. The VHC is calculated based on the volumetric efficiency ($\eta_{vol}$), the density of the working fluid at the compressor inlet ($\rho_{comp,in}$) and the difference in enthalpy over the condenser or gas cooler as shown in Equation 4.4.

$$VHC = \eta_{vol} \cdot \rho_{comp,in} \cdot (h_{cd,in} - h_{cd,out}) \tag{4.4}$$

#### 4.2.1.5 Model validation

To validate the thermodynamic model, case studies reported in the literature are simulated and the COP is compared. Next to implementing the heat source and sink boundary conditions, modeling assumptions such as PPTD or efficiencies are also adapted. An overview of the COP simulated by the thermodynamic model of this work and the COP reported in the literature can be found in Table 4.2. The table also indicates whether the working fluid operates in the subcritical regime or the transcritical regime.

Table 4.2: Comparison of the results of the developed model with the results reported in the literature.

| working fluid | Operational mode | COP: Current work | COP: Literature | Deviation (%) | Reference |
|---|---|---|---|---|---|
| Propane | Transcritical | 2.63 | 2.66 | 1.26 | [56] |
| Propane/Iso-pentane (50/50 wt %) | Subcritical | 3.05 | 3.09 | 0.97 | [56] |
| Propane/n-Pentane (40/60 wt %) | Subcritical | 2.99 | 3.02 | 0.99 | [56] |
| Propane/n-Pentane (80/20 wt %) | Subcritical | 3.00 | 3.04 | 1.31 | [56] |
| Propane/n-Butane (80/20 wt %) | Subcritical | 2.90 | 2.90 | 0 | [56] |
| Ethanol | Subcritical | 3.66 | 3.62 | 1.1 | [162] |
| R161 | Subcritical | 4.14 | 4.04 | 2.47 | [163] |

Based on Table 4.2 it can be concluded that the outcomes of the model align well with the results reported within the literature. Possible explanations for the small differences in COP could be differences in the REFPROP version, or rounding errors in the reported boundary conditions and results.

### 4.2.2 Optimization model

In the optimization algorithm, the COP calculated by the thermodynamic model (i.e. objective function), for a specific working fluid, is maximized. This objective function is maximized through optimizing the following input variables: superheat at the evaporator ($\Delta T_{sh}$), subcooling at the condenser ($\Delta T_{sc}$), pressure during heat extraction ($p_{low}$), pressure during heat delivery ($p_{high}$) and molar fraction of the first constituent in case of binary mixtures ($x_{mole}$). For each working fluid, both the heat pump cycle with and without IHX will be optimized.

The objective function contains many local maxima, hence a state-of-the-art global optimizer implemented in SciPy [164] is used to find the global optimum. The basin-hopping global optimizer was chosen as it showed the most robust and best results for a specified number of function evaluations. Prior to running the basin-hopping algorithm, a dual annealing optimization with a low number of function evaluations is performed to provide an initial guess for the basin-hopping algorithm.

In the optimization method several constraints are implemented on the output values. These constraints cannot be directly applied by putting bounds on the input variables because they require an evaluation of the actual heat pump cycle using the thermodynamic model. Hence penalties (i.e. soft constraints) are applied to the objective function when the constraints are not met. The penalty functions are tuned so that the optimization algorithm quickly converges to a solution for which none of the constraints are violated. Soft constraints are applied on three output values, namely the PPTD at the condenser or gascooler, the PPTD at the evaporator and the presence of wet compression. Constraints are imposed on the PPTD, because the COP would be optimal for a PPTD of zero, which would require infinitely large heat exchangers. Therefore, a PPTD of 5 K is imposed, which gives a suitable trade-off between COP and heat exchanger size [143]. Within each function evaluation of the optimization, the PPTD between working fluid and secondary medium is determined also by using an optimizer. This optimizer locates the point where the temperature difference between the two fluids is minimal.

The optimization strategy is computationally expensive due to the many local maxima of the objective function and the high number of working fluids to be considered. Hence, several techniques are applied to speed up the

optimization. First, the optimization can be parallelized over all available processor cores, so that on each core the cycle is optimized for a different working fluid. Second, different bounds on the optimization variables are chosen for subcritical, transcritical and supercritical cycles. By reducing the search space the optimization can be accelerated.
Overall, the optimization problem can be presented by:

$$
\begin{aligned}
&\textit{Maximize} && COP = f(p_{low}, p_{high}, \Delta T_{sh}, \Delta T_{sc}, (x_{mole}))\\
&\textit{Variables} && p_{low}, p_{high}, \Delta T_{sh}, \Delta T_{sc}, (x_{mole})\\
&\textit{Subject to} && PPTD_{high} = f(p_{high}, \Delta T_{sh}, \Delta T_{sc}, (x_{mole})) \geq 5\\
& && PPTD_{low} = f(p_{low}, \Delta T_{sh}, (x_{mole})) \geq 5\\
& && \chi_{comp,min} = f(p_{low}, p_{high}, \Delta T_{sh}) \notin [0, 1]\\
& && p_{low}^{L} \leq p_{low} \leq p_{low}^{U}\\
& && p_{high}^{L} \leq p_{high} \leq p_{high}^{U}\\
& && \Delta T_{sh}^{L} \leq \Delta T_{sh} \leq \Delta T_{sh}^{U}\\
& && \Delta T_{sc}^{L} \leq \Delta T_{sc} \leq \Delta T_{sc}^{U}\\
& && 0 \leq x_{mole} \leq 1
\end{aligned}
$$

with $\chi_{comp,min}$ the minimum working fluid vapour quality that occurs during the compression process, and the superscript 'L' referring to lower boundary and 'U' to upper boundary.

### 4.2.3 Working fluid selection

Most studies are restricted to working fluids that are currently used in practice. In this study however, all pure fluids within REFPROP 10.0 are being considered as potential working fluid. Nevertheless, these working fluids are first screened in terms of environmental aspects, thermal stability, toxicity and flammability. Only if they pass the screening procedure they will be simulated.

Based on all pure fluids that passed the screening procedure a pool of all binary possible mixtures is created. From this pool, mixtures where both constituents have a critical temperature below 160 °C are eliminated as the aim is to study these mixtures in the subcritical regime. It should be noted that for several binary mixtures, no binary interaction parameters (BIPs) are available. In these scenarios, the BIPs of similar working fluids are used or the BIPs are estimated. These BIPs influence the thermophysical properties of the mixtures, which can affect the performance and operating conditions of the optimized cycle. This is shown in the work of Abedini et al. [165], who showed that for the R1234ze(Z)/acetone mixture the optimized COP was 3.95 using the estimated BIPs. After tuning the BIPs based on experimental data, the COP changed to 3.94 (± 0.25 % change). For the R1234ze(Z)/isohexane

mixture, the COP using estimated BIPs was 3.90, while the optimum COP using BIPs based on experimental data was 3.83 (± 1.7 % change). Binary mixtures for which the BIPs are not available are still considered in this analysis. This is because the aim of this theoretical model is to provide a preliminary assessment of potential working fluids as a basis for experimental research. If BIPs are not available for the reported mixtures, this is mentioned throughout the analysis.

Additional elimination of working fluids, both pure as binary mixtures, may follow during post-processing when the enforced technical constrains, explained in Section 4.2.4, are not respected.

#### 4.2.3.1 Environmental aspects

All working fluids that have a GWP below 150 and do not deplete the ozone layer (ODP ≈ 0) are considered in this study. In this way, the EU-regulations regarding fluorinated GHG [166] and substances that deplete the ozone layer [167] are met.

#### 4.2.3.2 Thermal stability

The thermal stability/reactivity of the working fluid at higher temperatures can be characterized by the instability grade of the NFPA 704 standard [168]. This grade rates the chemical stability of a substance at elevated pressures and temperatures on a scale from 0 to 4. Substances with an instability grade of 1 can already become unstable at elevated pressures and temperatures. Therefore, working fluids with an instability grade equal to, or higher than, 1 are disregarded. Examples of well performing working fluids that are discarded due to their low chemical stability are: dimethyl ether, dimethyl carbonate, 1-pentene, 1,3-butadiene, trans-2-butene, or 1-butyne.

Whereas the NFPA 704 thermal stability grade gives an indication of violent chemical changes at higher pressures and temperatures such as explosive decomposition or detonation, the working fluid can also decompose over time when subjected to high pressures and temperatures (i.e. thermolysis). Decomposition of the working fluid can lead to a reduction in thermal efficiency because of the change in operating conditions [169]. Moreover, decomposition products such as non-condensable gases or deposits could damage the components and induce safety concerns [169]. In addition, if the working fluid would depreciate over a short time interval it would show less favourable financial appraisal than expected [170]. Therefore, it is crucial that the working fluid shows no, to low, thermolysis at the targeted temperatures and pressures. Consequently, working fluids that start to decompose below 200 °C are eliminated.

#### 4.2.3.3 Flammability

Flammability and explosion concerns may withhold use of working fluids such as hydrocarbons. An exception is the chemical industry where the processes may already be protected [171]. However, when correctly handled and installed, flammable working fluids are safe to use [172]. Several use cases of such flammable working fluids at high temperatures and pressures can be found. Bamigbetan et al. [23] constructed a laboratory-scale HTHP, supplying heat up to 115 °C. The heat pump is a cascaded cycle making use of propane in the low-temperature cycle and butane in the high-temperature cycle. The heap pump design is based on components that are commercially available. Furthermore, several HTHP manufacturers (Mayekawa, Johnson Controls, etc.) offer commercial available HTHPs making use of hydrocarbons for supply temperatures up to 145 °C [13]. In the field of ORCs, the use of hydrocarbons is more prevalent. Galindo et al. [173], constructed an experimental ORC making use of ethanol as working fluid to recover waste heat from a gasoline engine. For this set-up exhaust gas inlet temperatures up to 673 °C were tested. Furthermore, several ORC manufacturers (Ormat, Turboden, Atlas Copco, etc.) make use of hydrocarbons such as cyclo-pentane, iso-pentane or n-butane for waste heat temperatures well above 200 °C [174]. Therefore, no constraint is placed upon the flammability. Instead, in contrast to most literature, two scenarios are considered: one where flammable fluids are allowed and one where they are not allowed. For the flammability grade, the ASHRAE 34 standard [175] is used which classifies the flammability in four grades. In the scenario that flammability is a concern, highly flammable fluids (class 3) and flammable fluids (class 2) will be disregarded whereas non-flammable fluids (class 1) and mildly flammable fluids (class 2L) will be considered.

Whereas no direct limitation is placed upon the flammability grade a limitation will be placed upon the auto-ignition temperature. If the compressor discharge temperature without (external) cooling method exceeds the auto-ignition temperature the fluid will be eliminated from the results. In this way the system can safely operate even when the (external) cooling fails.

#### 4.2.3.4 Toxicity

Ideally, the working fluid is non-toxic. However, toxic working fluids such as ammonia are widely used in heat pumps and refrigeration machines. Ammonia has the highest toxicity grade according to the ASHRAE 34 standard (class B) and a health-grade of 3 out of 4 according to the NFPA 704 standard. With ammonia set as boundary for the maximum toxicity, working fluids with an NFPA 704 health-grade of 4 will be disregarded from the analysis.

#### 4.2.3.5 Overview of selected working fluids

An overview of the working fluid selection of the pure working fluids can be found in Appendix E. In this appendix it is indicated whether the working fluid passed the imposed GWP limitation, ODP limitation, NFPA 704 instability limitation and NFPA 704 health limitation. For some working fluids no NFPA 704 standard was found, so the instability and health grade was named 'unknown'. These working fluids were not eliminated by the screening procedure. However, when these working fluids show to be among the best performing working fluids, its instability grade and health hazard should be carefully studied.

### 4.2.4 Technical constraints

As indicated in the optimization model and fluid selection, some working fluids may not be considered because they result in unrealistic technical requirements. The imposed technical requirements are described in the upcoming sections.

#### 4.2.4.1 Compressor discharge temperature

The compressor discharge temperature should be kept as low as possible for various reasons. First of all, the working fluid-oil mixture might become thermally unstable at higher temperatures when the compressor is lubricated [12]. In addition, oil degradation may occur when subjected to prolonged high temperatures [23]. Furthermore, a high compressor discharge temperature poses challenges in the heat management and wear of the compressor and materials of the equipment [12].

Whereas high compressor discharge temperatures may cause severe issues when not appropriately handled, no constraint is placed upon the compressor discharge temperature because several techniques exist to reduce it. Examples are: two-phase compression, vapour or liquid injection and intercooling [176, 177]. These cooling techniques can reduce the specific compressor power. However, it may involve a trade-off because less heat will be delivered during heat rejection when the discharge temperature decreases. Furthermore, for applications with a large temperature glide, the reduction of the compressor discharge temperature leads to an increase in pressure during heat rejection in order to respect the implemented PPTD, as can be observed in Figure 4.6. A similar behaviour was observed in the work of Arpagaus et al. [129], who found that for applications with large temperature glide a transcritical cycle with parallel compression did not lead to improved COPs compared to a conventional transcritical cycle with IHX. The reason for this is that the

cycle making use of parallel compression reduces the discharge temperature. For applications with lower temperature glides, the effect is however less outspoken.

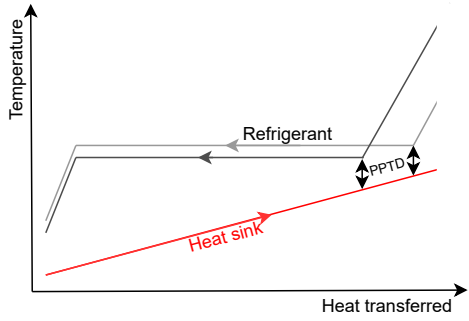


Figure 4.6: Illustration of the effect of a decrease of compressor discharge temperature on the heat rejection pressure.

For these reasons, it is expected that these methods to reduce the discharge temperature do not offer any, or limited, advantages in terms of COP for applications with large temperature glides. For applications with lower temperatures glides this is may not be true. However, no cycle configuration to reduce the compressor discharge temperature is implemented. This because a large amount of configurations exists. Furthermore, no exact boundary can be defined on the maximum discharge temperature as this strongly depends on the compressor design.

#### 4.2.4.2 Pressure ratio

The pressure ratio should be as low as possible. For high pressure ratios, multiple compression stages may be required. This would strongly increase the investment cost and the complexity of the heat pump system. Considering that single compressor units typically have a pressure ratio of about 4-5 [178–181], this study imposes a maximum pressure ratio of 20 so that no more than two compression stage should be used.

#### 4.2.4.3 Pressure levels

The maximum allowable discharge pressure for most commercial working fluid compressors is around 30 bar [12, 178–180, 182, 183]. However, some compressors are being designed for pressures in the range of 50 bar to 60 bar [12, 178, 179, 182, 184], e.g for use of ammonia or R32. Furthermore, some transcritical $CO_2$ compressors are specifically designed for discharge

pressures up to 140 bar to 150 bar [124, 178, 179, 184]. Because of, among others, the low pressure ratio of $CO_2$ compressors, these compressors are not suitable for other working fluids [124]. Therefore, a maximum compressor discharge pressure of 60 bar is assumed for all other working fluids than $CO_2$ in this study. For $CO_2$, a maximum compressor discharge pressure of 150 bar is implemented.

Next to the limitations on the maximum discharge pressure, there is a limitation on the minimum pressure within the heat pump system. If the minimum pressure is below the atmospheric pressure, air may infiltrate in the system, if not well sealed. This may introduce undesired effects on the operation of the heat pump system. However, a moderate level of vacuum is permissible. A boundary of 0.5 bar as minimum pressure is selected as also applied by Frate et al. [150]. This constraint caused for example the elimination of dimethyl carbonate.

### 4.2.5 Boundary conditions

As previously stressed, transcritical operation can show beneficial effects in the event of large temperature glides at the heat sink side. Therefore, three representative industrial case studies with large heat sink temperature glides ($\geq$ 60 K) are selected, rather than generic data. The thermal oil heating case study, superheated steam drying case study and spray drying with external heat source case study described in Section 2.4.3 are considered. The temperature glides at the heat sink side for these case studies are 60 K, 81 K and 105 K respectively.

Regarding the zeotropic binary mixtures, applications are selected where the temperature glides are of a lower magnitude because of the risk of fractionation. Furthermore, there is also a focus on the temperature glide of the heat source, rather than the heat sink alone. Unlike for the transcritical operation, generic case studies are now considered. Four case studies are selected which differ in temperature glide at the heat source and heat sink. The heat source and heat sink inlet and outlet temperatures of the four case studies can be found in Table 4.3. The small heat source temperature glide of 20 K is typically found in cooling loops, while the heat sink temperature glide of 20 K is typically found in a wide range of applications such as (pressurized) hot water production or thermal oil heating.

Table 4.3: Selected generic temperature profiles for the zeotropic mixture boundary conditions.

| **Case** | $T_{source,in}$ [°C] | $T_{source,out}$ [°C] | $T_{sink,in}$ [°C] | $T_{sink,out}$ [°C] |
|---|---|---|---|---|
| I | 120 | 100 | 160 | 180 |
| II | 120 | 100 | 180 | 180 |
| III | 100 | 100 | 160 | 180 |
| IV | 100 | 100 | 180 | 180 |

These case studies differ in the sense that they either show a temperature glide at both the heat source and heat sink (Case I), a temperature glide only at the heat source (Case II), a temperature glide only at the heat sink (Case III), or no temperature glide at all (Case IV).

## 4.3 Results - Transcritical operation

For each case study selected for transcritical operation, the best performing working fluids with their optimized operating conditions ($p_{low}$, $p_{high}$, $\Delta T_{sh}$ and $\Delta T_{sc}$) are reported in a table. The table also reports the pressure ratio (PR), COP, VHC, compressor discharge temperature ($T_{comp,d}$), cycle type, i.e. subcritical (SC) or transcritical (TC), and whether or not the cycle optimally makes use of an IHX.

### 4.3.1 Case I: Thermal oil heating

The results of the best performing working fluids in terms of COP for the thermal oil heating case can be found in Table 4.4.

Table 4.4: Results of the best performing fluids for the thermal oil heating case.

| Fluid | $p_{low}$ [bar] | $p_{high}$ [bar] | PR [-] | $\Delta T_{sh}$ [°C] | $\Delta T_{sc}$ [°C] | COP [-] | VHC $[kJ/m^3]$ | $T_{comp,d}$ [°C] | Cycle [-] | IHX [-] |
|---|---|---|---|---|---|---|---|---|---|---|
| Acetone | 2.5 | 23.1 | 9.4 | 0.0 | 44.2 | 3.34 | 2545 | 250 | SC | Yes |
| Benzene | 1.2 | 13.6 | 11.7 | 0.0 | 51.5 | 3.33 | 1315 | 232 | SC | Yes |
| Ethanol | 1.3 | 23.4 | 18.2 | 10.2 | 43.0 | 3.31 | 1858 | 300 | SC | Yes |
| Cyclobutene | 10.6 | 53.3 | 5.0 | 10.4 | 29.9 | 3.30 | 7454 | 231 | TC | Yes |
| Methanol | 2.1 | 31.7 | 14.9 | 0.7 | 42.6 | 3.29 | 3047 | 296 | SC | No |
| Cyclohexane | 1.1 | 13.7 | 12.1 | 9.7 | 56.3 | 3.29 | 1243 | 213 | SC | Yes |
| Cyclopentane | 2.8 | 25.0 | 8.8 | 10.4 | 50.7 | 3.29 | 2681 | 224 | SC | Yes |
| Pentane | 4.1 | 31.2 | 7.5 | 10.3 | 46.6 | 3.28 | 3371 | 210 | SC | Yes |
| R1336mzz(Z) | 4.9 | 35.9 | 7.4 | 10.3 | 26.4 | 3.26 | 3815 | 209 | TC | Yes |
| R1233zd(E) | 7.4 | 43.1 | 5.9 | 10.0 | 21.5 | 3.26 | 5338 | 217 | TC | Yes |
| Isopentane | 5.1 | 35.0 | 6.9 | 10.1 | 42.2 | 3.26 | 3878 | 208 | TC | Yes |
| Isohexane | 2.1 | 21.8 | 10.5 | 9.6 | 57.1 | 3.25 | 1945 | 207 | SC | Yes |
| 3-Methylpentane | 1.9 | 20.7 | 10.9 | 10.3 | 58.5 | 3.24 | 1812 | 206 | SC | Yes |
| 2.3-Dimethylbutane | 2.2 | 22.5 | 10.3 | 9.0 | 59.4 | 3.23 | 2019 | 205 | SC | Yes |
| 2.2-Dimethylbutane | 2.7 | 25.7 | 9.4 | 9.4 | 58.4 | 3.22 | 2357 | 205 | SC | Yes |

#### 4.3.1.1 Working fluids and performance

Based on the reported results in Table 4.4 it can be observed that classical subcritical cycles have a slightly higher COP compared to transcritical cycles for this case study with a heat sink temperature glide of 60 K. For subcritical cycles COPs up to 3.34 are observed, while for transcritical cycles COPs up to 3.30 are observed. Acetone, benzene and ethanol, which are not yet used in HTHPs, are found to be the best performing fluids for subcritical cycles whereas cyclobutene, R1336mzz(Z) and R1233zd(E) are found to be the best performing fluids resulting in transcritical cycles.

All reported fluids, with the exception of methanol, have a higher COP when an IHX is added. Methanol already has a compressor discharge temperature of about 300 °C, even without IHX. The addition of an IHX would strongly increase this temperature and would therefore also induce a lot of exergy destruction.

#### 4.3.1.2 Operating conditions

Both the subcritical and transcritical cycles have a considerable amount of subcooling (i.e. $\Delta T_{sc}$) when optimized in order to maximize the heat output for a given amount of compression work. These high subcooling values can be observed in the T,s-diagrams of the best performing subcritical and transcritical cycles as illustrated in Figure 4.7. In these cycles an IHX is used. Typically, the optimal amount of subcooling is adjusted so that, next to an

already existing pinch point, a new pinch point nearly appears at the location where the working fluid leaves the heat exchanger. This behaviour is also observed in the literature [142]. A similar behaviour is sometimes, although not always, observed for the superheat. The increase in superheat for subcritical cycles however leads to a high compressor discharge temperature, involving a trade-off. For transcritical cycles however, the discharge temperature is limited because of the temperature match at the gas cooler.

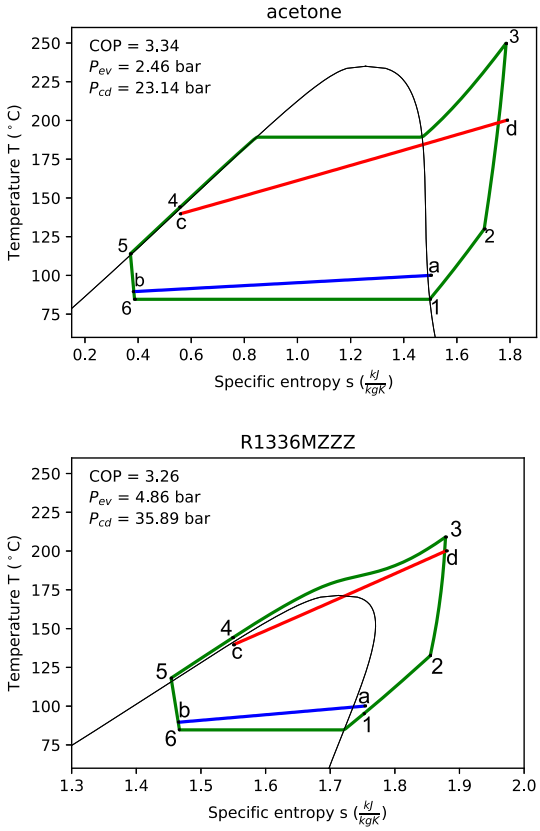


Figure 4.7: T,s-diagram, with scaled entropy for secondary fluid, for the best performing subcritical cycle (top) and transcritical cycle (bottom) for the thermal oil heating case study.

Next to the lower compressor discharge temperature it can be observed that transcritical cycles have much higher VHCs and considerably lower pressure ratios. For the reported transcritical cycles, the VHC varies between 3815-7454 kJ/$m^3$ and the pressure ratio between 5-7.5, whereas for subcritical cycles the

VHC varies between 1065-3371 kJ/$m^3$ and the pressure ratio varies between 7.5-18.2. Therefore, use of transcritical cycles could already be beneficial for heat sink temperature glides of 60 K and lower when considering the heat pump design next to the performance. Cyclobutene, whose potential is not yet reported in literature, is found to be particularly suitable because of the combination of its high COP and high VHC. A particular disadvantage of transcritical operation however is the associated high compressor discharge pressure. For the subcritical cycles the compressor discharge pressure varies between 13.6-31.7 bar whereas for the transcritical cycles it varies between 35-53.3 bar.

### 4.3.2 Case II: Superheated steam drying

The results of the working fluids with the highest COP for the SSD case are reported in Table 4.5.

Table 4.5: Results of the best performing fluids for the superheated steam drying case.

| Fluid | $p_{low}$ [bar] | $p_{high}$ [bar] | PR [-] | $\Delta T_{sh}$ [°C] | $\Delta T_{sc}$ [°C] | COP [-] | VHC [$kJ/m^3$] | $T_{comp,d}$ [°C] | Cycle [-] | IHX [-] |
|---|---|---|---|---|---|---|---|---|---|---|
| R1336mzz(Z) | 6.2 | 43.3 | 6.9 | 0.0 | 50.4 | 4.32 | 5607 | 202 | TC | Yes |
| R1234ze(Z) | 12.1 | 57.1 | 4.7 | 1.5 | 29.1 | 4.31 | 9488 | 202 | TC | Yes |
| R1233zd(E) | 9.3 | 47.8 | 5.1 | 1.1 | 45.5 | 4.30 | 7708 | 202 | TC | Yes |
| Cyclobutene | 13.1 | 54.3 | 4.1 | 2.3 | 53.9 | 4.29 | 10204 | 208 | TC | Yes |
| Cis-2-Butene | 12.8 | 55.6 | 4.4 | 1.5 | 41.6 | 4.26 | 9643 | 203 | TC | Yes |
| Isopentane | 6.4 | 40.0 | 6.2 | 0.0 | 66.2 | 4.26 | 5456 | 202 | TC | Yes |
| Pentane | 5.3 | 35.0 | 6.6 | 0 | 75.6 | 4.20 | 4746 | 202 | TC | Yes |
| R1224yd(Z) | 10.3 | 55.3 | 5.4 | 1.8 | 34.5 | 4.20 | 8256 | 202 | TC | Yes |
| Acetone | 3.3 | 23.1 | 7.1 | 2.99 | 68.0 | 4.20 | 3585 | 222 | SC | Yes |
| Ethanol | 1.9 | 22.4 | 12.0 | 0.0 | 64.9 | 4.13 | 2817 | 258 | SC | Yes |
| Methanol | 3.0 | 28.5 | 9.5 | 0.0 | 61.3 | 4.12 | 4307 | 267 | SC | No |
| Cyclopentane | 3.7 | 26.8 | 7.3 | 0.0 | 79.8 | 4.03 | 3732 | 204 | SC | Yes |
| Benzene | 1.6 | 14.2 | 9.1 | 0.0 | 78.2 | 4.01 | 1871 | 209 | SC | Yes |

#### 4.3.2.1 Working fluids and performance

Now, for a case study with a temperature glide of 81 K at the heat sink side, transcritical cycles show better performance in terms of COP compared to subcritical cycles. The COP of the best performing transcritical cycle is 4.32 whereas the COP of the best performing subcritical cycle is 4.13. Consequently, a COP increase of 4.6 % can be achieved by using transcritical cycles. The HFOs or HCFOs R1336mzz(Z), R1234ze(Z) and R1233zd(E) are found to be the best performing fluids for transcritical cycles. These working fluids are already

being experimentally investigated for HTHPs, but at lower temperatures (< 160 °C), operating in the subcritical regime [144, 185, 186]. Its potential for higher operational temperatures, by operating in the transcritical region, is yet to be unlocked. Ethanol, methanol and acetone are found to be the best performing fluids for subcritical cycles. Again, the most optimal heat pump cycle always makes use of an IHX, with the exception of methanol.

#### 4.3.2.2 Operating conditions

As for the thermal oil heating case study, the subcooling is high and almost induces a new pinch point. The amount of superheat however, is now often close to zero because of the latent heat source. The transcritical cycles again show much higher VHCs, lower pressure ratios and lower compressor discharge temperatures on average. For almost all transcritical cycles, with the exception of cyclobutene and cis-2-butene, the minimum possible compressor discharge temperature of 202 °C is observed. The compressor discharge pressures for transcritical cycles are again high and are somewhat increased compared to the thermal oil heating case, even though the heat sink outlet temperature of the SSD case study (197 °C) is 3 °C lower compared to the thermal oil heating case study (200 °C). The increase in compressor discharge pressure is a result of the lower heat sink inlet temperature, while the heat source temperature remains similar. For lower heat sink inlet temperature the potential for the IHX decreases. Consequently, higher compressor discharge pressures are observed for this case study. It causes an increase of compressor discharge pressure of 26 % for R1336mzz(Z) when comparing the SSD case with the thermal oil heating case. This is clearly shown in Figure 4.8, which shows the T,s-diagram of R1336mzz(Z) for both the thermal oil heating case study and the SSD case study.

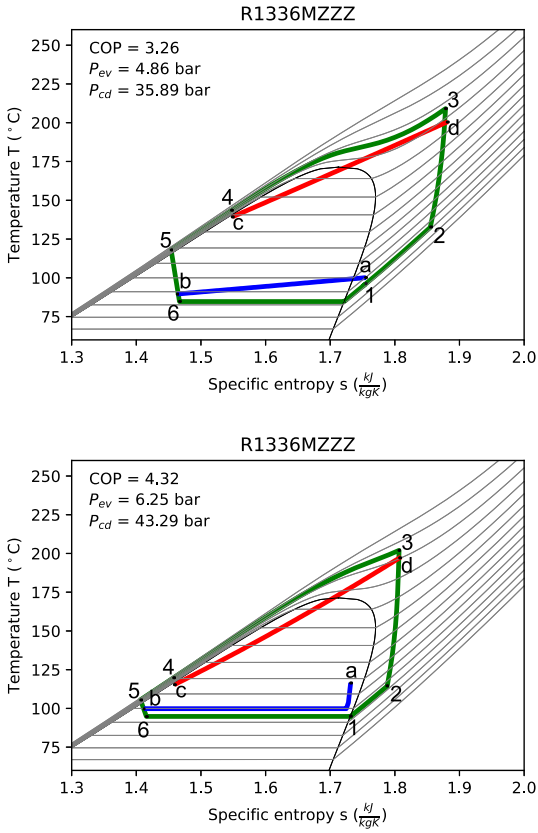


Figure 4.8: T,s-diagram of R1336mzz(Z), with scaled entropy for the secondary fluid and isobars, when applied to the thermal oil heating case study (top) and the SSD case study (bottom).

### 4.3.3 Case III: Spray drying with external heat source

The results of the best performing working fluids for the spray drying with external heat source case study are reported in Table 4.6.

Table 4.6: Results of the best performing optimized fluids for the spray drying case study with external heat source.

| Fluid | $p_{low}$ [bar] | $p_{high}$ [bar] | PR [-] | $\Delta T_{sh}$ [°C] | $\Delta T_{sc}$ [°C] | COP [-] | VHC $[kJ/m^3]$ | $T_{comp,d}$ [°C] | Cycle [-] | IHX [-] |
|---|---|---|---|---|---|---|---|---|---|---|
| R1336mzz(Z) | 4.7 | 53.4 | 11.3 | 0.0 | 71.4 | 4.25 | 4855 | 205 | TC | Yes |
| R1233zd(E) | 7.2 | 52.9 | 7.4 | 11.4 | 66.5 | 4.18 | 6887 | 205 | TC | Yes |
| Isopentane | 5.0 | 43.1 | 8.6 | 11.4 | 83.4 | 4.14 | 4727 | 205 | TC | Yes |
| Cyclobutene | 10.4 | 56.0 | 5.4 | 11.4 | 74.9 | 4.12 | 9194 | 208 | TC | Yes |
| Pentane | 4.0 | 36.9 | 9.1 | 11.3 | 90.0 | 4.03 | 4009 | 205 | TC | Yes |
| Acetone | 2.4 | 23.6 | 9.8 | 11.3 | 90.3 | 3.96 | 2957 | 222 | SC | Yes |
| Methanol | 2.1 | 25.4 | 12.3 | 8.1 | 76.8 | 3.89 | 3233 | 296 | SC | No |
| Ethanol | 1.2 | 23.2 | 18.6 | 0.0 | 87.6 | 3.89 | 2141 | 250 | SC | No |
| Cyclopentane | 2.8 | 28.7 | 10.3 | 11.1 | 103.5 | 3.83 | 3156 | 205 | SC | Yes |
| Benzene | 1.1 | 15.5 | 13.6 | 10.8 | 104.7 | 3.77 | 1528 | 205 | SC | No |

#### 4.3.3.1 Working fluids and performance

Now, for an application where the heat sink has a temperature glide of 105 K, transcritical cycles have even better performance compared to subcritical cycles. The best performing transcritical cycle with R1336mzz(Z) as working fluid has a COP of 4.25 while the best performing subcritical cycle, using acetone as a working fluid, has a COP of 3.96. This corresponds to a COP increase of 7.3%. Acetone, methanol and ethanol are again the best performing subcritical fluids while R1336mzz(Z), R1233zd(E) and isopentane are the best performing transcritical fluids. R1234ze(Z) also showed good performance but was eliminated from the results because the imposed maximum compressor discharge pressure of 60 bar was exceeded due to the low potential for internal heat exchange.

#### 4.3.3.2 Operating conditions

Similar operating conditions as for the previous case studies are found. Namely that transcritical cycles mostly have more favourable pressure ratios, higher VHCs and lower compressor discharge temperatures. However, again they have high compressor discharge pressures. Moreover, a similar behaviour in optimal superheating and subcooling is observed as for previous cases.

### 4.3.4 Influence of the internal heat exchanger

Based on the results of the three case studies it can be observed that most working fluids can attain a higher COP when an IHX is included in the cycle. Although the use of an IHX is common practice in heat pumps, its influence on the cycle performance and operating conditions for applications with high

temperatures and large temperature glides at the heat sink is less studied. Consequently, this section analyzes the effect of the IHX on the cycle performance and operating conditions for the three considered case studies. Therefore, the COP, compressor discharge pressure, pressure ratio and compressor discharge temperature for two subcritical fluids and two transcritical fluids are reported in Table 4.7, both for the scenario with IHX and without IHX. Acetone and benzene are selected as subcritical fluids whereas R1336mzz(Z) and R1233zd(E) are selected as transcritical fluids.

Table 4.7: Influence of IHX on two subcritical fluids and two transcritical fluids for the three selected case studies.

| Working fluid | IHX | COP [-] | $p_{high}$ [bar] | PR [-] | $T_{comp,d}$ [°C] |
|---|---|---|---|---|---|
| Case 1: Thermal oil heating | | | | | |
| R1336mzz(Z) | ✓ | 3.26 | 35.9 | 7.4 | 209 |
| | ✗ | 2.67 | 56.2 | 11.3 | 205 |
| R1233zd(E) | ✓ | 3.26 | 43.1 | 5.9 | 217 |
| | ✗ | 2.80 | 55.8 | 7.5 | 205 |
| Acetone | ✓ | 3.34 | 23.1 | 9.4 | 250 |
| | ✗ | 3.18 | 25.9 | 10.2 | 223 |
| Benzene | ✓ | 3.33 | 13.8 | 11.7 | 233 |
| | ✗ | 3.11 | 15.6 | 13.3 | 205 |
| Case 2: Superheated steam drying | | | | | |
| R1336mzz(Z) | ✓ | 4.32 | 43.3 | 6.9 | 202 |
| | ✗ | 3.71 | 51.0 | 10.0 | 202 |
| R1233zd(E) | ✓ | 4.30 | 47.8 | 5.1 | 202 |
| | ✗ | 4.04 | 58.1 | 6.3 | 202 |
| Acetone | ✓ | 4.17 | 23.1 | 7.1 | 222 |
| | ✗ | 4.05 | 25.4 | 7.8 | 210 |
| Benzene | ✓ | 4.00 | 14.2 | 9.1 | 209 |
| | ✗ | 3.69 | 14.9 | 11.3 | 202 |
| Case 3: Spray drying with external heat source | | | | | |
| R1336mzz(Z) | ✓ | 4.25 | 53.4 | 11.3 | 205 |
| | ✗ | 4.24 | 54.4 | 11.6 | 205 |
| R1233zd(E) | ✓ | 4.18 | 52.9 | 7.4 | 205 |
| | ✗ | 4.11 | 59.8 | 8.3 | 205 |
| Acetone | ✓ | 3.96 | 23.6 | 9.8 | 222 |
| | ✗ | 3.94 | 24.1 | 10.0 | 219 |
| Benzene | ✓ | 3.77 | 15.4 | 10.6 | 206 |
| | ✗ | 3.77 | 15.5 | 13.6 | 206 |

For the thermal oil heating case, it can be observed that the use of an IHX has a large influence on the heat pump cycle. For R1336mzz(Z) a COP increase of 22

% and a gas cooler pressure decrease of 57 % is observed, while the compressor discharge temperature increased with about 4 °C. For the other working fluids, smaller but still considerable COP increases and pressure decreases are being observed. Because of the decrease in compressor discharge pressure, the pressure ratio also decreased. For subcritical cycles however the increase in performance due to the use of an IHX is typically lower. R1336mzz(Z) showed an exceptionally strong increase in COP because of its overhanging fluid saturation curve. More generally, IHXs provide a very efficient way to avoid wet compression when wet fluids are used. The advantages of the IHX may come at the cost of an increased compressor discharge temperature. Especially for subcritical cycles, the compressor discharge temperatures show an increase when using an IHX. For transcritical cycles this is less of an issue.

For the SSD case similar conclusions as for the thermal oil heating case can be drawn. A difference however, is that now the minimum compressor discharge temperature is found for the transcritical cycles regardless of the use of an IHX.

For the spray drying with external heat source, use of an IHX has minimal influence on the heat pump cycle states and therefore the COP and operating conditions. The reason is that the heat sink and heat source inlet temperatures slightly cross. Consequently, only a limited amount of heat can be internally recuperated as displayed in Figure 4.9.

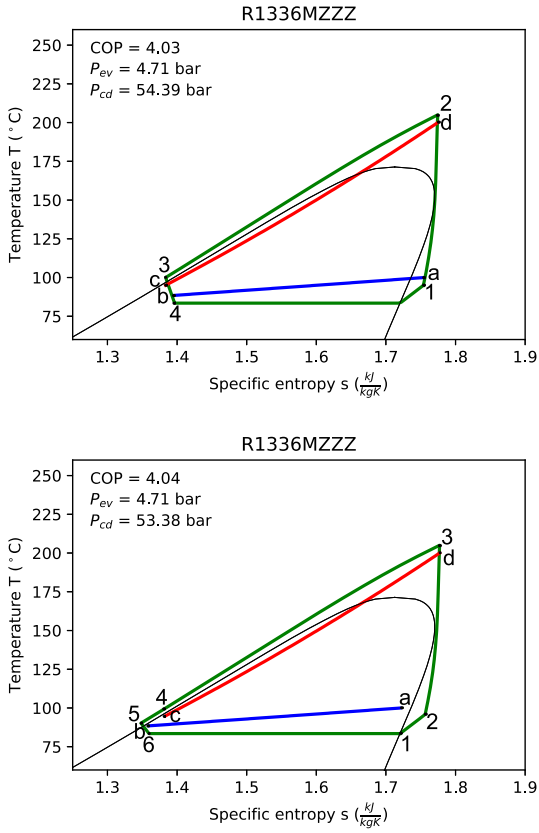


Figure 4.9: T,s-diagram of R1336mzz(Z), with scaled entropy for secondary fluid, without (top) and with (bottom) IHX for the spray drying with external heat source case study.

### 4.3.5 The use of non-flammable or low-flammability working fluids

All reported subcritical fluids (e.g. acetone, benzene or methanol) are highly flammable. For the transcritical cycles, some highly flammable fluids are observed as well (e.g. isopentane, cyclobutene). However, HFOs and HCFOs were frequently the best performing fluids with transcritical cycles. The HFOs/HCFOs are either inflammable or mildly flammable. Therefore, if highly flammable fluids or flammable fluids would not be allowed on the industrial site, the impact for the transcritical cycles would be minimal, or there would be no impact at all. For the subcritical cycles however the impact would be larger. The only appropriate pure working fluid would be water. Using water

as working fluid for these selected cases shows however lower COPs and less favourable operating conditions compared to the HFOs/HCFOs. The results for water as working fluid for each case study can be found in Table 4.8.

Table 4.8: Results of the best performing non-flammable or mildly flammable subcritical cycles for the selected case studies.

| Case | Fluid | $p_{low}$ [bar] | $p_{high}$ [bar] | PR [-] | $\Delta T_{sh}$ [°C] | $\Delta T_{sc}$ [°C] | COP [-] | VHC $[kJ/m^3]$ | $T_{comp,d}$ [°C] | IHX [-] |
|---|---|---|---|---|---|---|---|---|---|---|
| Oil heating | Water | 0.58 | 12.2 | 21.2 | 0.0 | 43.9 | 3.09 | 1065 | 569 | No |
| SSD | Water | 0.84 | 10.8 | 12.9 | 0.0 | 62.4 | 3.75 | 1477 | 488 | No |
| Hot air drying | Water | 0.54 | 9.8 | 18.1 | 0.0 | 79.1 | 3.47 | 1045 | 534 | No |

This table shows that use of water as a working fluid is at first sight less advantageous compared to the HFOs/HCFOs. The pressure during heat extraction is below the atmospheric pressure. This may result in potential air infiltration. Furthermore the low pressure induces a low density of the water vapour at the compressor inlet, resulting in low VHCs, ranging from 1065-1477 $kJ/m^3$. The VHCs of the HFOs/HCFOs on the other hand range from 3815-9488 $kJ/m^3$. Moreover, the low pressures during heat extraction results in large pressure ratios. Pressure ratios in the range of 12.89-21.20 are observed when using water, whereas for the HFOs/HCFOs they range from 4.7 to 11.7. Furthermore, the compressor discharge temperature is high (up to 569 °C) when using water as working fluid. Therefore, a method to reduce the compressor discharge temperature will be required, whereas for the HFOs/HCFOs this is not needed as the compressor discharge temperatures are low. Water has, however, next to its favourable environmental properties the advantage of not needing an IHX. Compared to the best performing HFO/HCFO, the COP of water is 5.5%, 15.2% and 22.5% lower for the oil heating case, SSD case and the hot air drying case respectively. Again, it can be observed that for larger temperature glides, transcritical cycles become more efficient.

## 4.4 Results - Zeotropic binary mixtures

The analysis for zeotropic mixtures is similar as for transcritical cycles (Section 4.3), but different cases are used. For each case the best performing working fluid is selected and the results of the optimized operating conditions are reported in a table, combined with the PR, COP, VHC, $T_{comp,d}$ and whether the cycle optimally makes use of an IHX. Two tables are now however made, one for the mixtures and one for the pure working fluids. When the results of the mixtures are reported, the optimized molar fraction ($x_{mole}$) of the first constituent is directly given after the name of the working fluid.

### 4.4.1 Case I: Temperature glide at both the heat sink and heat source

In case I there is a temperature glide of 20 K at both the heat source and heat sink. The results of the five best performing binary mixtures in terms of COP for case I, can be found in Table 4.9. The results of three the best performing pure working fluids can be found in Table 4.10.

Table 4.9: Results of the five best performing binary mixtures - Case I. * BIPs not available for fluid.

| Fluid | $p_{low}$ [bar] | $p_{high}$ [bar] | PR [-] | $\Delta T_{sh}$ [°C] | $\Delta T_{sc}$ [°C] | COP [-] | VHC $[kJ/m^3]$ | $T_{comp,d}$ [°C] | IHX [-] |
|---|---|---|---|---|---|---|---|---|---|
| Acetone/toluene (0.48) | 1.83 | 9.50 | 5.2 | 0 | 0 | 4.30 | 1754 | 220 | Yes |
| Cyclopentane/toluene (0.48)* | 1.82 | 9.15 | 5.0 | 0 | 0 | 4.28 | 1521 | 212 | Yes |
| Decane/toluene (0.17) | 0.51 | 3.52 | 6.9 | 3.8 | 4 | 4.27 | 518 | 207 | Yes |
| Acetone/water (0.43) | 2.69 | 16.19 | 6 | 0 | 8.24 | 4.22 | 3023 | 253 | No |
| Benzene/methanol (0.75) | 2.97 | 15.24 | 5.1 | 0 | 0 | 4.16 | 2764 | 229 | Yes |

Table 4.10: Results of the three best performing pure working fluids - Case I.

| Fluid | $p_{low}$ [bar] | $p_{high}$ [bar] | PR [-] | $\Delta T_{sh}$ [°C] | $\Delta T_{sc}$ [°C] | COP [-] | VHC $[kJ/m^3]$ | $T_{comp,d}$ [°C] | IHX [-] |
|---|---|---|---|---|---|---|---|---|---|
| Toluene | 0.64 | 5.3 | 8.33 | 20 | 19.3 | 3.85 | 642 | 223 | Yes |
| Benzene | 1.57 | 10.40 | 6.62 | 20 | 15.69 | 3.81 | 1396 | 231 | Yes |
| Cyclohexane | 1.53 | 9.90 | 6.49 | 20 | 16.41 | 3.78 | 3.78 | 212 | Yes |

#### 4.4.1.1 Working fluids and performance

Based on the reported results in Table 4.9 and Table 4.10 it can be observed that binary mixtures can attain higher COPs compared to the pure working fluids for this case study. For the pure working fluids a maximum COP of 3.85 is found, while for the binary mixtures a maximum COP of 4.30 is found, resulting in a COP increase of 11.7 %. The improvement in COP can be predominantly attributed to the characteristic temperature glide of the mixtures during phase change, which matches the temperature glide of the secondary media, reducing the exergy destruction during heat transfer. As an illustration, the T,s-diagrams of the benzene and methanol mixture and pure toluene are shown in Figure 4.10.

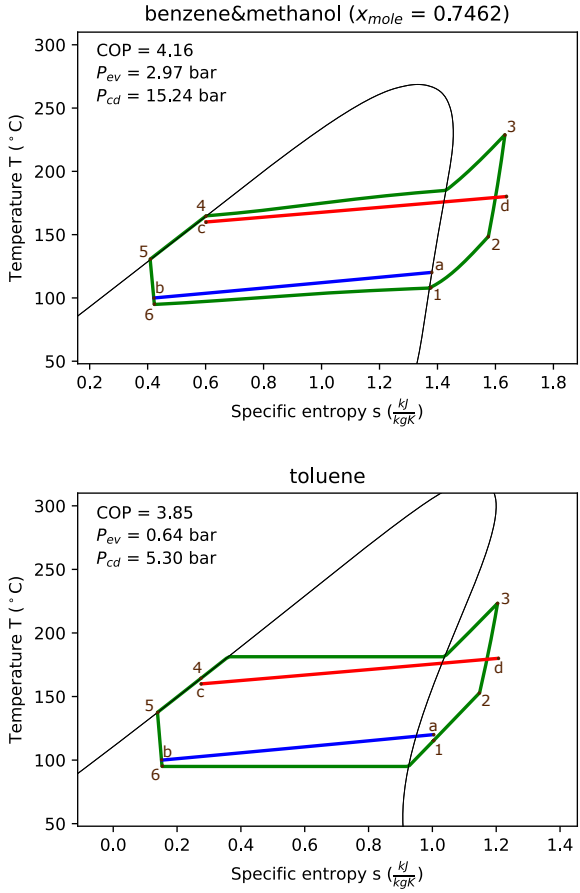


Figure 4.10: T,s-diagram of the heat pump cycle with IHX for the benzene and methanol mixture (top) and toluene (bottom), with scaled entropy for secondary fluid - Case I.

It is remarkable that only natural working fluids are found among the best performing pure and binary working fluids reported. This is also because the synthetic working fluids typically have lower critical temperatures, often below 175 °C. Therefore, the synthetic working fluids show a tendency to operate as a transcritical cycle. However, as shown in the previous section, transcritical cycles are from a performance point of view however only interesting starting at temperatures glides of 60 K. The hydrocarbon natural working fluids have higher critical temperatures and therefore operate as a subcritical cycle, which is now more suited. They are however all flammable. An exception is water which is sometimes also found as a constituent in a binary mixture. It is

notable that only when water is one of the constituents, the use of an IHX is not optimal.

#### 4.4.1.2 Operating conditions

The optimized subcooling and superheating typically has a value so that, next to an already existing pinch point, a new pinch point nearly appears at the location where the working fluid leaves the heat exchanger as can be seen in Figure 4.10, and as also observed in the previous section. For pure working fluids this results in a superheat which equals the temperature glide of the the heat source (i.e. 20 K). The subcooling is somewhat lower compared to the temperature glide of the heat sink (i.e. 20 K). This is because of the heat transferred from the working fluid to the secondary medium during desuperheating, prior to condensation. For the mixtures the optimized superheat values are much lower or zero, because of their temperature glide during phase change.

Operating conditions such as pressure levels, pressure ratio, volumetric heating capacity or compressor discharge temperature are in the same order of magnitude when comparing zeotropic mixtures with pure working fluids. Moreover, the operating conditions strongly depends on the mixtures constituents and the composition. Depending on the molar fraction, however, a trade-off between these parameters could however be achieved. Although, often not all of them are improved at the same time or in the same order of magnitude as was found for transcritical cycles.

### 4.4.2 Case II: Temperature glide only at the heat source

The results of the five best performing binary mixtures in terms of COP for case study II, where there is only a temperature glide (20 K) at the heat source, can be found in Table 4.11. The results of three the best performing pure working fluids can be found in Table 4.12.

Table 4.11: Results of the five best performing binary mixtures - Case II. * BIPs not available for fluid.

| Fluid | $p_{low}$ [bar] | $p_{high}$ [bar] | PR [-] | $\Delta T_{sh}$ [°C] | $\Delta T_{sc}$ [°C] | COP [-] | VHC $[kJ/m^3]$ | $T_{comp,d}$ [°C] | IHX [-] |
|---|---|---|---|---|---|---|---|---|---|
| Acetone/water (0.42) | 2.66 | 19.97 | 7.51 | 0 | 0 | 3.56 | 2866 | 337 | Yes |
| Decane/toluene (0.13) | 0.54 | 5.03 | 9.37 | 6.43 | 0 | 3.50 | 575 | 234 | Yes |
| Heptane/water (0.13) | 0.71 | 9.34 | 13.20 | 0 | 0 | 3.46 | 1010 | 307 | No |
| Toluene/water* (0.17) | 0.70 | 9.12 | 13.08 | 0 | 0 | 3.45 | 1005 | 322 | No |
| Methanol/water (0.20) | 1.34 | 16.09 | 12.0 | 0 | 0 | 3.44 | 1764 | 402 | No |

Table 4.12: Results of the three best performing pure working fluids - Case II.

| Fluid | $p_{low}$ [bar] | $p_{high}$ [bar] | PR [-] | $\Delta T_{sh}$ [°C] | $\Delta T_{sc}$ [°C] | COP [-] | VHC $[kJ/m^3]$ | $T_{comp,d}$ [°C] | IHX [-] |
|---|---|---|---|---|---|---|---|---|---|
| Toluene | 0.64 | 5.69 | 8.96 | 20 | 0 | 3.47 | 599 | 240 | Yes |
| Benzene | 1.57 | 11.20 | 7.13 | 20 | 0 | 3.42 | 1307 | 250 | Yes |
| Cyclohexane | 1.53 | 10.53 | 6.90 | 20 | 0 | 3.39 | 1199 | 229 | Yes |

#### 4.4.2.1 Working fluids and performance

Again, it can be observed that the five best performing binary mixtures have a higher COP than the three best performing pure working fluids, although the increase is marginal. The highest COP found among the binary mixtures (3.56) is now just about 2.6 % higher compared to the highest COP found among the pure working fluids (3.47).

Despite that there is only a temperature glide at the heat source, binary mixtures still have benefits in temperature matching compared to pure working fluids. This is because the temperature glide of the mixture is among others also a function of the pressure. Therefore, it is possible that the temperature glide of the evaporator is larger than the temperature glide at the condenser. An example for a water and acetone mixture is shown in Figure 4.11. For these conditions the temperature glide in the evaporator is about 19.1 K, while the temperature glide in the condenser is 7.7 K.

It is also possible that next to zeotropic binary mixtures, near-azeotropic or azeotropic binary mixtures are also found among the best performing working fluids. These exhibit small or no temperature glide during phase change. They can still achieve higher COPs than pure working fluids due to a trade-off in thermophysical properties.

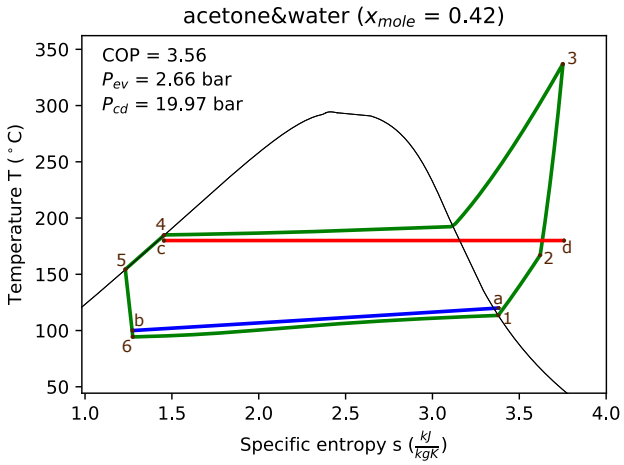


Figure 4.11: T,s-diagram of the heat pump cycle with IHX for the water and acetone mixture, with scaled entropy for secondary fluid - Case II.

### 4.4.3 Case III: Temperature glide only at the heat sink

The results of the best performing binary mixtures in terms of COP for case study III, where there is only a temperature glide (20 K) at the heat sink, can be found in Table 4.13. Only four mixtures where found which outperform their respective pure working fluids. The results of the best performing pure working fluids can be found in Table 4.14.

Table 4.13: Results of the best performing binary mixtures - Case III. * BIPs not available for fluid.

| Fluid | $p_{low}$ [bar] | $p_{high}$ [bar] | PR [-] | $\Delta T_{sh}$ [°C] | $\Delta T_{sc}$ [°C] | COP [-] | VHC $[kJ/m^3]$ | $T_{comp,d}$ [°C] | IHX [-] |
|---|---|---|---|---|---|---|---|---|---|
| Heptane/water (0.32) | 0.64 | 6.5 | 10.2 | 0 | 13.76 | 3.85 | 829 | 269 | Yes |
| Toluene/water* (0.68) | 0.60 | 5.53 | 9.25 | 0 | 15.24 | 3.85 | 728 | 245 | Yes |
| Ethanol/methanol (0.53) | 2.90 | 26.37 | 9.08 | 0 | 12.5 | 3.70 | 3245 | 260 | No |
| Ethanol/water (0.68) | 1.82 | 20.00 | 11.00 | 0 | 15.6 | 3.65 | 2183 | 260 | No |

Table 4.14: Results of the best performing pure working fluids - Case III.

| Fluid | $p_{low}$ [bar] | $p_{high}$ [bar] | PR [-] | $\Delta T_{sh}$ [°C] | $\Delta T_{sc}$ [°C] | COP [-] | VHC $[kJ/m^3]$ | $T_{comp,d}$ [°C] | IHX [-] |
|---|---|---|---|---|---|---|---|---|---|
| Toluene | 0.64 | 5.34 | 8.39 | 0 | 16.63 | 3.80 | 637 | 219 | Yes |
| Benzene | 1.57 | 10.45 | 6.66 | 0 | 16.00 | 3.77 | 1386 | 227 | Yes |
| Cyclohexane | 1.53 | 9.98 | 6.53 | 0 | 16.86 | 3.72 | 1280 | 208 | Yes |

#### 4.4.3.1 Working fluids and performance

For the binary mixtures considered, typically the temperature glide at the evaporator is larger than the temperature glide at the condenser. Therefore, benefits of temperature matching of binary mixtures are small compared to pure working fluids. The best performing mixtures are thus azeotropic, or near-azeotropic, mixtures as illustrated in Figure 4.12. As indicated earlier, the benefits for these working fluids lies in its ability to find a trade-off between the thermodynamic properties of the two constituents, although the effect is rather limited. The COP of the best performing binary mixture (3.85) is just about 1.3 % higher than for the best performing pure fluid (3.80).

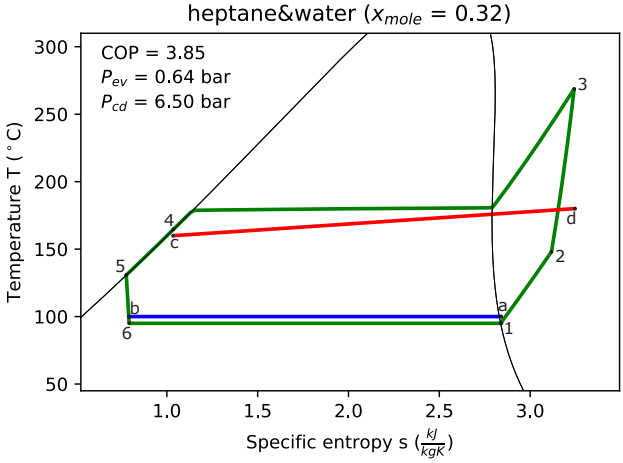


Figure 4.12: T,s-diagram of the heat pump cycle with IHX for the heptane and water mixture, with scaled entropy for secondary fluid - Case III.

### 4.4.4 Case IV: No temperature glides

The results of the best performing binary mixtures in terms of COP for case IV, where there are no temperature glides at both the heat source and heat sink, can be found in Table 4.15. Only four binary mixtures are found which outperform their respective pure working fluids. The results of the best performing pure working fluids can be found in Table 4.16.

Table 4.15: Results of the best performing binary mixtures - Case IV. * BIPs not available for fluid.

| Fluid | $p_{low}$ [bar] | $p_{high}$ [bar] | PR [-] | $\Delta T_{sh}$ [°C] | $\Delta T_{sc}$ [°C] | COP [-] | VHC $[kJ/m^3]$ | $T_{comp,d}$ [°C] | IHX [-] |
|---|---|---|---|---|---|---|---|---|---|
| Toluene/water* (0.66) | 0.60 | 6.15 | 10.25 | 0 | 0 | 3.49 | 692 | 268 | Yes |
| Heptane/water (0.40) | 0.64 | 7.09 | 11.10 | 0 | 0 | 3.48 | 767 | 273 | Yes |
| Acetone/water (0.87) | 3.15 | 21.88 | 6.9 | 0 | 0 | 3.24 | 2496 | 276 | Yes |
| Ethanol/water (0.76) | 1.87 | 22.17 | 11.85 | 0 | 0 | 3.24 | 2027 | 332 | Yes |

Table 4.16: Results of the best performing pure working fluids - Case IV.

| Fluid | $p_{low}$ [bar] | $p_{high}$ [bar] | PR [-] | $\Delta T_{sh}$ [°C] | $\Delta T_{sc}$ [°C] | COP [-] | VHC $[kJ/m^3]$ | $T_{comp,d}$ [°C] | IHX [-] |
|---|---|---|---|---|---|---|---|---|---|
| Toluene | 0.64 | 5.70 | 8.91 | 0 | 0 | 3.45 | 595 | 237 | Yes |
| Benzene | 1.57 | 11.20 | 7.13 | 0 | 0 | 3.39 | 1295 | 245 | Yes |
| Water | 0.84 | 11.23 | 13.36 | 0 | 0 | 3.36 | 1180 | 224 | No |

#### 4.4.4.1 Working fluids and performance

Like for the previous case study, where only a temperature glide was present at the heat sink side, predominantly the same azeotropic binary mixtures are found to be optimal. Again, the improvement in COP (+1.1 %) is small compared to the pure working fluids, which can again be attributed to the trade-off in thermophysical properties.

### 4.4.5 Influence of the internal heat exchanger

Because the use of an IHX shows similar influences on both the binary zeotropic mixtures and pure working fluids, the influence of the IHX and the corresponding comparison is not further investigated.

### 4.4.6 The use of non-flammable or low-flammability working fluids

With the exception of water, all reported working fluids are highly flammable. The non-flammable or mildy flammable HFOs and HCFOs, which result in transcritical cycles for these temperature profiles, show much lower COPs for these applications. The COP of the best pure working fluid is thus water. The results when using water as the working fluid for each case study are summarized in Table 4.17. The performance decrease compared to the best performing pure working fluids are small, namely; -6.2 % for Case I, -3.2 % for Case II, - 5.3% for Case III and -2.6 % for Case IV. Moreover, next to its

favourable environmental properties it has the advantage of not needing an IHX.

Table 4.17: Results of the best performing non-flammable or mildly flammable pure fluid for the four selected case studies.

| Case | Fluid | $p_{low}$ [bar] | $p_{high}$ [bar] | PR [-] | $\Delta T_{sh}$ [°C] | $\Delta T_{sc}$ [°C] | COP [-] | VHC $[kJ/m^3]$ | $T_{comp,d}$ [°C] | IHX [-] |
|---|---|---|---|---|---|---|---|---|---|---|
| Case I | Water | 0.85 | 10.1 | 11.9 | 0 | 15.3 | 3.61 | 1238 | 473 | No |
| Case II | Water | 0.85 | 11.2 | 13.3 | 0 | 0 | 3.36 | 1217 | 494 | No |
| Case III | Water | 0.85 | 10.1 | 11.9 | 0 | 15.3 | 3.61 | 1238 | 473 | No |
| Case IV | Water | 0.85 | 11.2 | 13.3 | 0 | 0 | 3.36 | 1217 | 494 | No |

When considering binary mixtures, overall they are few or no well-performing non-flammable or mildly-flammable binary mixtures. An exception is for the case with a temperature glide at both the heat source and the heat sink (Case I). The COP of water can then be improved by adding ammonia to the water. In Table 4.18, a comparison between water/ammonia and water is made for Case I. Next to the increase in COP (+7 %), the evaporator pressure becomes above the atmospheric pressure level (+32 %), the pressure ratio decreases (-24 %), the VHC increases (+25 %) and the compressor outlet temperature decreases (-34.4° C). A minor disadvantage is a small increase in pressure level at the condenser (+7.6 %).

Table 4.18: Comparison of the performance of optimized water and ammonia mixture and water for Case I.

| Fluid | COP | $p_{low}$ [bar] | $p_{high}$ [bar] | PR [-] | VHC $[kJ/m^3]$ | $T_{comp,d}$ [°C] |
|---|---|---|---|---|---|---|
| water/ammonia (0.94) | 3.87 | 1.12 | 10.77 | 9.6 | 1725 | 439 |
| water | 3.61 | 0.85 | 10.01 | 11.9 | 1375 | 473 |

When the water and ammonia mixture is compared to the flammable pure working fluids, it is observed that its COP is slightly better than the best pure working fluid (+ 0.5 %), but the COP is still 10 % lower compared to the best binary mixture for this particular case study.

## 4.5 Conclusion

The goal of this chapter is to analyze the potential for improving the COP of heat pump cycles through achieving temperature matching in the heat exchangers. This is done in two ways, first the potential of transcritical cycles

is assessed for three applications with large temperature glides at the heat sink and no, or limited, temperature glides at the heat source. The transcritical operation is investigated and applied to three relevant case studies, namely: thermal oil heating, spray drying and superheated steam drying. These case studies have heat sink temperature glides of respectively 60 K, 81 K and 105 K. Second, the potential for zeotropic mixtures is assessed for four generic case studies with small (20 K), or no temperature glides at the heat source and/or heat sink. In this aspect, a unique thermodynamic model is developed, allowing for a robust optimization, maximizing the COP.

The results show that, starting from a heat sink temperature glide of 60 K, transcritical cycles allow for higher COPs. For the case study with a heat sink temperature glide of 81 K, transcritical cycles allowed for a COP increase of 4.6 % whereas this increased to 7.3 % for the case with a heat sink temperature glide of 105 K. Transcritical cycles also introduce higher volumetric heating capacities, require lower pressure ratios and have lower compressor discharge temperatures. Furthermore, for high heat sink temperature glides, techniques to reduce the compressor discharge temperature increase the condenser/gas cooler pressure and may decrease the COP, while also increasing complexity. Therefore, from a practical and financial point of view, transcritical cycles may already be recommended for heat sink temperature glides below 60 K. One overall disadvantage of the transcritical cycles is the high compressor discharge pressure.

The best performing transcritical working fluids often are HFOs and HCFOs. More specifically R1336mzz(Z), R1234ze(Z) and R1233zd(E) often showed the best performance. However, the natural working fluids cyclobutene, cis-2-butene, isopentane and pentane in the transcritical regime also shows similar thermodynamic advantages over subcritical cycles. These working fluids, with the exception of cyclobutene and cis-2-butene, are well-known but are not yet used in the transcritical regime. For the subcritical cycles, acetone, ethanol and methanol were marked as best performing working fluids. These working fluids are not yet used in HTHPs. They are also highly flammable. If these flammable working fluids would be omitted, water shows the highest COP as subcritical working fluid. Unfortunately, for these boundary conditions, water results in strongly reduced COPs and volumetric heating capacities and strongly increased pressures ratios and compressor discharge temperatures, hence far less favourable financial appraisal is expected.

The results also show that the optimized subcooling and superheat vary according to the working fluid and case study. The degree of subcooling and superheating should be controlled so that, next to an already existing pinch point, a new pinch point is nearly created at the location where the working fluid leaves the heat exchanger. Moreover, for transcritical cycles, the gas

cooler pressure is also of particular importance.

Furthermore, the influence of an IHX was studied. Internal heat exchangers often allow for a large increase in COP and a decrease in compressor discharge pressure and therefore pressure ratio. The influence was especially high for the transcritical cycles. However, for some scenarios, especially in case of subcritical cycles, the compressor discharge temperature increased, although this was not typically the case for transcritical cycles. The potential of the internal heat exchanger however diminishes as the difference between heat source inlet temperature and heat sink outlet temperature becomes smaller.

The binary mixtures are investigated for four generic case studies with or without a temperature glide at the heat source and heat sink of 20 K. When there is a temperature glide at both the heat source and/or heat sink, zeotropic mixtures are able to increase the COP with 11.7 % compared to pure working fluids. When there is only a temperature glide at the heat source, zeotropic mixtures can still have a benefit in terms of temperature matching. This is because the temperature glide is a function of the pressure resulting in a larger temperature glide in the evaporator than the condenser. The COP increase compared to pure working fluids is however limited to 2.6 %. In case that there is only a temperature glide at the heat sink, or no temperature glide at all, zeotropic mixtures offer no advantage in terms of temperature matching. In this case, azeotropic, or near-azeotropic, mixture are however found that show larger COPs than pure working fluids. This may be a result of the trade-off in thermodynamic properties of the binary mixture. The COP increases are however limited to 1.3 %.

Regarding the working fluids, natural working fluids or mixtures of natural working fluids are found as optimal. With the exception of water they are however all highly flammable. If flammability would be a concern water would be the recommended working fluid. However, for the scenario that there is a temperature glide at both the heat source and heat sink (Case I), adding ammonia to the water resulted in a higher COP, lower pressure ratio, higher volumetric heating capacity and lower compressor discharge temperature.

# 5

# Techno-economic screening of vapour compression high-temperature heat pump working fluids

*This Chapter is based on the Journal paper:*

*E. Vieren, T. Demeester, W. Beyne, M. P. Andersen, B. Elmegaard, A. Arteconi, M. De Paepe and S. Lecompte, "Selection of pure and binary working fluids for high-temperature heat pumps: A financial approach",* Applied Thermal Engineering*, vol. 252, p. 123 615, 2024, ISSN: 1359-4311. DOI:* https://doi.org/10.1016/j.applthermaleng.2024.123615*. [Online]. Available:* https://www.sciencedirect.com/science/article/pii/S1359431124012833

## 5.1 Introduction

In the previous chapter it is shown that working fluids with a high COP may have a low VHC or a high pressure ratio, introducing the need for large compressors or multiple stages. On the contrary, the transcritical cycle did, by a small margin, not have the highest COPs for the thermal oil heating case

study with a temperature glide of 60 K. However, much larger VHCs and lower pressure ratios were found. These considerations are also true when looking into the different subcritical cycles or when using zeotropic mixtures. On the other hand, while the improved temperature match of transcritical cycles and zeotropic mixtures may lead to higher COPs, it also increases the required heat transfer surface. It is thus expected that there may be a compromise between thermodynamic and financial optima, as has been shown for ORCs [188]. Therefore, the heat pump with the highest COP may not be the most financially competitive.

Kosmadakis et al. [83] investigated the financial aspects of HTHPs for excess heat recovery, with the aim of identifying the most cost-effective heat pump cycle for various heat source temperatures (< 100 °C) and heat sink temperatures (< 150 °C). These heat source and heat sink temperatures were assumed to be constant, thus showing no temperature glide. They considered both single-stage and double-stage cycles and the use of an IHX. Three low-GWP synthetic working fluids were used. Their general conclusion is that single-stage cycles with an IHX shows the best financial appraisal when the temperature lift is below 50 °C. For higher temperature lifts two-stage cycles show superior cost-effectiveness.

Ommen et al. [182] studied the technical and economic working domains of HTHPs with heat sink temperatures up to 120 °C. The working fluids under consideration were the natural working fluids propane (R290), isobutane (R600a), $CO_2$ (R744) and ammonia (R717), as well as the synthetic working fluid R134a, which was used as a reference. In the event that the aforementioned working fluids were to reject heat at temperatures above the critical point (i.e. transcritical cycle), the heat rejection pressure was optimized. The heat pump cycle was however limited to a single-stage cycle without IHX. In contrast to the work of Kosmadakis et al. [83], however, four different sets of sink/source temperature glides were studied: 10 K/10 K, 20 K/10 K, 20 K/20 K and 40 K/10 K. This was done for temperature lifts varying from 10 K to 70 K. Depending on the temperature levels of the heat source and sink, different working fluids emerged as optimal solution. Overall, ammonia systems proved to be the best available technology for lower heat sink outlet temperatures (< 90 °C). Above this temperature the compressor discharge pressure became too high. For higher heat sink outlet temperatures, isobutane proved to be the best available technology. Transcritical $CO_2$ cycles were the most optimal for the 40 K/10 K glide when the heat sink outlet temperature was low (< 75 °C), and the temperature lift was high (> 50 °C). The other working fluids were never optimal.

Zühlsdorf et al. [189] also carried out a financial optimization for different working fluids, building on the work of Ommen et al. [182]. A set of 14 natural

working fluids and 4 low-GWP synthetic working fluids were considered as potential candidates. In addition, all possible binary mixtures of these working fluids were considered. A single-stage heat pump cycle with and without IHX was considered. The optimization was applied to a district heating application (up to 75 °C) for two different heat source temperature profiles. The work identified zeotropic mixtures that could boost thermodynamic efficiency by 30 % to 35 % and simultaneously lower the LCOH by 8 % to 10 %.

Vannoni et al. [190] performed a COP maximization and total cost of investment (TCI) minimization, also taking into account technical limitations. The study focused on the natural working fluids R290, R717, R600 and R600a, and on the HFO R1234yf. The HFCs R134a, a (deprecated) reference for low and medium temperature heat pumps, and R245a, a (deprecated) reference for HTHPs, were also considered. The source temperatures were considered to be between 30 °C and 70 °C, while supply temperatures were considered to be between 60 °C and 150 °C. For each point within the aforementioned range, the superheat at the compressor suction, the fraction of superheating provided by the evaporator and the minimum PPTD at the condenser, subcooler, evaporator and IHX were optimized. The results demonstrated that there is an inverse relationship between COP and TCI. Different Pareto fronts of optimal working fluids were identified for COP maximization and TCI minimization.

de Raad et al. [191] identified techno-economic improvements for a steam-generating heat pump using exergy-based cost minimization. The focus was on the production of 2 bar(a) steam, using condensate with an initial temperature of 80 °C. The steam has a mass flow rate of 10 t/h, while the water has a mass flow rate of 50 kg/s. Four different heat pump configurations were considered: a simple heat pump, a two-stage compression heat pump with intercooling, a heat pump with IHX and a two-stage heat pump with open economizer. All of these configurations used R1234ze(Z) as the working fluid. The IHX cycle was identified as the most promising. The incorporation of an IHX resulted in a 0.5 M€ increase in the investment cost, yet led to a 0.6 M€ reduction in the total cost of ownership after five years. This was achieved by enhancing the COP of the heat pump from 2.3 to 2.8.

Several studies are thus performed on financially optimal HTHP solutions. These however mostly consider few working fluids, a reduced set of configurations, and limited or specific applications. Furthermore, the operating temperatures are limited below 150 °C. This work aims to close these gaps. This is achieved by the financial optimization of various heat pump cycles (single-stage and double-stage, with and without IHX) for supply temperatures up to 200 °C. A large set of both synthetic and natural working fluids and their binary mixtures are considered as working fluid candidates. These working fluids may operate in the subcritical, transcritical or supercritical

regime. To perform the financial comparison, a methodology is developed to compute the LCOH. The methodology is applied to a large set of generic temperature profiles relevant to a wide range of industrial applications. The focus is on process temperatures between 160 °C and 200 °C and heat source temperatures between 80 °C and 120 °C.

The work performed in this chapter makes four main contributions. First, it examines and illustrates the potential mismatch between thermodynamic and financial optima. Second, it provides recommendations on the selection of suitable working fluids for a wide range of applications operating at temperatures in the range 160 °C to 200 °C. Third, it provides detailed results and thus insights into optimizing the financial aspects of heat pump cycles. Fourth, it provides an in-depth analysis of the sensitivity of the financial appraisal depending on various parameters. Furthermore, the results are also presented in a generic, yet insightful manner.

In what follows, the financial model is introduced and the set of generic temperature profiles is presented. The post-processing of the results is also explained. The results are then thoroughly presented and analyzed. First, a specific temperature profile is discussed in detail and then all results are discussed in a general but insightful way, using the generic set of temperature profiles. Afterwards, a sensitivity analysis of the most influential parameters is presented. Finally, a discussion is provided and a conclusion is drawn.

## 5.2 Methods

The Methods section is based on the thermodynamic model (Section 4.2.1) and the working fluid selection (Section 4.2.3) introduced in Chapter 4. These two sections establish the basis for the financial model which will be explained in the upcoming section (Section 5.2.1). Section 5.2.2 then provides insight into the generalized heat source and heat sink temperature profiles. Lastly, Section 5.2.3 discusses the post-processing of the results.

### 5.2.1 Financial model

The purpose of the financial model is to minimize the LCOH. As the LCOH depends on the COP, the robust thermodynamic model is a suitable basis for the financial model. The main adaptations to the existing thermodynamic model are listed below:

- Removal of the PPTD constraint: In the thermodynamic model, a PPTD of 5 K is imposed in the evaporator and condenser/gas cooler. This is because, from a thermodynamic point of view, the PPTD would optimally

converge to zero, resulting in a maximum COP but infinitely large heat exchangers. However, when a cost is assigned to these heat exchangers, the need for a predetermined PPTD disappears. This because a smaller PPTD results in a progressive increase in heat exchanger cost.

- Implementation of multiple compression stages: Only a single compression stage has been considered in the theoretical thermodynamic model. The use of multiple compression stages could, however, be necessary from a technical point of view, influencing the investment cost and therefore the LCOH. Consequently, the use of multiple compression stages is implemented. A maximum compression ratio of 6 per stage has been chosen. For higher pressure ratios, the compressor is split into two compressors with the intermediate pressure the geometric mean of the condensing and evaporating pressures [192].
- Implementation of the mechanical and drive efficiency. In the thermodynamic model an ideal mechanical and drive efficiency was considered. Now a mechanical and drive efficiency of 95 % [57] has been implemented, as this results in higher electricity costs.

The integration of the financial model alongside the thermodynamic model is unique. A flowchart of the robust financial model is shown in Figure 5.1.

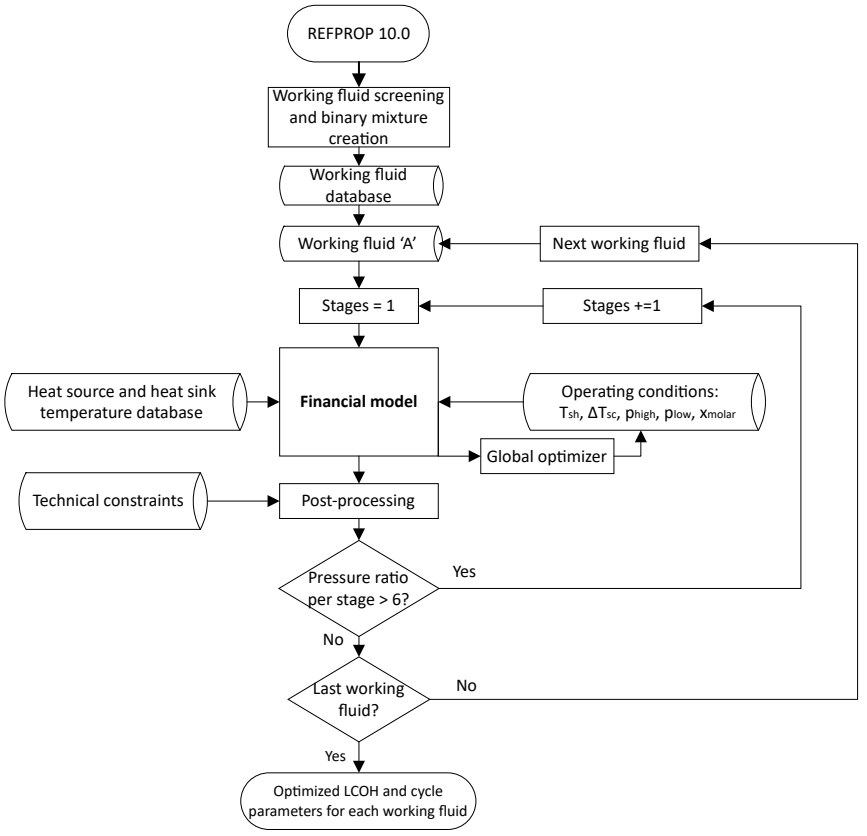


Figure 5.1: Flowchart of the financial model.

The LCOH represents the net present value of all costs associated with generating a unit of heat over the lifetime of a system (€/kWh). It is calculated using Equation 5.1.

$$LCOH = \frac{C_{CAPEX} + \sum_{t=1}^{n} \frac{C_{OPEX,t}}{(1+i)^t}}{\sum_{t=1}^{n} \frac{Q_t}{(1+i)^t}} \tag{5.1}$$

In this equation $C_{CAPEX}$ is the capital expenditure (€), $C_{OPEX,t}$ the operational expenditure at year $t$ (€/year), $n$ the lifetime of the heat pump (year), $i$ the interest rate (%) and $Q_t$ the amount of heat produced at year $t$ (kWh/year). The detailed calculations of capital and operating expenditures, as well as the financial constraints, are explained below.

#### 5.2.1.1 Capital expenditure

The capital expenditure (i.e. investment cost) of the heat pump is calculated using the method presented by Turton et al. [193]. This method should provide estimates in the accuracy range of -25 % to +40 %. First, the equipment purchase cost of each component is calculated. These historical component costs are then multiplied by a time factor to account for inflation. The inflated equipment costs are then used to calculate a total module cost, which represents the CAPEX.

**Heat exchanger equipment cost**

Plate frame heat exchangers are chosen because of their compactness, effectiveness, design flexibility and low cost [194]. For this type of heat exchanger, several cost functions are available in the literature [87, 182, 188, 193, 195–198]. The heat exchanger equipment cost function ($C^0_{hex}$) reported by Towler et al. [198] is selected. This cost function, shown in Equation 5.2, with $A_{tot}$ the total heat transfer area (m²), is valid for areas between 1 m² and 500 m².

$$C^0_{hex} = 0.88 \cdot (1600 + 210 \cdot {A_{tot}}^{0.95}) \tag{5.2}$$

To calculate the required heat transfer area, the heat supply and heat rejection are divided into sections where both media have an estimated constant heat transfer coefficient (HTC), e.g. gas-to-gas, liquid-to-gas, two-phase-to-two-phase. For each section, the heat transfer area ($A_{section}$) is determined based on Equation 5.3.

$$\dot{Q}_{section} = U_{section} \cdot A_{section} \cdot LMTD \tag{5.3}$$

where $\dot{Q}_{section}$ is the heat transfer rate in the section, $U_{section}$ is the overall heat transfer coefficient and LMTD is the logarithmic mean temperature difference across the heat exchanger. The LMTD for a counter flow heat exchanger is defined by Equation 5.4:

$$LMTD = \frac{(T_{wf,i} - T_{sm,o}) - (T_{wf,o} - T_{sm,i})}{\ln\left(\frac{T_{wf,i} - T_{sm,o}}{T_{wf,o} - T_{sm,i}}\right)} \tag{5.4}$$

where $T_{wf,i}$ and $T_{wf,o}$, are the temperatures of the working fluid at the inlet and outlet of the section and $T_{sm,i}$ and $T_{sm,o}$ the temperatures of the secondary medium at the inlet and outlet of the section. This equation is however only valid when the specific heat capacity is constant. For zeotropic mixtures and operation above the critical point this approximation cannot be made. Therefore, in these scenarios, a discretization is made. For plate frame heat exchangers with a negligible wall resistance and without fouling, the overall heat transfer coefficient of each section can be calculated by Equation 5.5:

$$\frac{1}{U_{section}} = \frac{1}{\alpha_{wf}} + \frac{1}{\alpha_{sm}} \tag{5.5}$$

where $\alpha_{wf}$ and $\alpha_{sm}$ are the HTCs of the working fluid and secondary medium respectively. These HTCs depend on the working fluid, the Reynolds number and the Prandtl number. Taking these dependencies into account for all working fluids and their mixtures would require a large number of heat transfer correlations, often with large uncertainties, especially for mixtures and (near-) transcritical operation. Moreover, it would also require detailed dimensioning of the heat exchangers. In addition, the computational effort would increase drastically as these equations rely on local fluid properties that have to be extracted from libraries. Therefore, in this study, the HTCs are based on typical HTCs given in the VDI Heat Atlas [199]. For each phase a fixed HTC was chosen, independent of the working fluid, as shown in Table 5.1. For condensation and evaporation the same HTCs are chosen and they are categorized as 'two-phase'. For supercritical operation, the same HTC is chosen as for liquid. No heat transfer deterioration was considered for the zeotropic mixtures, as the deterioration in heat transfer coefficient strongly depends on the boundary conditions, mixture constituents and the molar fraction.

Table 5.1: Used heat transfer coefficient for each phase, based on extrapolation of data reported in the VDI Heat Atlas [199].

| **Phase** | **Heat transfer coefficient** $\alpha$ $[W/(m^2K)]$ |
|---|---|
| Liquid | 2000 |
| Two-phase | 3000 |
| Gas | 100 |
| Supercritical | 2000 |

The total heat transfer area of the heat exchanger is the sum of the area of each section as shown in Equation 5.6.

$$A_{tot} = \sum_{section} A_{section} \tag{5.6}$$

**Compressor equipment cost**

The cost of a compressor is often expressed as a function of its power use [193, 195, 200]. However, it is not necessarily the power use but the volume flow rate at the compressor inlet, which determines the compressor size. This volume flow rate is highly dependent on the working fluid. Therefore, a compressor cost function is chosen that is a function of the compressor inlet volume flow rate. The cost function reported by Ommen et al. [182], for reciprocating compressors, shown in Equation 5.7, is used.

$$C^0_{comp} = 19850 \cdot \left(\frac{\dot{V}_{comp,in}}{279.8}\right)^{0.73} \tag{5.7}$$

With $\dot{V}_{comp,in}$ the volume flow rate at the inlet of the compressor ($m^3/s$). The cost function aligns well with the cost functions of Astolfi [201] and Frate et al. [202], as shown in Figure 5.2. All these cost functions are derived from compressor manufacturer data.

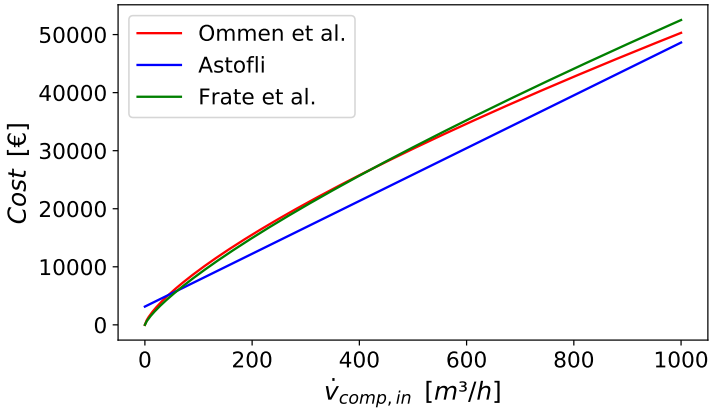


Figure 5.2: Overview of the compressor cost as a function of the volume flow rate at the compressor inlet for different cost functions.

The reported compressor costs do not include the cost of the electric drive. The electric drive however can be expressed as a function of its power use $\dot{W}_{drive}$ (W) [182], as shown in Equation 5.8.

$$C^0_{drive} = 10710 \cdot \left(\frac{\dot{W}_{drive}}{250000}\right)^{0.65} \tag{5.8}$$

**Expansion valve equipment cost**

For the expansion valve, a cost function reported by Sanaye and Shirazi [203] is used. In this equation (Equation 5.9), the expansion valve cost ($C^0_{valve}$) is expressed as a function of the working fluid mass flow rate $\dot{m}_{wf}$ (kg/s).

$$C^0_{valve} = 114.5 \cdot \dot{m}_{wf} \tag{5.9}$$

**Total module cost**

To account for inflation, each purchased equipment cost is indexed to the year 2021 using the Chemical Engineering Plant Cost Index (CEPCI) [204] as shown in Equation 5.10.

$$C^0_{2021} = C^0_x \cdot \frac{CEPCI_{2021}}{CEPCI_x} \tag{5.10}$$

Where $C^0_{2021}$ represents the purchased equipment cost in the year 2021 and $C^0_x$ denotes the purchased equipment cost in the year when the cost function was

developed. Similarly, $CEPCI_{2021}$ refers to the CEPCI in 2021, while $CEPCI_x$ represents the CEPCI in the year when the cost function was developed.

The indexed purchased equipment costs $C^0_{2021}$ are multiplied by a bare module cost factor ($F_{BM}$) to calculate the bare module cost ($C_{BM}$) of each component as shown in Equation 5.11.

$$C_{BM} = C^0_{2021} \cdot F_{BM} \tag{5.11}$$

This bare module cost factor takes into account direct costs (e.g. labour) and indirect costs (e.g. engineering expenses).

An overview of the CEPCI at the year when the cost function was developed, together with the bare module cost factor of each component is shown in Table 5.2. The CEPCI at the reference year (2021) is 726 [204].

Table 5.2: CEPCI [204] and bare module factor ($F_{BM}$) for each component [193].

| **Component** | **CEPCI (year)** | $F_{BM}$ |
|---|---|---|
| Plate heat exchanger | 551 (2010) | 1.16 |
| Positive displacement compressor | 567 (2013) | 2.4 |
| Compressor drive | 567 (2013) | 1.5 |
| Expansion valve | 567 (2013) | 2 |

The total module cost ($C_{TM}$), which equals the capital expenditure, is the sum of each bare module cost plus 15 % and 3 % for contingency costs and fees respectively, as shown in Equation 5.12.

$$C_{CAPEX} = C_{TM} = 1.18 \cdot \sum_{i=1}^{n} C_{BM,i} \tag{5.12}$$

#### 5.2.1.2 Operational expenditure

The operational expenditure is the sum of the annual electricity cost ($C_{el}$) and the annual maintenance cost ($C_{maint}$) as shown in Equation 5.13.

$$C_{OPEX} = C_{el} + C_{maint} \tag{5.13}$$

The annual electricity cost is determined multiplying the specific cost of electricity ($c_{el}$) with the electricity demand ($\dot{W}_{el}$) and the annual operating hours ($h_a$) as shown in Equation 5.14.

$$C_{el} = c_{el} \cdot \dot{W}_{el} \cdot h_a \tag{5.14}$$

The electricity demand is calculated by dividing the compressor power with the selected mechanical and drive efficiency ($\eta_{m\&d}$), as shown in Equation

5.15. With the compressor power coming from the thermodynamic model (Equation 4.1).

$$\dot{W}_{el} = \frac{\dot{W}_{comp}}{\eta_{m\&d}} \tag{5.15}$$

The maintenance cost is determined as a fraction ($f_{maint}$) of the capital expenditure as shown in Equation 5.16.

$$C_{maint} = f_{maint} \cdot C_{CAPEX} \tag{5.16}$$

#### 5.2.1.3 Financial boundary conditions

Calculating the LCOH requires several boundary conditions which depend on the industrial process, industry or location. Here, financial boundary conditions are chosen that represent a typical energy-intensive industry in Belgium as shown in Table 5.3. A relatively high maintenance cost fraction is selected because of the lower maturity of heat pumps supplying heat up to 200 °C and the high number of operational hours.

Table 5.3: Overview of the considered financial boundary conditions.

| Parameter | Value | Reference |
|---|---|---|
| Heat pump lifetime ($n$) | 15 years | [87, 182, 205] |
| Interest rate ($i$) | 5 % | - |
| Maintenance cost fraction ($f_{maint}$) | 0.06 | [87, 206, 207] |
| Annual operating hours ($h_a$) | 7000 | [57, 87] |
| Specific electricity cost ($c_{el}$) | 0.0806 €/kWh | [92] |

For the specific electricity cost, the bi-annual electricity costs reported by Eurostat for Belgium between 2016 and 2020 [92] are averaged. This was done for the prices reported in the annual electricity use range of 500 MWh to 2000 MWh. According to Eurostat, most of the EU non-household consumers fall within this use range. Furthermore, it is important to note that the LCOH depends on the heating capacity, as non-linear cost functions are used. Therefore, a modular heat pump with a heating capacity of 500 kW is considered, which is in line with the heating capacities of (near) industrial HTHPs [12].

### 5.2.2 Generalized heat source and heat sink temperatures

The financial model is applied to a wide set of generic temperature profiles rather than case studies. The generic temperature profiles vary both in absolute temperature levels and temperature glides. Depending on whether the

heat source or sink is of sensible or latent nature, the generic temperature profiles are classified into four groups as shown in Table 5.4. The table also shows how many combinations of temperature profiles are selected for each scenario. Due to the additional degree of freedom when the secondary medium is of sensible nature, the number of combinations is increased for these cases. For each combination the heat sink outlet either has a temperature of 160 °C or 200 °C, and the heat source has an inlet temperature of 80 °C or 120 °C. In the event that the secondary medium is of sensible nature, a temperature glide of 10 K, 20 K and 30 K is considered for the heat source, whereas for the heat sink a temperature glide of 20 K, 40 K and 60 K is considered. Several relevant industrial applications are also given for each classification. Steam production can be found in each category as it can be generated from both sensible (e.g. hot water) or latent (residual low pressure steam) heat sources and the steam can be generated either directly in a boiler [61, 208] or indirectly by a flashing process [62–64].

Table 5.4: Overview of the four temperature profile classifications depending on the nature of the heat source or sink.

| Heat source | Heat sink | Sets of temperature profiles | Relevant applications |
|---|---|---|---|
| Latent | Latent | 4 | Distillation |
| | | | Steam production (direct) |
| | | | Product evaporation |
| | | | Chemical reactor |
| Sensible | Latent | 12 | Steam production (direct) |
| | | | Product evaporation |
| | | | Chemical reactor |
| Latent | Sensible | 12 | Thermal oil heating |
| | | | Superheated steam drying |
| | | | Steam production (flashing) |
| | | | Pressurized hot water heating |
| | | | Fluid (pre)heating |
| Sensible | Sensible | 36 | Thermal oil heating |
| | | | Steam production (flashing) |
| | | | Pressurized hot water heating |
| | | | Fluid (pre)heating |

With regard to the HTC of the secondary medium, 'liquid' was used if the secondary medium was of sensible nature, while 'two-phase' was used if the secondary medium was of latent nature. Both HTCs are given in Table 5.1.

The increased complexity of the techno-economic optimization compared to the thermodynamic optimization, together with the larger number of boundary conditions considered, resulted in a higher computational effort than in the previous chapter. For this reason, extensive use was made of the Stevin high-performance computing infrastructure at Ghent University.

### 5.2.3 Post-processing of the results

All the results are processed by evaluating whether the maximum discharge pressure of 60 bar is exceeded. In addition, for the binary mixtures, a minimum deviation of 2 % in molar fraction and LCOH from the respective pure fluids is imposed. This is done to ensure a clear distinction between pure fluids and binary mixtures.

## 5.3 Results

The results are generalized in the form of a 'selection matrix'. This selection matrix indicates the best performing types of working fluid(s) for each type of heat source and sink. Before discussing this generalized selection matrix, a single temperature profile is first discussed. This is done to give an example of how the selection matrix can be used. Moreover, it also allows for providing more detailed results, such as a breakdown of the LCOH and the optimal heat pump cycle.

### 5.3.1 Application to a specific temperature profile

A 'sensible-sensible' temperature profile is chosen where the heat source is cooled from 120 °C to 100 °C, while the heat sink is heated from 160 °C to 180 °C. Based on the financial model the optimum LCOH is calculated for all working fluids. The five working fluids with the lowest LCOH are shown in Table 5.5. The table shows the working fluid, molar fraction of the first component (for binary mixtures), number of compression stages, use of an IHX, COP, LCOH and the specific investment cost ($c_{inv}$). The latter is the ratio between the CAPEX and the heating capacity.

Table 5.5: Overview of the five working fluids with the lowest LCOH for the selected temperature profile. * BIPs not available for fluid.

| Working fluid | Molar fraction first component | Stages | IHX | COP | LCOH [€/kWh] | $c_{inv}$ [€/kW] |
|---|---|---|---|---|---|---|
| Methanol&ammonia | 0.685 | 1 | No | 3.85 | 0.0290 | 372 |
| Cyclopentane&methanol* | 0.230 | 1 | Yes | 3.95 | 0.0294 | 425 |
| Cis-2-Butene&methanol | 0.110 | 1 | Yes | 3.83 | 0.0304 | 363 |
| Benzene&methanol | 0.647 | 1 | Yes | 4.10 | 0.0307 | 511 |
| Cyclobutene&octane* | 0.974 | 1 | Yes | 3.49 | 0.0309 | 359 |

This table shows that the working fluids with the lowest LCOHs are (zeotropic) binary mixtures, consisting exclusively of natural working fluids, namely hydrocarbons and ammonia. It also shows that among the five best perform-

ing working fluids the variation in LCOH is rather low. To get an insight into the added value of using mixtures, each of them are compared with its main constituent with the highest molar fraction. The results for these pure working fluids are shown in Table 5.6. This table also shows the relative change in COP, LCOH and specific investment cost compared to the binary mixture reported in Table 5.5. Cyclobutene is compared to cyclobutene&octane, methanol is compared to methanol&ammonia and benzene is compared to benzene&methanol.

Table 5.6: Overview of the financially best performing pure working fluids for the selected temperature profile. In between brackets the comparison with cyclobutene&octane, methanol&ammonia and benzene&methanol respectively (Table 5.5).

| Working fluid | Stages | IHX | COP | LCOH [€/kWh] | $c_{inv}$ [€/kW] |
|---|---|---|---|---|---|
| Cyclobutene | 1 | Yes | 3.37 [-3.4%] | 0.0317 [+2.6%] | 357 [-0.5%] |
| Methanol | 2 | No | 3.71 [-3.3%] | 0.0331 [+14.1%] | 528 [+41.9%] |
| Benzene | 2 | Yes | 3.82 [-6.8%] | 0.0400 [+30.3%] | 871 [+70.4%] |

Furthermore, a breakdown of the LCOH for the working fluids, reported in Table 5.5 and Table 5.6, is shown in Figure 5.3. The numbers next to the bars indicate the part of the LCOH due to the electricity use (red colour) and the part due to the heat pump investment and maintenance (blue colour).

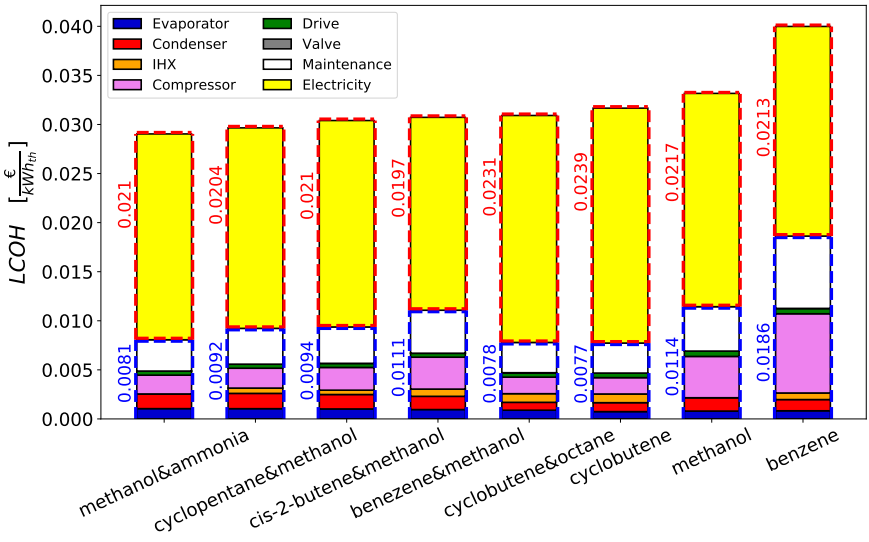


Figure 5.3: Breakdown of the LCOH of the best performing zeotropic mixtures and pure working fluids for the considered temperature profile.

Based on Table 5.5, Table 5.6 and Figure 5.3 several conclusions can be formulated:

- Compared to pure fluids, mixtures can potentially increase the COP while reducing the specific investment costs. One of the reasons for their capacity to increase the COP can be attributed to their non-isothermal phase change, reducing the exergy destruction during heat transfer. An example of the temperature match is shown in Figure 5.4, where the T,Q-diagrams of methanol&ammonia (COP = 3.85) and methanol (COP = 3.72) in the evaporator and condenser are shown. Another way to increase the COP may be a trade-off in thermophysical properties of mixtures compared to pure working fluids. Furthermore, the pressure levels shown at the top of each T,Q-diagram indicate that the addition of ammonia to methanol increases the pressure levels, which here has beneficial effects. As the evaporator pressure increases relatively more than the condenser pressure, the compression ratio decreases from about 8 to 5.7, hence only one compression stage is required. Furthermore, at the given molar fraction and the higher evaporator pressure, the mixture has a lower volume flow rate at the compressor inlet compared to the main constituent: 0.083 $m^3/s$ for methanol&ammonia compared to 0.130 $m^3/s$ for pure methanol. Both aspects results in a significant reduction in compressor cost as found in Figure 5.3. For the methanol&ammonia mixture the compressor has an equivalent LCOH of 0.0019 €/kW whereas for pure methanol the compressor has an equivalent LCOH of 0.0042 €/kW, which is about 2.2 times as high.

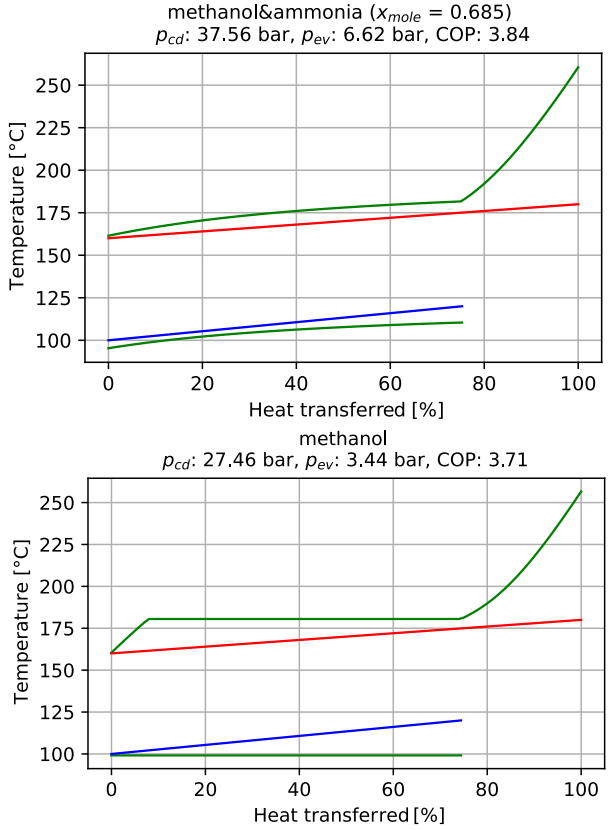


Figure 5.4: T,Q-diagram of methanol/ammonia (top) and methanol (bottom) for the considered case study.

- The main cost driver in the life cycle of the heat pump is the electricity use. However, for this specific case, the costs associated with the investment and maintenance of the heat pump represent a significant share, ranging from 24 % to 47 %, and thus cannot be neglected. Therefore, the heat pump with the highest COP does not necessarily have the lowest LCOH. For example, benzene has a COP (3.82) that is about 13 % higher than the COP of cyclobutene (3.37). Nevertheless, a heat pump using benzene would have a LCOH that is 26 % higher than a heat pump using cyclobutene. That is because a heat pump with benzene has an expected specific investment cost of 871 €/kW, compared to 357 €/kW for cyclobutene. The remarkably high investment cost of a benzene heat pump is a consequence of the high normal boiling point (NBP) of benzene (80.1 °C), resulting in a low evaporation pressure. Due to this

low evaporation pressure the compression ratio will be high, resulting in the need for two compression stages. In addition, the low evaporation pressure results in a low suction density and therefore a high volume flow rate, increasing the compressor cost.

- Figure 5.3 shows that, when not considering the electricity costs, the maintenance cost (white) and compressor cost (violet) are the most dominant. The compressor cost contribution however is highly variable and strongly depends on the working fluid. For the working fluids reported in Figure 5.3, the compressor cost represents between 36 % and 72 % of the total component cost. The contribution of the compressor drive is small, but cannot be neglected as it contributes to 5 % to 10 % of the total component cost. The contribution of the expansion valve (<< 0.5 %), however, can be neglected. The heat exchangers also have a significant contribution (between 7 % to 30 % for the condenser or evaporator) and cannot be neglected. It can also be observed that the binary mixtures have a higher evaporator and condenser cost, which is a result of the improved temperature matching.

### 5.3.2 Financial selection matrix

By applying the financial model to the large set of heat source and sink temperatures (Table 5.4) a selection matrix is made and presented in Figure 5.5. This matrix shows the working fluids with primarily the lowest LCOH for each combination of heat source and sink types. Within each combination of heat source and sink types more than one working fluid is listed. This because of three main reasons:

1. Each combination covers multiple sets of temperature levels, each of which may have an optimal working fluid. Consequently, Figure 5.5 also indicates the temperature level (low, medium, and high) of the heat source/sink for which the working fluid is recommended.
2. Working fluids that perform close to the optimum working fluid are also reported. Because there is some uncertainty in the LCOH, these fluids may also be the financially best performing fluids in practice.
3. Since flammable working fluids may withhold the integration of a heat pump, a distinction is made between non- or mildly flammable working fluids and flammable working fluids.

| | | Heat Source | |
|---|---|---|---|
| | | Latent | Sensible |
| Heat Sink | Latent | Subcritical pure fluid<br>**Flammable**<br>• Acetone, methanol, ethanol (always)<br>• Cyclobutene (low $T_{source}$ and $T_{sink}$)<br>**Non- or mildly flammable**<br>• Water (high $T_{source}$)<br>• HFOs and HCFOs (low $T_{source}$ and $T_{sink}$) | Subcritical pure fluid<br>**Flammable**<br>• Cyclobutene, Cyclopentane, Cis-2-Butene (low $T_{sink}$)<br>• Acetone, Methanol, Ethanol (high $T_{sink}$)<br>**Non- or mildly flammable**<br>• Water (high $T_{sink}$ and $T_{source}$)<br>• HFOs and HCFOs (low $T_{sink}$ and $T_{source}$) |
| | | (near-) azeotropic mixtures<br>**Flammable**<br>• Mixtures of hydrocarbons (always)<br>• Mixtures of water and hydrocarbons (medium $T_{source}$)<br>**Non- or mildly flammable**<br>• None | Zeotropic mixtures<br>**Flammable**<br>• Mixtures of hydrocarbons and mixtures of hydrocarbons and ammonia (always)<br>• Mixtures of water and hydrocarbons (medium $T_{source}$)<br>**Non- or mildly flammable**<br>• Water/ammonia (high $T_{source}$) |
| | Sensible | Subcritical and transcritical pure fluids<br>**Flammable**<br>• Cyclobutene and Cis-2-Butene (low and medium $T_{sink}$)<br>**Non- or mildly flammable**<br>• HFOs and HCFOs (low and medium $T_{sink}$)<br>• Water (high $T_{source}$ and $T_{sink}$) | Zeotropic mixtures<br>**Flammable**<br>• Mixtures of hydrocarbons and mixtures of hydrocarbons and ammonia (always)<br>• Mixtures of water and hydrocarbons (medium $T_{source}$)<br>**Non- or mildly flammable**<br>• Water/ammonia (medium $T_{source}$) |
| | | (near-) azeotropic mixtures<br>**Flammable**<br>• Mixtures of hydrocarbons (high $T_{sink}$)<br>• Mixtures of hydrocarbons with water or ammonia (high $T_{source}$ and high $T_{sink}$)<br>**Non- or mildly flammable**<br>• None | |

Figure 5.5: Generalization of the financially best performing working fluids.

In what follows, each quadrant of the selection matrix will be discussed in more detail.

#### 5.3.2.1 Latent heat source – latent heat sink

If both heat source and heat sink are of latent nature, the lowest LCOH is sometimes achieved with pure fluids and sometimes with binary mixtures. Overall, no general trend could be observed. However, all fluids operate in the subcritical regime.

The mixtures with a low LCOH usually have an azeotropic point in their vapour-liquid equilibrium (VLE). Therefore, at molar concentrations close to this point, they have similar temperature profiles as pure working fluids. Nevertheless, these mixtures may exhibit more advantageous LCOHs than their pure constituents, due to the earlier mentioned trade-off in their thermophysical properties. This may potentially increase COP or decrease specific investment costs. The best performing mixtures are mixtures of hydrocarbons with other hydrocarbons or water. The hydrocarbons are often acetone, methanol, benzene and cyclopentane. It should be noted that the potential of mixing water with hydrocarbons was also identified by Invernizzi et al. [209], for use in ORCs. They concluded that these water-based mixtures require smaller turbomachinery compared to pure water and reduce the po-

tential flammability and toxicity of the other fluid. No suitable non- or mildly flammable mixtures were found.

Regarding the pure working fluids, acetone, methanol and ethanol are often found to be optimal at all temperatures. These hydrocarbons generally result in a high COP, but also a relatively high investment cost due to the need for a large compressor. A heat pump using cyclobutene is found to be optimal at lower heat source and sink temperatures, due to its very low investment cost, even though its COP for this application is not among the best. It is particularly interesting for low heat source temperatures since, unlike other fluids, a small compressor can be used owing to its lower NBP (2 °C). At high heat sink temperatures, however, the compressor discharge pressure becomes too high for cyclobutene. Furthermore, its COP drastically drops when the heat sink temperature approaches the critical point of the working fluid (175 °C), as the transition to transcritical cycles impairs a lot of exergy destruction when heat is transferred to a heat sink at constant temperature. When non- or mildly-flammable working fluids are considered, the HFOs and HCFOs have the lowest LCOH for low heat source and sink temperatures, for the same reasons as discussed for cyclobutene. For higher heat source temperatures (>100 °C), water has the lowest LCOH for the non- or mildly flammable working fluids as its compressor cost strongly decreases because of the higher suction densities at increased heat source temperatures.

An illustration of the trade-off between COP and investment cost, for a case study with a constant heat sink temperature of 160 °C and heat source temperature of 120 °C, is illustrated in Figure 5.6. This figure shows the COP plotted against the LCOH for the 150 working fluids with the lowest LCOH, with a colour scale indicating the specific investment cost. Although the LCOH generally decreases with the COP, the working fluid with the lowest LCOH does not necessarily have the highest COP. The working fluids with the lowest LCOH ranks as working fluid with only the 13th highest COP. The better-performing working fluids in terms of COP have largely increased specific investment costs, rendering them financially less attractive. The working fluid with the highest COP results in a heat pump with a specific investment cost slightly above 1000 €/kW and therefore has about the same LCOH as heat pumps using working fluids resulting in half the COP. Here, the influence of the specific investment cost is particularly high because a case study is shown with a low temperature lift, resulting in high COPs and therefore less influence of the electricity cost. Nevertheless, the same trends are observed for other temperature profiles.

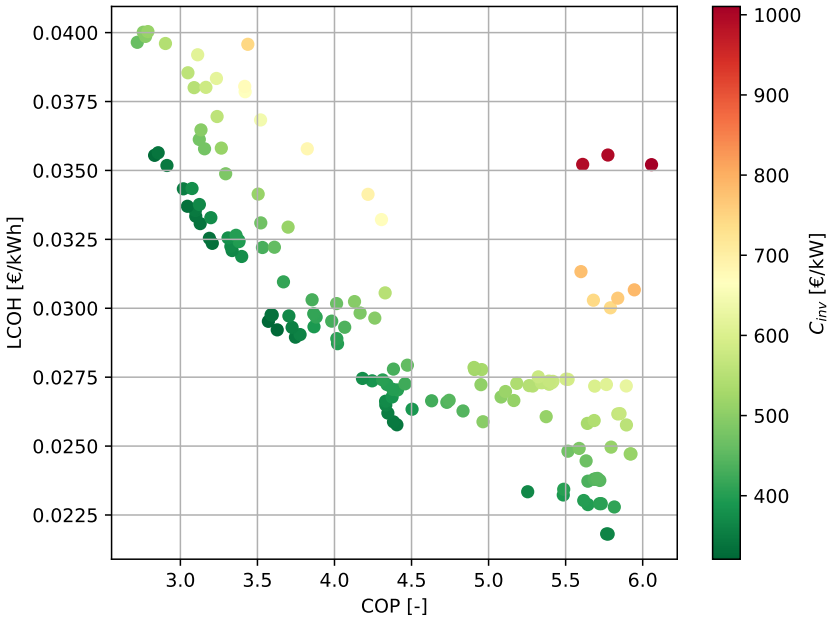


Figure 5.6: Illustration of the LCOH as a function of the COP, using a colour scale according to the specific investment cost. The illustration is for a latent heat sink of 160 °C and a latent heat source of 120 °C.

#### 5.3.2.2 Sensible heat source - latent heat sink

If the heat source is of a sensible nature and the heat sink of a latent nature, zeotropic mixtures can lead to improved temperature matching, in addition to the potential trade-off in thermophysical properties. Interestingly, the temperature glide of the mixture is also a function of the pressure, as illustrated by the VLE diagram of water&acetone in Figure 5.7 (a), where the VLE is drawn for both the evaporating and condensing pressures. Therefore, the temperature glide during condensation and evaporation is not necessarily the same. As a result, a suitable temperature match can be achieved between the working fluid and the secondary medium, even though these media show different temperature glides. This is also shown in the T,Q-diagram of water&acetone with a molar fraction of 0.437 water (Figure 5.7 (b)), where the heat source is cooled from 120 °C to 90 °C and the heat sink is at a constant temperature of 160 °C. Furthermore, the match in temperature allows for higher suction densities at the compressor inlet.

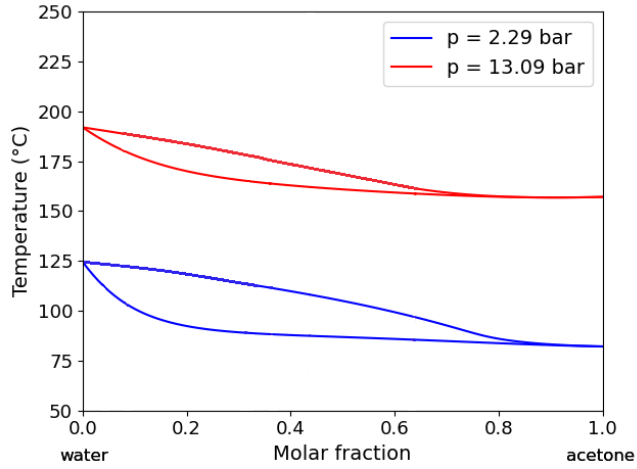


(a)

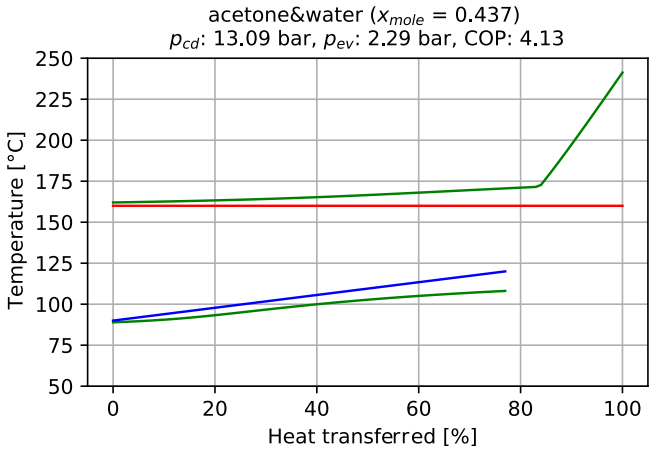


(b)

Figure 5.7: (a) Vapour-liquid equilibrium diagram for the water&acetone mixture at the evaporator and condenser pressure with the corresponding optimized T,Q-diagram (b) for the sensible (120 °C to 90 °C) latent (160 °C) case study.

Figure 5.8 illustrates the temperature glide at the evaporator ($\Delta T_{ev}$) and condenser ($\Delta T_{cd}$) for the 100 working fluids with the lowest LCOH in the aforementioned temperature profile. It is evident that the most effective working fluids exhibit a higher glide at the evaporator compared to the condenser. Some working fluids exhibit a temperature glide at the evaporator that is nearly 20 K greater than the temperature glide at the condenser. Further-

more, it can be observed that the temperature glide at the evaporator is limited to 30 K, which is the same temperature glide as the heat source. For other 'sensible latent' temperature profiles similar trends are being observed.

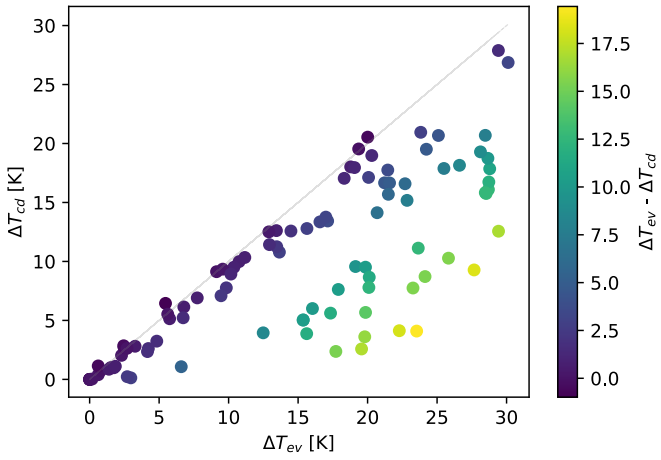


Figure 5.8: Illustration of temperature glide of the working fluid at the condenser and evaporator for the 100 best performing working fluid for the sensible (120 °C to 90 °C) latent (160 °C) case study. Colour scaled according to the difference in temperature glide between evaporator and condenser.

Similar zeotropic mixtures are observed as for the 'latent latent' scenario, although the molar compositions are different. For the pure working fluids, the same conclusions can be drawn as for the 'latent latent' scenario. One overall difference is that mixtures with ammonia also appear. This, either mixed with hydrocarbons or water. The later can be classified as a non- or mildly flammable working fluid.

#### 5.3.2.3 Latent heat source - sensible heat sink

Since the temperature glide of mixtures generally decreases with increasing pressure, as shown for water&acetone in Figure 5.7 (a), zeotropic mixtures show no benefits in terms of temperature matching in this scenario. Hence, the best performing mixtures operate close to the azeotropic point.

Particularly well performing are pure working fluids such as cyclobutene and cis-2-butene (flammable) or HFOs and HCFOs (non- or mildly flammable) operating in the transcritical regime. The advantage of this cycle is twofold:

1. The transcritical cycle allows for a high COP due to favourable temperature matching during both heat extraction and rejection, resulting in

high COPs

2. Typically, the lower the critical temperature is the lower the NBP of the working fluid. Therefore, these working fluids have higher pressures during heat extraction. As a result, the volume flow rate at the compressor inlet is typically low, resulting in a low heat pump investment cost. Combined with a high COP this gives rise to a low LCOH.

On the downside, the transcritical cycle results in high compressor discharge pressures, although this can be greatly reduced by temperature matching. Nonetheless, this can become problematic at higher heat sink temperatures, so in that case subcritical fluids are recommended, either as a pure fluid or as a mixture. It is shown here that by minimizing the LCOH, transcritical cycles become a preferable choice starting at temperature glides of 40 K, compared to 60 K when optimizing the COP.

#### 5.3.2.4 Sensible heat source - sensible heat sink

Zeotropic mixtures show the best performance when both the heat source and heat sink are of sensible nature, as has been elaborately shown in Section 5.3.1. Again, mixtures of hydrocarbons with other hydrocarbons, ammonia or water are found to be the most optimal. If a non- or mildly flammable working fluid is required, water&ammonia shows the best performance.

## 5.4 Sensitivity analysis

The results of the financial model may be sensitive to financial parameters which generally vary over time, or may depend on the country or type of industry where the heat pump is to be integrated. It may also be sensitive to the cost functions used. Therefore, a sensitivity analysis is performed.

Figure 5.3, which displays the cost breakdown of the LCOH, shows that the electricity use is the main contribution in the LCOH. Therefore, the cost of electricity may have a large influence on the results. In addition, the yearly electricity cost is also determined by the annual operating hours. Furthermore, the breakdown of the LCOH shows that the heat pump investment cost also plays a role. The specific investment cost depends on the heating capacity of the heat pump. Therefore, different heating capacities are analyzed. Furthermore, the compressor is the most expensive component, and thus can also have a large influence on the specific investment cost. However, as the compressor cost function is derived from manufacturer data and is consistent with other compressor cost functions (Figure 5.2), the sensitivity is not further

investigated. The heat exchangers, compressor drive and expansion valve often have less impact on the LCOH. Therefore, the influence of these costs is not considered. There is also no sensitivity considered towards thermodynamic modeling assumptions such as isentropic efficiency, IHX effectiveness, or heat transfer coefficients. This is because a lower impact is expected. For example, Zühlsdorf et al. [210] varied the isentropic efficiency between 50 % and 80 % and found little effect on the financial ranking of the different mixtures. It could be argued that the maintenance cost also has a significant impact on the LCOH. While this is true, it should not vary as much between industrial sites, or over time, such as the electricity costs.

In what follows, the sensitivity on the results of the financial model regarding variations in electricity cost, annual operating hours and heating capacity is analyzed. To keep the results clear and concise and to limit the computational time, the sensitivity analysis is performed on the temperature profiles selected in Section 5.3.1.

### 5.4.1 Influence of the electricity price

In Section 5.2.1.3 a base electricity price of 0.0806 €/kWh has been considered. To illustrate the impact of this cost, the electricity cost is increased by +50 % (0.1209 €/kWh) and decreased by -50 % (0.0403 €/kWh). An overview of the LCOH, COP and specific investment cost of the five best working fluids for each electricity price is shown in Figure 5.9, with more detailed information in Table F.1 of Appendix F.

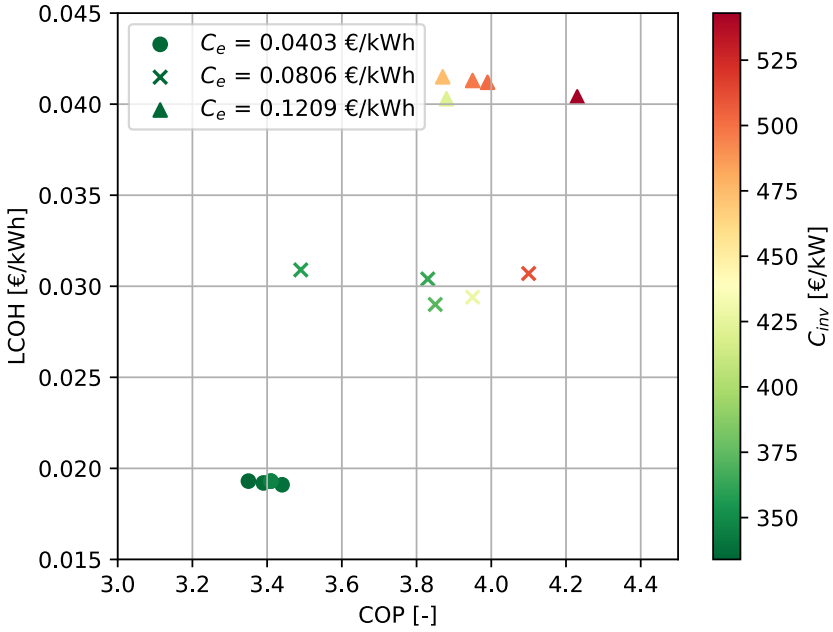


Figure 5.9: Illustration of the LCOH, COP and specific investment cost of the five best performing working fluids under different electricity prices. Applied to the 'sensible-sensible' case study.

Several conclusions can be drawn from this information:

- The LCOH rises sharply with the electricity price. For an electricity price of 0.1209 €/kWh (+ 50 %), the LCOH is on average about 2.1 times higher than for an electricity price of 0.0403 €/kWh (-50 %). It can therefore be concluded that the LCOH is highly sensitive to changes in the electricity price.
- As the electricity price decreases, the optimum heat pump cycle goes towards configurations with the COP pooled around 3.4. For higher electricity prices the electricity usage, and thus the COP, becomes more relevant. The trade-off between COP and specific investment cost is thus largely influenced by the electricity price. Nevertheless, a COP variation between 3.8 and 4.3 is shown. In all scenarios low COPs always result in lower specific investment costs, whether the five best working fluids are compared for a specific electricity price or whether the three electricity price scenarios are compared against each other.
- The best performing working fluids vary with the electricity price. Nev-

ertheless, the same type of working fluids (i.e. mixtures of hydrocarbons) are still observed for other electricity prices. It can therefore be concluded that the results of the general selection matrix (Figure 5.5) are valid for a wider range of electricity prices. One of the reasons is that, in case of binary mixtures, the mixture composition adapt to the electricity price, so that an optimal trade-off between COP and specific investment cost can be found.

### 5.4.2 Influence of the annual operating hours

In Section 5.2.1.3 7000 annual operating hours were considered. However, for industries that do not operate continuously, 3500 operating hours is more appropriate [69, 182]. An overview of the LCOH, COP and specific investment cost of the five best working fluids for each number of annual operating hours is shown in Figure 5.10, with more detailed information in Table F.2 of Appendix F.

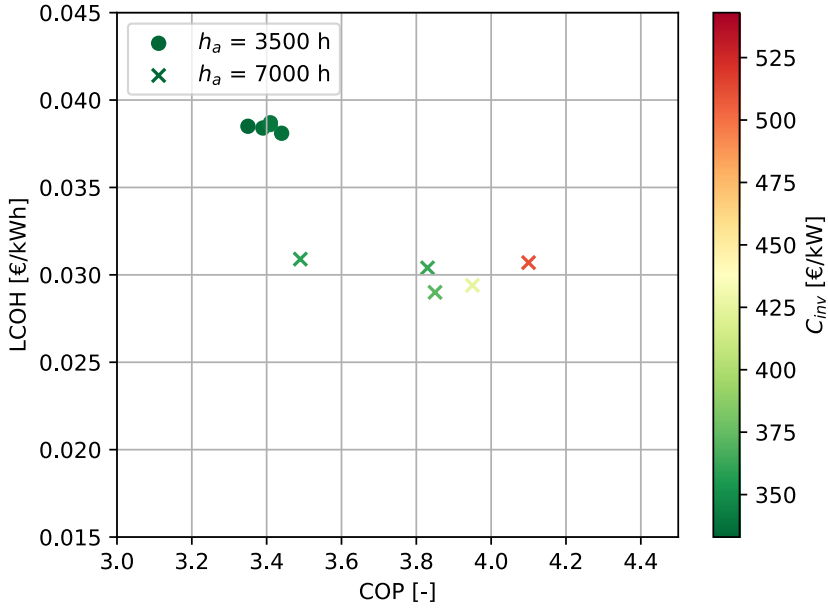


Figure 5.10: Illustration of the LCOH, COP and specific investment cost of the five best performing working fluids under different annual operating hours. Applied to the 'sensible sensible' case study.

Based on this several conclusions can be made:

- The LCOH increases as the annual operating hours decrease. When the annual operating hours are reduced from 7000 h to 3500 h, the LCOH almost increases by 30 %. This is due to the fact that the heat pump will deliver less heat during its lifetime. Thus the LCOH is highly sensitive to the annual operating hours, although to a lesser extent than the electricity price.
- At lower annual operating hours, the influence of the specific investment costs becomes more apparent. As a result, the best performing fluids may have lower COPs.
- As with the electricity price, the ranking of the best performing working fluids depends on the annual operating hours. However, again, the same types of working fluids are observed.

### 5.4.3 Influence of the heat pump capacity

A heating capacity of 500 kW was considered during this work. To determine the sensitivity towards the heating capacity, the heat pump capacity is doubled (1000 kW) and halved (250 kW). Heat pumps with capacities of several MW are also relevant for energy-intensive industries, such as the (petro)chemical industry [14]. However, these heat pump systems make use of turbomachinery. Since in this work, a cost function and a typical compression ratio of a positive displacement machine is used, these capacities are not considered. An overview of the LCOH, COP and specific investment cost of the five best working fluids for each heating capacity is shown in Figure 5.11, with more detailed information in Table F.3 of Appendix F.

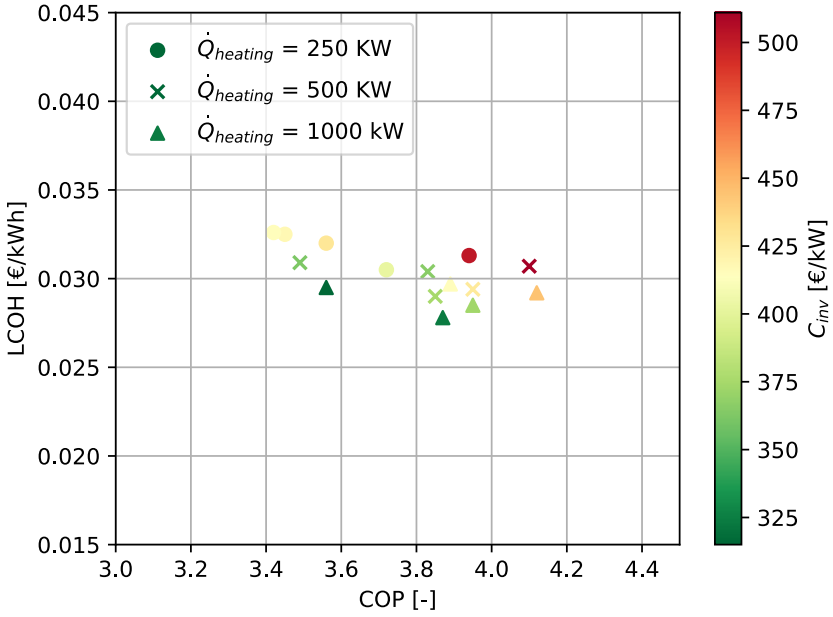


Figure 5.11: Illustration of the LCOH, COP and specific investment cost of the five best performing working fluids under different heat pump capacities. Applied to the 'sensible sensible' case study.

Based on this figure multiple conclusions can be formulated:

- The component costs, and hence the LCOH, decreases with the heating capacity. Although the effect is found to be considerably small over the studied range of heating capacities.
- For higher heating capacities, the molar fraction of the binary mixtures shifts, increasing the COP. For example, methanol&ammonia has an optimum COP at a molar fraction of 0.79. However, the financial optimum occurs at lower methanol molar fractions. This is because methanol greatly increases the cost of the compressor cost due to its high NBP. With increasing heating capacities, the relative cost of the compressor decreases as economics of scales applies. Hence, the mixture shifts towards a molar composition with a higher fraction of methanol.
- It can be concluded that the ranking of the best performing working fluids changes only slightly over the heating capacity range studied.

## 5.5 Discussion

Within this work the LCOH is optimized for different heat pump cycles, working fluids and secondary media temperature profiles. It is noteworthy that within the literature the payback period is often used instead of the LCOH, which may be misleading. This is because the payback period does not consider the period after the investment has been paid back, and it is dependent on external boundary conditions such as gas prices. Consequently, if the payback period would be optimized, the configurations with the lowest payback period inherently tend to be those with the lowest investment costs. However, these heat pumps may not have the lowest total cost of ownership. Therefore, the LCOH should provide a better estimate of the financial appraisal.

Based on the optimized LCOHs, a ranking of the financial appraisal can be made of different working fluids and configurations for each set of temperature profiles. This may act as the basis for designing a heat pump for a specific application, or specific set of applications. Next to ranking, it is also possible to observe the influence of the thermophysical properties of the working fluid on the financial appraisal. The model also provides insight into how the financial appraisal is determined and how it can be optimized. Particularly interesting is the breakdown of the LCOH, showing that the investment cost cannot be neglected and thus induces a discrepancy between thermodynamic and financial optima. Furthermore, binary (zeotropic) mixtures and transcritical cycles other than $CO_2$ demonstrate favourable results. However, there is limited experimental research conducted for these working fluids or cycles, creating a gap in the experimental literature.

Regarding the LCOH calculation, it should be taken into consideration that the model cannot exactly determine the absolute value of the LCOH and there may be some deviation in the initial ranking compared to the practical case. This is one of the reasons why not only the best performing working fluid is reported. To more exactly determine the LCOH the following aspects should, among others, be integrated into the model:

- The heat transfer coefficient correlations. In practice, the heat transfer coefficient is dependent on the properties of the working fluid.
- The cost of the working fluid. Particularly since the synthetic working fluids show overall much larger costs than natural working fluids.
- The influence of material compatibility or pressure on equipment costs.
- The off-design behaviour.
- The isentropic compression efficiency. It has been show that the isentropic efficiency depends on the properties of the working fluid [147].
- The impact of costs related to ATEX compliance.

- Specific compressor design. The analysis was carried out considering a maximum compression ratio per stage of 6. At higher compression ratios, the LCOH of working fluids requiring high pressure ratios (>6) can be reduced, while the LCOH of those requiring low pressure ratios (<6) remains unchanged. Generally, this could result in a more favourable LCOH for working fluids with high NBPs, such as water or benzene, as a high NBP often results in high compression ratios. For a lower maximum compression ratio, the opposite trend will be observed.

A sensitivity analysis of the results was carried out with respect to electricity price, annual operating hours and heat pump capacity. Regarding the annual operating hours it should be mentioned that the lifetime was considered constant under varying annual operating hours. On the other hand, future cash and heat flows would however be strongly discounted. While the sensitivity of the results towards the electricity price, annual operating hours and heat pump capacity were discussed in detail, the sensitivity towards the component costs was not. For the compressor cost function, this is mainly because it is consistent with cost functions reported in other literature. Nevertheless, a sensitivity analysis towards the compressor cost was performed by changing the compressor cost by -25 %, +50 % and + 100 %. For higher compressor costs, the working fluids with higher NBPs were additionally penalized in their LCOH and vice versa. However, within the cost range considered, the results showed little influence on the relative ranking of the working fluids. For the other component cost functions the influence is much lower.

## 5.6 Conclusion

This work presents a robust financial optimization method to minimize the LCOH for HTHPs providing heat ranging from 160 °C up to 200 °C. The LCOH is optimized rather than the COP. Optimizing COP is common in the literature, but the results should be considered carefully as it does not take into account investment costs.

The presented optimization involves adjusting the heat pump's operational parameters ($p_{high}$, $p_{low}$, $\Delta T_{sh}$, $\Delta T_{sc}$), and in case of mixtures, the binary mixture composition ($x_{mole}$), to minimize the LCOH. Furthermore, the model incorporates a working fluid screening process applied to a large set of pure and binary working fluids. The financial model is applied to wide set of generic temperature profiles, categorized into four groups based on the nature of the heat source and sink (sensible or latent). The results are then subjected to a post-processing procedure. The optimization of the LCOH for a large set of pure and binary working fluids, applied to a large database of

generic temperature profiles for temperatures up to 200 °C is not found in the literature. Novel key findings from this analysis are summarized as:

- There is a discrepancy between optimum COP and optimum LCOH. This is because the fluid or configuration with the highest COP often does not have the lowest capital cost.
- The advantages of binary mixtures are twofold. Firstly, if the mixture is zeotropic and the heat source and/or heat sink are not latent, their non-isothermal phase change can match the temperature profile of the secondary media. This can increase the COP and reduce the compression ratio. However, it increases the cost of the heat exchanger. Secondly, a compromise in the thermophysical properties of the mixture can increase the COP and improve the operating conditions, reducing the LCOH. Particularly well performing were mixtures of natural working fluids.
- The use of binary mixtures is not limited to applications where the heat sink and heat source have similar temperature glides. The temperature glide of the binary mixture is a function of pressure and the molar fraction of its constituents. Furthermore, at defined pressures and molar fractions, the mixture can undergo a (near) isothermal phase change. Consequently, binary mixtures can be employed in scenarios where neither the heat sink nor the heat source exhibits a temperature glide, or where the temperature glide of the heat source exceeds that of the heat sink. An exception is when the temperature glide of the heat sink is greater than that of the heat source, as the temperature glide of mixtures generally decreases with pressure.
- For applications with large temperature glides at the heat sink ($\geq$ 40 K) and small or no temperature glides at the heat source, transcritical cycles using an IHX gives the best performance. Cyclobutene, not used in heat pump cycles, was found to be particularly well performing. However, the synthetic HFOs and HCFOs also showed good performance.
- Most of the reported pure working fluids or binary mixtures are or contain flammable working fluids. If the use of flammable working fluids would not be permitted, the HFOs and HCFOs showed the best financial appraisal at lower heat source and sink temperatures. At higher heat source and sink temperatures, water gave the best financial assessment. When the heat source or heat source and heat sink showed temperature glides, the addition of ammonia to the water improved the LCOH.
- The specific case study analysis showed that the price of electricity had a significant impact on LCOH and changed the ranking of the optimal

working fluids. However, natural working fluid mixtures consistently outperformed other options in this case study. The annual operating hours had less effect on LCOH and ranking. The heating capacity had a marginal effect, mainly due to the limited range considered.

To minimize the cost of heat production of HTHPs it is crucial that these findings are taken into account in the design of the heat pump for the specific application. Furthermore, experimental research on zeotropic mixtures and transcritical cycles, not using $CO_2$, are scarce. Further research is needed on this topic.

# 6

# Design of a water and water-ammonia vapour compression high-temperature heat pump

*This Chapter is based on the Conference publication:*

*E. Vieren, K. Couvreur, M. De Paepe and S. Lecompte, "Design of a high-temperature heat pump providing heat up to 200 °c", eng, in* 16th IIR-Gustav Lorentzen Conference on Natural Refrigerants*, College Park, Maryland, USA: University of Maryland, 2024, p. 11,* ISBN*: 978-2-36215-062-3. [Online]. Available:* http://doi.org/10.18462/iir.gl2024.1229

## 6.1 Introduction

As highlighted in the state-of-the-art section (Section 2.3), closed-cycle vapour compression HTHPs supplying heat above 160 °C are not commercially available, but are still in the prototype stage. In this chapter a HTHP concept is developed based on the insights gained in previous chapters. The boundary conditions are:

- Supply temperatures up to 200 °C should be attainable.

- Natural working fluids should be used.
- Working fluids should be non or mildly flammable.

These constraints differentiate with what is currently available for either prototypes or commercial HTHPs. An overview of commercial HTHPs is provided in the IEA HPT Annex 58 [13]. It shows that several closed-cycle VCHP manufacturers still use synthetic working fluids. These working fluids however have unfavourable characteristics regarding their GWP and/or ODP and/or PFAS formation. Due to these unfavourable characteristics of synthetic working fluids, companies are shifting more and more towards the use of natural working fluids. For supply temperatures below 95 °C, ammonia (R718) is widely used. Its high condensing pressure (51 bar at 91 °C), and the lack of ammonia compressors for higher pressures, however limits its application potential for HTHPs. Moreover, even when the compressor discharge pressure is no limitation, its low critical temperature of about 132 °C would result in transcritical cycles for heat sinks temperatures above about approximately 130 °C. Consequently, as has been shown in Chapter 4 and Chapter 5, ammonia may only be suitable for applications with large temperature glides at the heat sink, when considering high sink temperatures above 130 °C. For supply temperatures above 95 °C, the most commonly used natural working fluids are $CO_2$ (R744) or hydrocarbons (HCs). However, the low critical temperature of $CO_2$ (31.1 °C) results in transcritical or supercritical operation for higher-temperature applications, making it only suitable for heating industrial processes that experience substantial temperature glides. In contrast to ammonia, however, high-pressure compressor technology for $CO_2$ is available. Regarding the use of HCs, multiple HCs exists that are suitable for temperatures up to 200 °C. These HCs are highly flammable, but can be safely used if the right safety precautions are taken [171]. Nevertheless, industrial end-users may be reluctant to use them. To fill this gap, water (R718) is increasingly proposed as a natural working fluid solution due to its numerous favourable properties [212, 213].

Although there are numerous advantages of water, there are some challenges involved when using water as a working fluid. Its high NBP (100 °C) may result in sub-atmospheric pressures, high pressure ratios and low volumetric heating capacities. In addition, its high critical pressure (220.6 bar) may result in a high compressor discharge temperature. A potential solution for these challenges can be found by mixing working fluids, which may result in enhanced operational conditions and performance. A promising natural constituent to mix with water, which is only mildly flammable, is ammonia. Ammonia offers a high volumetric heating capacity and a low pressure ratio but, unlike water, operates under high pressures. Furthermore, it also is a natural working fluid which is not highly flammable like the HCs.

The potential for improving the operational conditions and the performance of water by adding ammonia to the water was highlighted in Chapter 4. The potential for improving the financial aspects on the other hand was highlighted in Chapter 5. There it was shown that water and ammonia can have the lowest LCOH when non-or mildly flammable working fluids are considered. The potential for improving the COP by adding ammonia was however only observed when both secondary media have a temperature glide.

The abovementioned reasons led to the selection of both water and the mixture of water/ammonia as working fluid for the experimental design. With the aim of using the mixture water/ammonia as a working fluid when both secondary media have a temperature glide and water otherwise. Consequently, this chapter further investigates the potential of adding ammonia to water and provides specific insights into designing a heat pump using water or water-ammonia for temperatures up to 200 °C. Here, a strong focus will be placed upon the compressor technology. Furthermore, an overview will be given what the expected performance could be.

## 6.2 Methods

The method section starts with a brief discussion on the water and ammonia mixture (Section 6.2.1). Furthermore, in this section, generic boundary conditions will also be introduced, allowing for a more in-depth performance comparison between pure water and water and ammonia. Afterwards, the challenges related to the high compressor discharge temperature, and how to solve these, are discussed (Section 6.2.2). In this section, the design of the water and water and ammonia heat pump is then discussed. Consequently, the compressor model is extended based on the specific heat pump design (Section 6.2.3), allowing to analyze the impact on the heat pump operation. Lastly, the nominal design conditions of the HTHP are discussed (Section 6.2.4).

### 6.2.1 Applicability range of the water and ammonia mixture

Mixing water with ammonia results in a zeotropic mixture which undergoes a temperature glide during the phase change. The temperature glide of the mixture, as a function of the water molar fraction at different pressures, is shown in Figure 6.1. Depending on the desired temperature glide, the molar fraction of the mixture can be tuned so that a maximum temperature glide of 95 K can be achieved. This temperature glide is nearly insensitive to the operational pressure. For water molar fractions above 0.8 the temperature glide approaches, or is lower than, 40 K. Remarkable is that at low water

fractions, the temperature glide increases very sharply with a small additional fraction of water. This results in a high sensitivity of the temperature glide as a result of errors in charging or compositions shift. For high water fractions, the sensitivity is much lower.

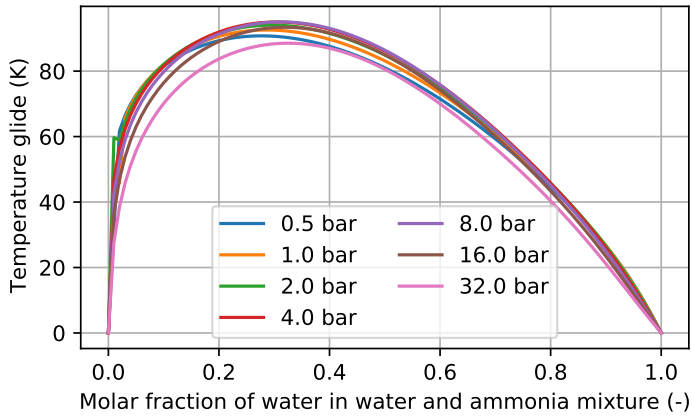


Figure 6.1: Temperature glide of the water and ammonia mixture for different water molar fractions under different pressures.

Depending on the temperature profiles seen in an application, different molar fractions of ammonia, or no ammonia at all, may be optimal from a thermodynamic point of view. To investigate and quantify when adding ammonia to water could be interesting, and how much ammonia is needed, the use of the mixture will be screened for different heat source and heat sink temperature glides. In this analysis, the heat sink outlet temperature is fixed at 200 °C, as the aim is heat production at 200 °C. The heat source inlet temperature is fixed at 120 °C, so that the temperature lift stays reasonable. Temperature glides of 0 K, 10 K, 20 K, 30 K and 40 K are considered for the secondary media, resulting in 25 different temperature profiles.

The model developed in Chapter 4 will be used to simulate the heat pump cycle. An IHX is not used as it does not have a positive effect when water is used as the medium.

### 6.2.2 Heat pump design for use of water or water-ammonia as a working fluid

High compressor discharge temperatures are problematic if not properly handled. It can lead to high thermal stresses or jamming of the compressor due to thermal expansion. However, there are numerous techniques to limit this temperature. Common techniques to reduce the compressor discharge

temperature are [176, 177]: two-phase suction, liquid injection, two-phase injection, vapour-injection or providing intercooling between different stages.

Due to the particularly high compressor discharge temperature of water and water and ammonia, liquid injection is the most common method, as also reported in experimental research studies [212, 213]. The water injection can be done during or before compression, with the latter resulting in two-phase suction at the compressor inlet.

Of particular interest for liquid injection is the twin-screw compressor. These compressors are more tolerant to liquid carryover than reciprocating and centrifugal machines because screw compressors do not have valves or thin blades that can be damaged by the impact of liquid droplets [214]. Moreover, the use of valves can lead to liquid slugging and failure. Another advantage of twin-screw compressors is their wide application range in terms of volume flow rate, which overlaps with medium and large reciprocating compressors and small and medium centrifugal compressors [214]. In addition, the typical compression ratios for twin-screw compressors are high, ranging from 2 to 15 [214]. This allows for high temperature lifts per compression stage, reducing the number of compression stages required to achieve the desired temperature lift.

Compressors for heat pumps often use lubrication oil to protect moving components from wear [215], reduce leakage paths and therefore allowing looser tolerances [215] and assist in heat dissipation [216]. However, a disadvantage for high-temperature applications is the possible thermal dissociation of the lubricating oil. Oil-free designs are therefore increasingly being considered for high-temperature applications. In oil-free compressors the previous listed advantages of using oil disappears, but could be achieved by injecting liquid working fluid into the compressor. Furthermore, it will act more effectively as a coolant since it may also evaporate during the compression process [217]. It should however be noted that the conventional 'oil-free' compressor require an expensive and complicated sealing system to prevent oil-leakage from the bearings into the working chamber, or working fluid leak into the lubricating oil, both being highly undesired [218].

All the abovementioned aspects let to the selection of a liquid-injected twin-screw compressor which is oil-free. For this a compressor manufacturer was found which is able to deliver a compressor considering the use of water and ammonia and the targeted supply temperatures up to 200 °C. The compressor is an oil-free water injected air compressor which will be adapted for this purpose. To avoid the complicated sealing system and allow for true oil-free operation, the compressor will use the working fluid as a lubricant for the bearings. This is possible using hydrostatic or hydrodynamic bearings. An illustration of a simplified heat pump design, proposed in this research, is

shown in Figure 6.2. This design has two additional loops compared to a basic heat pump cycle, namely the 'bearing lubrication loop' (olive green) and the 'two-phase injection control loop' (orange).

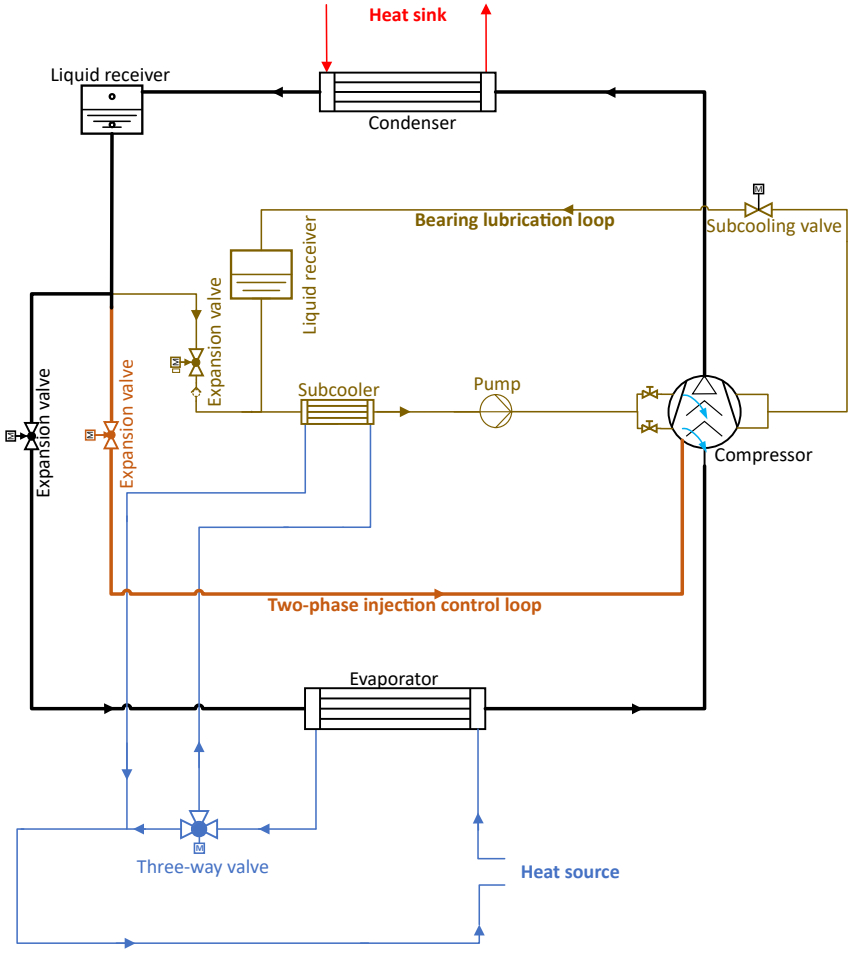


Figure 6.2: Simplified illustration of the proposed heat pump design.

In the bearing lubrication loop subcooled working fluid circulates through the high-pressure side and low-pressure side bearings of the compressor. A part of this flow inevitably leaks to the compressor, as shown by the light blue arrows in Figure 6.2. The leakage flow from the low-pressure side bearing leaks to the inlet of the compressor, while the leakage flow from the high-pressure side bearing leaks at an intermediate pressure. Because of this leakage flow, the bearing lubrication loop is not closed. To compensate for the leakage, it is

connected to the main heat pump circuit. Furthermore, due to heat transfer from the bearings to the working fluid, the working fluid needs to maintain a subcooled state to avoid boiling, hence avoiding damaging the bearings. The subcooling is done by the heat source. A liquid receiver and an associated subcooling valve are also installed to provide smooth control of the bearing lubrication loop.

At present it is however unknown to what extent the working fluid will leak from the bearing lubrication circuit into the main compressor flow. This is because the leakage rate depends on factors such as seals and tolerances. Therefore, in the event that the bearing lubrication leakage flow is not sufficient, an additional loop is used, called the 'two-phase compression control loop'. This loop expands liquid from the liquid receiver to the working fluid flow after the evaporator, allowing the compressor inlet to be controlled in the two-phase region.

### 6.2.3 Modelling of the proposed heat pump cycle

To predict the influence of the bearing lubrication leakage on the cycle performance and cycle operating parameters a model is required that simulates the full cycle introduced in Figure 6.2.

The model to simulate the proposed heat pump cycle extends the model explained in Chapter 4 by including a more detailed compressor sub-model. The compressor now has four inlet streams, namely the main inlet, i.e. the flow from the evaporator, the flow from the two-phase compression control loop, the leakage flow from the low-pressure side bearing and the leakage flow from the high-pressure side bearing. The first three are at the compressor inlet, while the last one is at an intermediate pressure.

The complete compressor, with liquid injection, is modeled using different compressor stages. Furthermore, since the flow at the inlet of the compressor stage may have a liquid fraction, a pump stage is placed in parallel with the compressor stage in the model. The pressure of the gas phase is increased by the compressor stage, while the pressure of the liquid phase is increased, to the same pressure of the compressor outlet, by the pump stage. Different sets of a parallel compressor and pump stages are placed in series. A specific amount of working fluid is considered to evaporate between each set, so that the superheated vapour at the compressor outlet becomes saturated. The corresponding mass and energy balances for each injection can be found in Equation 6.1 and Equation 6.2 respectively.

$$\dot{m}_{wf,superheated\ vapour} + \dot{m}_{wf,subcooled\ liquid} = \dot{m}_{wf,saturated\ vapour} \tag{6.1}$$

$$\begin{aligned} &\dot{m}_{wf,superheated\ vapour} \cdot h_{wf,superheated\ vapour} + \\ &\quad \dot{m}_{wf,subcooled\ liquid} \cdot h_{Wf,subcooled\ liquid} = \\ &\quad \dot{m}_{wf,saturated\ vapour} \cdot h_{wf,superheated\ vapour} \end{aligned} \tag{6.2}$$

An unknown is the number of stages in series that most closely mimics the real compression. Too many stages would result in compression following the saturated gas phase, representing slow heat transfer between the vapour phase and the liquid phase. Too few stages would result in a single compression stage with subsequent desuperheating, representing ideal heat transfer between vapour phase and liquid phase. An intermediate scenario takes place in the actual compression process. In this analysis, four compression stages are considered and the leakage from the high pressure side bearing is assumed to occur after the second compression stage as shown in Figure 6.3, mimicking liquid injection from the high pressure side bearing at 50 % of the built-in volume ratio.

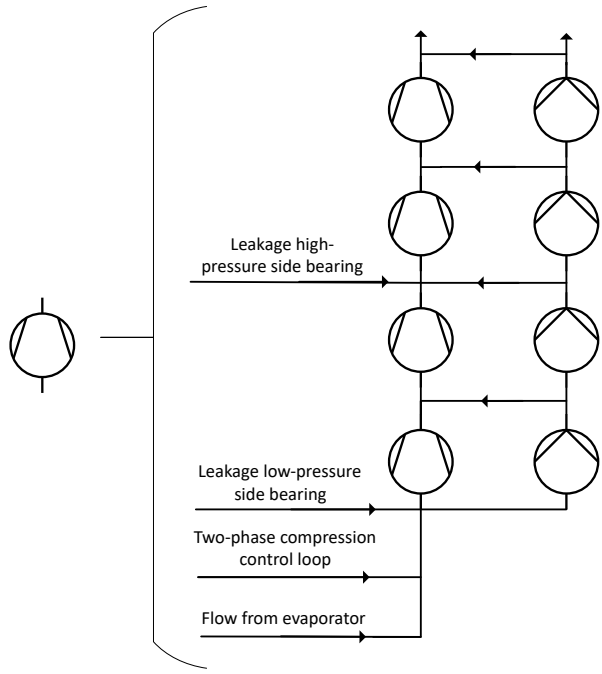


Figure 6.3: Schematic overview of the compressor within the model.

### 6.2.4 Boundary conditions and case specific design

The model will be tested and analyzed on a set of boundary conditions, listed in Table 2. These boundary conditions are the targeted operating conditions of the concept HTHP. Therminol 66 will be used as heat source and heat sink media.

Table 6.1: Overview of the experimental boundary conditions.

| Parameters | Value |
|---|---|
| Heat source inlet temperature | 120 °C |
| Heat source outlet temperature | 100 °C |
| Heat sink inlet temperature | 170 °C |
| Heat sink outlet temperature | 200 °C |
| Drive power | 30 kW |

Furthermore, according to the compressor manufacturer, the majority of the leakage, 63 %, comes from the low-pressure side bearing. Conversely, 37 % of the leakage is from the high pressure side bearing. Moreover, the compressor is designed for a maximum compressor discharge temperature of 250 °C.

## 6.3 Results

The result section is split into two parts. First, a performance comparison is made to assess when water should be used as a working fluid and when the water/ammonia mixture should be used (Section 6.3.1). Afterwards, the influence of the compressor injection is studied for both water and the water and ammonia mixture (Section 6.3.2).

### 6.3.1 Applicability range of the water and ammonia mixture

The COP, PR and VHC for water and the water-ammonia mixture under different heat source and heat sink temperature glides, when using the model without compressor injection (Chapter 4), can be found in Figure 6.4. The corresponding optimum molar fraction of ammonia is also given for the water-ammonia mixture. The figure is mapped in green according to the COP increase of the water and ammonia mixture compared to pure water.

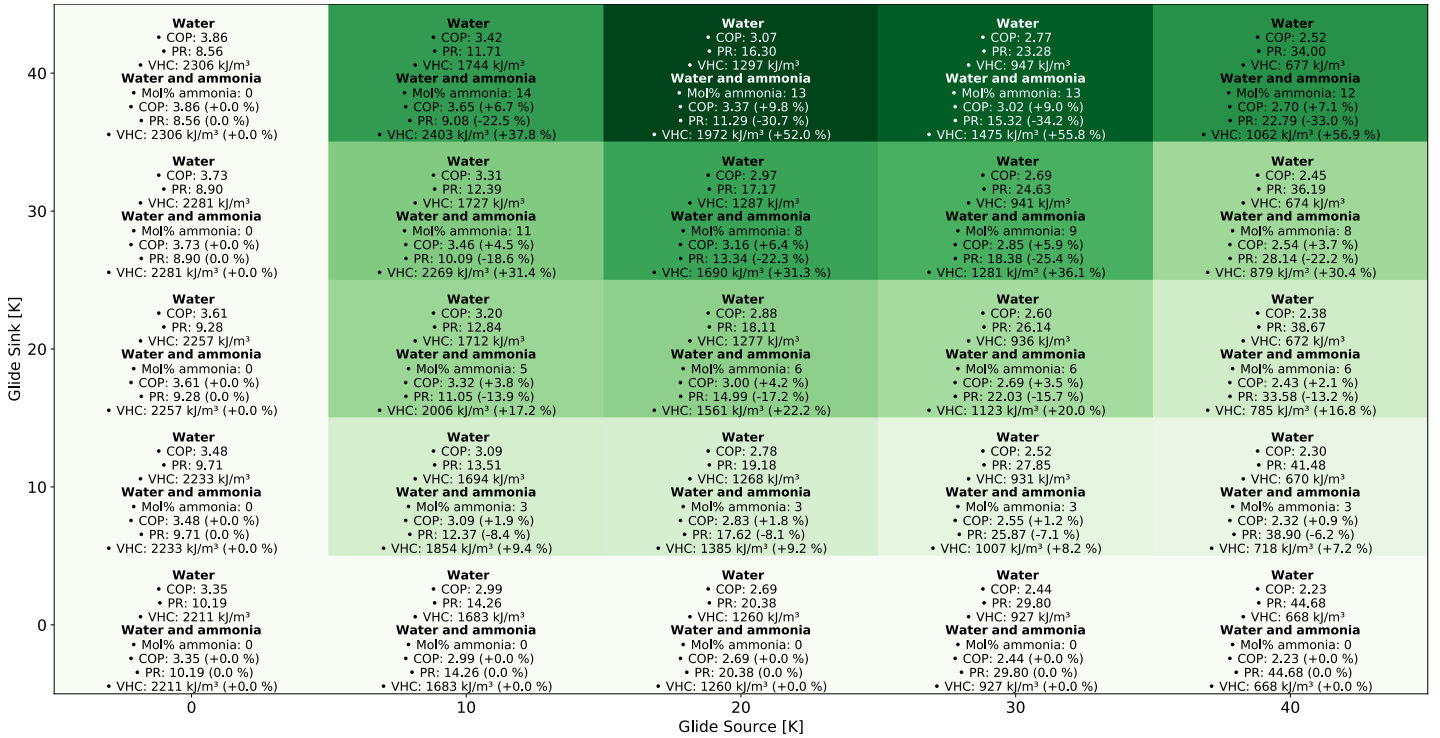


Figure 6.4: COP, PR and VHC for water and the water-ammonia mixture under different heat sink and heat source glides for a heat sink inlet temperature of 120 °C and a heat sink outlet temperature of 200 °C. Figure colour scaled in green according to the COP increase of the water/ammonia mixture over pure water.

Several conclusions can be formulated based on this figure:

- The addition of ammonia to water is beneficial in terms of COP as soon that there is a temperature glide at both the heat source and the heat sink. For these scenarios, COP increases up to about 10 % are observed. The optimum ammonia fraction goes up to 14 mol%. When there is no temperature glide at either the heat source or the heat sink, pure water has the highest COP. Hence, the optimum ammonia fraction is 0 mol%.
- Next to the potential increase in COP, there is an increase in VHC and a decrease in pressure ratio possible by adding ammonia to the water. VHC increases up to 55.8 % can be observed, while pressure ratio decreases of 34.2 % can be observed. The reason for this is twofold:

    1. The ammonia content increases. A higher ammonia fraction leads to an increase in the evaporation pressure, which among others, increases the suction density and thus the VHC. Moreover, the increase in evaporation pressure is relatively greater than the increase in condensation pressure. The pressure ratio therefore decreases.
    2. The mixtures becomes zeotropic. The corresponding match in temperature profile of this mixture and the secondary media results in a higher dew point temperature, therefore the evaporation pressure increases. This increases the suction density and reduces the pressure ratio.

- The figure also shows that for the design boundary conditions, given in Table 6.1, 8 mol% ammonia is optimal. The addition of this fraction of ammonia would result in a 6.4 % increase in COP, a 22.3 % decrease in pressure ratio and a 31.3 % increase in VHC.

### 6.3.2 Compressor injection for lowering the compressor discharge temperature

In this subsection the advanced compressor sub-model is used. Consequently, this section evaluates the effect of bearing lubrication leakage into the compressor chamber. For different leakage rates, the effect on the compressor discharge temperature and the COP will be assessed. This is done using the model discussed in Section 6.2.3, applied to the boundary conditions discussed in Section 6.2.4. The analysis will be carried out for pure water first and then for the water-ammonia mixture.

#### 6.3.2.1 Pure water

The compressor discharge temperature and COP as a function of the leakage mass flow rate, when using water as the working fluid are, is shown in Figure 6.5.

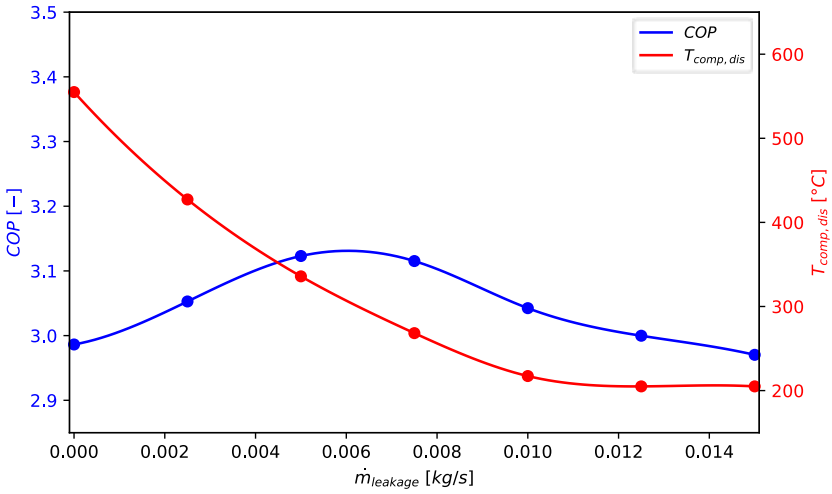


Figure 6.5: COP and compressor discharge temperature as a function of the leakage mass flow rate using water as working fluid.

As expected, the compressor discharge temperature decreases with increasing leakage mass flow rate. For mass flow rates above 0.012 kg/s, the compressor discharge temperature remains fixed at 205 °C. Considering that the heat sink outlet temperature is 200 °C and the PPTD is 5 °C, this is the minimum compressor discharge temperature that can be achieved. Higher leakage flow rates would result in a two-phase outlet at the compressor.

The COP shows a different trend. It first increases, reaching a maximum COP of about 3.13 at 0.0061 kg/s, and then decreases. This is due to two opposing effects as the leakage rate increases. First, as the compressor discharge temperature decreases, the specific compressor work decreases as the compression process more closely approaches isothermal compression. However, a lower compressor discharge temperature means that less heat is transferred from the working fluid to the heat sink during desuperheating. Therefore, the pinch point occurs closer to the heat sink outlet temperature of 200 °C and further from the heat sink inlet temperature of 170 °C (see Figure 4.6). This increases the condensing pressure and therefore the pressure ratio. In addition, as less heat is transferred during desuperheating, the enthalpy dif-

ference across the condenser decreases. This means that expansion losses have a greater relative influence. Both the pressure ratio and the enthalpy difference across the condenser as a function of the leakage flow rate can be found in Figure 6.6. The influence is quite large. In the range of leakage flow rates studied, the pressure ratio increases by 19 % while the enthalpy difference across the condenser decreases by 36 %.

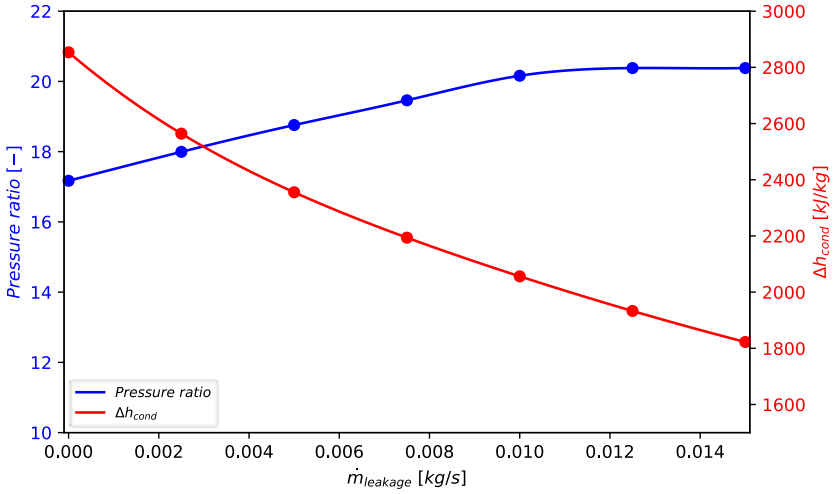


Figure 6.6: Pressure ratio and enthalpy difference over the condenser as a function of the leakage mass flow rate using water as working fluid.

Also notable is that the optimum COP occurs at a leakage flow rate for which the compressor discharge temperature is around 375 °C. For this scenario the COP improvement compared to no injection is about 4.9 %. For the actual compressor however the compressor discharge temperature should be limited to 250 °C. In this scenario, the COP improvement compared to no injection is 3.7 %.

#### 6.3.2.2 Water-ammonia mixture

The compressor discharge temperature and COP as a function of the leakage mass flow rate using water-ammonia, with an optimized molar fraction, as the working fluid can be found in Figure 6.7. The pressure ratio and enthalpy difference over the condenser are shown in Figure 6.8. In both figures pure water is added as a reference.

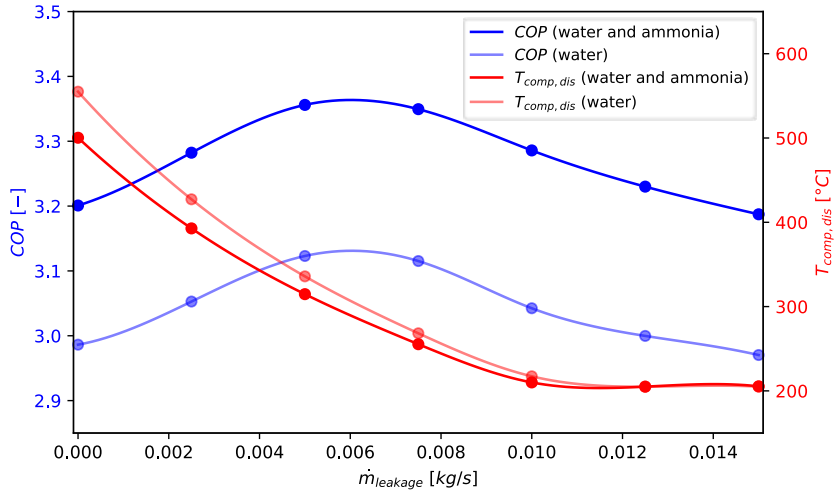


Figure 6.7: COP and compressor discharge temperature as a function of the leakage mass flow rate using water-ammonia as working fluid, with water as a reference.

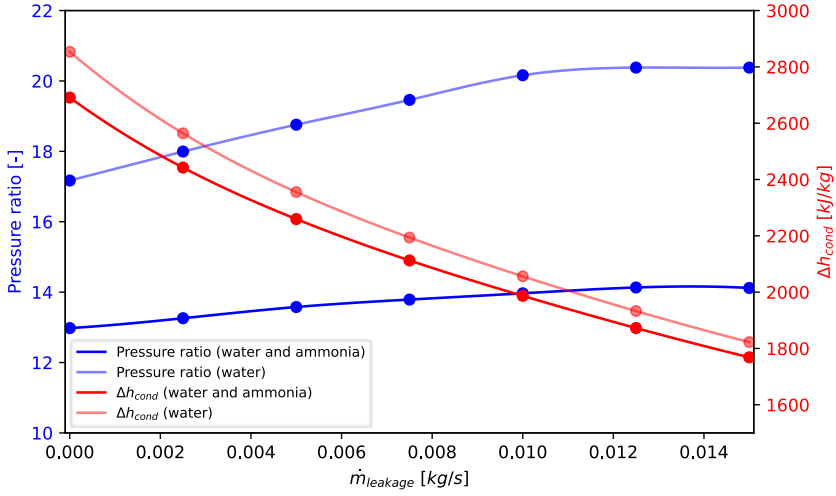


Figure 6.8: Pressure ratio and enthalpy difference over the condenser as a function of the leakage mass flow rate using water-ammonia as working fluid, with water as a reference.

The same conclusion can be drawn as for pure water. Again, a COP increase

up to 5.2 % is observed at the optimum leakage flow rate. Considering the constraint of a maximum compressor discharge temperature of 250 °C, the COP increase is limited to 4.6 %. It can also be observed that the increase in pressure ratio is less pronounced. Over the studied range of injection leakage flow rates the pressure ratio only increases with 9 % compared to 18 % for pure water.

The pressure ratio increase is less outspoken for water-ammonia because of the flexibility in ammonia fraction. This leads that larger ammonia fractions are optimal at higher leakage flow rates. A higher leakage flow rate leads to a lower compressor discharge temperature, and therefore less heat transferred during desuperheating. Consequently, with injection, the pinch point will shift closer to the heat sink outlet temperature of 200 °C and further from the heat sink inlet temperature of 170 °C. When there is no injection, the desuperheating of the working fluids results in a temperature increase of 7 °C of the thermal oil. This means that the temperature glide of the thermal oil is 23 °C during condensation of the water and ammonia mixture. When the injection is so high that the compressor outlet state is at saturated conditions, the thermal oil will experience a temperature glide of 30 °C during condensation of the water and ammonia mixture. This allows for using a mixture with a higher glide, and thus higher a ammonia fraction as optimal working fluid. When the compressor discharge temperature is controlled at 250 °C, the optimum ammonia fraction shifts from 8 mol% to 13.5 mol%. The increased addition of ammonia leads to a lower pressure ratio. Furthermore, it leads to a higher volumetric heating capacity. Therefore, here, benefits can be achieved through liquid injection, especially when using water-ammonia mixtures.

## 6.4 Conclusion

Water is one of the few environmentally safe and non-flammable working fluids and is increasingly being proposed for HTHP applications. However, it can present some issues in relation to the design of the compressor. This because the use of water as a working fluid can result in sub-atmospheric pressures, high pressure ratios, low volumetric heating capacities and high compressor discharge temperatures. When the heat sink and heat source both have a temperature glide, adding ammonia to water, to form a mixture, can improve the pressure ratio, sub-atmospheric pressures, pressure ratio and volumetric heating capacity while simultaneously increasing the COP. When limiting the temperature glide of the secondary media to 40 K, the pressure ratio decreases by up to 34.2 % and volumetric heating capacity increases by up to 55.8 % when comparing water-ammonia as a working fluid with pure

water for cases with temperature glides. At the same time, COP increases of up to 9.8 % are found. Even more promising improvements are expected for higher temperature glides. If either the heat source or the heat sink has no temperature glide, no improvement in pressure ratio, sub-atmospheric pressures or pressure ratio could be found with a simultaneous increase in COP.

Working fluid injection has been investigated to reduce the compressor discharge temperature. This is done by developing a compressor sub-model that allows for adding injection. The nominal design conditions of a HTHP are used for the simulation. It was concluded that working fluid injection could increase the COP for both water and the mixture water-ammonia. There is however an optimum injection mass flow rate. At the optimum working fluid injection the compressor discharge temperature is still too high for the selected compressor. However, the decrease in COP when the compressor discharge temperature was reduced to 250 °C was minor. Furthermore, compressor injection was found to be particularly advantageous for water-ammonia mixtures, as it enabled higher ammonia fractions, enhancing the operational conditions.

# 7 Conclusions

## 7.1 Conclusions

Climate change and the large volumes of pollutants released into the atmosphere are direct outcomes of the rising global demand for energy. A significant share of this energy is used by the industrial sector, with the majority required in the form of heat. Since this heat is primarily generated through the combustion of fossil fuels, transitioning away from fossil fuel boilers offers a major opportunity to combat climate change and reduce pollutant emissions. One promising solution for providing low-temperature heat are heat pump technologies, which captures residual heat and transfer it to industrial processes at higher temperatures, thereby significantly lowering primary energy use. Different heat pump technologies exist, but the focus here was on the vapour compression heat pump, which is commonly electrically-driven. Next to reducing primary energy use this makes it possible to fully transition away from fossil fuels in heat production. Some challenges are however to be tackled to accelerate the deployment of these vapour compression heat pumps in the industry. This thesis focused on three of these challenges.

The first challenge identified is the competition with other heating technologies. Therefore, a financial framework was developed, able to calculate the levelized cost of heat for the vapour compression heat pump, but also

for the heat transformer, electrical boiler and natural gas boiler as competing technologies. Based on this framework, an analysis was performed able to indicate the best performing working scope of each technology. This was done under different energy prices and considering variations in temperature lift and residual heat availability. In conclusion, the heat transformer is only viable in regions where there is an excess of residual heat relative to heat demand. The electric boiler did not have the lowest levelized cost of heat for the boundary conditions studied. Otherwise, the technology with the lowest levelized cost of heat is either the vapour compression heat pump or the natural gas boiler. The decision between using a vapour compression heat pump or a natural gas boiler depends largely on the interplay between energy costs and the required temperature lift. The vapour compression heat pump tends to give the most favourable results for high energy prices, a low electricity-to-gas price ratio, and moderate temperature lifts. If this is not the case, it is also a viable technology compared to the natural gas boiler, but only until a maximum financially feasible temperature lift. To gain a deeper insight, two case studies were also compared, each with specific temperature lifts and levels of residual heat available, while considering variations in technology costs. The solution with the lowest levelized cost of heat varied depending on the country. Additionally, a sensitivity analysis examined factors such as annual operating hours, emission trading schemes, and the availability of residual heat. The vapour compression heat pump was preferred in scenarios with high operating hours, high emission trading costs, and abundant residual heat. However, in cases where residual heat significantly exceeds demand, the heat transformer may offer the lowest levelized cost of heat.

The second challenge identified is the lack of environmental friendly working fluids that can be used in the high temperature range. Particularly lacking in the current state-of-the-art high-temperature heat pumps, are working fluids which matches their temperature profiles with the temperature profile of the secondary media during heat transfer. This can strongly increase the performance, and thus adoption rate, of the heat pump. In this context, a comprehensive thermodynamic heat pump simulation and optimization framework was developed, with a primary focus on applications involving temperature glides at the heat source and/or heat sink. The initial focus was on applications with large temperature glides at the heat sink and smaller ones at the heat source, focusing on transcritical cycles. Here, it was shown that transcritical cycles outperform conventional subcritical cycles when the temperature glide at the heat sink exceeds 60 K. Next, applications with smaller or no temperature glides at both the heat source and heat sink were examined, focusing on binary (zeotropic) mixtures. Here, binary zeotropic mixtures were found to enhance performance due to their temperature glide characteris-

tics. Furthermore, interestingly, the temperature glides during condensation and evaporation are not always identical, which means zeotropic mixtures can be used in applications where the temperature glides at the heat source and heat sink differ. Additionally, in cases where there are no temperature glides, (near-) azeotropic binary mixtures can also offer advantages due to their balanced thermophysical properties. The model was then extended to incorporate costs associated to the components, allowing for optimizing the levelized cost of heat rather than just performance. This analysis was conducted under a wide range of boundary conditions. Overall, it was concluded that there is often a trade-off between achieving maximum performance and minimizing the levelized cost of heat, as the highest-performing solution does not always result in the lowest cost. Here, however, the potential of binary mixtures and transcritical cycles was even more pronounced. In the scenario of optimized levelized cost of heat, transcritical cycles were already effective at temperature glides starting from 40 K.

The third challenge is that depending on the application, the heat pump technology may not be commercially available, particularly at temperatures above 160 °C. Furthermore, for some industries, there may be concerns regarding potential flammability of the working fluid of the commercially available technologies. To overcome these constraints, a new vapour compression heat pump has been designed, capable of delivering heat up to 200 °C. This system can utilize either water or a water-ammonia mixture as the working fluid, both of which were selected for their excellent performance characteristics. Additionally, both fluids are natural, have zero global warming and ozone depletion potential, do not form PFAS, and are non-flammable or only mildly flammable. An oil-free twin-screw compressor with hydrodynamic bearings and working fluid injection, powered by a 30 kW drive, was chosen for this design. Furthermore, the influence of the injection on the heat pump operation, for a water and a water and ammonia heat pump was studied. The analysis showed an optimum injection rate and particularly showed benefits of the injection for the water and ammonia heat pump design.

## 7.2 Future work

In this work a design of a high-temperature heat pump was made. The high-temperature heat pump makes use of a water and ammonia mixture and has an oil-free, working fluid lubricated, twin-screw compressor. The heat source and heat sink circuits are thermal oil circuits. First, a piping and instrumentation diagram of the high-temperature heat pump and the thermal oil circuits was made. This diagram can be found in Appendix G. Consequently, based on a limitation of the electrical drive power of the compressor (30 kW) and

the nominal operating temperature levels, all components in this piping and instrumentation diagram were sized, configured and ordered from a multitude of different component manufacturers. Based on all these components a 3-D design was made, shown in Appendix H. Furthermore, a control strategy and a hazard and operability study of the heat pump is also made, and the electrical cabinet is designed. The next step is the assembly of all components and the commissioning of the set-up in the lab. Once the set-up is successfully commissioned, the following aspects should be studied:

- **Steady-state performance mapping of the high-temperature heat pump:** This involves mapping the Coefficient of Performance of the heat pump under a set of operating conditions. The different operating conditions will involve changes in: heat source and heat sink temperature profiles, heat pump load, ammonia composition and compressor injection rates. By steadily increasing the ammonia fraction, the optimum mixture composition for different operational conditions can be experimentally verified. This may differ from simulations among other because of fractionation, which can be observed and studied in the experimental test rig trough heat balances and density measurements of the Coriolis flow meters. Moreover, the complete compressor performance can be characterized. Also important is that the data extracted from these measurements allows for the development, or scaling of, heat transfer and pressure drop correlations for water and ammonia mixtures at high temperatures and high pressures.
- **Dynamic performance of the high-temperature heat pump:** This aspect involves studying how fast and stable the high-temperature heat pump can control changes in process parameters such as heat source inlet temperature or heat sink inlet temperature, or set points of heat sink outlet temperatures or heating loads.
- **Development of an advanced heat pump model:** Based on the experimental data an advanced heat pump model can be developed, by making semi-empirical component models of the compressor, heat exchangers and expansion valve. This can be done by implementing heat transfer and pressure drop correlations in the heat exchangers and flow coefficients for the leakage paths and non-equilibrium relaxation time coefficients for the compressor. This aspect would be an extension from the model developed in Chapter 6. The model would allow for virtually simulating operating conditions out of the design range of the heat pump, or for studying the use of the compressor for mechanical vapour recompression.

Further research gaps that deserves further investigation could include:

- **Extending and developing a tool of the financial model in Chapter 3:** In Chapter 3 a financial model was made for comparing the performance of the vapour compression heat pump, heat transformer, electric boiler and natural gas boiler. If more cost data on the heat pump technologies becomes available, the cost should be correlated as a function of the temperatures and temperature lift, which was not done because of the lack in data. Also interesting would be including part-load performance data. Consequently, it would be interesting to develop a tool that end-users can use to get a better idea of the financial performance of each technology given a case study. This tool should include user-defined inputs such as energy prices, thermal load profiles or additional costs related to heat recovery.
- **Extending the thermodynamic and financial screening:** In Chapter 4 and Chapter 5 the use of mixtures was limited to the subcritical regime and to binary mixtures. Furthermore, the financial model developed in Chapter 5 could be extended by several points as discussed in Section 5.5. Both aspects were not done in this thesis because of the associated high computational time. Therefore, if one should study this, the cycle simulation and cycle optimization time should first be drastically reduced.

# A Publications

## A.1 Publications as first author in peer-reviewed international journals

E. Vieren, K. Couvreur, M. De Paepe and S. Lecompte, "High-temperature heat pumps in industrial heating networks: A study on energy use, emissions, and economics", *Applied Thermal Engineering*, vol. 259, p. 124 799, 2025, ISSN: 1359-4311. DOI: https://doi.org/10.1016/j.applthermaleng.2024.124799. [Online]. Available: https://www.sciencedirect.com/science/article/pii/S1359431124024670

E. Vieren, T. Demeester, W. Beyne, M. P. Andersen, B. Elmegaard, A. Arteconi, M. De Paepe and S. Lecompte, "Selection of pure and binary working fluids for high-temperature heat pumps: A financial approach", *Applied Thermal Engineering*, vol. 252, p. 123 615, 2024, ISSN: 1359-4311. DOI: https://doi.org/10.1016/j.applthermaleng.2024.123615. [Online]. Available: https://www.sciencedirect.com/science/article/pii/S1359431124012833

E. Vieren, T. Demeester, W. Beyne, A. Arteconi, M. De Paepe and S. Lecompte, "The thermodynamic potential of high-temperature transcritical heat pump cycles for industrial processes with large temperature glides", *Applied Thermal Engineering*, vol. 234, p. 121 197, 2023, ISSN: 1359-4311. DOI: https://doi.org/10.1016/j.applthermaleng.2023.121197. [Online].

Available: https://www.sciencedirect.com/science/article/pii/S1359431123012267

E. Vieren, T. Demeester, W. Beyne, C. Magni, H. Abedini, C. Arpagaus, S. Bertsch, A. Alessia, M. De Paepe and S. Lecompte, "The potential of vapor compression heat pumps supplying process heat between 100 and 200 °c in the chemical industry", *Energies*, vol. 16, no. 18, 2023, ISSN: 1996-1073. DOI: 10.3390/en16186473. [Online]. Available: https://www.mdpi.com/1996-1073/16/18/6473

## A.2 Publications as co-author in peer-reviewed international journals

A. Degelin, R. Tassenoy, E. Vieren, T. Demeester, I. T'Jollyn, M. De Paepe, "Influence of supply temperature and booster technology on the energetic performance and levelized cost of heat of a district heating network with central heat pump", *Energy*, vol. 312, p. 133 589, 2024, ISSN: 0360-5442. DOI: https://doi.org/10.1016/j.energy.2024.133589. [Online]. Available: https://www.sciencedirect.com/science/article/pii/S036054422403367X

T. Zhu, E. Vieren, J. Liang, J. E. Thorsen, M. De Paepe, S. Lecompte and B. Elmegaard, "Booster heat pump with drop-in zeotropic mixtures applied in ultra-low temperature district heating system", *Energy*, vol. 305, p. 132 292, 2024, ISSN: 0360-5442. DOI: https://doi.org/10.1016/j.energy.2024.132292. [Online]. Available: https://www.sciencedirect.com/science/article/pii/S0360544224020668

H. Abedini, E. Vieren, T. Demeester, W. Beyne, S. Lecompte, S. Quoilin and A. Arteconi, "A comprehensive analysis of binary mixtures as working fluid in high temperature heat pumps", *Energy Conversion and Management*, vol. 277, p. 116 652, 2023, ISSN: 0196-8904. DOI: https://doi.org/10.1016/j.enconman.2022.116652. [Online]. Available: https://www.sciencedirect.com/science/article/pii/S0196890422014303

## A.3 Publications in proceedings of international conferences

S. Abbasi, E. Vieren, K. Couvreur, S. Lecompte and A. Arteconi, "Impact of composition adjustment on the performance of a water-ammonia high-temperature heat pump", eng, West Lafayette, Indiana, 2024, p. 10. [Online]. Available: https://docs.lib.purdue.edu/iracc/2541/

E. Vieren, K. Couvreur, M. De Paepe and S. Lecompte, "Design of a high-temperature heat pump providing heat up to 200 °c", eng, in *16th IIR-Gustav Lorentzen Conference on Natural Refrigerants*, College Park, Maryland, USA: University of Maryland, 2024, p. 11, ISBN: 978-2-36215-062-3. [Online]. Available: http://doi.org/10.18462/iir.gl2024.1229

E. Vieren, K. Couvreur, M. De Paepe and S. Lecompte, "Analysis of heat pump-integrated heating network topologies for decarbonization in industrial clusters", eng, in *Proceedings of ECOS 2024 37th International Conference on Efficiency, Cost, Optimization, Simulation and Environmental Impact of Energy Systems*, Rhodos, Greece, 2024, p. 12. [Online]. Available: https://ecos2024.com/proceedings/

E. Vieren, W. Beyne, T. Demeester, K. Couvreur, S. Abbasi, A. Arteconi, M. De Paepe and S. Lecompte, "High-temperature heat pumps: Thermodynamic, economic and experimental perspectives for enhanced integration", in *Proceedings of High-Temperature Heat Pump Symposium 2024*, Copenhagen, Denmark: Technical University of Denmark, 2024. [Online]. Available: https://orbit.dtu.dk/en/publications/4th-high-temperature-heat-pump-symposium-book-of-presentations

A. Degelin, R. Tassenoy, E. Vieren, T. Demeester, I. T'Jollyn and M. De Paepe, "Energetic and financial evaluation of a district heating network under varying supply temperatures and booster technologies", in *Proceedings of 9th edition of the European Thermal Sciences Conference (Eurotherm 2024*, vol. 2766, Bled, Slovenia: IOP Publishing, 2024. [Online]. Available: http://doi.org/10.1088/1742-6596/2766/1/012095

E. Vieren, K. Couvreur, T. Demeester, W. Beyne, M. De Paepe and S. Lecompte, "Experimental design of a high-temperature heat pump with sink temperatures up to 200°c", in *Proceedings of 26th IIR International Congress of Refrigeration (ICR2023)*, Paris, France: International Institute of Refrigeration (IIR), 2023

E. Vieren, W. Beyne, T. Demeester, M. De Paepe and S. Lecompte, "Theoretical assessment of industrial heating technologies up to 250°c", in *Proceedings of 26th IIR International Congress of Refrigeration (ICR2023)*, Paris, France: In-

ternational Institute of Refrigeration (IIR), 2023. [Online]. Available: http://doi.org/10.18462/iir.icr.2023.0324

E. Vieren, T. Demeester, W. Beyne, M. P. Andersen, B. Elmegaard, M. De Paepe and S. Lecompte, "Techno-economic optimization of high-temperature heat pumps using pure fluids and binary mixtures", in *Proceedings of the 14th IEA Heat Pump Conference (HPC2023*, Chicago, Illinois: Technology Collaboration Programme on Heat Pumping Technologies by IEA (HPT TCP), 2023

A. Degelin, R. Tassenoy, E. Vieren, T. Demeester and M. De Paepe, "Influence of supply temperature and booster technology on the energetic performance of a district heating network", in *Book of abstracts : 9th International Conference on Smart Energy Systems (SESAAU2023)*, Copenhagen, Denmark: Aalborg University, 2023, pp. 357–358. [Online]. Available: https://vbn.aau.dk/da/publications/book-of-abstracts-9th-international-conference-on-smart-energy-sy

X. van Heule, T. Schoonjans, E. Vieren, W. Faes, D. Beets, M. Bijnens and M. De Paepe, "Experimental comparison of two fin geometries for cast iron air preheaters", in *Proceedings of the 17th International Heat Transfer Conference (IHTC-17)*, Cape Town, South Africa, 2023, 67:1–67:9. [Online]. Available: http://doi.org/10.1615/IHTC17.210-50

E. Vieren, H. Abedini, T. Demeester, W. Beyne, A. Arteconi, M. De Paepe and S. Lecompte, "Optimal temperature matching in high-temperature heat pumps", in *Proceedings of the High-Temperature Heat Pump Symposium 2022*, Copenhagen, Denmark: Technical University of Denmark, 2022, pp. 225–229, ISBN: 9788774756972. [Online]. Available: https://orbit.dtu.dk/en/publications/3rd-high-temperature-heat-pump-symposium-2022-book-of-presentatio

E. Vieren, T. Demeester, W. Beyne, H. Abedini, A. Arteconi, M. De Paepe and S. Lecompte, Steven, "Natural refrigerants versus synthetic refrigerants for steam-generating heat pumps", in *Proceedings of the 15th IIR-Gustav Lorentzen Conference on Natural Refrigerants (GL2022)*, Trondheim, Norway: International Institute of Refrigeration (IIR), 2022. [Online]. Available: http://doi.org/10.18462/iir.gl2022.0020

X. van Heule, E. Vieren, M. De Paepe and S. Lecompte, "Design of a two-phase reciprocating expansion test-rig for model validation", in *International Compressor Engineering Conference, Proceedings*, West-Lafayette, USA, 2022, p. 10. [Online]. Available: https://docs.lib.purdue.edu/cgi/viewcontent.cgi?article=3802&context=icec

E. Vieren, K. Couvreur, J. Vander Heyde, M. De Paepe and S. Lecompte,

"Techno-economic analysis of high temperature heat pumps: A case study", in *Proceedings of the 15th International Conference on Heat Transfer, Fluid Mechanics and Thermodynamics (HEFAT2021)*, Online, 2021, pp. 2109–2114, ISBN: 9781775922162

R. Tassenoy, E. Vieren, M. De Paepe and S. Lecompte, "Carnot battery : Introduction of a high-level, application based sizing model", in *Proceedings of the 15th International Conference on Heat Transfer, Fluid Mechanics and Thermodynamics (HEFAT2021)*, Online, 2021, pp. 382–387, ISBN: 9781775922162

E. Vieren, K. Couvreur, J. Vander Heyde, M. De Paepe and S. Lecompte, "Simulation, optimization and design of a heating network at an industrial plant", in *Proceedings of the International Conference on Efficiency, Cost, Simulation and Environmental Impact of Energy Systems (ECOS2021)*, Taormina, Italy, 2021, pp. 1981–1992

A full list of articles can be found on the academic bibliography of Ghent University:
https://biblio.ugent.be/person/C6CCFCF8-23FE-11E4-8DF0-78A0B5D1D7B1

# B

# Overview of the selected case studies

## B.1 Steam production case study

The steam production case study is based on data retrieved from the industry. The corresponding process parameters can be found in Table B.1.

Table B.1: Information on the heat source and heat sink for the steam production case study, with $p$ the pressure, $\dot{m}$ the mass flow rate, $T$ the temperature, $x$ the quality and $\dot{Q}$ the heat flow rate.

| | Heat Source | | | | | | Heat Sink | | | | |
|---|---|---|---|---|---|---|---|---|---|---|---|
| Fluid | $p$ [bar] | $\dot{m}$ [kg/s] | $T_{in}$ [°C] | $T_{out}$ [°C] | $\dot{Q}$ [kW] | Fluid | $p$ [bar] | $\dot{m}$ [kg/s] | $x_{in}$ [-] | $x_{out}$ [-] | $\dot{Q}$ [kW] |
| Water | 1 | 9.32 | 78 | 60 | 702.3 | Water | 1.58 | 0.213 | 0 | 1 | 474 |

In this case study there is a steam demand at a pressure of 1.58 bar (saturation temperature of 111.4 °C). The steam network is a closed loop where the water is recirculated and therefore needs to be heated from the saturated liquid state ($x_{in} = 0$) to the saturated vapour state ($x_{out} = 1$). The total heat demand is 474 $kW_{th}$, resulting in a steam mass flow rate of 0.213 kg/s. In the respective industrial site there is also a cooling water circuit. This cooling water circuit operates at a pressure of 1 bar and has a supply temperature of 78 °C and a return temperature of 60 °C. The cooling water has a mass flow rate of 9.32 kg/s, so that 702.3 $kW_{th}$ of heat needs to be cooled. This heat available could

act as a heat source for a heat pump to generate steam.

## B.2 Thermal oil heating case study

The thermal oil heating case study is based on data retrieved from the industry. At the industrial site, thermal oil (Therminol 66) is heated from 140 °C to 200 °C, corresponding with a thermal oil temperature glide of 60 K. Taking into account the demand in mass flow rate, this results in a heat demand of 1254 $kW_{th}$. The same integrated site also has a pressurized hot water residual heat stream available at 100 °C. This residual heat source could be used for a HTHP to heat the thermal oil. The temperature levels, mass flow rate and pressure level of the heat source and sink are reported in Table B.2.

Table B.2: Information on the heat source and heat sink for the thermal oil heating case study, with $p$ the pressure, $\dot{m}$ the mass flow rate, $T$ the temperature and $\dot{Q}$ the heat flow rate.

| | **Heat Source** | | | | | | **Heat Sink** | | | | |
|---|---|---|---|---|---|---|---|---|---|---|---|
| Fluid | $p$ [bar] | $\dot{m}$ [kg/s] | $T_{in}$ [°C] | $T_{out}$ [°C] | $\dot{Q}$ [kW] | Fluid | $p$ [bar] | $\dot{m}$ [kg/s] | $T_{in}$ [°C] | $T_{out}$ [°C] | $\dot{Q}$ [kW] |
| Water | 20 | 20 | 100 | - | - | Therminol 66 | 1 | 10 | 140 | 200 | 1254 |

## B.3 Pressurized hot water production case study

The data in this case study is also based on data retrieved from the industry. Here, the heat sink is pressurized water at 55 bar, which is heated from 140 °C to 200 °C, resulting in a temperature glide of 60 K. Taking into account the mass flow rate, this results in a heat demand of about 7860 $kW_{th}$. The heat source for potential heat pump integration is a residual hot water stream with a temperature of 110 °C and a pressure of 3 bar. The key specifications of the heat sink and heat source streams are presented in Table B.3.

Table B.3: Information on the heat source and heat sink for the pressurized hot water production case study, with $p$ the pressure, $\dot{m}$ the mass flow rate, $T$ the temperature and $\dot{Q}$ the heat flow rate.

| | **Heat Source** | | | | | | **Heat Sink** | | | | |
|---|---|---|---|---|---|---|---|---|---|---|---|
| Fluid | $p$ [bar] | $\dot{m}$ [kg/s] | $T_{in}$ [°C] | $T_{out}$ [°C] | $\dot{Q}$ [kW] | Fluid | $p$ [bar] | $\dot{m}$ [kg/s] | $T_{in}$ [°C] | $T_{out}$ [°C] | $\dot{Q}$ [kW] |
| Water | 3 | 70 | 110 | - | - | Water | 55 | 30 | 140 | 200 | 7860 |

## B.4 Superheated steam drying case study

The data reported in the work of Bang-Møller et al. [237] is used for this case study. In their work the performance of biomass-fueled combined heat and power plants is studied. The first process of the plant is drying of wet wood (42 % water) by means of SSD. Here, the SSD process is isolated and heat pump integration is considered. A schematic of the heat pump assisted SSD process can be found in Figure B.1. In this particular process, superheated steam needs to be heated from 116 °C to 197 °C, resulting in a total heat demand of 370 $kW_{th}$. For this, some superheated steam, with a condensation temperature of 100 °C, is available at 115 °C. If the slightly superheated excess steam completely condenses, about 298 $kW_{th}$ of heat can be extracted. More information regarding the different thermodynamic states can be found in Table B.4. It must be noted that in the actual plant some steam is mixed with the dry wood, as also found in other literature [238]. In this study however it is assumed that all steam can be recuperated from the dried product, which should be possible if air infiltration is avoided [53].

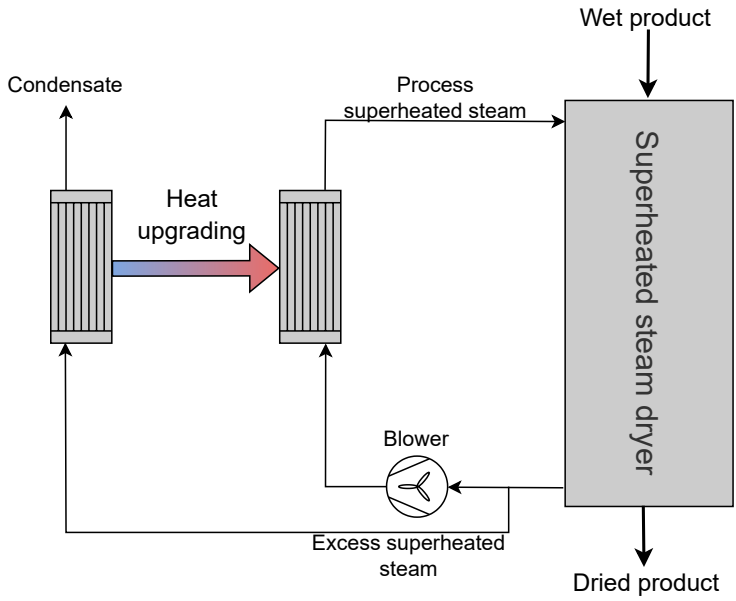


Figure B.1: Scheme of a heat pump assisted superheated steam dryer configuration.

Table B.4: Mass flow rate $\dot{m}$, pressure $p$, temperature $T$ and specific enthalpy $h$ of each state indicated on Figure B.1, data according to Bang-Møller et al. [237].

| State | $\dot{m}$ [kg/s] | $p$ [bar] | $T$ [°C] | $h$ [kJ/(kg·K)] |
|---|---|---|---|---|
| a | 0.32 | 1.013 | 15 | - |
| b | 0.19 | 1.008 | 115 | - |
| 1 | 2.40 | 1.008 | 115 | 2706 |
| 2 | 2.27 | 1.008 | 115 | 2706 |
| 3 | 2.27 | 1.018 | 116 | 2708 |
| 4 | 2.27 | 1.013 | 197 | 2869 |
| 5 | 0.13 | 1.008 | 115 | 2706 |

The information regarding the heat source and sink can be found in Table B.5.

Table B.5: Information on the heat source and heat sink for the SSD case study, with $p$ the pressure, $\dot{m}$ the mass flow rate, $T$ the temperature and $\dot{Q}$ the heat flow rate, data according to Bang-Møller et al. [237].

| Heat Source | | | | | | Heat Sink | | | | | |
|---|---|---|---|---|---|---|---|---|---|---|---|
| Fluid | $p$ [bar] | $\dot{m}$ [kg/s] | $T_{in}$ [°C] | $T_{out}$ [°C] | $\dot{Q}$ [kW] | Fluid | $p$ [bar] | $\dot{m}$ [kg/s] | $T_{in}$ [°C] | $T_{out}$ [°C] | $\dot{Q}$ [kW] |
| Superheated steam | 1 | 0.13 | 115 | - | - | Superheated steam | 1 | 2.27 | 116 | 197 | 370 |

## B.5 Spray drying with external heat source case study

In spray drying an external residual heat source is typically needed to maintain reasonable temperature lifts. Therefore, in this generic case study, an external residual heat stream at a temperature level of 105 °C is considered. Nevertheless, the exhaust air of the spray dryer will still be used for preheating the dry inlet air as shown in Figure B.2. It is assumed that the dry inlet air has a mass flow rate of 1 kg/s and is heated up to 60 °C by the exhaust air. The preheated dry inlet air is then further preheated up to 95 °C by use of the hot water waste heat, considering a temperature difference of 10 K at the pinch point in the respective counter flow heat exchanger. If the outlet temperature of the hot water stream is assumed to be 100 °C, it would imply that there is 1.69 kg/s of hot water available at 100 °C to heat the preheated inlet air from 95 °C to 200 °C by use of a heat pump. This implies a slightly crossing temperature profile of the heat source and sink throughout the heat upgrading.

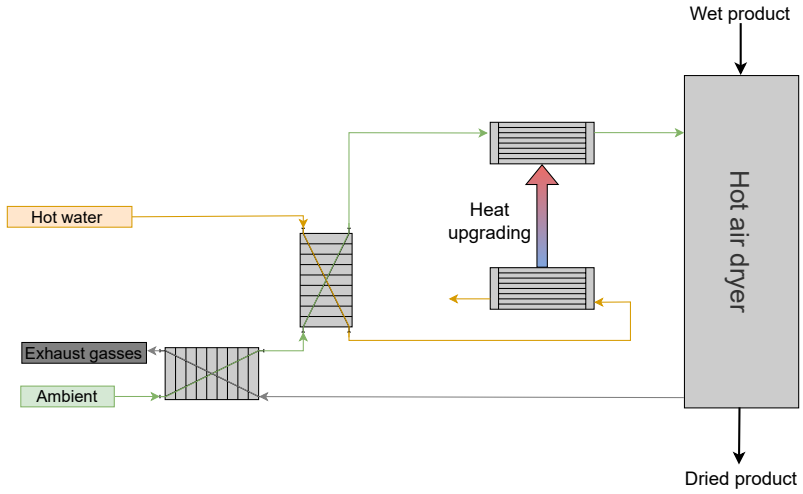


Figure B.2: Considered heat recovery configuration for spray drying case study.

An overview of the process parameters of the heat pump system can be found in Table B.6.

Table B.6: Information on the heat source and heat sink for the spray drying with external heat source case study, with $p$ the pressure, $\dot{m}$ the mass flow rate, $T$ the temperature and $\dot{Q}$ the heat flow rate.

| **Heat Source** | | | | | | **Heat Sink** | | | | | |
|---|---|---|---|---|---|---|---|---|---|---|---|
| Fluid | $p$ [bar] | $\dot{m}$ [kg/s] | $T_{in}$ [°C] | $T_{out}$ [°C] | $\dot{Q}$ [kW] | Fluid | $p$ [bar] | $\dot{m}$ [kg/s] | $T_{in}$ [°C] | $T_{out}$ [°C] | $\dot{Q}$ [kW] |
| Water | 1.5 | 1.69 | 100 | - | - | dry air | 1 | 1 | 95 | 200 | 106.2 |

## B.6 Distillation case study

This case study is based on the work of Chew et al. [49], who studied several concepts for improving the energy efficiency of a distillation dividing-wall column (DWC). A DWC allows for the separation of multi-component mixtures (e.g. tertiary mixture) in a single tower [239, 240]. Consequently the need of a second unit is eliminated, reducing the CAPEX and OPEX due to its compactness and large energy savings.

An example selected here is the tertiary separation of benzene (B), toluene

(T) and ethyl benzene (EB) in DWC configuration, as depicted in Figure B.3. The corresponding properties of interest of each state are given in Table B.7.

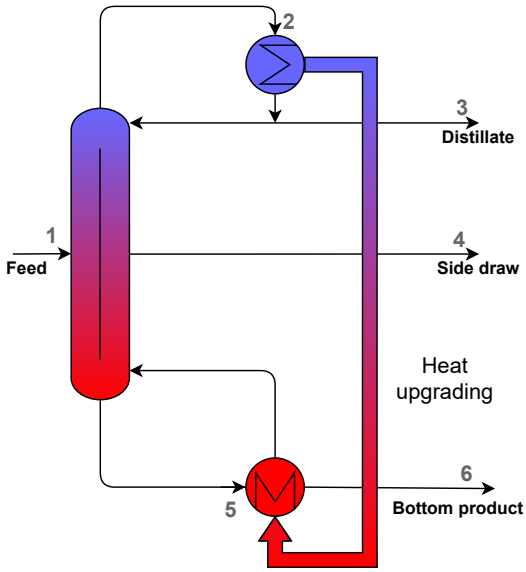


Figure B.3: Illustration of the distillation of benzene, toluene and ethyl benzene in DWC configuration, based on Chew et al. [49].

Table B.7: Thermodynamic properties corresponding to the states depicted in Figure B.3, data according to Chew et al. [49].

| State | $T$ (°C) | $p$ (bar) | Molar flow (kmol/h) | Mol % B | Mol % T | Mol % EB |
|---|---|---|---|---|---|---|
| 1 | 122.9 | 1.75 | 500 | 34 | 33 | 33 |
| 2 | 97.3 | 1.65 | 805.9 | 99.5 | 0.5 | - |
| 3 | 97.2 | 1.65 | 165.5 | 99.5 | 0.5 | - |
| 4 | 133.4 | 1.83 | 163.9 | 0.2 | 96 | 3.8 |
| 5 | 161.2 | 2.00 | 908.3 | - | 6.4 | 93.6 |
| 6 | 162.0 | 2.00 | 170.6 | - | 4.0 | 96.0 |

For this particular case study, 6654 $kW_{th}$ of heat is released at the condenser of the distillation column. As a zeotropic mixture is condensed, its temperature decreases from 97.3 °C to 97.2 °C during condensation. At the same time, 6974 $kW_{th}$ of high quality heat is demanded in the reboiler, also increasing the

temperature from 161.2 °C to 162 °C. Hence, a temperature lift of around 65 °C is needed. The properties of these two streams are reported in Table B.8.

From observing the energy balances, it can be concluded that the reboiler needs 321 $kW_{th}$ more heat than rejected at the condenser. If the energy balance does not allow to provide the heat requested, an externally driven (trim) reboiler should be considered, or an additional residual heat source should be integrated.

Table B.8: Information on the heat source and heat sink for the distillation case study, with $p$ the pressure, $\dot{m}$ the mass flow rate, $T$ the temperature and $\dot{Q}$ the heat flow rate, data based on Chew et al. [49].

| **Heat Source** | | | | | | **Heat Sink** | | | | | |
|---|---|---|---|---|---|---|---|---|---|---|---|
| Fluid | $p$ [bar] | $\dot{m}$ [kg/s] | $T_{in}$ [°C] | $T_{out}$ [°C] | $\dot{Q}$ [kW] | Fluid | $p$ [bar] | $\dot{m}$ [kg/s] | $T_{in}$ [°C] | $T_{out}$ [°C] | $\dot{Q}$ [kW] |
| 99.5% B 0.5% T | 1.65 | 17.5 | 97.3 | 97.2 | 6 654 | 93.6% EB 6.4% T | 2 | 26.56 | 161.2 | 162 | 6 974 |

# C

# Financial appraisal of the high-temperature heat pump technologies: results for other technology costs

## C.1 Generalized vapour compression heat pump financial performance

The LCOH of a VCHP as function of the RHR and the GTL for a specific investment cost of 250 €/$kW_{th}$ and 900 €/$kW_{th}$ under both the high and low electricity price are shown in Figure C.1 and Figure C.2 respectively.

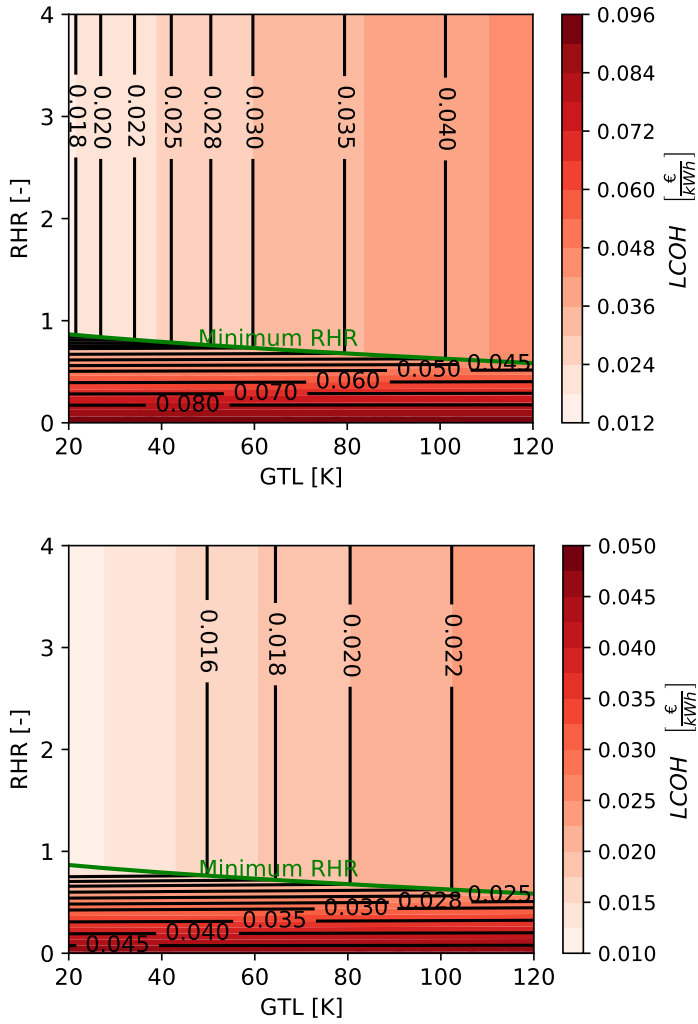


Figure C.1: LCOH of a VCHP as a function of the GTL and RHR, for an electricity price of 0.0945 €/$kWh_e$ (top) and 0.04725 €/$kWh_e$ (bottom) at a VCHP specific investment cost of 250 €/$kW_{th}$.

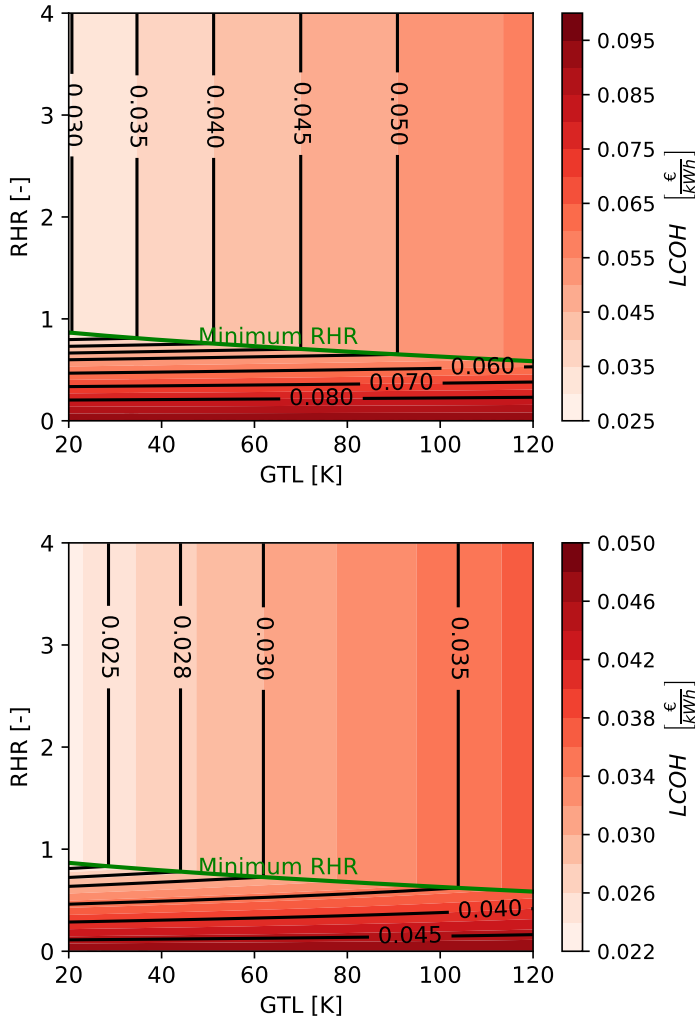


Figure C.2: LCOH of a VCHP as a function of the GTL and RHR, for an electricity price of 0.0945 €/$kWh_e$ (top) and 0.04725 €/$kWh_e$ (bottom) at a VCHP specific investment cost of 900 €/$kW_{th}$.

## C.2 Generalized heat transformer financial performance

The LCOH of a HTF as function of the RHR and the GTL for a specific investment cost of 1000 €/$kW_{th}$ and 2000 €/$kW_{th}$ under both the high and low electricity price are shown in Figure C.3 and Figure C.4 respectively.

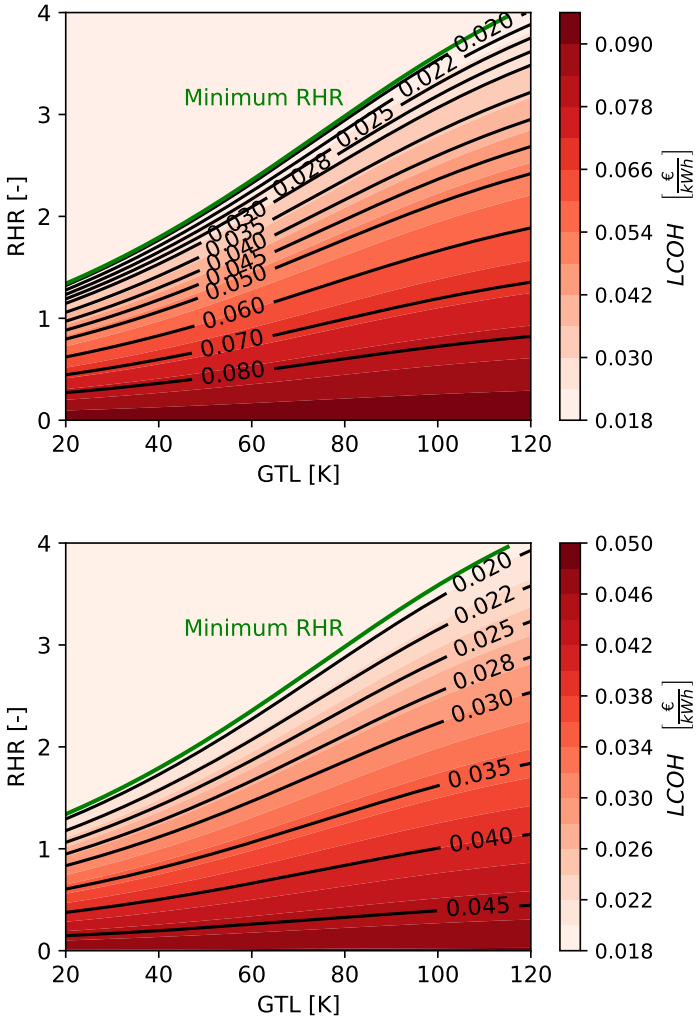


Figure C.3: LCOH of a HTF as a function of the GTL and RHR, for an electricity price of 0.0945 €/$kWh_e$ (top) and 0.04725 €/$kWh_e$ (bottom) at a HTF specific investment cost of 1000 €/$kW_{th}$.

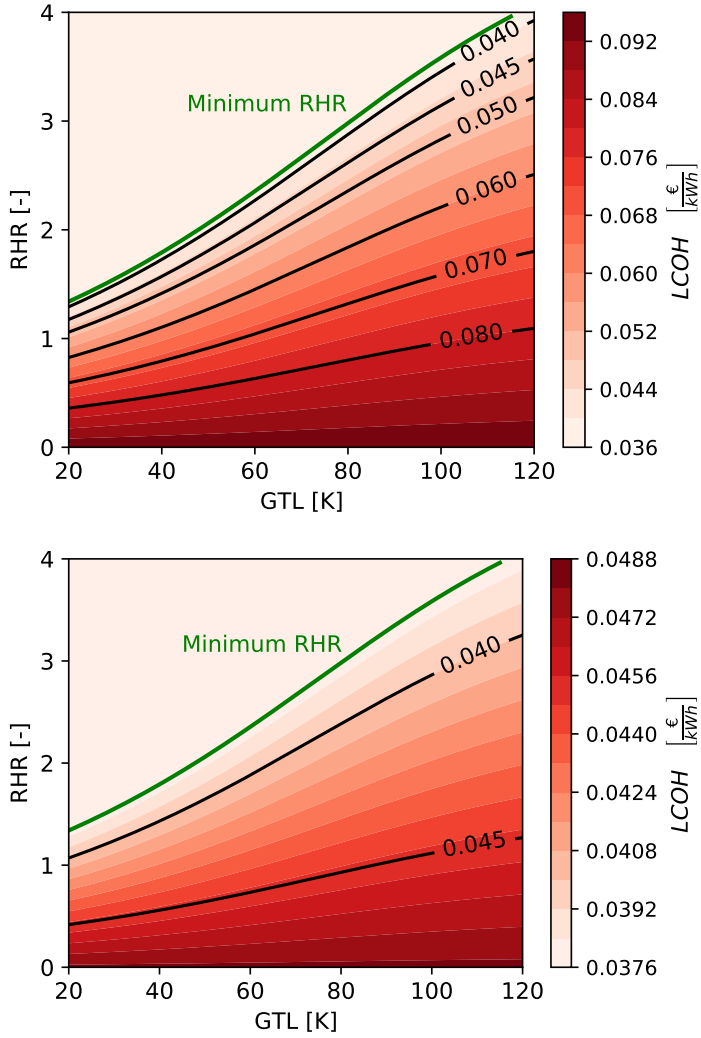


Figure C.4: LCOH of a HTF as a function of the GTL and RHR, for an electricity price of 0.0945 €/$kWh_e$ (top) and 0.04725 €/$kWh_e$ (bottom) at a HTF specific investment cost of 2000 €/$kW_{th}$.

## C.3 Generalized comparison of all renewable technologies

The renewable technology with the lowest LCOH, depending on the GTL and the RHR, for a low technology investment cost and a high technology investment cost can be found in Figure C.5 and Figure C.6 respectively.

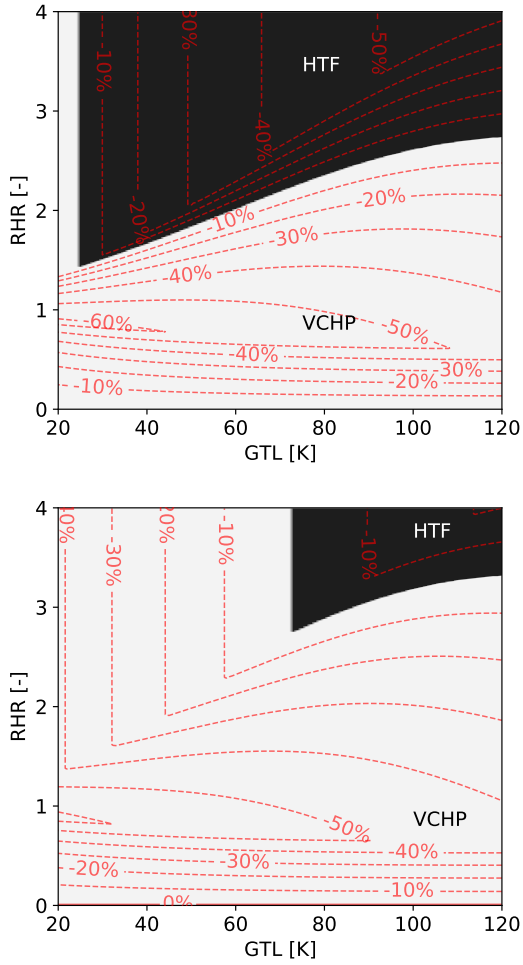


Figure C.5: Renewable technology with the lowest LCOH as a function of the GTL and RHR, for an electricity price of 0.0945 €/$kWh_e$ (top) and 0.04725 €/$kWh_e$ (bottom) at the low specific investment costs. Red lines indicate the relative difference in LCOH (%) between the technology with the lowest LCOH and the second-lowest LCOH.

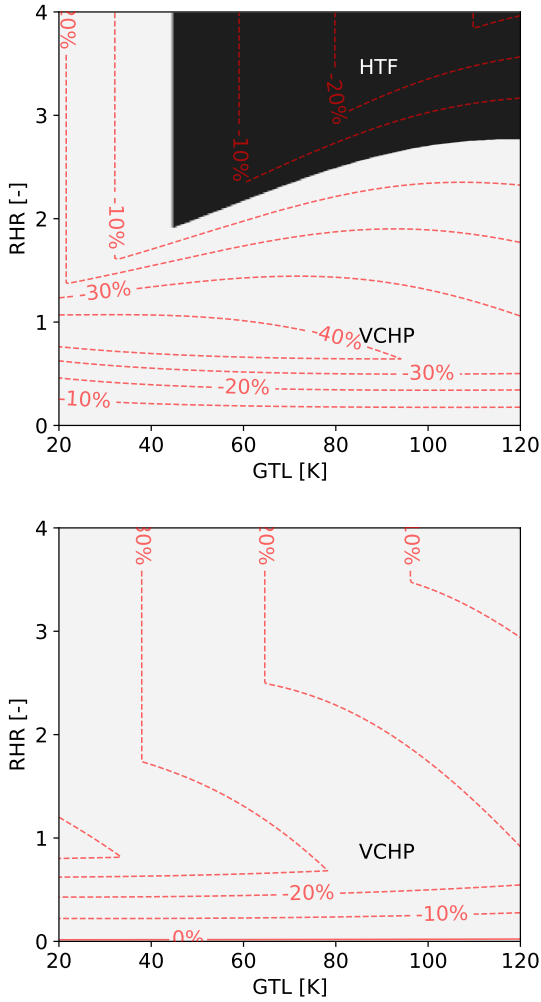


Figure C.6: Renewable technology with the lowest LCOH as a function of the GTL and RHR, for an electricity price of 0.0945 €/$kWh_e$ (top) and 0.04725 €/$kWh_e$ (bottom) at the high specific investment costs. Red lines indicate the relative difference in LCOH (%) between the technology with the lowest LCOH and the second-lowest LCOH.

## C.4 Generalized comparison of all heating technologies

An overview of the technology with the lowest LCOH for the different electricity prices and EGPRs, considering low technology costs can be found in Figure C.7. Figure C.8 shows the same figure but considers a high technology investment cost.

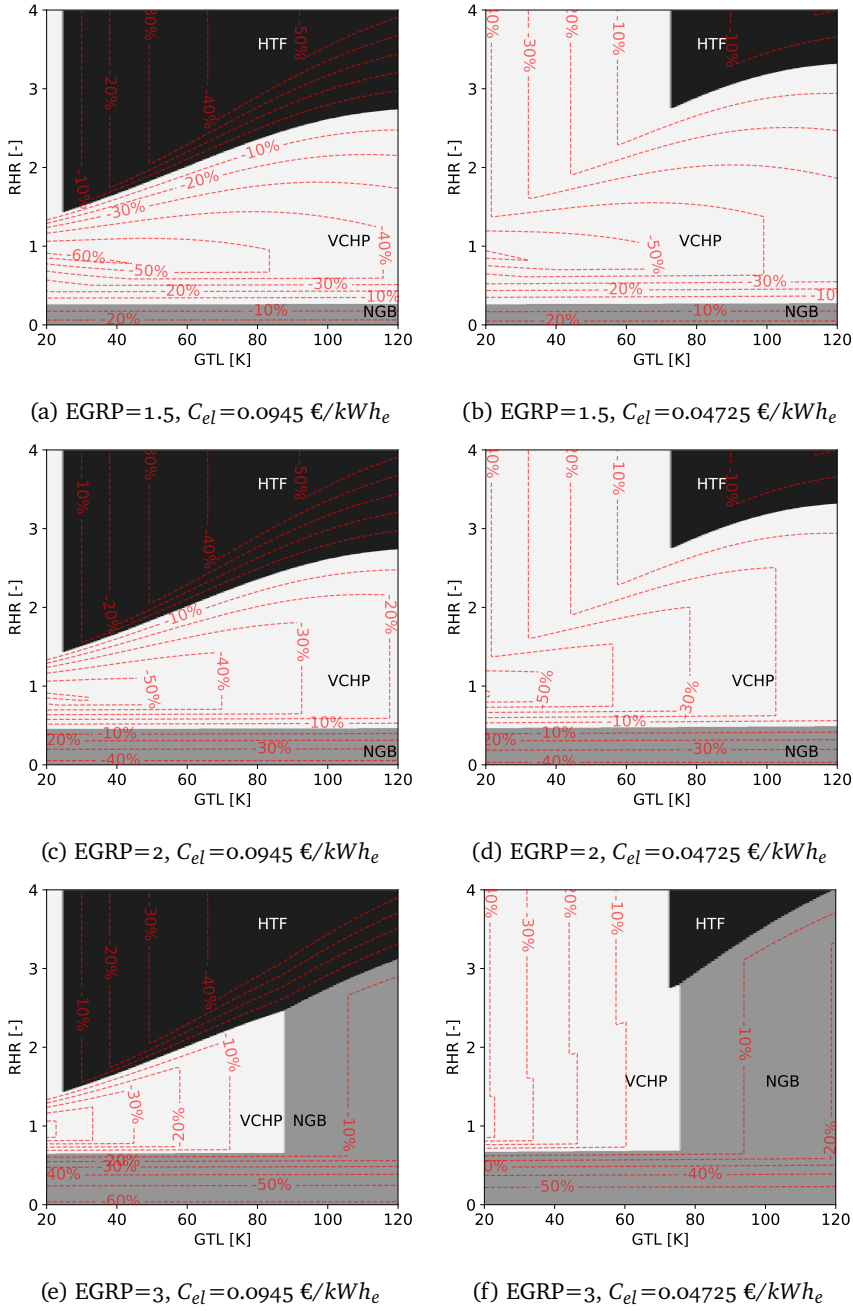


(a) EGRP=1.5, $C_{el}$=0.0945 €/$kWh_e$

(b) EGRP=1.5, $C_{el}$=0.04725 €/$kWh_e$

(c) EGRP=2, $C_{el}$=0.0945 €/$kWh_e$

(d) EGRP=2, $C_{el}$=0.04725 €/$kWh_e$

(e) EGRP=3, $C_{el}$=0.0945 €/$kWh_e$

(f) EGRP=3, $C_{el}$=0.04725 €/$kWh_e$

Figure C.7: Technology with the lowest LCOH as a function of the RHR and GTL, for the different electricity prices and EGPRs, considering low technology investment costs. Red lines indicate the relative difference in LCOH (%) between the technology with the lowest LCOH and the second-lowest LCOH.

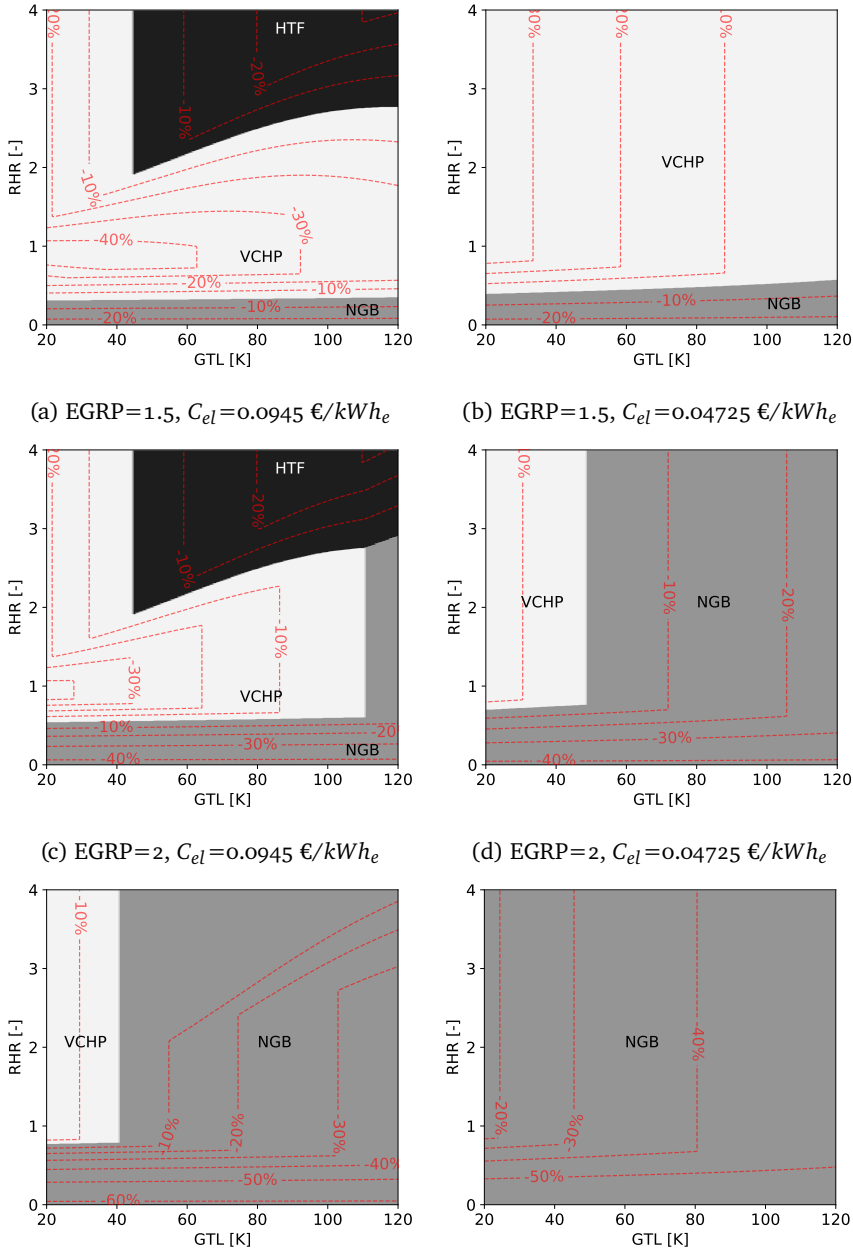


(a) EGRP=1.5, $C_{el}$=0.0945 €/$kWh_e$

(b) EGRP=1.5, $C_{el}$=0.04725 €/$kWh_e$

(c) EGRP=2, $C_{el}$=0.0945 €/$kWh_e$

(d) EGRP=2, $C_{el}$=0.04725 €/$kWh_e$

(e) EGRP=3, $C_{el}$=0.0945 €/$kWh_e$

(f) EGRP=3, $C_{el}$=0.04725 €/$kWh_e$

Figure C.8: Technology with the lowest LCOH as a function of the RHR and GTL, for the different electricity prices and EGPRs, considering high technology investment costs. Red lines indicate the relative difference in LCOH (%) between the technology with the lowest LCOH and the second-lowest LCOH.

# D

# Fundamentals of vapour compression heat pump technology

## D.1 Working principle

An idealized heat pump, transferring heat from a cold body at temperature $T_c$ to a hot body at temperature $T_h$, is represented by the reversed Carnot cycle. In the reversed Carnot cycle all processes (i.e. isentropic compression, isothermal compression, isentropic expansion and isothermal expansion) are internally reversible. The second law of thermodynamic defines the maximum achievable COP given the constant temperatures of the cold and hot body, as shown in Equation D.1.

$$COP_{Carnot} = \frac{T_h}{T_h - T_c} \tag{D.1}$$

However, to operate between a heat sink being heated from $T_{sink,in}$ to $T_{sink,out}$ and a heat source being cooled from $T_{source,in}$ to $T_{source,out}$, the Carnot cycle should operate between the highest temperature ($T_{sink,out}$) and the lowest temperature ($T_{source,out}$). This would result in the non-optimal COP given in Equation D.2.

$$COP_{Carnot,glide} = \frac{T_{sink,out}}{T_{sink,out} - T_{source,out}} \tag{D.2}$$

In these scenarios the Lorenz cycle results in the highest COP possible. The Lorenz cycle is an alternative idealized cycle but considers that heat addition and rejection to the cycle is non-isothermal. Consequently, the heat transfer occurs at the thermodynamic average temperatures of the heat source ($\bar{T}_{sink}$) and heat sink ($\bar{T}_{source}$), resulting in the COP definition shown in Equation D.3.

$$COP_{Lorenz} = \frac{\bar{T}_{sink}}{\bar{T}_{sink} - \bar{T}_{source}} \tag{D.3}$$

For streams with constant heat capacity, $\bar{T}$ equals:

$$\bar{T} = \frac{T_1 - T_2}{ln(\frac{T_1}{T_2})} \tag{D.4}$$

A realization of the reversed Carnot or Lorenz cycle is the reversed Rankine cycle, on which the vapour compression heat pump is based. A schematic and T,s-diagram of an ideal reversed Rankine cycle can be found in Figure D.1. Within this cycle a continuous flow of working fluid passes several components shown in Figure D.1 (a). Here, the evaporator inlet will be considered as starting point. The working fluid enters the inlet of the evaporator as a two-phase liquid vapour mixture. The working fluid then starts to evaporate at constant pressure until point 1 as a result of heat transfer from the cold body, at temperature $T_c$, to the working fluid, providing cooling at the cold body. Consequently, the two-phase liquid-vapour mixture is adiabatically compressed from state 1 to the saturated vapour pressure (state 2). This results in an increase of pressure and temperature of the working fluid. Now, the working fluid goes to the condenser, where the saturated vapour condenses at constant pressure as it transfers heat to the warm body at temperature $T_h$, until it reaches the saturated liquid state (state 3). The working fluid then returns to the inlet of the evaporator by adiabatically expanding it through an expander, recovering compression work.

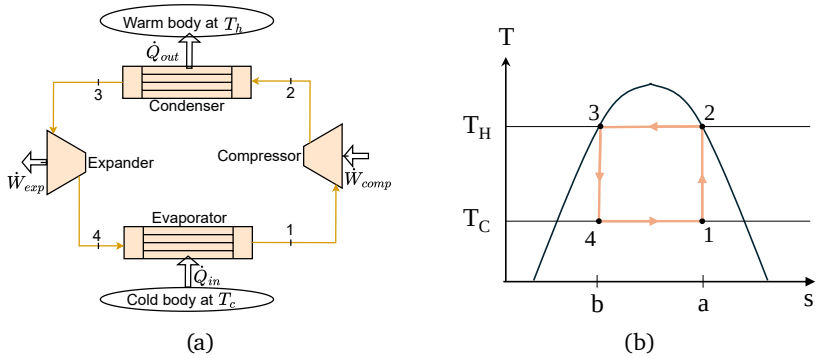


Figure D.1: Schematic (a) and T,s-diagram (b) of a Carnot cycle.

A practical reversed Rankine cycle however deviates from this idealized reversed Rankine cycle in multiple aspects:

- The heat transfer in the heat exchangers is not reversible, leading to a temperature difference between the hot and cold medium. Furthermore, heat losses and pressure drops occur in the heat exchangers.
- The inlet state of the compressor is generally not a two-phase liquid-vapor mixture. This would result in 'wet compression', which is commonly avoided due to the presence of liquid droplets which can damage the compressor. Typical compressors are thus 'dry compressors' which compress vapour only. These compressors require a saturated state at the evaporator outlet at minimum. In practice, the vapour is typically superheated to avoid liquid droplets.
- The compression process is not reversible. It is often characterized by an isentropic efficiency, or by an polytropic efficiency when heat losses are accounted for. Depending on the inlet conditions of the working fluid at the compressor inlet and the vapour saturation curve, this typically results in a superheated vapour state at the compressor outlet.
- The expansion process is not reversible. Furthermore, when the expansion happens over the saturation dome, the expansion work is typically small compared to the compression work. Therefore, a throttling valve, with lower initial and maintenance costs, is often used.
- For applications with temperature glides, improvements are possible with superheating at the evaporator outlet and subcooling at the condenser outlet.

The schematic of an actual VCHP and the corresponding T,s-diagram can be found in Figure D.2. The figure shows the superheat at the evaporator outlet

($\Delta T_{sh}$), subcooling at the condenser outlet ($\Delta T_{sc}$) and the state that would be achieved when the compression is isentropic ($2s$). No influence of pressure drops are shown.

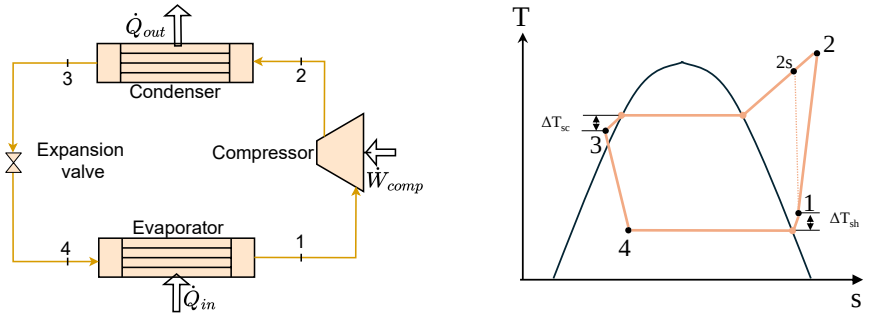


Figure D.2: Schematic (a) and T,s-diagram (b) of an actual cycle.

In part, because of the deviations of the practical VCHP cycle from the idealized Carnot and Lorenz cycles, the COP of these cycles will be lower. In order to benchmark the actual COP with the Carnot COP and Lorenz COP, the Carnot efficiency ($\eta_{Carnot}$) and Lorenz efficiency ($\eta_{Lorenz}$) are often introduced, as shown in Equation D.5 and Equation D.6 respectively.

$$\eta_{Carnot} = \frac{COP}{COP_{Carnot}} \tag{D.5}$$

$$\eta_{Lorenz} = \frac{COP}{COP_{Lorenz}} \tag{D.6}$$

Typical order of magnitudes for these efficiencies are 40 % to 50 % [241].

## D.2 Working fluids

### D.2.1 Historical use and working fluid legislations

An overview of the historical use of working fluid types can be found in Figure D.3.

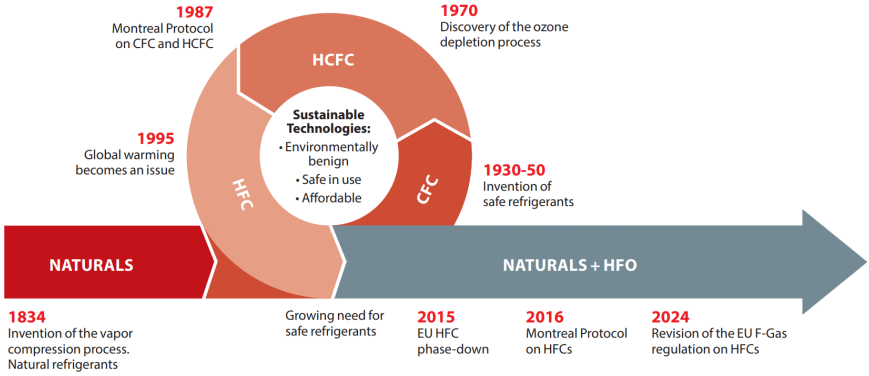


Figure D.3: Historical cycle of the use of working fluids. Figure copied from Refrigeration options report Danfoss [242].

In 1834 Jacob Perkings invented the mechanical cooling system using ethylether as working fluid [243]. In these early days of refrigeration, natural (i.e. substances that naturally occur) and industrially used substances were employed as working fluids. However, by the 1930s, safety concerns emerged due to incidents involving fires and poisoning from working fluid leaks. This led to the development of synthetic working fluids (i.e. synthetically developed substances), specifically chlorofluorocarbons (CFCs), which were safer and quickly adopted worldwide. The development of these type of synthetic working fluids continued in the 1950s with the introduction of hydrochlorofluorocarbons (HCFCs), which were only partially chlorinated. In the early 1970s, it was however discovered that working fluids containing CFCs and HCFCs contributed to the degradation of the ozone layer, due to the presence of chloride atoms. CFCs were found to have a particularly high ozone depletion potential (ODP), and although HCFCs have a comparatively lower ODP, they still caused significant damage. Consequently, the Montreal Protocol, an international treaty aimed at phasing out CFCs and HFCs, was established in 1987. This protocol has since been recognized as a major global success in reducing the emission of hazardous chemicals. Accordingly, there has been a strong push towards substitute working fluids, called hydrofluorocarbons (HFCs), which have an ODP of zero. While the ODP of HFCs is zero they exhibit a relatively high global warming potential (GWP), although lower than for the CFC. In 1995, however, global warming becomes of increased concern. In this aspect the Kyoto Protocol was signed by industrialized nations on December 11, 1997. This protocol aimed to reduce greenhouse gas (GHG) emissions, specifically targeting carbon dioxide ($CO_2$), methane ($CH_4$), sulfur hexafluoride ($SF_6$), nitrogen oxides ($NO_x$), perfluorocarbons (PFCs), and hydrofluorocarbons (HFCs) [243]. This pushed the use of working fluids

slowly back to the natural working fluids, although they never completely disappeared. Even a new group of synthetic refrigerants appeared, namely hydrofluoroolefins (HFOs) and hydrochlorofluroolefins (HCFOs). The HCFOs are often also referred to as HFOs, as also done in Figure D.3. The natural working fluids that are most pushed forward are ammonia, carbon dioxide, hydrocarbons and water. In 2015, the European Union's F-gas regulation (EU 2014/517) [244], established in 2014, came into effect, aiming to phase down HFCs. The aim of this F-gas regulation is to reduce equivalent CO2 emissions by 2030 to two-thirds by their 2014 levels [243]. On October 15, on a global initiative, 2016, the Kigali Amendment to the Montreal Protocol was adopted aiming at a global phase down of HFCs. The EU's updated F-gas Regulation (EU 2024/573) [245], effective March 11, 2024, introduces stricter HFC reduction measures to align with the Green Deal and "Fit for 55" targets. It builds on the 2014 version, mandating a steeper phase-down of HFCs with a full phase-out by 2050.

Currently used working fluids have zero ODP and are pushed towards low GWP. This can be achieved through using natural working fluids and synthetic H(C)FOs. However, recently there is increased attention towards the atmospheric breakdown products of synthetic working fluids. Compounds with a '$CF_3$' group can react in the atmosphere to produce trifluoroacetic acid (TFA), which is a type of per- and polyfluoroalkyl substance (PFAS). TFA quickly dissolves in water and is washed out of the atmosphere by rain. Although it is efficiently removed from the air, TFA poses a toxicity risk to aquatic organisms and is very slow to break down in the environment [246]. Particularly for HFOs and HCFOs the TFA depositions may be an issue. Due to their extremely short atmospheric lifetime, local depositions of TFAs may be an issue. It is important to note that not all F-gases are classified as PFAS, as they do not all contain a '$CF_3$' group. Among PFAS-classified HFOs and HCFOs, some produce only small amounts of TFA upon breakdown, while others can result in nearly 100% TFA formation. The TFA yield depends on the working fluid's chemical composition and involves a complex interaction of various atmospheric factors [242]. This is one of the reasons why the REACH restriction proposal was developed and submitted by five national authorities (the Netherlands, Germany, Sweden, Norway, and Denmark), aimed at regulating the manufacture, market placement (including import), and use of PFAS [247].

### D.2.2 Desired properties of the working fluid

A large amount of working fluids exists, each with their own characteristics. An overview of the desired properties of working fluids can be found in Table D.1.

Table D.1: Desired properties of a working fluid [12, 162, 248].

| Category | Required properties |
|---|---|
| Thermodynamic suitability | Pressure at standstill and during operation > 1 atm |
| | Low compressor discharge temperature |
| | Low compression ratio |
| | High COP at full operating range |
| | High volumetric heating capacity |
| Environmental compatibility | Low GWP, preferably below 10 |
| | Zero ODP |
| | No PFAS breakdown products |
| Safety | Non-toxic |
| | Non-flammable |
| Availability | Low cost |
| | Widely available |
| Technical aspects | Low viscosity (small pressure drops) |
| | High heat transfer coefficients |
| | Good solubility in oil |
| | Good thermal stability of working fluid-oil mixture |
| | Good lubrication properties at full operating range |
| | Good material compatibility (aluminum, steel, copper) |
| | Good thermal stability of the working fluid at full operating range |
| | Good chemical stability of the working fluid at full operating range |

More information regarding the thermophysical properties and the different working fluids can be found in the literature [12, 19, 21, 184, 249, 250].

### D.2.3 Vapour saturation curve

Depending on the shape of the vapour saturation curve, a working fluid for use in heat pumps can be categorized as: dry fluid ($dT/ds < 0$), wet fluid ($dT/ds > 0$) or isentropic fluid ($dT/ds = \infty$) as shown in Figure D.4. A working fluid classified as 'wet' goes through the two-phase region during isentropic compression when starting from saturated vapour state. When the compressor is however not designed to handle compression in the two-phase region, a certain amount of superheat at the evaporator outlet will required for wet fluids [146]. Another option to avoid wet compression is employing an IHX [251]. For a dry or isentropic working fluids, no superheat or IHX is required to avoid wet compression.

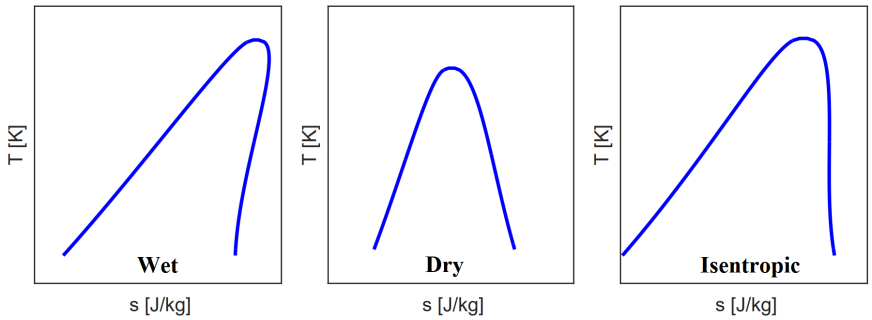


Figure D.4: T,s-diagram of a wet, dry and isentropic working fluid. Figure adapted from Lecompte [252].

## D.3 Importance of flexible operation

The increasing integration of intermittent renewables into the electricity grid threatens the stable operation of the grid. It can also lead to large price fluctuations in the electricity market. Both the need for stable grid operation and the existence of highly volatile energy prices require flexibility on the demand side. Flexibility services can be divided into two types [253]: implicit and explicit flexibility. Implicit flexibility refers to the voluntary adjustment of electricity use by users in order to reduce the costs associated with electricity price fluctuations or to reduce the overall electricity tariff expenditure. On the other hand, explicit flexibility involves a formal agreement or participation in a flexibility market where the supplier offers its ability to adjust electricity use as a service. It is expected that electricity price operation will favour on-off operation, whereas flexibility operation will favour part-load operation. The start-up time of a heat pump is in the range of a few minutes, but excessive start-up and shut-down is avoided, as it can be detrimental to the heat pump and also increase maintenance costs [253]. However, for some heat pump designs it should be possible to start and stop the heat pump frequently. The capacity of the heat pump can be adjusted by changing the load of the compressor(s). The compressor load is changed either by using a variable speed drive or by shutting down one or more compressors in parallel systems. Typical reported minimum loads, limited by a minimum compressor speed and poor drive efficiency, are in the order of 20 % to 40 % [254–256].

# E

# Overview of the working fluid screening

Table E.1: Overview of the working fluid screening.

| Short name | Short Formula | Critical temperature [°C] | Critical pressure [bar] | Passed working fluid screening? | GWP ≤ 150? | ODP ≈ 0? | NFPA health hazard ≤ 4? | NFPA Reactivity = 0? |
|---|---|---|---|---|---|---|---|---|
| 1,3-Butadiene | $C_4H_6$ | 152.0 | 43.1 | No | Yes | Yes | Yes | No |
| 1-Butyne | $C_4H_6$ | 158.9 | 41.4 | No | Yes | Yes | Yes | No |
| 1-Pentene | $C_5H_{10}$ | 192.6 | 36.0 | No | Yes | Yes | Yes | No |
| 2,2-Dimethylbutane | $C_6H_{14}$ | 216.9 | 31.4 | Yes | Yes | Yes | Yes | Yes |
| 2,3-Dimethylbutane | $C_6H_{14}$ | 227.5 | 31.6 | Yes | Yes | Yes | Yes | Yes |
| 3-Methylpentane | $C_6H_{14}$ | 232.9 | 31.8 | Yes | Yes | Yes | Yes | Yes |
| Acetone | $C_3H_6O$ | 235.0 | 46.9 | Yes | Yes | Yes | Yes | Yes |
| Acetylene | $C_2H_2$ | 35.2 | 59.9 | No | Yes | Yes | Yes | No |
| Ammonia (R-717) | $NH_3$ | 132.4 | 113.6 | Yes | Yes | Yes | Yes | Yes |
| Argon (R-740) | Ar | -122.5 | 48.6 | Yes | Yes | Yes | Yes | Yes |
| Benzene | $C_6H_6$ | 288.9 | 49.1 | Yes | Yes | Yes | Yes | Yes |
| Butane (R-600) | $C_4H_{10}$ | 152.0 | 38.0 | Yes | Yes | Yes | Yes | Yes |
| Butene | $C_4H_8$ | 146.1 | 40.1 | Yes | Yes | Yes | Yes | Yes |
| Carbon dioxide (R-744) | $CO_2$ | 31.0 | 73.8 | Yes | Yes | Yes | Yes | Yes |
| Carbon monoxide | CO | -140.3 | 34.9 | Yes | Yes | Yes | Yes | Yes |
| Carbonyl sulfide | COS | 105.6 | 63.7 | No | Yes | Yes | Yes | No |
| Chlorine | $Cl_2$ | 143.7 | 76.4 | No | Yes | No | No | Yes |
| Chlorobenzene | $C_6H_5Cl$ | 359.2 | 45.2 | No | Yes | No | Yes | Yes |
| cis-Butene | $C_4H_8$ | 162.6 | 42.3 | Yes | Yes | Yes | Yes | Yes |
| Cyclobutene | $C_4H_6$ | 174.9 | 51.5 | Yes | Yes | Yes | Yes | Yes |
| Cyclohexane | $C_6H_{12}$ | 280.5 | 40.8 | Yes | Yes | Yes | Yes | Yes |
| Cyclopentane | $C_5H_{10}$ | 238.6 | 45.8 | Yes | Yes | Yes | Yes | Yes |
| Cyclopropane | $C_3H_6$ | 125.2 | 55.8 | Yes | Yes | Yes | Yes | Yes |
| D4 | $C_8H_{24}O_4Si_4$ | 313.4 | 13.5 | Yes | Yes | Yes | Yes | Yes |
| D5 | $C_{10}H_{30}O_5Si_5$ | 345.2 | 10.9 | Yes | Yes | Yes | Yes | Yes |
| D6 | $C_{12}H_{36}Si_6O_6$ | 372.6 | 9.6 | Yes | Yes | Yes | Yes | Yes |
| DEA | $C_4H_{11}NO_2$ | 463.4 | 49.5 | Yes | Yes | Yes | Yes | Yes |
| Decane | $C_{10}H_{22}$ | 344.6 | 21.0 | Yes | Yes | Yes | Yes | Yes |
| Deuterium | $D_2$ | -234.8 | 16.8 | Yes | Yes | Yes | Yes | Yes |
| Dichloroethane (R-150) | $C_2H_4Cl_2$ | 288.5 | 52.3 | No | Yes | No | Yes | Yes |
| Diethyl ether | $C_4H_{10}O$ | 193.6 | 37.2 | No | Yes | Yes | Yes | No |
| Dimethyl carbonate | $C_3H_6O_3$ | 283.9 | 49.1 | Yes | Yes | Yes | Yes | Yes |
| Dimethyl ether (RE-170) | $C_2H_6O$ | 127.2 | 53.4 | No | Yes | Yes | Yes | No |
| Docosane | $C_{22}H_{46}$ | 519.1 | 11.7 | Yes | Yes | Yes | Yes | Yes |
| Dodecane | $C_{12}H_{26}$ | 385.0 | 18.2 | Yes | Yes | Yes | Yes | Yes |
| Ethane (R-170) | $C_2H_6$ | 32.2 | 48.7 | Yes | Yes | Yes | Yes | Yes |
| Ethanol | $C_2H_6O$ | 241.6 | 62.7 | Yes | Yes | Yes | Yes | Yes |
| Ethylene glycol | $C_2H_6O_2$ | 445.9 | 105.1 | Yes | Yes | Yes | Yes | Yes |
| Ethylbenzene | $C_8H_{10}$ | 344.0 | 36.2 | Yes | Yes | Yes | Yes | Yes |
| Ethylene (R-1150) | $C_2H_4$ | 9.2 | 50.4 | No | Yes | Yes | Yes | No |
| Ethylene oxide | $C_2H_4O$ | 195.8 | 73.0 | No | Yes | Yes | Yes | No |
| Fluorine | $F_2$ | -128.7 | 51.7 | No | Yes | Yes | No | No |
| Heavy water | $D_2O$ | 370.7 | 216.6 | No | Yes | Yes | No | No |
| Helium (R-704) | He | -268.0 | 2.3 | Yes | Yes | Yes | Yes | Yes |
| Heptane | $C_7H_{16}$ | 267.1 | 27.4 | Yes | Yes | Yes | Yes | Yes |

| Short name | Short Formula | Critical temperature [°C] | Critical pressure [bar] | Passed working fluid screening? | GWP ≤ 150? | ODP ≈ 0? | NFPA health hazard ≤ 4? | NFPA Reactivity = 0? |
|---|---|---|---|---|---|---|---|---|
| Hexadecane | $C_{16}H_{34}$ | 449.0 | 14.8 | Yes | Yes | Yes | Yes | Yes |
| Hexane | $C_6H_{14}$ | 234.7 | 30.4 | Yes | Yes | Yes | Yes | Yes |
| Hydrogen (R-702) | $H_2$ | -240.0 | 13.0 | Yes | Yes | Yes | Yes | Yes |
| Hydrogen chloride | HCl | 51.5 | 83.1 | No | Yes | No | Yes | No |
| Hydrogen sulfide | $H_2S$ | 100.0 | 90.0 | No | Yes | Yes | No | Yes |
| Isobutane (R-600a) | $C_4H_{10}$ | 134.7 | 36.3 | Yes | Yes | Yes | Yes | Yes |
| Isobutene | $C_4H_8$ | 144.9 | 40.1 | No | Yes | Yes | Yes | No |
| Isohexane | $C_6H_{14}$ | 224.6 | 30.4 | Yes | Yes | Yes | Yes | Yes |
| Isooctane | $C_8H_{18}$ | 270.9 | 25.7 | Yes | Yes | Yes | Yes | Yes |
| Isopentane (R-601a) | $C_5H_{12}$ | 187.2 | 33.8 | Yes | Yes | Yes | Yes | Yes |
| Krypton (R-784) | Kr | -63.7 | 55.3 | Yes | Yes | Yes | Yes | Yes |
| MD2M | $C_{10}H_{30}Si_4O_3$ | 326.3 | 11.4 | Yes | Yes | Yes | Unkown | Unkown |
| MD3M | $C_{12}H_{36}Si_5O_4$ | 355.8 | 9.6 | Yes | Yes | Yes | Unkown | Unkown |
| MD4M | $C_{14}H_{42}O_5Si_6$ | 380.1 | 8.4 | Yes | Yes | Yes | Unkown | Unkown |
| MDM | $C_8H_{24}O_2Si_3$ | 292.2 | 14.4 | Yes | Yes | Yes | Unkown | Unkown |
| MEA | $C_2H_7NO$ | 398.3 | 81.3 | Yes | Yes | Yes | Yes | Yes |
| Methane (R-50) | $CH_4$ | -82.6 | 46.0 | Yes | Yes | Yes | Yes | Yes |
| Methanol | $CH_4O$ | 240.2 | 82.2 | Yes | Yes | Yes | Yes | Yes |
| Methyl linoleate | $C_{19}H_{34}O_2$ | 525.9 | 13.4 | Yes | Yes | Yes | Unkown | Unkown |
| Methyl linolenate | $C_{19}H_{32}O_2$ | 498.9 | 13.7 | Yes | Yes | Yes | Unkown | Unkown |
| Methyl oleate | $C_{19}H_{36}O_2$ | 508.9 | 12.5 | Yes | Yes | Yes | Unkown | Unkown |
| Methyl palmitate | $C_{17}H_{34}O_2$ | 481.9 | 13.5 | Yes | Yes | Yes | Unkown | Unkown |
| Methyl stearate | $C_{19}H_{38}O_2$ | 501.9 | 12.4 | Yes | Yes | Yes | Yes | Yes |
| Methylcyclohexane | $C_7H_{14}$ | 299.1 | 34.7 | Yes | Yes | Yes | Yes | Yes |
| MM | $C_6H_{18}OSi_2$ | 245.6 | 19.3 | Yes | Yes | Yes | Unkown | Unkown |
| m-Xylene | $C_8H_{10}$ | 343.7 | 35.3 | Yes | Yes | Yes | Yes | Yes |
| Neon(R-720) | Ne | -228.8 | 26.6 | Yes | Yes | Yes | Unkown | Unkown |
| Neopentane | $C_5H_{12}$ | 160.6 | 32.0 | Yes | Yes | Yes | Yes | Yes |
| Nitrogen (R-728) | $N_2$ | -147.0 | 34.0 | Yes | Yes | Yes | Unkown | Unkown |
| Nitrogen trifluoride | $F_3N$ | -39.2 | 44.6 | Yes | Yes | Yes | Unkown | Unkown |
| Nitrous oxide (R-744A) | $N_2O$ | 36.4 | 72.5 | No | No | Yes | Unkown | Unkown |
| Nonane | $C_9H_{20}$ | 321.4 | 22.8 | Yes | Yes | Yes | Yes | Yes |
| Novec 649, 1230 | $C_6F_{12}O$ | 168.7 | 18.7 | Yes | Yes | Yes | Unkown | Unkown |
| Octane | $C_8H_{18}$ | 295.6 | 24.8 | Yes | Yes | Yes | Yes | Yes |
| Orthohydrogen(R-702) | $H_2$ | -239.9 | 13.1 | Yes | Yes | Yes | Yes | Yes |
| Oxygen (R-732) | $O_2$ | -118.6 | 50.4 | Yes | Yes | Yes | Yes | Yes |
| o-Xylene | $C_8H_{10}$ | 357.1 | 37.4 | Yes | Yes | Yes | Yes | Yes |
| Parahydrogen(R-702p) | $H_2$ | -240.2 | 12.9 | Yes | Yes | Yes | Yes | Yes |
| Pentane (R-601) | $C_5H_{12}$ | 196.6 | 33.7 | Yes | Yes | Yes | Yes | Yes |
| Perfluorobutane | $C_4F_{10}$ | 113.2 | 23.2 | No | No | Yes | Unkown | Unkown |
| Perfluorohexane | $C_6F_{14}$ | 174.9 | 17.4 | No | No | Yes | Unkown | Unkown |
| Perfluoropentane | $C_5F_{12}$ | 147.9 | 20.6 | No | No | Yes | Unkown | Unkown |
| Propadiene | $C_3H_4$ | 124.9 | 52.2 | Yes | Yes | Yes | Unkown | Unkown |
| Propane (R-290) | $C_3H_8$ | 96.7 | 42.5 | Yes | Yes | Yes | Yes | Yes |
| Propylcyclohexane | $C_9H_{18}$ | 357.7 | 28.6 | Yes | Yes | Yes | Unkown | Unkown |
| Propylene (R-1270) | $C_3H_6$ | 91.1 | 45.6 | No | Yes | Yes | Yes | No |
| Propylene oxide | $C_3H_6O$ | 215.0 | 54.4 | No | Yes | Yes | Yes | No |
| Propyne | $C_3H_4$ | 129.2 | 56.3 | No | Yes | Yes | Yes | No |
| p-Xylene | $C_8H_{10}$ | 343.0 | 35.3 | Yes | Yes | Yes | Yes | Yes |
| R11 | $CCl_3F$ | 198.0 | 44.1 | No | No | No | Unkown | Unkown |
| R1123 | $C_2HF_3$ | 58.6 | 45.4 | Yes | Yes | Yes | Unkown | Unkown |
| R113 | $C_2Cl_3F_3$ | 214.1 | 33.9 | No | No | No | Unkown | Unkown |
| R114 | $C_2Cl_2F_4$ | 145.7 | 32.6 | No | No | No | Yes | Yes |
| R115 | $C_2ClF_5$ | 80.0 | 31.3 | No | No | No | Yes | Yes |
| R116 | $C_2F_6$ | 19.9 | 30.5 | No | No | Yes | Yes | Yes |
| R12 | $CCl_2F_2$ | 112.0 | 41.4 | No | No | No | Yes | Yes |
| R1216 | $C_3F_6$ | 85.8 | 31.5 | No | Yes | Yes | Yes | No |
| R1224yd(Z) | $C_3HClF_4$ | 155.5 | 33.4 | Yes | Yes | Yes | Yes | Yes |
| R123 | $C_2HCl_2F_3$ | 183.7 | 36.6 | No | Yes | No | Yes | No |
| R1233zd(E) | $C_3H_2ClF_3$ | 166.5 | 36.2 | Yes | Yes | Yes | Yes | Yes |
| R1234yf | $C_3F_4H_2$ | 94.7 | 33.8 | Yes | Yes | Yes | Yes | Yes |
| R1234ze(E) | $C_3F_4H_2$ | 109.4 | 36.3 | Yes | Yes | Yes | Yes | Yes |
| R1234ze(Z) | $C_3F_4H_2$ | 150.1 | 35.3 | Yes | Yes | Yes | Yes | Yes |
| R124 | $C_2HClF_4$ | 122.3 | 36.2 | No | No | No | Unkown | Unkown |
| R1243zf | $C_3H_3F_3$ | 103.8 | 35.2 | Yes | Yes | Yes | Unkown | Unkown |
| R125 | $C_2HF_5$ | 66.0 | 36.2 | No | No | Yes | Unkown | Unkown |
| R13 | $CClF_3$ | 28.9 | 38.8 | No | No | No | Unkown | Unkown |
| R1336mzz(Z) | $C_4H_2F_6$ | 171.4 | 29.0 | Yes | Yes | Yes | Yes | Yes |
| R134a | $C_2H_2F_4$ | 101.1 | 40.6 | No | No | Yes | Yes | No |
| R13I1 | $CF_3I$ | 123.3 | 39.5 | No | Yes | No | Unkown | Unkown |
| R14 | $CF_4$ | -45.6 | 37.5 | No | No | Yes | Unkown | Unkown |
| R141b | $C_2H_3Cl_2F$ | 204.4 | 42.1 | No | No | No | Yes | Yes |
| R142b | $C_2H_3ClF_2$ | 137.1 | 40.6 | No | No | No | Yes | Yes |
| R143a | $C_2H_3F_3$ | 72.7 | 37.6 | No | No | Yes | Unkown | Unkown |
| R152a | $C_2H_4F_2$ | 113.3 | 45.2 | Yes | Yes | Yes | Unkown | Unkown |
| R161 | $C_2H_5F$ | 102.1 | 50.5 | Yes | Yes | Yes | Unkown | Unkown |
| R21 | $CHCl_2F$ | 178.3 | 51.8 | No | No | No | Unkown | Unkown |
| R218 | $C_3F_8$ | 71.9 | 26.4 | No | No | Yes | Unkown | Unkown |
| R22 | $CHClF_2$ | 96.1 | 49.9 | No | No | No | Yes | No |
| R227ea | $C_3HF_7$ | 101.8 | 29.3 | No | No | Yes | Yes | No |
| R23 | $CHF_3$ | 26.1 | 48.3 | No | No | Yes | Yes | Yes |
| R236ea | $C_3H_2F_6$ | 139.3 | 34.2 | No | No | Yes | Yes | Yes |
| R236fa | $C_3H_2F_6$ | 124.9 | 32.0 | No | No | Yes | Yes | Yes |
| R245ca | $C_3H_3F_5$ | 174.4 | 39.4 | No | No | Yes | Unkown | Unkown |
| R245fa | $C_3H_3F_5$ | 153.9 | 36.5 | No | No | Yes | Yes | Yes |
| R32 | $CH_2F_2$ | 78.1 | 57.8 | No | No | Yes | Yes | Yes |
| R365mfc | $C_4H_5F_5$ | 186.9 | 32.7 | No | No | No | Yes | Yes |
| R40 | $CH_3Cl$ | 143.2 | 66.9 | No | Yes | No | Yes | Yes |
| R41 | $CH_3F$ | 44.1 | 59.0 | Yes | Yes | Yes | Yes | Yes |
| RC318 | $C_4F_8$ | 115.2 | 27.8 | No | No | Yes | Unkown | Unkown |
| RE143a | $C_2H_3F_3O$ | 104.8 | 36.4 | No | No | Yes | Unkown | Unkown |
| RE245cb2 | $C_3H_3F_5O$ | 133.7 | 28.9 | No | No | Yes | Unkown | Unkown |
| RE245fa2 | $C_3H_3F_5O$ | 171.7 | 34.3 | No | No | Yes | Unkown | Unkown |
| RE347mcc (HFE-7000) | $C_4H_3F_7O$ | 164.6 | 24.8 | No | No | Yes | Unkown | Unkown |
| Sulfur dioxide (R-764) | $O_2S$ | 157.5 | 78.9 | Yes | Yes | Yes | Yes | Yes |
| Sulfur hexafluoride | $SF_6$ | 45.6 | 37.5 | No | No | Yes | Unkown | Unkown |
| Toluene | $C_7H_8$ | 318.6 | 41.3 | Yes | Yes | Yes | Yes | Yes |
| trans-Butene | $C_4H_8$ | 155.5 | 40.3 | No | Yes | Yes | Yes | No |
| Undecane | $C_{11}H_{24}$ | 365.7 | 19.9 | Yes | Yes | Yes | Yes | Yes |
| Vinyl chloride (R-1140) | $C_2H_3Cl$ | 151.8 | 55.9 | No | Yes | No | Yes | No |
| Water (R-718) | $H_2O$ | 373.9 | 220.6 | Yes | Yes | Yes | Yes | Yes |
| Xenon | Xe | 16.6 | 58.4 | Yes | Yes | Yes | Unkown | Unkown |

# F

# Techno-economic screening of high-temperature heat pump configurations: detailed results of the sensitivity analysis

## F.1 Influence of the electricity price

Table F.1: Overview of the five best performing working fluids for the 'sensible sensible' temperature profile under different electricity prices. * BIPs not available for fluid.

| Working fluid | Molar fraction first component | Stages | IHX | COP | LCOH [€/kWh] | $C_{inv}$ [€/kW] |
|---|---|---|---|---|---|---|
| $c_e$ = 0.0403 €/kWh | | | | | | |
| Cis-2-butene&methanol | 0.569 | 1 | Yes | 3.44 | 0.0191 | 338 |
| Cyclobutene&toluene* | 0.957 | 1 | Yes | 3.39 | 0.0192 | 337 |
| Benzene&cyclobutene* | 0.084 | 1 | Yes | 3.35 | 0.0193 | 334 |
| Cyclobutene&octane* | 0.976 | 1 | Yes | 3.41 | 0.0193 | 344 |
| Cyclobutene&heptane* | 0.954 | 1 | Yes | 3.41 | 0.0193 | 346 |
| $c_e$ = 0.0806 €/kWh (base case) | | | | | | |
| Methanol&ammonia | 0.685 | 1 | No | 3.85 | 0.0290 | 372 |
| Cyclopentane&methanol* | 0.230 | 1 | No | 3.99 | 0.0294 | 425 |
| Cis-2-butene&methanol | 0.110 | 1 | Yes | 3.91 | 0.0274 | 497 |
| Benzene&methanol | 0.647 | 1 | Yes | 4.10 | 0.0307 | 511 |
| Cyclobutene&octane* | 0.974 | 1 | No | 3.49 | 0.0309 | 359 |
| $c_e$ = 0.1209 €/kWh | | | | | | |
| Cyclopentane&methanol* | 0.168 | 1 | Yes | 3.88 | 0.0403 | 421 |
| Benzene&ethanol | 0.677 | 1 | Yes | 4.23 | 0.0404 | 543 |
| Cyclopentane&ethanol | 0.304 | 1 | Yes | 3.99 | 0.0412 | 502 |
| Cyclopentane&methanol* | 0.735 | 1 | Yes | 4.10 | 0.0412 | 497 |
| Benzene&cyclobutene* | 0.185 | 1 | Yes | 3.87 | 0.0415 | 474 |

## F.2 Influence of the annual operating hours

Table F.2: Overview of the five best performing working fluids for the 'sensible sensible' temperature profile under different annual operating hours. * BIPs not available for fluid.

| Working fluid | Molar fraction first component | Stages | IHX | COP | LCOH [€/kWh] | $C_{inv}$ [€/kW] |
|---|---|---|---|---|---|---|
| Annual operating hours = 7000 h (base case) | | | | | | |
| Methanol&ammonia | 0.685 | 1 | No | 3.85 | 0.0290 | 372 |
| Cyclopentane&methanol* | 0.230 | 1 | Yes | 3.95 | 0.0294 | 425 |
| Cis-2-Butene&methanol* | 0.110 | 1 | Yes | 3.83 | 0.0304 | 363 |
| Benzene&methanol* | 0.647 | 1 | Yes | 4.10 | 0.0307 | 511 |
| Cyclobutene&octane* | 0.974 | 1 | No | 3.49 | 0.0309 | 359 |
| Annual operating hours = 3500 h | | | | | | |
| Cis-2-Butene&methanol | 0.569 | 1 | Yes | 3.44 | 0.0381 | 337 |
| Cyclobutene&toluene* | 0.962 | 1 | Yes | 3.39 | 0.0384 | 336 |
| Cyclobutene&benzene* | 0.926 | 1 | Yes | 3.35 | 0.0385 | 333 |
| Cyclobutene&heptane* | 0.958 | 1 | Yes | 3.41 | 0.0386 | 344 |
| Cyclobutene&cyclohexane* | 0.942 | 1 | Yes | 3.36 | 0.0387 | 340 |

## F.3 Influence of the heat pump capacity

Table F.3: Overview of the five best performing working fluids for the 'sensible sensible' temperature profile under different heating capacities. * BIPs not available for fluid.

| Working fluid | Molar fraction first component | Stages | IHX | COP | LCOH [€/kWh] | $C_{inv}$ [€/kW] |
|---|---|---|---|---|---|---|
| Heating capacity = 250 kW | | | | | | |
| Methanol&ammonia | 0.659 | 1 | No | 3.72 | 0.0305 | 406 |
| Cyclopentane&methanol* | 0.233 | 1 | Yes | 3.94 | 0.0313 | 501 |
| Cis-2-butene&methanol | 0.584 | 1 | Yes | 3.56 | 0.032 | 431 |
| Cyclobutene&toluene* | 0.962 | 1 | Yes | 3.45 | 0.0325 | 421 |
| Cyclobutene&heptane* | 0.960 | 1 | Yes | 3.42 | 0.0326 | 418 |
| Heating capacity = 500 kW (base case) | | | | | | |
| Methanol&ammonia | 0.685 | 1 | No | 3.85 | 0.0290 | 372 |
| Cyclopentane&methanol* | 0.230 | 1 | Yes | 3.95 | 0.0294 | 425 |
| Cis-2-butene&methanol | 0.110 | 1 | Yes | 3.83 | 0.0304 | 363 |
| Benzene&methanol | 0.647 | 1 | Yes | 4.10 | 0.0307 | 511 |
| Cyclobutene&octane* | 0.974 | 1 | Yes | 3.49 | 0.0309 | 359 |
| Heating capacity = 1000 kW | | | | | | |
| Methanol&ammonia | 0.724 | 1 | No | 3.87 | 0.0278 | 323 |
| Cyclopentane&methanol* | 0.224 | 1 | Yes | 3.95 | 0.0285 | 373 |
| Benzene&methanol | 0.656 | 1 | Yes | 4.12 | 0.0292 | 444 |
| Cis-2-butene&methanol | 0.585 | 1 | Yes | 3.56 | 0.0295 | 315 |
| Cyclopentane&ethanol | 0.483 | 1 | Yes | 3.89 | 0.0297 | 414 |

# G

# Piping and instrumentation diagram of the high-temperature heat pump design

An overview of the piping and instrumentation diagram of the HTHP design can be found in Figure G.1. The design consists of four main circuits; (1) the thermal oil heat source circuit (blue), (2) the refrigerant heat pump circuit (black), (3) an intermediate thermal oil heat sink circuit (red) and (4) the water and ethylene glycol heat rejection circuit (yellow). Both the heat rejection circuit and the thermal oil heater (including auxiliary components such as pump, storage, accumulator and air vent) were already present in the lab prior to the design of the heat pump, as they were used for experimental research on organic Rankine cycles. Therefore, they are given in a green box. All other parts had to be designed. Because the water with ethylene glycol circuit is designed for temperatures below 100 °C, an intermediate thermal oil circuit is designed, capable for handling temperatures up to 250 °C. Both oil circuits make use of therminol 66. The refrigerant circuit consists of the main loop, a bearing lubrication loop and a two-phase injection loop. All circuits are also equipped with different types of sensors allowing for an in depth analysis of the experimental design. All components have a tag existing of six characters. The first two characters are letters indicating the component name, as shown in the legend at the right bottom of Figure G.1. The next four

characters are digits with the first two indicating the circuit number and the last two the tag number within the circuit.

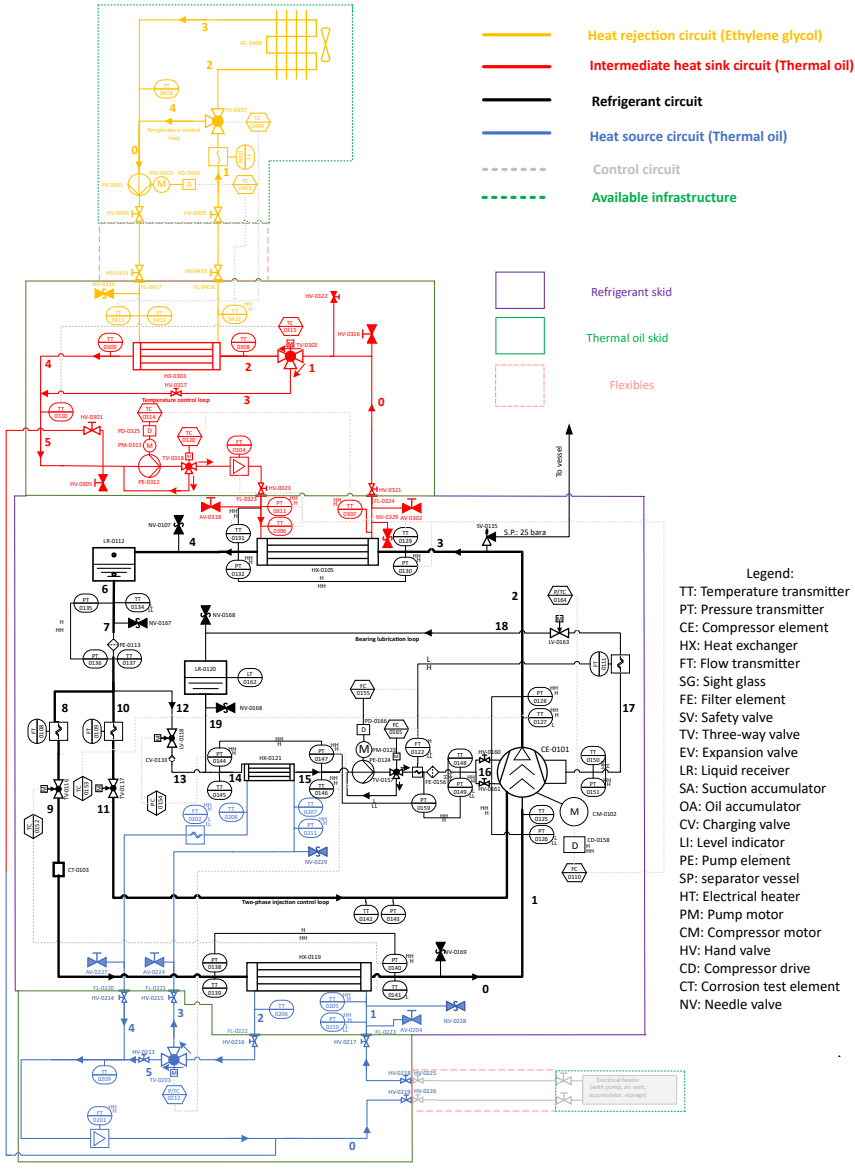


Figure G.1: Piping and instrumentation diagram of the experimental high-temperature heat pump design.

# H

# 3-D design of the high-temperature heat pump

The HTHP will be installed in the Sustainable Thermo-Fluid Energy Systems research group's lab in Kortrijk. Considering the lab structure and arrangement, and the components selected, the 3-D design of the high-temperature heat pump was made. A view of the design from different angles can be found in Figures H.1 and H.2.

The design of the heat pump consists of two skids, namely the 'refrigerant skid' and the 'thermal oil skid'. Both are also indicated in the P&ID diagram shown in Appendix G. The refrigerant skid consists of the refrigerant circuit, while the thermal oil skid consists of both the thermal oil heat source and heat sink circuit. Splitting up the design in two skids allows for a wider use of these skids. When split up, the thermal oil skid can be used more conveniently for other heat pump designs. Each skid will be placed in the lab on a heavy-duty workbench. The connections between the different skids and the thermal oil heater and heat rejection circuit will be made using flexibles.

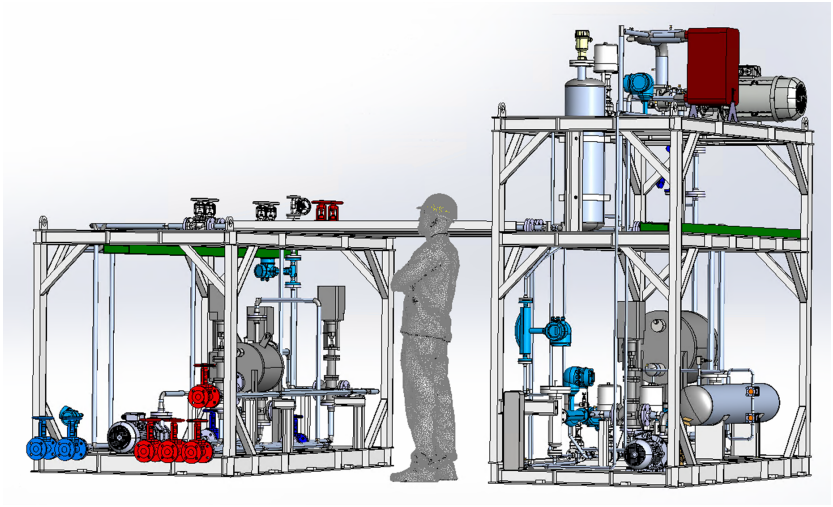

Figure H.1: 3-D design of the experimental high-temperature heat pump - view 1.

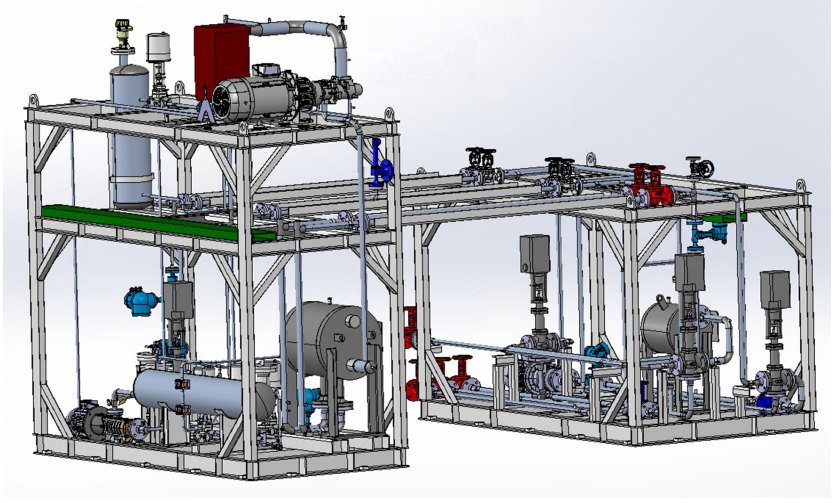

Figure H.2: 3-D design of the experimental high-temperature heat pump - view 2.

# Bibliography


[1] R. Dhillon and G. von Wuehlisch, "Mitigation of global warming through renewable biomass", *Biomass and Bioenergy*, vol. 48, pp. 75–89, 2013, ISSN: 0961-9534. DOI: https://doi.org/10.1016/j.biombioe.2012.11.005. [Online]. Available: https://www.sciencedirect.com/science/article/pii/S0961953412004734.

[2] United Nations Framework Convention on Climate Change, "The paris agreement", *Conference of the Parties: Twenty-first Session*, Dec. 2015, Accessed: 2024-08-02. [Online]. Available: https://unfccc.int/process-and-meetings/conferences/past-conferences/paris-climate-change-conference-november-2015/cop-21.

[3] R. Lindsey and L. Dahlman, *Climate change: Global temperature*, Accessed: 2024-08-02, Jan. 2024. [Online]. Available: https://www.climate.gov/news-features/understanding-climate/climate-change-global-temperature.

[4] H. D. Matthews and S. Wynes, "Current global efforts are insufficient to limit warming to 1.5°c", *Science*, vol. 376, no. 6600, pp. 1404–1409, 2022. DOI: 10.1126/science.abo3378.

[5] K. O. Yoro and M. O. Daramola, "Chapter 1 - co2 emission sources, greenhouse gases, and the global warming effect", in *Advances in Carbon Capture*, M. R. Rahimpour, M. Farsi, and M. A. Makarem, Eds., Woodhead Publishing, 2020, pp. 3–28, ISBN: 978-0-12-819657-1. DOI: https://doi.org/10.1016/B978-0-12-819657-1.00001-3. [Online]. Available: https://www.sciencedirect.com/science/article/pii/B9780128196571000013.

[6] Our World in Data. "Greenhouse gas emissions by sector". Accessed: 2024-08-02. (2024), [Online]. Available: https://ourworldindata.org/ghg-emissions-by-sector.

[7] R. de Boer *et al.*, "Strengthening industrial heat pump innovation: Decarbonizing industrial heat", SINTEF Energi AS, 2020, Accessed: 2024-06-24. [Online]. Available: https://hthp-symposium.org/high-temperature-heat-pumps/white-paper-strengthening-industrial-heat-pump-innovation.

[8] Global Carbon Project, *Supplemental data of global carbon budget 2019 (version 1.0)*, 2019. DOI: 10.18160/gcp-2019. [Online]. Available: https://doi.org/10.18160/gcp-2019.

[9] R. D. Brook *et al.*, "Particulate matter air pollution and cardiovascular disease", *Circulation*, vol. 121, no. 21, pp. 2331–2378, 2010. DOI: 10.1161/CIR.0b013e3181dbece1. eprint: https://www.ahajournals.org/doi/pdf/10.1161/CIR.0b013e3181dbece1. [Online]. Available: https://www.ahajournals.org/doi/abs/10.1161/CIR.0b013e3181dbece1.

[10] K. Vohra, A. Vodonos, J. Schwartz, E. A. Marais, M. P. Sulprizio, and L. J. Mickley, "Global mortality from outdoor fine particle pollution generated by fossil fuel combustion: Results from geos-chem", *Environmental Research*, vol. 195, p. 110754, 2021, ISSN: 0013-9351. DOI: https://doi.org/10.1016/j.envres.2021.110754. [Online]. Available: https://www.sciencedirect.com/science/article/pii/S0013935121000487.

[11] Fraunhofer ISI, *Direct electrification of industrial process heat: An assessment of technologies, potentials and future prospects for the eu*, Study on behalf of Agora Industry, 2024.

[12] C. Arpagaus, F. Bless, M. Uhlmann, J. Schiffmann, and S. S. Bertsch, "High temperature heat pumps: Market overview, state of the art, research status, refrigerants, and application potentials", *Energy*, vol. 152, pp. 985–1010, 2018, ISSN: 0360-5442. DOI: https://doi.org/10.1016/j.energy.2018.03.166. [Online]. Available: https://www.sciencedirect.com/science/article/pii/S0360544218305759.

[13] International Energy Agency (IEA); Heat Pump Technologies (HPT), *Annex58 task 1: Technologies – state of the art and ongoing developments for systems and components*, https://heatpumpingtechnologies.org/annex58/task1/, Accessed: 2022-07-07, 2022.

[14] A. Marina, S. Spoelstra, H. Zondag, and A. Wemmers, "An estimation of the european industrial heat pump market potential", *Renewable and Sustainable Energy Reviews*, vol. 139, p. 110545, 2021, ISSN: 1364-0321. DOI: https://doi.org/10.1016/j.rser.2020.110545. [Online]. Available: https://www.sciencedirect.com/science/article/pii/S1364032120308297.

[15] E. Vieren, T. Demeester, W. Beyne, C. Magni, H. Abedini, C. Arpagaus, S. Bertsch, A. Alessia, M. De Paepe and S. Lecompte, "The potential of vapor compression heat pumps supplying process heat between 100 and 200 °c in the chemical industry", *Energies*, vol. 16, no. 18, 2023, ISSN: 1996-1073. DOI: 10.3390/en16186473. [Online]. Available: https://www.mdpi.com/1996-1073/16/18/6473.

[16] M. Khamooshi, K. Parham, M. Yari, S. Babadi, F. Egelioglu, and H. Salati, "Thermodynamic analysis and optimization of a high temperature triple absorption heat transformer", *The Scientific World Journal*, vol. 2014, Jul. 2014. DOI: 10.1155/2014/980452.

[17] V. Mounier, L. C. Mendoza, and J. Schiffmann, "Thermo-economic optimization of an orc driven heat pump based on small scale turbomachinery and comparison with absorption heat pumps", *International Journal of Refrigeration*, vol. 81, pp. 96–110, 2017, ISSN: 0140-7007. DOI: https://doi.org/10.1016/j.ijrefrig.2017.05.021. [Online]. Available: https://www.sciencedirect.com/science/article/pii/S0140700717302128.

[18] Z. Xu and R. Wang, "Absorption heat pump for waste heat reuse: current states and future development", *Frontiers in Energy*, vol. 11, no. 4, pp. 414–436, 2017, ISSN: 20951698. DOI: 10.1007/s11708-017-0507-1.

[19] D. Wu, B. Hu, and R. Wang, "Vapor compression heat pumps with pure low-gwp refrigerants", *Renewable and Sustainable Energy Reviews*, vol. 138, p. 110 571, 2021, ISSN: 1364-0321. DOI: https://doi.org/10.1016/j.rser.2020.110571. [Online]. Available: https://www.sciencedirect.com/science/article/pii/S136403212030856X.

[20] C. Mateu-Royo, J. Navarro-Esbrí, A. Mota-Babiloni, M. Amat-Albuixech, and F. Molés, "Theoretical evaluation of different high-temperature heat pump configurations for low-grade waste heat recovery", *International Journal of Refrigeration*, vol. 90, pp. 229–237, 2018, ISSN: 0140-7007. DOI: https://doi.org/10.1016/j.ijrefrig.2018.04.017. [Online]. Available: https://www.sciencedirect.com/science/article/pii/S0140700718301233.

[21] J. Jiang, B. Hu, R. Wang, N. Deng, F. Cao, and C.-C. Wang, "A review and perspective on industry high-temperature heat pumps", *Renewable and Sustainable Energy Reviews*, vol. 161, p. 112 106, 2022, ISSN: 1364-0321. DOI: https://doi.org/10.1016/j.rser.2022.112106. [Online]. Available: https://www.sciencedirect.com/science/article/pii/S1364032122000351.

[22] E. Vieren, T. Demeester, W. Beyne, A. Arteconi, M. De Paepe, and S. Lecompte, "The thermodynamic potential of high-temperature transcritical heat pump cycles for industrial processes with large temperature glides", *Applied Thermal Engineering*, vol. 234, p. 121 197, 2023, ISSN: 1359-4311. DOI: https://doi.org/10.1016/j.applthermaleng.2023.121197. [Online]. Available: https://www.sciencedirect.com/science/article/pii/S1359431123012267.

[23] O. Bamigbetan, T. M. Eikevik, P. Nekså, M. Bantle, and C. Schlemminger, "Experimental investigation of a prototype r-600 compressor for high temperature heat pump", *Energy*, vol. 169, pp. 730–738, 2019, ISSN: 0360-5442. DOI: https://doi.org/10.1016/j.energy.2018.12.020. [Online]. Available: https://www.sciencedirect.com/science/article/pii/S0360544218323867.

[24] D. Boman, A. Raymond, and S. Garimella, *Adsorption Heat Pumps: Fundamentals and Applications*. Jan. 2021, ISBN: 978-3-030-72179-4. DOI: 10.1007/978-3-030-72180-0.

[25] A. Hepbasli, Z. Erbay, F. Icier, N. Colak, and E. Hancioglu, "A review of gas engine driven heat pumps (gehps) for residential and industrial applications", *Renewable and Sustainable Energy Reviews*, vol. 13, no. 1, pp. 85–99, 2009, ISSN: 1364-0321. DOI: https://doi.org/10.1016/j.rser.2007.06.014. [Online]. Available: https://www.sciencedirect.com/science/article/pii/S1364032107001268.

[26] U.S. Department of Energy, *Industrial heat pumps for steam and fuel savings*, https://www.energy.gov/eere/amo/downloads/industrial-heat-pumps-steam-and-fuel-savings, Accessed: 10-08-2021, 2020.

[27] A. Kühn, Ed., *Thermally driven heat pumps for heating and cooling*. Berlin: Universitätsverlag der TU Berlin, 2013. DOI: 10.14279/depositonce-3726. [Online]. Available: http://dx.doi.org/10.14279/depositonce-3726.

[28] W. Wu, B. Wang, W. Shi, and X. Li, "Absorption heating technologies: A review and perspective", *Applied Energy*, vol. 130, pp. 51–71, 2014, ISSN: 0306-2619. DOI: https://doi.org/10.1016/j.apenergy.2014.05.027. [Online]. Available: https://www.sciencedirect.com/science/article/pii/S0306261914005224.

[29] H. Demir, M. Mobedi, and S. Ülkü, "A review on adsorption heat pump: Problems and solutions", *Renewable and Sustainable Energy Reviews*, vol. 12, no. 9, pp. 2381–2403, 2008, ISSN: 1364-0321. DOI: https://doi.org/10.1016/j.rser.2007.06.005. [Online]. Available: https://www.sciencedirect.com/science/article/pii/S1364032107000998.

[30] K. Parham, M. Khamooshi, D. B. K. Tematio, M. Yari, and U. Atikol, "Absorption heat transformers - A comprehensive review", *Renewable and Sustainable Energy Reviews*, vol. 34, pp. 430–452, 2014, ISSN: 1364-0321. DOI: https://doi.org/10.1016/j.rser.2014.03.036. [Online]. Available: http://www.sciencedirect.com/science/article/pii/S136403211400197X.

[31] P. Donnellan, K. Cronin, and E. Byrne, "Recycling waste heat energy using vapour absorption heat transformers: A review", *Renewable and Sustainable Energy Reviews*, vol. 42, pp. 1290–1304, 2015, ISSN: 1364-0321. DOI: https://doi.org/10.1016/j.rser.2014.11.002. [Online]. Available: https://www.sciencedirect.com/science/article/pii/S1364032114009319.

[32] A. Sözen and H. S. Yücesu, "Performance improvement of absorption heat transformer", *Renewable Energy*, vol. 32, no. 2, pp. 267–284, 2007, ISSN: 0960-1481. DOI: https://doi.org/10.1016/j.renene.2006.01.017. [Online]. Available: https://www.sciencedirect.com/science/article/pii/S0960148106000450.

[33] X. Ma *et al.*, "Application of absorption heat transformer to recover waste heat from a synthetic rubber plant", *Applied Thermal Engineering*, vol. 23, no. 7, pp. 797–806, 2003, ISSN: 1359-4311. DOI: https://doi.org/10.1016/S1359-4311(03)00011-5. [Online]. Available: https://www.sciencedirect.com/science/article/pii/S1359431103000115.

[34] *High-Temperature Heat Pumps: Task 1 – Technologies: Task Report*, English. IEA Heat Pump Centre, 2023.

[35] S. Klute, M. Budt, M. van Beek, and C. Doetsch, "Steam generating heat pumps – overview, classification, economics, and basic modeling principles", *Energy Conversion and Management*, vol. 299, p. 117882, 2024, ISSN: 0196-8904. DOI: https://doi.org/10.1016/j.enconman.2023.117882. [Online]. Available: https://www.sciencedirect.com/science/article/pii/S0196890423012281.

[36] G. Kosmadakis, "Estimating the potential of industrial (high-temperature) heat pumps for exploiting waste heat in eu industries", *Applied Thermal Engineering*, vol. 156, pp. 287–298, 2019, ISSN: 1359-4311. DOI: https://doi.org/10.1016/j.applthermaleng.2019.04.082. [Online]. Available: https://www.sciencedirect.com/science/article/pii/S1359431118376087.

[37] M. H. Bade and S. Bandyopadhyay, "Minimization of thermal oil flow rate for indirect integration of multiple plants", *Industrial & Engineering Chemistry Research*, vol. 53, no. 33, pp. 13 146–13 156, 2014. DOI: 10.1021/ie502059f. eprint: https://doi.org/10.1021/ie502059f. [Online]. Available: https://doi.org/10.1021/ie502059f.

[38] S. Ai, B. Wang, X. Li, and W. Shi, "Analysis of a heat recovery system of the spray-drying process in a soy protein powder plant", *Applied Thermal Engineering*, vol. 103, pp. 1022–1030, 2016, ISSN: 1359-4311. DOI: https://doi.org/10.1016/j.applthermaleng.2016.04.108. [Online]. Available: https://www.sciencedirect.com/science/article/pii/S1359431116305968.

[39] K. Matsuda, D. Kurosaki, D. Hayashi, and K. Aoyama, "Industrial heat pump study using pinch technology for a large scale petrochemical site", *Chemical Engineering Transactions*, vol. 29, pp. 67–72, Sep. 2012. DOI: 10.3303/CET1229012. [Online]. Available: https://www.cetjournal.it/index.php/cet/article/view/CET1229012.

[40] Q. Zhang *et al.*, "Economically and thermodynamically efficient heat pump-assisted side-stream pressure-swing distillation arrangement for separating a maximum-boiling azeotrope", *Applied Thermal Engineering*, vol. 173, p. 115 228, 2020, ISSN: 1359-4311. DOI: https://doi.org/10.1016/j.applthermaleng.2020.115228. [Online]. Available: https://www.sciencedirect.com/science/article/pii/S1359431119361691.

[41] H. Shahandeh, M. Jafari, N. Kasiri, and J. Ivakpour, "Economic optimization of heat pump-assisted distillation columns in methanol-water separation", *Energy*, vol. 80, pp. 496–508, 2015, ISSN: 0360-5442. DOI: https://doi.org/10.1016/j.energy.2014.12.006. [Online]. Available: https://www.sciencedirect.com/science/article/pii/S0360544214013632.

[42] A. Marina and S. Spoelstra and H.A. Zondag and A.K. Wemmers, "Industrial process and waste heat data for eu28", *Mendeley Data*, p. V1, 2020, Cited by: 1. [Online]. Available: https://www.scopus.com/inward/record.uri?eid=2-s2.0-85099634332&partnerID=40&md5=ec5a5b218e02c574d7d9221cb3e40204.

[43] H. Bauer, J. Ehrmaier, L. Gigliotti, F. Liebach, T. Schleyer, and A. Simoncini, "Industrial heat pumps: Five considerations for future growth", *McKinsey & Company*, 2024, Accessed: 2024-08-26. [Online]. Available: https://www.mckinsey.com/industries/industrials-and-electronics/our-insights/industrial-heat-pumps-five-considerations-for-future-growth.

[44] O. Dumont, G. F. Frate, A. Pillai, S. Lecompte, M. De paepe, and V. Lemort, "Carnot battery technology: A state-of-the-art review", *Journal of Energy Storage*, vol. 32, p. 101 756, 2020, ISSN: 2352-152X. DOI: https://doi.org/10.1016/j.est.2020.101756. [Online]. Available: https://www.sciencedirect.com/science/article/pii/S2352152X20315930.

[45] A. A. Kiss and R. Smith, "Rethinking energy use in distillation processes for a more sustainable chemical industry", *Energy*, vol. 203, p. 117 788, 2020, ISSN: 0360-5442. DOI: https://doi.org/10.1016/j.energy.2020.117788. [Online]. Available: https://www.sciencedirect.com/science/article/pii/S0360544220308951.

[46] H. Luo, C. S. Bildea, and A. A. Kiss, "Novel heat-pump-assisted extractive distillation for bioethanol purification", *Industrial & Engineering Chemistry Research*, vol. 54, no. 7, pp. 2208–2213, 2015. DOI: 10.1021/ie504459c. eprint: https://doi.org/10.1021/ie504459c. [Online]. Available: https://doi.org/10.1021/ie504459c.

[47] A. Jana, "Advances in heat pump assisted distillation column: A review", *Energy Conversion and Management*, vol. 77, pp. 287–297, 2014.

[48] A. A. Kiss, S. J. F. Landaeta, and C. A. I. Ferreira, "Towards energy efficient distillation technologies – making the right choice", *Energy*, vol. 47, no. 1, pp. 531–542, 2012, ISSN: 0360-5442. DOI: 10.1016/j.energy.2012.09.038. [Online]. Available: https://www.sciencedirect.com/science/article/pii/S0360544212007165.

[49] J. M. Chew, C. Reddy, and G. Rangaiah, "Improving energy efficiency of dividing-wall columns using heat pumps, organic rankine cycle and kalina cycle", *Chemical Engineering and Processing: Process Intensification*, vol. 76, pp. 45–59, 2014, ISSN: 0255-2701. DOI: https://doi.org/10.1016/j.cep.2013.11.011. [Online]. Available: https://www.sciencedirect.com/science/article/pii/S0255270113002754.

[50] A. Kazemi, A. Mehrabani-Zeinabad, and M. Beheshti, "Recently developed heat pump assisted distillation configurations: A comparative study", *Applied Energy*, vol. 211, pp. 1261–1281, 2018, ISSN: 0306-2619. DOI: https://doi.org/10.1016/j.apenergy.2017.12.023. [Online]. Available: https://www.sciencedirect.com/science/article/pii/S0306261917317373.

[51] X. You, I. Rodriguez-Donis, and V. Gerbaud, "Reducing process cost and co2 emissions for extractive distillation by double-effect heat integration and mechanical heat pump", *Applied Energy*, vol. 166, pp. 128–140, 2016, ISSN: 0306-2619. DOI: https://doi.org/10.1016/j.apenergy.2016.01.028. [Online]. Available: https://www.sciencedirect.com/science/article/pii/S0306261916300083.

[52] L. J. Goh, M. Y. Othman, S. Mat, H. Ruslan, and K. Sopian, "Review of heat pump systems for drying application", *Renewable and Sustainable Energy Reviews*, vol. 15, no. 9, pp. 4788–4796, 2011, ISSN: 1364-0321. DOI: https://doi.org/10.1016/j.rser.2011.07.072. [Online]. Available: https://www.sciencedirect.com/science/article/pii/S1364032111003170.

[53] A. Mujumdar, *Handbook of Industrial Drying*. CRC Press, 2006, ISBN: 9781420017618.

[54] *Dryficiency project*, http://dry-f.eu/, Accessed: 2021-07-26.

[55] J. Wang, C. Brown, and D. Cleland, "Heat pump heat recovery options for food industry dryers", *International Journal of Refrigeration*, vol. 86, pp. 48–55, 2018, ISSN: 0140-7007. DOI: https://doi.org/10.1016/j.ijrefrig.2017.11.028. [Online]. Available: https://www.sciencedirect.com/science/article/pii/S0140700717304826.

[56] B. Zühlsdorf, F. Bühler, R. Mancini, S. Cignitti, and B. Elmegaard, "High temperature heat pump integration using zeotropic working fluids for spray drying facilities", English, in *Proceedings of the 12th IEA Heat Pump Conference 2017*, 12th IEA Heat Pump Conference ; Conference date: 15-05-2017 Through 18-05-2017, 2017.

[57] B. Zühlsdorf, F. Bühler, M. Bantle, and B. Elmegaard, "Analysis of technologies and potentials for heat pump-based process heat supply above 150 °c", *Energy Conversion and Management: X*, vol. 2, p. 100 011, 2019, ISSN: 2590-1745. DOI: https://doi.org/10.1016/j.ecmx.2019.100011. [Online]. Available: https://www.sciencedirect.com/science/article/pii/S2590174519300091.

[58] C. L. Law, H. H. Chen, and A. S. Mujumdar, "Food Technologies: Drying", *Encyclopedia of Food Safety*, vol. 3, pp. 156–167, 2014. DOI: 10.1016/B978-0-12-378612-8.00268-7.

[59] H. Romdhana, C. Bonazzi, and M. Esteban-Decloux, "Superheated steam drying: An overview of pilot and industrial dryers with a focus on energy efficiency", *Drying Technology*, vol. 33, no. 10, pp. 1255–1274, 2015. DOI: 10.1080/07373937.2015.1025139. eprint: https://doi.org/10.1080/07373937.2015.1025139. [Online]. Available: https://doi.org/10.1080/07373937.2015.1025139.

[60] N. Hampel, K. H. Le, A. Kharaghani, and E. Tsotsas, "Continuous modeling of superheated steam drying of single rice grains", *Drying Technology*, vol. 37, no. 12, pp. 1583–1596, 2019. DOI: 10.1080/07373937.2018.1518917. eprint: https://doi.org/10.1080/07373937.2018.1518917. [Online]. Available: https://doi.org/10.1080/07373937.2018.1518917.

[61] F. Bless, C. Arpagaus, S. S. Bertsch, and J. Schiffmann, "Theoretical analysis of steam generation methods - energy, co2 emission, and cost analysis", *Energy*, vol. 129, pp. 114–121, 2017, ISSN: 0360-5442. DOI: https://doi.org/10.1016/j.energy.2017.04.088. [Online]. Available: https://www.sciencedirect.com/science/article/pii/S0360544217306540.

[62] G. Lee *et al.*, "Development of steam generation heat pump through refrigerant replacement approach", 2017. [Online]. Available: https://api.semanticscholar.org/CorpusID:198232472.

[63] D. H. Kang, S.-I. Na, and M. S. Kim, "Recent researches on steam generation heat pump system", *International Journal of Air-Conditioning and Refrigeration*, vol. 25, no. 04, p. 1 730 005, 2017. DOI: 10.1142/S2010132517300051. [Online]. Available: https://doi.org/10.1142/S2010132517300051.

[64] T. Kaida, I. Sakuraba, K. Hashimoto, and H. Hasegawa, "Experimental performance evaluation of heat pump-based steam supply system", *IOP Conference Series: Materials Science and Engineering*, vol. 90, no. 1, p. 012 076, Jul. 2015. DOI: 10.1088/1757-899X/90/1/012076. [Online]. Available: https://dx.doi.org/10.1088/1757-899X/90/1/012076.

[65] A. Alicilar, M. Doğan, and M. Gürü, "Optimization of a double stage flash system", *International Journal of Energy Research*, vol. 19, no. 2, pp. 169–179, 1995, ISSN: 1099114X. DOI: 10.1002/er.4440190209.

[66] E. Vieren, W. Beyne, T. Demeester, M. De Paepe and S. Lecompte, "Theoretical assessment of industrial heating technologies up to 250°c", in *Proceedings of 26th IIR International Congress of Refrigeration (ICR2023)*, Paris, France: International Institute of Refrigeration (IIR), 2023. [Online]. Available: http://doi.org/10.18462/iir.icr.2023.0324.

[67] M. Dumont, R. Wang, D. Wenzke, K. Blok, and R. Heijungs, "The techno-economic integrability of high-temperature heat pumps for decarbonizing process heat in the food and beverages industry", *Resources, Conservation and Recycling*, vol. 188, p. 106 605, 2023, ISSN: 0921-3449. DOI: https://doi.org/10.1016/j.resconrec.2022.106605. [Online]. Available: https://www.sciencedirect.com/science/article/pii/S0921344922004396.

[68] M. J. S. Zuberi, A. Hasanbeigi, and W. Morrow, "Techno-economic evaluation of industrial heat pump applications in us pulp and paper, textile, and automotive industries", *Energy Efficiency*, vol. 16, no. 19, pp. 1–19, 2023. DOI: 10.1007/s12053-023-10089-6.

[69] F. Schlosser, M. Jesper, J. Vogelsang, T. Walmsley, C. Arpagaus, and J. Hesselbach, "Large-scale heat pumps: Applications, performance, economic feasibility and industrial integration", *Renewable and Sustainable Energy Reviews*, vol. 133, p. 110 219, 2020, ISSN: 1364-0321. DOI: https://doi.org/10.1016/j.rser.2020.110219. [Online]. Available: https://www.sciencedirect.com/science/article/pii/S1364032120305086.

[70] F. Schlosser, S. Zysk, T. G. Walmsley, L. Kong, B. Zühlsdorf, and H. Meschede, "Break-even of high-temperature heat pump integration for milk spray drying", *Energy Conversion and Management*, vol. 291, p. 117 304, 2023, ISSN: 0196-8904. DOI: https://doi.org/10.1016/j.enconman.2023.117304. [Online]. Available: https://www.sciencedirect.com/science/article/pii/S0196890423006507.

[71] M. Sadeghi, T. Petersen, Z. Yang, B. Zühlsdorf, and K. S. Madsen, "Thermal design and optimization of high-temperature heat pump integrated with district heating benchmarked in denmark for process heat supply", *International Journal of Refrigeration*, vol. 159, pp. 356–370, 2024, ISSN: 0140-7007. DOI: https://doi.org/10.1016/j.ijrefrig.2023.12.025. [Online]. Available: https://www.sciencedirect.com/science/article/pii/S0140700723004814.

[72] S. Spoelstra, W. Haije, and J. Dijkstra, "Techno-economic feasibility of high-temperature high-lift chemical heat pumps for upgrading industrial waste heat", *Applied Thermal Engineering*, vol. 22, no. 14, pp. 1619–1630, 2002, ISSN: 1359-4311. DOI: https://doi.org/10.1016/S1359-4311(02)00077-7. [Online]. Available: https://www.sciencedirect.com/science/article/pii/S1359431102000777.

[73] S. Yang, Y. Qian, Y. Wang, and S. Yang, "A novel cascade absorption heat transformer process using low grade waste heat and its application to coal to synthetic natural gas", *Applied Energy*, vol. 202, pp. 42–52, 2017, ISSN: 0306-2619. DOI: https://doi.org/10.1016/j.apenergy.2017.04.028. [Online]. Available: https://www.sciencedirect.com/science/article/pii/S0306261917304257.

[74] P. Saini, M. Ghasemi, C. Arpagaus, F. Bless, S. Bertsch, and X. Zhang, "Techno-economic comparative analysis of solar thermal collectors and high-temperature heat pumps for industrial steam generation", *Energy Conversion and Management*, vol. 277, p. 116623, 2023, ISSN: 0196-8904. DOI: https://doi.org/10.1016/j.enconman.2022.116623. [Online]. Available: https://www.sciencedirect.com/science/article/pii/S0196890422014017.

[75] S. Meyers, B. Schmitt, and K. Vajen, "The future of low carbon industrial process heat: A comparison between solar thermal and heat pumps", *Solar Energy*, vol. 173, pp. 893–904, 2018, ISSN: 0038-092X. DOI: https://doi.org/10.1016/j.solener.2018.08.011. [Online]. Available: https://www.sciencedirect.com/science/article/pii/S0038092X18307801.

[76] M. Jesper, F. Schlosser, F. Pag, T. G. Walmsley, B. Schmitt, and K. Vajen, "Large-scale heat pumps: Uptake and performance modelling of market-available devices", *Renewable and Sustainable Energy Reviews*, vol. 137, p. 110646, 2021, ISSN: 1364-0321. DOI: https://doi.org/10.1016/j.rser.2020.110646. [Online]. Available: https://www.sciencedirect.com/science/article/pii/S1364032120309308.

[77] C. Arpagaus, F. Bless, and S. S. Bertsch, "Techno-economic analysis of steam-generating heat pumps in distillation processes", in *High-Temperature Heat Pump Symposium*, Eastern Switzerland University of Applied Science, Institute for Energy Systems, Copenhagen, Denmark, 2022. [Online]. Available: mailto:Cordin.Arpagaus@ost.ch.

[78] U.S. Department of Energy, *Electric resistance heating*, https://www.energy.gov/energysaver/electric-resistance-heating, Accessed: 2024-06-06, 2024. [Online]. Available: https://www.energy.gov/energysaver/electric-resistance-heating.

[79] S. Meyers, B. Schmitt, M. Chester-Jones, and B. Sturm, "Energy efficiency, carbon emissions, and measures towards their improvement in the food and beverage sector for six european countries", *Energy*, vol. 104, pp. 266–283, 2016, ISSN: 0360-5442. DOI: https://doi.org/10.1016/j.energy.2016.03.117. [Online]. Available: https://www.sciencedirect.com/science/article/pii/S0360544216303644.

[80] T. Ommen, J. K. Jensen, W. B. Markussen, L. Reinholdt, and B. Elmegaard, "Technical and economic working domains of industrial heat pumps: Part 1 – single stage vapour compression heat pumps", *International Journal of Refrigeration*, vol. 55, pp. 168–182, 2015, ISSN: 0140-7007. DOI: https://doi.org/10.1016/j.ijrefrig.2015.02.012. [Online]. Available: https://www.sciencedirect.com/science/article/pii/S0140700715000444.

[81] S. Lemmens and S. Lecompte, "Case study of an organic Rankine cycle applied for excess heat recovery: Technical, economic and policy matters", *Energy Conversion and Management*, vol. 138, pp. 670–685, 2017, ISSN: 01968904. DOI: 10.1016/j.enconman.2017.01.074. [Online]. Available: http://dx.doi.org/10.1016/j.enconman.2017.01.074.

[82] F. Bless, C. Arpagaus, and S. Bertsch, "Theoretical investigation of high-temperature heat pump cycles for steam generation", *13th IEA Heat Pump Conference, May 11-14, 2020, Jeju, Korea, postponed to 26-29 April 2021*, pp. 1–9, 2020.

[83] G. Kosmadakis, C. Arpagaus, P. Neofytou, and S. Bertsch, "Techno-economic analysis of high-temperature heat pumps with low-global warming potential refrigerants for upgrading waste heat up to 150 °C", *Energy Conversion and Management*, vol. 226, no. September, 2020, ISSN: 01968904. DOI: 10.1016/j.enconman.2020.113488.

[84] F. Cudok *et al.*, "Absorption heat transformer - state-of-the-art of industrial applications", *Renewable and Sustainable Energy Reviews*, vol. 141, p. 110 757, 2021, ISSN: 1364-0321. DOI: https://doi.org/10.1016/j.rser.2021.110757. [Online]. Available: https://www.sciencedirect.com/science/article/pii/S1364032121000526.

[85] Y. Han, B. Shen, and T. Zhang, "A techno-economic assessment of fuel switching options of addressing environmental challenges of coal-fired industrial boilers: An analytical work for china", *Energy Procedia*, vol. 142, pp. 3083–3087, 2017, Proceedings of the 9th International Conference on Applied Energy, ISSN: 1876-6102. DOI: https://doi.org/10.1016/j.egypro.2017.12.448. [Online]. Available: https://www.sciencedirect.com/science/article/pii/S1876610217362033.

[86] H. Yan, B. Hu, and R. Wang, "Air-source heat pump for distributed steam generation: A new and sustainable solution to replace coal-fired boilers in china", *Advanced Sustainable Systems*, vol. 4, no. 11, p. 2 000 118, 2020. DOI: https://doi.org/10.1002/adsu.202000118. eprint: https://onlinelibrary.wiley.com/doi/pdf/10.1002/adsu.202000118. [Online]. Available: https://onlinelibrary.wiley.com/doi/abs/10.1002/adsu.202000118.

[87] G. B. Wang and X. R. Zhang, "Thermoeconomic analysis of optimization potential for CO2 vapor compression cycle: From transcritical to supercritical operation for waste heat recovery from the steam condenser", *International Journal of Energy Research*, vol. 43, no. 1, pp. 297–312, 2019, ISSN: 1099114X. DOI: 10.1002/er.4263.

[88] S.-F. Lee, *Thermoeconomics of lithium bromide/water absorption chillers and heat transformers*. University of Florida, 1999.

[89] J. H. R. Enslin, "Economic aspects of utilizing heat transformer technology", 2019.

[90] A. Pensini, C. N. Rasmussen, and W. Kempton, "Economic analysis of using excess renewable electricity to displace heating fuels", *Applied Energy*, vol. 131, pp. 530–543, 2014, ISSN: 0306-2619. DOI: https://doi.org/10.1016/j.apenergy.2014.04.111. [Online]. Available: https://www.sciencedirect.com/science/article/pii/S0306261914004772.

[91] M. R. Akhtari, I. Shayegh, and N. Karimi, "Techno-economic assessment and optimization of a hybrid renewable earth - air heat exchanger coupled with electric boiler, hydrogen, wind and pv configurations", *Renewable Energy*, vol. 148, pp. 839–851, 2020, ISSN: 0960-1481. DOI: https://doi.org/10.1016/j.renene.2019.10.169. [Online]. Available: https://www.sciencedirect.com/science/article/pii/S0960148119316660.

[92] European Commission, *Eurostat: Electricity prices for non-household consumers - bi-annual data (from 2007 onwards)*, Accessed: April 26, 2022. [Online]. Available: https://ec.europa.eu/eurostat/databrowser/view/nrg_pc_205/default/table?lang=en.

[93] European Commission, *Eurostat: Natural gas prices for non-household consumers - bi-annual data (from 2007 onwards)*, Accessed: April 26, 2022. [Online]. Available: https://ec.europa.eu/eurostat/databrowser/view/nrg_pc_203/default/table?lang=en.

[94] European Energy Exchange AG, *Eua emission spot primary market auction report - history*, https://www.eex.com/en/market-data/environmental-markets/eua-primary-auction-spot-download, Accessed: May 26, 2022, 2022.

[95] J. Chau, T. Sowlati, S. Sokhansanj, F. Preto, S. Melin, and X. Bi, "Techno-economic analysis of wood biomass boilers for the greenhouse industry", *Applied Energy*, vol. 86, no. 3, pp. 364–371, 2009, ISSN: 0306-2619. DOI: https://doi.org/10.1016/j.apenergy.2008.05.010. [Online]. Available: https://www.sciencedirect.com/science/article/pii/S0306261908001372.

[96] Enerdata, *Carbon price forecast 2030-2050: Assessing market stability & future challenges*, Accessed: 2024-09-30, 2023. [Online]. Available: https://www.enerdata.net/publications/executive-briefing/carbon-price-projections-eu-ets.html.

[97] T. Gilbert, A. K. Menon, C. Dames, and R. Prasher, "Heat source and application-dependent levelized cost of decarbonized heat", *Joule*, vol. 7, no. 1, pp. 128–149, 2023, ISSN: 2542-4351. DOI: https://doi.org/10.1016/j.joule.2022.11.006. [Online]. Available: https://www.sciencedirect.com/science/article/pii/S2542435122005645.

[98] D. Walraven, B. Laenen, and W. D'haeseleer, "Minimizing the levelized cost of electricity production from low-temperature geothermal heat sources with orcs: Water or air cooled?", *Applied Energy*, vol. 142, pp. 144–153, 2015, ISSN: 0306-2619. DOI: https://doi.org/10.1016/j.apenergy.2014.12.078. [Online]. Available: https://www.sciencedirect.com/science/article/pii/S030626191401335X.

[99] V. L. Le, A. Kheiri, M. Feidt, and S. Pelloux-Prayer, "Thermodynamic and economic optimizations of a waste heat to power plant driven by a subcritical orc (organic rankine cycle) using pure or zeotropic working fluid", *Energy*, vol. 78, pp. 622–638, 2014, ISSN: 0360-5442. DOI: https://doi.org/10.1016/j.energy.2014.10.051. [Online]. Available: https://www.sciencedirect.com/science/article/pii/S0360544214012018.

[100] J. Ziemele and E. Dace, "An analytical framework for assessing the integration of the waste heat into a district heating system: Case of the city of riga", *Energy*, vol. 254, p. 124 285, 2022, ISSN: 0360-5442. DOI: https://doi.org/10.1016/j.energy.2022.124285. [Online]. Available: https://www.sciencedirect.com/science/article/pii/S0360544222011884.

[101] L. Fu, Y. Li, Y. Wu, X. Wang, and Y. Jiang, "Low carbon district heating in china in 2025- a district heating mode with low grade waste heat as heat source", *Energy*, vol. 230, p. 120 765, 2021, ISSN: 0360-5442. DOI: https://doi.org/10.1016/j.energy.2021.120765. [Online]. Available: https://www.sciencedirect.com/science/article/pii/S0360544221010136.

[102] J. Pelda, F. Stelter, and S. Holler, "Potential of integrating industrial waste heat and solar thermal energy into district heating networks in germany", *Energy*, vol. 203, p. 117 812, 2020, ISSN: 0360-5442. DOI: https://doi.org/10.1016/j.energy.2020.117812. [Online]. Available: https://www.sciencedirect.com/science/article/pii/S0360544220309191.

[103] E. Vieren, T. Demeester, W. Beyne, A. Arteconi, M. De Paepe and S. Lecompte, "The thermodynamic potential of high-temperature transcritical heat pump cycles for industrial processes with large temperature glides", *Applied Thermal Engineering*, vol. 234, p. 121 197, 2023, ISSN: 1359-4311. DOI: https://doi.org/10.1016/j.applthermaleng.2023.121197. [Online]. Available: https://www.sciencedirect.com/science/article/pii/S1359431123012267.

[104] B. Hu, D. Wu, L. Wang, and R. Wang, "Exergy analysis of r1234ze(z) as high temperature heat pump working fluid with multi-stage compression", *Frontiers in Energy*, vol. 11, pp. 493–502, Nov. 2017. DOI: 10.1007/s11708-017-0510-6.

[105] K.-M. Adamson *et al.*, "High-temperature and transcritical heat pump cycles and advancements: A review", *Renewable and Sustainable Energy Reviews*, vol. 167, p. 112 798, 2022, ISSN: 1364-0321. DOI: https://doi.org/10.1016/j.rser.2022.112798. [Online]. Available: https://www.sciencedirect.com/science/article/pii/S1364032122006827.

[106] B. Zühlsdorf, J. K. Jensen, S. Cignitti, C. Madsen, and B. Elmegaard, "Analysis of temperature glide matching of heat pumps with zeotropic working fluid mixtures for different temperature glides", *Energy*, vol. 153, pp. 650–660, 2018, ISSN: 0360-5442. DOI: https://doi.org/10.1016/j.energy.2018.04.048. [Online]. Available: https://www.sciencedirect.com/science/article/pii/S0360544218306522.

[107] C. Xu, H. Yang, X. Yu, H. Ma, M. Chen, and M. Yang, "Performance analysis for binary mixtures based on r245fa using in high temperature heat pumps", *Energy Conversion and Management: X*, vol. 12, p. 100 123, 2021, ISSN: 2590-1745. DOI: https://doi.org/10.1016/j.ecmx.2021.100123. [Online]. Available: https://www.sciencedirect.com/science/article/pii/S2590174521000489.

[108] W. Xu, R. Zhao, S. Deng, L. Zhao, and S. S. Mao, "Is zeotropic working fluid a promising option for organic rankine cycle: A quantitative evaluation based on literature data", *Renewable and Sustainable Energy Reviews*, vol. 148, p. 111 267, 2021, ISSN: 1364-0321. DOI: https://doi.org/10.1016/j.rser.2021.111267. [Online]. Available: https://www.sciencedirect.com/science/article/pii/S1364032121005542.

[109] H. Abedini *et al.*, "A comprehensive analysis of binary mixtures as working fluid in high temperature heat pumps", *Energy Conversion and Management*, vol. 277, p. 116 652, 2023, ISSN: 0196-8904. DOI: https://doi.org/10.1016/j.enconman.2022.116652. [Online]. Available: https://www.sciencedirect.com/science/article/pii/S0196890422014303.

[110] G. Bamorovat Abadi and K. C. Kim, "Investigation of organic rankine cycles with zeotropic mixtures as a working fluid: Advantages and issues", *Renewable and Sustainable Energy Reviews*, vol. 73, pp. 1000–1013, 2017, ISSN: 1364-0321. DOI: https://doi.org/10.1016/j.rser.2017.02.020. [Online]. Available: https://www.sciencedirect.com/science/article/pii/S1364032117302253.

[111] S. Lecompte, B. Ameel, D. Ziviani, M. van den Broek, and M. De Paepe, "Exergy analysis of zeotropic mixtures as working fluids in organic rankine cycles", *Energy Conversion and Management*, vol. 85, pp. 727–739, 2014, ISSN: 0196-8904. DOI: https://doi.org/10.1016/j.enconman.2014.02.028. [Online]. Available: https://www.sciencedirect.com/science/article/pii/S0196890414001472.

[112] J. Zhang, B. Elmegaard, and F. Haglind, "Condensation heat transfer and pressure drop characteristics of zeotropic mixtures of r134a/r245fa in plate heat exchangers", *International Journal of Heat and Mass Transfer*, vol. 164, p. 120 577, 2021, ISSN: 0017-9310. DOI: https://doi.org/10.1016/j.ijheatmasstransfer.2020.120577. [Online]. Available: https://www.sciencedirect.com/science/article/pii/S0017931020335134.

[113] F. Heberle, M. Preißinger, and D. Brüggemann, "Zeotropic mixtures as working fluids in organic rankine cycles for low-enthalpy geothermal resources", *Renewable Energy*, vol. 37, no. 1, pp. 364–370, 2012, ISSN: 0960-1481. DOI:

https://doi.org/10.1016/j.renene.2011.06.044. [Online]. Available: https://www.sciencedirect.com/science/article/pii/S0960148111003818.

[114] M. Chys, M. van den Broek, B. Vanslambrouck, and M. De Paepe, "Potential of zeotropic mixtures as working fluids in organic rankine cycles", *Energy*, vol. 44, no. 1, pp. 623–632, 2012, Integration and Energy System Engineering, European Symposium on Computer-Aided Process Engineering 2011, ISSN: 0360-5442. DOI: https://doi.org/10.1016/j.energy.2012.05.030. [Online]. Available: https://www.sciencedirect.com/science/article/pii/S0360544212004100.

[115] L. Rajapaksha, "Influence of special attributes of zeotropic refrigerant mixtures on design and operation of vapour compression refrigeration and heat pump systems", *Energy Conversion and Management*, vol. 48, no. 2, pp. 539–545, 2007, ISSN: 0196-8904. DOI: https://doi.org/10.1016/j.enconman.2006.06.001. [Online]. Available: https://www.sciencedirect.com/science/article/pii/S0196890406001993.

[116] G. Lorentzen, *Trans-critical vapour compression cycle device*, 1990.

[117] G. Lorentzen, "Revival of carbon dioxide as a refrigerant", *International Journal of Refrigeration*, vol. 17, no. 5, pp. 292–301, 1994, ISSN: 0140-7007. DOI: https://doi.org/10.1016/0140-7007(94)90059-0. [Online]. Available: https://www.sciencedirect.com/science/article/pii/0140700794900590.

[118] B. T. Austin and K. Sumathy, "Transcritical carbon dioxide heat pump systems: A review", *Renewable and Sustainable Energy Reviews*, vol. 15, no. 8, pp. 4013–4029, 2011, ISSN: 1364-0321. DOI: https://doi.org/10.1016/j.rser.2011.07.021. [Online]. Available: https://www.sciencedirect.com/science/article/pii/S1364032111002607.

[119] R. U. Rony, H. Yang, S. Krishnan, and J. Song, "Recent advances in transcritical co2 (r744) heat pump system: A review", *Energies*, vol. 12, no. 3, 2019, ISSN: 1996-1073. DOI: 10.3390/en12030457. [Online]. Available: https://www.mdpi.com/1996-1073/12/3/457.

[120] D. Yang, Y. Li, J. Xie, and J. Wang, "Research and application progress of transcritical CO2 refrigeration cycle system: a review", *International Journal of Low-Carbon Technologies*, vol. 17, pp. 245–256, Dec. 2021, ISSN: 1748-1317. DOI: 10.1093/ijlct/ctab086. eprint: https://academic.oup.com/ijlct/article-pdf/doi/10.1093/ijlct/ctab086/42446526/ctab086.pdf. [Online]. Available: https://doi.org/10.1093/ijlct/ctab086.

[121] Y. Ma, Z. Liu, and H. Tian, "A review of transcritical carbon dioxide heat pump and refrigeration cycles", *Energy*, vol. 55, pp. 156–172, 2013, ISSN: 0360-5442. DOI: https://doi.org/10.1016/j.energy.2013.03.030. [Online]. Available: https://www.sciencedirect.com/science/article/pii/S0360544213002181.

[122] M.-H. Kim, J. Pettersen, and C. Bullard, "Fundamental process and system design issues in co2 vapor compression systems", *Progress in Energy and Combustion Science*, vol. 30, pp. 119–174, 2004.

[123] S. Lecompte *et al.*, "Review of experimental research on supercritical and transcritical thermodynamic cycles designed for heat recovery application", *Applied Sciences*, vol. 9, p. 2571, Jun. 2019. DOI: 10.3390/app9122571.

[124] J. Sarkar, S. Bhattacharyya, and M. Ram Gopal, "Natural refrigerant-based subcritical and transcritical cycles for high temperature heating", *International Journal of Refrigeration*, vol. 30, no. 1, pp. 3–10, 2007, ISSN: 0140-7007. DOI: https://doi.org/10.1016/j.ijrefrig.2006.03.008. [Online]. Available: https://www.sciencedirect.com/science/article/pii/S0140700706000661.

[125] K. Besbes, A. Zoughaib, F. Carlan, and J.-L. Peureux, "A R-32 transcritical heat pump for high temperature industrial applications", in *Proceedings of the 24th IIR International Congress of Refrigeration*, Yokohama, Japan: ICR2015, 2015. DOI: 10.18462/iir.icr.2015.0599.

[126] G. Abi Chahla, Y. Beucher, A. Zoughaib, F. Carlan, and J. Pierrucci, "Transcritical industrial heat pump using HFO's for up to 150°C hot air supply", in *Proceedings of the 25th IIR International Congress of Refrigeration*, Montréal, Canada: ICR2019, 2019. DOI: 10.18462/iir.icr.2019.1184.

[127] T. Kimura *et al.*, "Development of a high temperature heat pump using reusable heat as the heat source", in *Proceedings of the JRAIA International Symposium 2018*, Japan: JRAIA2018, 2018.

[128] M. Verdnik and R. Rieberer, "Influence of operating parameters on the cop of an r600 high-temperature heat pump", *International Journal of Refrigeration*, vol. 140, pp. 103–111, 2022, ISSN: 0140-7007. DOI: https://doi.org/10.1016/j.ijrefrig.2022.05.010. [Online]. Available: https://www.sciencedirect.com/science/article/pii/S0140700722001621.

[129] C. Arpagaus, F. Bless, and S. Bertsch, "Theoretical analysis of transcritical HTHP cycles with low gwp hfo refrigerants and hydrocarbons for process heat up to 200 °C", in *Proceedings of the IIR Rankine Conference*, Glasgow, UK: IIR, 2020.

[130] E. W. Lemmon, I. H. Bell, M. L. Huber, and M. O. McLinden, *Nist standard reference database 23: Reference fluid thermodynamic and transport properties-refprop, version 10.0, national institute of standards and technology*, 2018. DOI: https://doi.org/10.18434/T4/1502528. [Online]. Available: https://www.nist.gov/srd/refprop.

[131] J. Quenel, M. Anders, and B. Atakan, "Propane-isobutane mixtures in heat pumps with higher temperature lift: An experimental investigation", *Thermal Science and Engineering Progress*, vol. 42, p. 101 907, 2023, ISSN: 2451-9049. DOI: https://doi.org/10.1016/j.tsep.2023.101907. [Online]. Available: https://www.sciencedirect.com/science/article/pii/S2451904923002603.

[132] L. P. Brendel *et al.*, "High-glide refrigerant blends in high-temperature heat pumps: Part 1 – coefficient of performance", *International Journal of Refrigeration*, vol. 165, pp. 84–96, 2024, ISSN: 0140-7007. DOI: https://doi.org/10.1016/j.ijrefrig.2024.05.005. [Online]. Available: https://www.sciencedirect.com/science/article/pii/S0140700724001622.

[133] J. Luo, K. Yang, Z. Zhao, G. Chen, and Q. Wang, "Experimental investigations on the performance of a single-stage compound air-source heat pump using co2/r600a in cold regions", *Applied Thermal Engineering*, vol. 205, p. 118050, 2022, ISSN: 1359-4311. DOI: https://doi.org/10.1016/j.applthermaleng.2022.118050. [Online]. Available: https://www.sciencedirect.com/science/article/pii/S1359431122000175.

[134] J. Liu, F. Zhou, N. Lyu, H. Fan, and X. Zhang, "Analysis of low gwp ternary zeotropic mixtures applied in high-temperature heat pump for waste heat recovery", *Energy Conversion and Management*, vol. 292, p. 117381, 2023, ISSN: 0196-8904. DOI: https://doi.org/10.1016/j.enconman.2023.117381. [Online]. Available: https://www.sciencedirect.com/science/article/pii/S0196890423007276.

[135] J. Gómez-Hernández, R. Grimes, J. Briongos, C. Marugán-Cruz, and D. Santana, "Carbon dioxide and acetone mixtures as refrigerants for industry heat pumps to supply temperature in the range 150–220 oc", *Energy*, vol. 269, p. 126821, 2023, ISSN: 0360-5442. DOI: https://doi.org/10.1016/j.energy.2023.126821. [Online]. Available: https://www.sciencedirect.com/science/article/pii/S0360544223002153.

[136] P. Ganesan and T. M. Eikevik, "New zeotropic co2-based refrigerant mixtures for cascade high-temperature heat pump to reach heat sink temperature up to 180 °c", *Energy Conversion and Management: X*, vol. 20, p. 100407, 2023, ISSN: 2590-1745. DOI: https://doi.org/10.1016/j.ecmx.2023.100407. [Online]. Available: https://www.sciencedirect.com/science/article/pii/S2590174523000636.

[137] B. Dai *et al.*, "Assessment of heat pump with carbon dioxide/low-global warming potential working fluid mixture for drying process: Energy and emissions saving potential", *Energy Conversion and Management*, vol. 222, p. 113225, 2020, ISSN: 0196-8904. DOI: https://doi.org/10.1016/j.enconman.2020.113225. [Online]. Available: https://www.sciencedirect.com/science/article/pii/S019689042030769X.

[138] P. A. Domanski, J. Steven Brown, J. Heo, J. Wojtusiak, and M. O. McLinden, "A thermodynamic analysis of refrigerants: Performance limits of the vapor compression cycle", *International Journal of Refrigeration*, vol. 38, pp. 71–79, 2014, ISSN: 0140-7007. DOI: https://doi.org/10.1016/j.ijrefrig.2013.09.036. [Online]. Available: https://www.sciencedirect.com/science/article/pii/S0140700713002703.

[139] B. Saleh and M. Wendland, "Screening of pure fluids as alternative refrigerants", *International Journal of Refrigeration*, vol. 29, no. 2, pp. 260–269, 2006, ISSN: 0140-7007. DOI: https://doi.org/10.1016/j.ijrefrig.2005.

05.009. [Online]. Available: https://www.sciencedirect.com/science/article/pii/S0140700705001106.

[140] D. Calleja-Anta, L. Nebot-Andrés, J. Catalán-Gil, D. Sánchez, R. Cabello, and R. Llopis, "Thermodynamic screening of alternative refrigerants for r290 and r600a", *Results in Engineering*, vol. 5, p. 100 081, 2020, ISSN: 2590-1230. DOI: https://doi.org/10.1016/j.rineng.2019.100081. [Online]. Available: https://www.sciencedirect.com/science/article/pii/S2590123019300817.

[141] P. Domanski, J. Brown, and E. Lemmon, *Cycle d: Nist vapor compression cycle design program, version 6.0; user's guide*, en, 2018-11-19 2018. DOI: https://doi.org/10.6028/NIST.NSRDS.49-2018.

[142] M. Pitarch, E. Hervas-Blasco, E. Navarro-Peris, J. Gonzálvez-Maciá, and J. M. Corberán, "Evaluation of optimal subcooling in subcritical heat pump systems", *International Journal of Refrigeration*, vol. 78, pp. 18–31, 2017, ISSN: 0140-7007. DOI: https://doi.org/10.1016/j.ijrefrig.2017.03.015. [Online]. Available: https://www.sciencedirect.com/science/article/pii/S014070071730110X.

[143] G. Kosmadakis and P. Neofytou, "Investigating the effect of nanorefrigerants on a heat pump performance and cost-effectiveness", *Thermal Science and Engineering Progress*, vol. 13, p. 100 371, 2019, ISSN: 2451-9049. DOI: https://doi.org/10.1016/j.tsep.2019.100371. [Online]. Available: https://www.sciencedirect.com/science/article/pii/S2451904919300204.

[144] C. Mateu-Royo, J. Navarro-Esbrí, A. Mota-Babiloni, F. Molés, and M. Amat-Albuixech, "Experimental exergy and energy analysis of a novel high-temperature heat pump with scroll compressor for waste heat recovery", *Applied Energy*, vol. 253, p. 113 504, 2019, ISSN: 0306-2619. DOI: https://doi.org/10.1016/j.apenergy.2019.113504. [Online]. Available: https://www.sciencedirect.com/science/article/pii/S030626191931178X.

[145] M. Astolfi, "Techno-economic optimization of low temperature csp systems based on orc with screw expanders", *Energy Procedia*, vol. 69, pp. 1100–1112, 2015, International Conference on Concentrating Solar Power and Chemical Energy Systems, SolarPACES 2014, ISSN: 1876-6102. DOI: https://doi.org/10.1016/j.egypro.2015.03.220. [Online]. Available: https://www.sciencedirect.com/science/article/pii/S1876610215005263.

[146] M. Yang, T. Li, X. Feng, and Y. Wang, "A simulation-based targeting method for heat pump placements in heat exchanger networks", *Energy*, vol. 203, p. 117 907, 2020, ISSN: 0360-5442. DOI: https://doi.org/10.1016/j.energy.2020.117907. [Online]. Available: https://www.sciencedirect.com/science/article/pii/S0360544220310148.

[147] D. Roskosch, V. Venzik, J. Schilling, A. Bardow, and B. Atakan, "Beyond temperature glide: The compressor is key to realizing benefits of zeotropic mixtures in heat pumps", *Energy Technology*, vol. 9, no. 4, p. 2 000 955, 2021. DOI: https://doi.org/10.1002/ente.202000955. eprint: https://onlinelibrary.wiley.com/doi/pdf/10.1002/ente.202000955. [Online].

Available: https://onlinelibrary.wiley.com/doi/abs/10.1002/ente.202000955.

[148] C. Underwood, "14 - heat pump modelling", in *Advances in Ground-Source Heat Pump Systems*, S. J. Rees, Ed., Woodhead Publishing, 2016, pp. 387–421, ISBN: 978-0-08-100311-4. DOI: https://doi.org/10.1016/B978-0-08-100311-4.00014-5. [Online]. Available: https://www.sciencedirect.com/science/article/pii/B9780081003114000145.

[149] B. Luo and P. Zou, "Performance analysis of different single stage advanced vapor compression cycles and refrigerants for high temperature heat pumps", *International Journal of Refrigeration*, vol. 104, pp. 246–258, 2019, ISSN: 0140-7007. DOI: https://doi.org/10.1016/j.ijrefrig.2019.05.024. [Online]. Available: https://www.sciencedirect.com/science/article/pii/S0140700719302208.

[150] G. F. Frate, L. Ferrari, and U. Desideri, "Analysis of suitability ranges of high temperature heat pump working fluids", *Applied Thermal Engineering*, vol. 150, pp. 628–640, 2019, ISSN: 1359-4311. DOI: https://doi.org/10.1016/j.applthermaleng.2019.01.034. [Online]. Available: https://www.sciencedirect.com/science/article/pii/S1359431118353602.

[151] O. Ibrahim, F. Fardoun, R. Younes, and H. Louahlia-Gualous, "Air source heat pump water heater: Dynamic modeling, optimal energy management and mini-tubes condensers", *Energy*, vol. 64, pp. 1102–1116, 2014, ISSN: 0360-5442. DOI: https://doi.org/10.1016/j.energy.2013.11.017. [Online]. Available: https://www.sciencedirect.com/science/article/pii/S0360544213009791.

[152] J. Van Nieuwenhuyse, S. Lecompte, and M. De Paepe, "Current status of the thermohydraulic behavior of supercritical refrigerants: A review", *Applied Thermal Engineering*, vol. 218, p. 119 201, 2023, ISSN: 1359-4311. DOI: https://doi.org/10.1016/j.applthermaleng.2022.119201. [Online]. Available: https://www.sciencedirect.com/science/article/pii/S1359431122011334.

[153] T. Deethayat, T. Kiatsiriroat, and C. Thawonngamyingsakul, "Performance analysis of an organic rankine cycle with internal heat exchanger having zeotropic working fluid", *Case Studies in Thermal Engineering*, vol. 6, pp. 155–161, 2015, ISSN: 2214-157X. DOI: https://doi.org/10.1016/j.csite.2015.09.003. [Online]. Available: https://www.sciencedirect.com/science/article/pii/S2214157X15300101.

[154] Z. Zhang, L. Tian, Y. Chen, and L. Tong, "Effect of an internal heat exchanger on performance of the transcritical carbon dioxide refrigeration cycle with an expander", *Entropy*, vol. 16, no. 11, pp. 5919–5934, 2014, ISSN: 1099-4300. DOI: 10.3390/e16115919. [Online]. Available: https://www.mdpi.com/1099-4300/16/11/5919.

[155] K. Yang, Y. Zhang, X. Li, and J. Xu, "Theoretical evaluation on the impact of heat exchanger in advanced adiabatic compressed air energy storage system", *Energy Conversion and Management*, vol. 86, pp. 1031–1044, 2014, ISSN: 0196-8904. DOI: https://doi.org/10.1016/j.enconman.2014.06.062. [Online]. Available: https://www.sciencedirect.com/science/article/pii/S0196890414005871.

[156] Y. Wang, Z. Ye, X. Yin, Y. Song, and F. Cao, "Energy, exergy and exergoeconomic evaluation of the air source transcritical co2 heat pump with internal heat exchanger for space heating", *International Journal of Refrigeration*, vol. 130, pp. 14–26, 2021, ISSN: 0140-7007. DOI: https://doi.org/10.1016/j.ijrefrig.2021.06.028. [Online]. Available: https://www.sciencedirect.com/science/article/pii/S0140700721002656.

[157] V. Pérez-García, A. Mota-Babiloni, and J. Navarro-Esbrí, "Influence of operational modes of the internal heat exchanger in an experimental installation using r-450a and r-513a as replacement alternatives for r-134a", *Energy*, vol. 189, p. 116 348, 2019, ISSN: 0360-5442. DOI: https://doi.org/10.1016/j.energy.2019.116348. [Online]. Available: https://www.sciencedirect.com/science/article/pii/S0360544219320432.

[158] N. Zheng and L. Zhao, "The feasibility of using vapor expander to recover the expansion work in two-stage heat pumps with a large temperature lift", *International Journal of Refrigeration*, vol. 56, pp. 15–27, 2015, ISSN: 0140-7007. DOI: https://doi.org/10.1016/j.ijrefrig.2014.11.010. [Online]. Available: https://www.sciencedirect.com/science/article/pii/S0140700714003405.

[159] G. Ferrara *et al.*, "A small power recovery expander for heat pump cop improvement", *Energy Procedia*, vol. 81, pp. 1151–1159, 2015, 69th Conference of the Italian Thermal Engineering Association, ATI 2014, ISSN: 1876-6102. DOI: https://doi.org/10.1016/j.egypro.2015.12.140. [Online]. Available: https://www.sciencedirect.com/science/article/pii/S1876610215027897.

[160] J. Sarkar, "Ejector enhanced vapor compression refrigeration and heat pump systems—a review", *Renewable and Sustainable Energy Reviews*, vol. 16, no. 9, pp. 6647–6659, 2012, ISSN: 1364-0321. DOI: https://doi.org/10.1016/j.rser.2012.08.007. [Online]. Available: https://www.sciencedirect.com/science/article/pii/S1364032112004765.

[161] X. Chen, S. Omer, M. Worall, and S. Riffat, "Recent developments in ejector refrigeration technologies", *Renewable and Sustainable Energy Reviews*, vol. 19, pp. 629–651, 2013, ISSN: 1364-0321. DOI: https://doi.org/10.1016/j.rser.2012.11.028. [Online]. Available: https://www.sciencedirect.com/science/article/pii/S1364032112006405.

[162] D. Mikielewicz and J. Wajs, "Performance of the very high-temperature heat pump with low gwp working fluids", *Energy*, vol. 182, pp. 460–470, 2019, ISSN: 0360-5442. DOI: https://doi.org/10.1016/j.energy.2019.05.203. [Online]. Available: https://www.sciencedirect.com/science/article/pii/S0360544219310916.

[163] H. Yan *et al.*, "Performance prediction of hfc, hc, hfo and hcfo working fluids for high temperature water source heat pumps", *Applied Thermal Engineering*, vol. 185, p. 116 324, 2021, ISSN: 1359-4311. DOI: https://doi.org/10.1016/j.applthermaleng.2020.116324. [Online]. Available: https://www.sciencedirect.com/science/article/pii/S1359431120338035.

[164] P. Virtanen *et al.*, "SciPy 1.0: Fundamental Algorithms for Scientific Computing in Python", *Nature Methods*, vol. 17, pp. 261–272, 2020. DOI: 10.1038/s41592-019-0686-2.

[165] H. Abedini, S. Tomassetti, G. Di Nicola, S. Quoilin, and A. Arteconi, "Zeotropic mixtures r1234ze(z)/acetone and r1234ze(z)/isohexane as refrigerants in high temperature heat pumps: Influence of the accuracy in thermodynamic properties evaluations", *International Journal of Refrigeration*, vol. 152, pp. 93–109, 2023, ISSN: 0140-7007. DOI: https://doi.org/10.1016/j.ijrefrig.2023.05.008. [Online]. Available: https://www.sciencedirect.com/science/article/pii/S0140700723001330.

[166] European Parliament, *Regulation (eu) no 517/2014 of the european parliament and of the council of 16 april 2014 on fluorinated greenhouse gases and repealing regulation (ec) no 842/2006*, https://eur-lex.europa.eu/eli/reg/2014/517/oj, Accessed: 2021-04-08, 2014.

[167] European Parliament, *Regulation (ec) no 1005/2009 of the european parliament and of the council of 16 september 2009 on substances that deplete the ozone layer*, https://eur-lex.europa.eu/legal-content/EN/TXT/?uri=CELEX:32009R1005j, Accessed: 2021-04-08, 2009.

[168] National Fire Protection Association (NFPA), *Nfpa 704: Standard system for the identification of the hazards of materials for emergency response*, https://www.nfpa.org/codes-and-standards/all-codes-and-standards/list-of-codes-and-standards/detail?code=704, Accessed: 2022-07-07, 2022.

[169] X. Dai, L. Shi, Q. An, and W. Qian, "Chemical kinetics method for evaluating the thermal stability of organic rankine cycle working fluids", *Applied Thermal Engineering*, vol. 100, pp. 708–713, 2016, ISSN: 1359-4311. DOI: https://doi.org/10.1016/j.applthermaleng.2016.02.091. [Online]. Available: https://www.sciencedirect.com/science/article/pii/S1359431116302344.

[170] W. C. Andersen and T. J. Bruno, "Rapid screening of fluids for chemical stability in organic rankine cycle applications", *Industrial & Engineering Chemistry Research*, vol. 44, no. 15, pp. 5560–5566, 2005. DOI: 10.1021/ie050351s. eprint: https://doi.org/10.1021/ie050351s. [Online]. Available: https://doi.org/10.1021/ie050351s.

[171] K. Harby, "Hydrocarbons and their mixtures as alternatives to environmental unfriendly halogenated refrigerants: An updated overview", *Renewable and Sustainable Energy Reviews*, vol. 73, pp. 1247–1264, 2017, ISSN: 1364-0321. DOI: https://doi.org/10.1016/j.rser.2017.02.039. [Online]. Available: https://www.sciencedirect.com/science/article/pii/S1364032117302551.

[172] E. Granryd, "Hydrocarbons as refrigerants — an overview", *International Journal of Refrigeration*, vol. 24, no. 1, pp. 15–24, 2001, ISSN: 0140-7007. DOI: https://doi.org/10.1016/S0140-7007(00)00065-7. [Online]. Available: https://www.sciencedirect.com/science/article/pii/S0140700700000657.

[173] J. Galindo *et al.*, "Experimental and thermodynamic analysis of a bottoming organic rankine cycle (orc) of gasoline engine using swash-plate expander", *Energy Conversion and Management*, vol. 103, pp. 519–532, 2015, ISSN: 0196-8904. DOI: https://doi.org/10.1016/j.enconman.2015.06.085. [Online]. Available: https://www.sciencedirect.com/science/article/pii/S0196890415006470.

[174] P. Colonna *et al.*, "Organic Rankine Cycle Power Systems: From the Concept to Current Technology, Applications, and an Outlook to the Future", *Journal of Engineering for Gas Turbines and Power*, vol. 137, no. 10, Oct. 2015, 100801, ISSN: 0742-4795. DOI: 10.1115/1.4029884. eprint: https://asmedigitalcollection.asme.org/gasturbinespower/article-pdf/137/10/100801/6165555/gtp_137_10_100801.pdf. [Online]. Available: https://doi.org/10.1115/1.4029884.

[175] The American Society of Heating, Refrigerating and Air-Conditioning Engineers (ASHRAE), *Ashrae 34 refrigerant designations*, https://www.ashrae.org/technical-resources/standards-and-guidelines/ashrae-refrigerant-designations, Accessed: 2022-07-07, 2022.

[176] M. Yang, B. Wang, X. Li, W. Shi, and L. Zhang, "Evaluation of two-phase suction, liquid injection and two-phase injection for decreasing the discharge temperature of the r32 scroll compressor", *International Journal of Refrigeration*, vol. 59, pp. 269–280, 2015, ISSN: 0140-7007. DOI: https://doi.org/10.1016/j.ijrefrig.2015.08.004. [Online]. Available: https://www.sciencedirect.com/science/article/pii/S0140700715002479.

[177] X.-Q. Cao, W.-W. Yang, F. Zhou, and Y.-L. He, "Performance analysis of different high-temperature heat pump systems for low-grade waste heat recovery", *Applied Thermal Engineering*, vol. 71, no. 1, pp. 291–300, 2014, ISSN: 1359-4311. DOI: https://doi.org/10.1016/j.applthermaleng.2014.06.049. [Online]. Available: https://www.sciencedirect.com/science/article/pii/S1359431114005298.

[178] BITZER, *Bitzer // technologies*, Feb. 2023. [Online]. Available: https://www.bitzer.de/gb/en/products/ (visited on 02/14/2023).

[179] Frascold, *Frascold products*, https://www.frascold.it/en/product-search?s=9, Accessed: 2022-07-07, 2022.

[180] Emerson Copeland, *Emerson copeland*, https://climate.emerson.com/en-us/brands/copeland, Accessed: 2022-07-07, 2022.

[181] SRMtec, *Srmtec compressors*, https://srmtec.it/en/, Accessed: 2022-07-07, 2022.

[182] T. Ommen, J. K. Jensen, W. B. Markussen, L. Reinholdt, and B. Elmegaard, "Technical and economic working domains of industrial heat pumps: Part 1 – single stage vapour compression heat pumps", *International Journal of Refrigeration*, vol. 55, pp. 168–182, 2015, ISSN: 0140-7007. DOI: https://doi.org/10.1016/j.ijrefrig.2015.02.012. [Online]. Available: https://www.sciencedirect.com/science/article/pii/S0140700715000444.

[183] Bock, *Bock products*, https://bock.de/en, Accessed: 2022-07-07, 2022.

[184] O. Bamigbetan, T. M. Eikevik, P. Nekså, and M. Bantle, "Review of vapour compression heat pumps for high temperature heating using natural working fluids", *International Journal of Refrigeration*, vol. 80, pp. 197–211, 2017, ISSN: 0140-7007. DOI: https://doi.org/10.1016/j.ijrefrig.2017.04.021. [Online]. Available: https://www.sciencedirect.com/science/article/pii/S0140700717301780.

[185] C. Arpagaus and S. Bertsch, "Experimental Comparison of HCFO and HFO R1224yd(Z), R1233zd(E), R1336mzz(Z), and HFC R245fa in a High Temperature Heat Pump up to 150 °C Supply Temperature", in *Proceedings of the 18th International Refrigeration and Air Conditioning Conference*, Purdue, USA: IRACC2021, 2021, Purdue, US.

[186] DryFiciency (Dry-F), *Dryficiency web page*, https://dryficiency.eu/, Accessed: 2022-12-08.

[187] E. Vieren, T. Demeester, W. Beyne, M. P. Andersen, B. Elmegaard, A. Arteconi, M. De Paepe and S. Lecompte, "Selection of pure and binary working fluids for high-temperature heat pumps: A financial approach", *Applied Thermal Engineering*, vol. 252, p. 123 615, 2024, ISSN: 1359-4311. DOI: https://doi.org/10.1016/j.applthermaleng.2024.123615. [Online]. Available: https://www.sciencedirect.com/science/article/pii/S1359431124012833.

[188] S. Quoilin, S. Declaye, B. F. Tchanche, and V. Lemort, "Thermo-economic optimization of waste heat recovery organic rankine cycles", *Applied Thermal Engineering*, vol. 31, no. 14, pp. 2885–2893, 2011, ISSN: 1359-4311. DOI: https://doi.org/10.1016/j.applthermaleng.2011.05.014. [Online]. Available: https://www.sciencedirect.com/science/article/pii/S1359431111002663.

[189] B. Zühlsdorf, J. K. Jensen, and B. Elmegaard, "Heat pump working fluid selection—economic and thermodynamic comparison of criteria and boundary conditions", *International Journal of Refrigeration*, vol. 98, pp. 500–513, 2019, ISSN: 0140-7007. DOI: https://doi.org/10.1016/j.ijrefrig.2018.11.034. [Online]. Available: https://www.sciencedirect.com/science/article/pii/S0140700718304870.

[190] A. Vannoni, A. Sorce, A. Traverso, and A. Fausto Massardo, "Large size heat pumps advanced cost functions introducing the impact of design cop on capital costs", *Energy*, vol. 284, p. 129 204, 2023, ISSN: 0360-5442. DOI: https://doi.org/10.1016/j.energy.2023.129204. [Online]. Available: https://www.sciencedirect.com/science/article/pii/S0360544223025987.

[191] B. W. de Raad, M. van Lieshout, L. Stougie, and A. Ramirez, "Identifying techno-economic improvements for a steam generating heat pump with exergy-based costs minimization", in *36th International Conference on Efficiency, Cost, Optimization, Simulation and Environmental Impact of Energy Systems (ECOS 2023)*, 2023, pp. 884–895.

[192] W. Gosney, *Principles of Refrigeration*. Cambridge University Press, 1982, ISBN: 9780521236713. [Online]. Available: https://books.google.be/books?id=_WV5QgAACAAJ.

[193] R. Turton, R. C. Bailie, W. B. Whiting, and J. A. Shaeiwitz, *Analysis, synthesis and design of chemical processes*. Pearson Education, 2008.

[194] J. Zhang, X. Zhu, M. E. Mondejar, and F. Haglind, "A review of heat transfer enhancement techniques in plate heat exchangers", *Renewable and Sustainable Energy Reviews*, vol. 101, pp. 305–328, 2019, ISSN: 1364-0321. DOI: https://doi.org/10.1016/j.rser.2018.11.017. [Online]. Available: https://www.sciencedirect.com/science/article/pii/S136403211830772X.

[195] M. Shamoushaki, P. H. Niknam, L. Talluri, G. Manfrida, and D. Fiaschi, "Development of cost correlations for the economic assessment of power plant equipment", *Energies*, vol. 14, no. 9, 2021, ISSN: 1996-1073. DOI: 10.3390/en14092665. [Online]. Available: https://www.mdpi.com/1996-1073/14/9/2665.

[196] S. Henchoz, C. Weber, F. Maréchal, and D. Favrat, "Performance and profitability perspectives of a co2 based district energy network in geneva's city centre", *Energy*, vol. 85, pp. 221–235, 2015, ISSN: 0360-5442. DOI: https://doi.org/10.1016/j.energy.2015.03.079. [Online]. Available: https://www.sciencedirect.com/science/article/pii/S0360544215003886.

[197] A. Mosaffa, L. G. Farshi, C. Infante Ferreira, and M. Rosen, "Exergoeconomic and environmental analyses of co2/nh3 cascade refrigeration systems equipped with different types of flash tank intercoolers", *Energy Conversion and Management*, vol. 117, pp. 442–453, 2016, ISSN: 0196-8904. DOI: https://doi.org/10.1016/j.enconman.2016.03.053. [Online]. Available: https://www.sciencedirect.com/science/article/pii/S0196890416301911.

[198] R. S. Gavin Towler, *Capital Cost Estimating*. 2013, vol. 76, pp. 114–142, ISBN: 9780080966595. DOI: 10.1021/ie50502a032.

[199] "Vdi heat atlas", *VDI Heat Atlas*, 2010. DOI: 10.1007/978-3-540-77877-6.

[200] R. Smith, *Chemical Process: Design and Integration*. Wiley, 2005, ISBN: 9780470011911. [Online]. Available: https://books.google.be/books?id=cdyiWR0d1o8C.

[201] M. Astolfi, "An innovative approach for the techno-economic optimization of organic rankine cycles", 2014.

[202] G. F. Frate, L. Ferrari, and U. Desideri, "Multi-criteria economic analysis of a pumped thermal electricity storage (ptes) with thermal integration", *Frontiers in Energy Research*, vol. 8, p. 528 376, 2020.

[203] S. Sanaye and A. Shirazi, "Four e analysis and multi-objective optimization of an ice thermal energy storage for air-conditioning applications", *International Journal of Refrigeration*, vol. 36, no. 3, pp. 828–841, 2013.

[204] M. Charles, *Cost indices*. [Online]. Available: https://www.toweringskills.com/financial-analysis/cost-indices/.

[205] S. Bertsch, C. Arpagaus, F. Bless, A. Weickgenannt, and J. Schiffmann, "Theoritical investigation of a high temperature heat pump using a micro turbo compressor and water as a refrigerant.", *13th IIR Gustav Lorentzen Conference on Natural Refrigerants (GL2018). Proceedings. Valencia, Spain, June 18-20th 2018.*, vol. 2018-June, pp. 490–498, 2018, ISSN: 01511637. DOI: 10.18462/IIR.GL.2018.1201. [Online]. Available: https://iifiir.org/en/fridoc/theoritical-investigation-of-a-high-temperature-heat-pump-using-a-micro-33562.

[206] A. Valero *et al.*, "Cgam problem: Definition and conventional solution", *Energy*, vol. 19, no. 3, pp. 279–286, 1994.

[207] H.-Y. Kwak, D.-J. Kim, and J.-S. Jeon, "Exergetic and thermoeconomic analyses of power plants", *Energy*, vol. 28, no. 4, pp. 343–360, 2003, ISSN: 0360-5442. DOI: https://doi.org/10.1016/S0360-5442(02)00138-X. [Online]. Available: https://www.sciencedirect.com/science/article/pii/S036054420200138X.

[208] S. Dusek, M. Lauermann, F. Helminger, and V. Wilk, "Analysis of a steam generating high temperature heat pump for industrial waste heat recovery", in *13th IEA Heat Pump Conference*, Paper No 097, HPT - Heat Pumping Technologies, Jeju, Korea, Aug. 2021. [Online]. Available: https://heatpumpingtechnologies.org/publications/paper-no-097-analysis-of-a-steam-generating-high-temperature-heat-pump-for-industrial-waste-heat-recovery-13th-iea-heat-pump-conference-jeju-korea/.

[209] C. Invernizzi, M. Binotti, P. Bombarda, G. Di Marcoberardino, P. Iora, and G. Manzolini, "Water mixtures as working fluids in organic rankine cycles", *Energies*, vol. 12, no. 13, 2019, ISSN: 1996-1073. DOI: 10.3390/en12132629. [Online]. Available: https://www.mdpi.com/1996-1073/12/13/2629.

[210] B. Zühlsdorf, W. Meesenburg, T. Ommen, J. Thorsen, W. Markussen, and B. Elmegaard, "Improving the performance of booster heat pumps using zeotropic mixtures", *Energy*, vol. 154, pp. 390–402, 2018, ISSN: 0360-5442. DOI: https://doi.org/10.1016/j.energy.2018.04.137. [Online]. Available: https://www.sciencedirect.com/science/article/pii/S0360544218307539.

[211] E. Vieren, K. Couvreur, M. De Paepe and S. Lecompte, "Design of a high-temperature heat pump providing heat up to 200 °c", eng, in *16th IIR-Gustav Lorentzen Conference on Natural Refrigerants*, College Park, Maryland, USA: University of Maryland, 2024, p. 11, ISBN: 978-2-36215-062-3. [Online]. Available: http://doi.org/10.18462/iir.gl2024.1229.

[212] M. Chamoun, R. Rulliere, P. Haberschill, and J.-L. Peureux, "Experimental and numerical investigations of a new high temperature heat pump for industrial heat recovery using water as refrigerant", *International Journal of Refrigeration*, vol. 44, pp. 177–188, 2014, ISSN: 0140-7007. DOI: https://doi.org/10.1016/j.ijrefrig.2014.04.019. [Online]. Available: https://www.sciencedirect.com/science/article/pii/S0140700714000954.

[213] D. Wu, J. Jiang, B. Hu, and R. Wang, "Experimental investigation on the performance of a very high temperature heat pump with water refrigerant", *Energy*, vol. 190, p. 116 427, 2020, ISSN: 0360-5442. DOI: https://doi.org/10.1016/j.energy.2019.116427. [Online]. Available: https://www.sciencedirect.com/science/article/pii/S036054421932122X.

[214] D. Zaytsev, "Development of wet compressor for application in compression-resorption heat pumps", 2003. [Online]. Available: https://api.semanticscholar.org/CorpusID:135557823.

[215] M. Youbi-Idrissi and J. Bonjour, "The effect of oil in refrigeration: Current research issues and critical review of thermodynamic aspects", *International Journal of Refrigeration*, vol. 31, no. 2, pp. 165–179, 2008, ISSN: 0140-7007. DOI: https://doi.org/10.1016/j.ijrefrig.2007.09.006. [Online]. Available: https://www.sciencedirect.com/science/article/pii/S0140700707001867.

[216] M. I. Smith, "Lubricants and lubrication.", 1987, ISSN: 0368-4504. DOI: 10.1201/9780429448867-5.

[217] N. Stosic, A. Kovacevic, and I. Smith, "An investigation of liquid injection in refrigeration screw compressors", Jan. 2005.

[218] C. Wang, Z. Xing, W. Chen, Q. Yang, and Z. He, "Development of an oil free water-lubricated twin-screw air compressor", *Applied Thermal Engineering*, vol. 143, pp. 396–402, 2018, ISSN: 1359-4311. DOI: https://doi.org/10.1016/j.applthermaleng.2018.07.119. [Online]. Available: https://www.sciencedirect.com/science/article/pii/S1359431118330023.

[219] E. Vieren, K. Couvreur, M. De Paepe and S. Lecompte, "High-temperature heat pumps in industrial heating networks: A study on energy use, emissions, and economics", *Applied Thermal Engineering*, vol. 259, p. 124 799, 2025, ISSN: 1359-4311. DOI: https://doi.org/10.1016/j.applthermaleng.2024.124799. [Online]. Available: https://www.sciencedirect.com/science/article/pii/S1359431124024670.

[220] A. Degelin, R. Tassenoy, E. Vieren, T. Demeester, I. T'Jollyn, M. De Paepe, "Influence of supply temperature and booster technology on the energetic performance and levelized cost of heat of a district heating network with central heat pump", *Energy*, vol. 312, p. 133 589, 2024, ISSN: 0360-5442. DOI: https://doi.org/10.1016/j.energy.2024.133589. [Online]. Available: https://www.sciencedirect.com/science/article/pii/S036054422403367X.

[221] T. Zhu, E. Vieren, J. Liang, J. E. Thorsen, M. De Paepe, S. Lecompte and B. Elmegaard, "Booster heat pump with drop-in zeotropic mixtures applied in ultra-low temperature district heating system", *Energy*, vol. 305, p. 132 292, 2024, ISSN: 0360-5442. DOI: https://doi.org/10.1016/j.energy.2024.132292. [Online]. Available: https://www.sciencedirect.com/science/article/pii/S0360544224020668.

[222] H. Abedini, E. Vieren, T. Demeester, W. Beyne, S. Lecompte, S. Quoilin and A. Arteconi, "A comprehensive analysis of binary mixtures as working fluid in high temperature heat pumps", *Energy Conversion and Management*, vol. 277, p. 116 652, 2023, ISSN: 0196-8904. DOI: https://doi.org/10.1016/j.enconman.2022.116652. [Online]. Available: https://www.sciencedirect.com/science/article/pii/S0196890422014303.

[223] S. Abbasi, E. Vieren, K. Couvreur, S. Lecompte and A. Arteconi, "Impact of composition adjustment on the performance of a water-ammonia high-temperature heat pump", eng, West Lafayette, Indiana, 2024, p. 10. [Online]. Available: https://docs.lib.purdue.edu/iracc/2541/.

[224] E. Vieren, K. Couvreur, M. De Paepe and S. Lecompte, "Analysis of heat pump-integrated heating network topologies for decarbonization in industrial clusters", eng, in *Proceedings of ECOS 2024 37th International Conference on Efficiency, Cost, Optimization, Simulation and Environmental Impact of Energy Systems*, Rhodos, Greece, 2024, p. 12. [Online]. Available: https://ecos2024.com/proceedings/.

[225] E. Vieren, W. Beyne, T. Demeester, K. Couvreur, S. Abbasi, A. Arteconi, M. De Paepe and S. Lecompte, "High-temperature heat pumps: Thermodynamic, economic and experimental perspectives for enhanced integration", in *Proceedings of High-Temperature Heat Pump Symposium 2024*, Copenhagen, Denmark: Technical University of Denmark, 2024. [Online]. Available: https://orbit.dtu.dk/en/publications/4th-high-temperature-heat-pump-symposium-book-of-presentations.

[226] A. Degelin, R. Tassenoy, E. Vieren, T. Demeester, I. T'Jollyn and M. De Paepe, "Energetic and financial evaluation of a district heating network under varying supply temperatures and booster technologies", in *Proceedings of 9th edition of the European Thermal Sciences Conference (Eurotherm 2024*, vol. 2766, Bled, Slovenia: IOP Publishing, 2024. [Online]. Available: http://doi.org/10.1088/1742-6596/2766/1/012095.

[227] E. Vieren, K. Couvreur, T. Demeester, W. Beyne, M. De Paepe and S. Lecompte, "Experimental design of a high-temperature heat pump with sink temperatures up to 200°c", in *Proceedings of 26th IIR International Congress of Refrigeration (ICR2023)*, Paris, France: International Institute of Refrigeration (IIR), 2023.

[228] E. Vieren, T. Demeester, W. Beyne, M. P. Andersen, B. Elmegaard, M. De Paepe and S. Lecompte, "Techno-economic optimization of high-temperature heat pumps using pure fluids and binary mixtures", in *Proceedings of the 14th IEA Heat Pump Conference (HPC2023*, Chicago, Illinois: Technology Collaboration Programme on Heat Pumping Technologies by IEA (HPT TCP), 2023.

[229] A. Degelin, R. Tassenoy, E. Vieren, T. Demeester and M. De Paepe, "Influence of supply temperature and booster technology on the energetic performance of a district heating network", in *Book of abstracts : 9th International Conference on Smart Energy Systems (SESAAU2023)*, Copenhagen, Denmark: Aalborg University, 2023, pp. 357–358. [Online]. Available: https://vbn.aau.dk/da/publications/book-of-abstracts-9th-international-conference-on-smart-energy-sy.

[230] X. van Heule, T. Schoonjans, E. Vieren, W. Faes, D. Beets, M. Bijnens and M. De Paepe, "Experimental comparison of two fin geometries for cast iron air preheaters", in *Proceedings of the 17th International Heat Transfer Conference (IHTC-17)*, Cape Town, South Africa, 2023, 67:1–67:9. [Online]. Available: http://doi.org/10.1615/IHTC17.210-50.

[231] E. Vieren, H. Abedini, T. Demeester, W. Beyne, A. Arteconi, M. De Paepe and S. Lecompte, "Optimal temperature matching in high-temperature heat pumps", in *Proceedings of the High-Temperature Heat Pump Symposium 2022*, Copenhagen, Denmark: Technical University of Denmark, 2022, pp. 225–229, ISBN: 9788774756972. [Online]. Available: https://orbit.dtu.dk/en/publications/3rd-high-temperature-heat-pump-symposium-2022-book-of-presentatio.

[232] E. Vieren, T. Demeester, W. Beyne, H. Abedini, A. Arteconi, M. De Paepe and S. Lecompte, Steven, "Natural refrigerants versus synthetic refrigerants for steam-generating heat pumps", in *Proceedings of the 15th IIR-Gustav Lorentzen Conference on Natural Refrigerants (GL2022)*, Trondheim, Norway: International Institute of Refrigeration (IIR), 2022. [Online]. Available: http://doi.org/10.18462/iir.gl2022.0020.

[233] X. van Heule, E. Vieren, M. De Paepe and S. Lecompte, "Design of a two-phase reciprocating expansion test-rig for model validation", in *International Compressor Engineering Conference, Proceedings*, West-Lafayette, USA, 2022, p. 10. [Online]. Available: https://docs.lib.purdue.edu/cgi/viewcontent.cgi?article=3802&context=icec.

[234] E. Vieren, K. Couvreur, J. Vander Heyde, M. De Paepe and S. Lecompte, "Techno-economic analysis of high temperature heat pumps: A case study", in *Proceedings of the 15th International Conference on Heat Transfer, Fluid Mechanics and Thermodynamics (HEFAT2021)*, Online, 2021, pp. 2109–2114, ISBN: 9781775922162.

[235] R. Tassenoy, E. Vieren, M. De Paepe and S. Lecompte, "Carnot battery : Introduction of a high-level, application based sizing model", in *Proceedings of the 15th International Conference on Heat Transfer, Fluid Mechanics and Thermodynamics (HEFAT2021)*, Online, 2021, pp. 382–387, ISBN: 9781775922162.

[236] E. Vieren, K. Couvreur, J. Vander Heyde, M. De Paepe and S. Lecompte, "Simulation, optimization and design of a heating network at an industrial plant", in *Proceedings of the International Conference on Efficiency, Cost, Simulation and Environmental Impact of Energy Systems (ECOS2021)*, Taormina, Italy, 2021, pp. 1981–1992.

[237] C. Bang-Møller, M. Rokni, B. Elmegaard, J. Ahrenfeldt, and U. Henriksen, "Decentralized combined heat and power production by two-stage biomass gasification and solid oxide fuel cells", *Energy*, vol. 58, pp. 527–537, 2013, ISSN: 0360-5442. DOI: https://doi.org/10.1016/j.energy.2013.06.046. [Online]. Available: https://www.sciencedirect.com/science/article/pii/S0360544213005458.

[238] L. R. Clausen, B. Elmegaard, J. Ahrenfeldt, and U. Henriksen, "Thermodynamic analysis of small-scale dimethyl ether (DME) and methanol plants based on the efficient two-stage gasifier", *Energy*, vol. 36, no. 10, pp. 5805–5814, 2011, ISSN: 03605442. DOI: 10.1016/j.energy.2011.08.047.

[239] A. A. Kiss and R. R. Rewagad, "Energy efficient control of a btx dividing-wall column", *Computers & Chemical Engineering*, vol. 35, no. 12, pp. 2896–2904, 2011, ISSN: 0098-1354. DOI: https://doi.org/10.1016/j.compchemeng.2011.03.024. [Online]. Available: https://www.sciencedirect.com/science/article/pii/S0098135411001141.

[240] N. Asprion and G. Kaibel, "Dividing wall columns: Fundamentals and recent advances", *Chemical Engineering and Processing: Process Intensification*, vol. 49, no. 2, pp. 139–146, 2010, ISSN: 0255-2701. DOI: https://doi.org/10.1016/j.cep.2010.01.013. [Online]. Available: https://www.sciencedirect.com/science/article/pii/S025527011000022X.

[241] P. A. Østergaard and A. N. Andersen, "Booster heat pumps and central heat pumps in district heating", *Applied Energy*, vol. 184, pp. 1374–1388, 2016, ISSN: 0306-2619. DOI: https://doi.org/10.1016/j.apenergy.2016.02.144. [Online]. Available: https://www.sciencedirect.com/science/article/pii/S0306261916303105.

[242] T. Funder-Kristensen, *Refrigerant options now and in the future*, Accessed: 2024-08-26, 2023. [Online]. Available: https://www.danfoss.com/en/about-danfoss/articles/dcs/refrigerant-options-now-and-in-the-future/.

[243] S. Dilshad, A. R. Kalair, and N. Khan, "Review of carbon dioxide (co2) based heating and cooling technologies: Past, present, and future outlook", *International Journal of Energy Research*, vol. 44, no. 3, pp. 1408–1463, 2020. DOI: https://doi.org/10.1002/er.5024. eprint: https://onlinelibrary.wiley.com/doi/pdf/10.1002/er.5024. [Online]. Available: https://onlinelibrary.wiley.com/doi/abs/10.1002/er.5024.

[244] *Regulation (eu) no 517/2014 of the european parliament and of the council of 16 april 2014 on fluorinated greenhouse gases and repealing regulation (ec) no 842/2006*, Text with EEA relevance, Apr. 16, 2014. [Online]. Available: http://data.europa.eu/eli/reg/2014/517/oj.

[245] *Regulation (eu) 2024/573 of the european parliament and of the council of 7 february 2024 on fluorinated greenhouse gases, amending directive (eu) 2019/1937 and repealing regulation (eu) no 517/2014*, Published in Official Journal of the European Union, L 45, 20 February 2024, Feb. 2024. [Online]. Available: https://eur-lex.europa.eu/eli/reg/2024/573/oj.

[246] M. O. McLinden, C. J. Seeton, and A. Pearson, "New refrigerants and system configurations for vapor-compression refrigeration", *Science*, vol. 370, no. 6518, pp. 791–796, 2020. DOI: 10.1126/science.abe3692. eprint: https://www.science.org/doi/pdf/10.1126/science.abe3692. [Online]. Available: https://www.science.org/doi/abs/10.1126/science.abe3692.

[247] European Chemicals Agency (ECHA), *Echa publishes pfas restriction proposal*, Accessed: 2024-08-27, 2023. [Online]. Available: https://echa.europa.eu/-/echa-publishes-pfas-restriction-proposal.

[248] S. Quoilin, M. V. D. Broek, S. Declaye, P. Dewallef, and V. Lemort, "Techno-economic survey of organic rankine cycle (orc) systems", *Renewable and Sustainable Energy Reviews*, vol. 22, pp. 168–186, 2013, ISSN: 1364-0321. DOI: https://doi.org/10.1016/j.rser.2013.01.028. [Online]. Available: https://www.sciencedirect.com/science/article/pii/S1364032113000592.

[249] D. Savitha, P. Ranjith, B. Talawar, and N. R. P. Reddy, "Refrigerants for sustainable environment – a literature review", *International Journal of Sustainable Energy*, vol. 41, no. 3, pp. 235–256, 2022. DOI: 10.1080/14786451.2021.1928129. eprint: https://doi.org/10.1080/14786451.2021.1928129. [Online]. Available: https://doi.org/10.1080/14786451.2021.1928129.

[250] N. Abas, A. R. Kalair, N. Khan, A. Haider, Z. Saleem, and M. S. Saleem, "Natural and synthetic refrigerants, global warming: A review", *Renewable and Sustainable Energy Reviews*, vol. 90, pp. 557–569, 2018, ISSN: 1364-0321. DOI: https://doi.org/10.1016/j.rser.2018.03.099. [Online]. Available: https://www.sciencedirect.com/science/article/pii/S1364032118301977.

[251] C. Kondou and S. Koyama, "Thermodynamic assessment of high-temperature heat pumps using low-gwp hfo refrigerants for heat recovery", *International Journal of Refrigeration*, vol. 53, pp. 126–141, 2015, ISSN: 0140-7007. DOI: https://doi.org/10.1016/j.ijrefrig.2014.09.018. [Online]. Available: https://www.sciencedirect.com/science/article/pii/S0140700714002576.

[252] S. Lecompte, "Performance evaluation of organic rankine cycle architectures : Application to waste heat valorisation", eng, Ph.D. dissertation, Ghent University, 2016, pp. XXXI, 239, ISBN: 9789085788973.

[253] M. Lindahl *et al.*, "Flexibility assessment and analyses of different options", IEA Heat Pumping Technologies Annex 57, Tech. Rep., Dec. 2023. [Online]. Available: https://heatpumpingtechnologies.org/annex57/wp-content/uploads/sites/69/2024/03/task-4-reportfinal-2.pdf.

[254] R. Padullés, M. L. Hansen, M. P. Andersen, B. Zühlsdorf, J. K. Jensen, and B. Elmegaard, "Optimal operation of industrial heat pumps with stratified thermal energy storage for emissions and cost reduction using day-ahead predictions", *Applied Thermal Engineering*, vol. 266, p. 125 703, 2025, ISSN: 1359-4311. DOI: https://doi.org/10.1016/j.applthermaleng.2025.

125703. [Online]. Available: https://www.sciencedirect.com/science/article/pii/S1359431125002947.

[255] G. F. Frate, L. Ferrari, P. Sdringola, U. Desideri, and A. Sciacovelli, "Thermally integrated pumped thermal energy storage for multi-energy districts: Integrated modelling, assessment and comparison with batteries", *Journal of Energy Storage*, vol. 61, p. 106 734, 2023, ISSN: 2352-152X. DOI: https://doi.org/10.1016/j.est.2023.106734. [Online]. Available: https://www.sciencedirect.com/science/article/pii/S2352152X23001317.

[256] Heaten, *Heaten technology*, Accessed: 2025-03-04, 2025. [Online]. Available: https://www.heaten.com/technology/.